HAKONE XVI

SEP 2-7, 2018, TSINGHUA UNIVERSITY, BEIJING, CHINA

16th International Symposium on High Pressure Low Temperature Plasma Chemistry

Organizers

TSINGHUA UNIVERSITY, BEIJING, CHINA

- **Department of Energy and Power Engineering;**

  http://www.te.tsinghua.edu.cn/publish/teen/index.html

- **Department of Engineering Physics;**

  http://www.engineeringphysics.tsinghua.edu.cn/

Contact

Room 201, Local Organizing Committee

Department of Energy and Power Engineering

Tsinghua University

Beijing, China, 100084

Email: hakone@tsinghua.edu.cn

Web

http://hakone.csp.escience.cn

Sponsors

- **National Natural Science Foundation of China**
  国家自然科学基金委

- **Department of Energy and Power Engineering**
  清华大学能源与动力工程系

- **Science and Technology on Plasma Dynamics Lab**
  等离子体动力学国家级重点实验室

- **Avantes**
  北京爱万提斯科技有限公司

- **Beijing Hiden Analytical Ltd.**
  北京英格海德分析技术有限公司

- **Nanjing Suman Plasma Technology Co.,Ltd**
  南京苏曼等离子科技有限公司

- **LONGKING**
  福建龙净环保股份有限公司

Location: Tsinghua University

Tsinghua University was established in 1911, originally under the name “Tsinghua Xuetang”. The school was renamed "Tsinghua School" in 1912. The university section was founded in 1925. The name “National Tsinghua University” was adopted in 1928.

The faculty greatly valued the interaction between Chinese and Western cultures, the sciences and humanities, the ancient and modern. Since China opened up to the world in 1978, Tsinghua University has developed at a breathtaking pace into a comprehensive research university. At present, the university has 14 schools and 56 departments with faculties in science, engineering, humanities, law, medicine, history, philosophy, economics, management, education and art. The University has now over 25,900 students, including 13,100 undergraduates and 12,800 graduate students. As one of China’s most renowned universities, Tsinghua has become an important institution for fostering talent and scientific research.

The educational philosophy of Tsinghua is to "train students with integrity." Among over 120,000 students who have graduated from Tsinghua since its founding are many outstanding scholars, eminent entrepreneurs and great statesmen remembered and respected by their fellow Chinese citizens.

With the motto of “Self-Discipline and Social Commitment” and the spirit of “Actions Speak Louder than Words”, Tsinghua University is dedicated to the well-being of Chinese society and to world development.

General information

High Pressure Low Temperature Plasma Chemistry Symposium (HAKONE) is a biennial international symposium, which brings together scientists and engineers from both of academic and industrial sphere working on subjects in the basic research and plasma processing of high pressure and low temperature plasma chemistry. The symposium provides for participants the opportunity to present the progress in their work and to discuss related problems of current interest in theory, experiment and applications in various areas. Moreover, HAKONE provides a forum for sharing knowledge, experience and creative ideas in a friendly atmosphere.

The series of High Pressure Low Temperature Plasma Chemistry Symposiums was initiated in Hakone (Japan, 1987). The next meetings were held in Kazimierz Dolny (Poland, 1989), Strasbourg (France, 1991), Bratislava (Slovakia, 1993), Milovy (Czech Republic, 1996), Cork (Ireland, 1998), Greifswald (Germany, 2000), Pühajärve (Estonia, 2002), Padova (Italy, 2004), Saga (Japan, 2006), Oléron Island (France, 2008), Trenčianske Teplice (Slovakia, 2010), Kazimierz Dolny (Poland, 2012) , Zinnowitz (Germany, 2014) and Brno (Czech Republic, 2016).

Topics

- Fundamental problems of high pressure discharges
- Modelling and diagnostics
- Molecular synthesis and decomposition
- Ozone generation and applications
- Generation of radiation in high pressure discharges
- Depollution and environmental applications
- Surface processing and technology (cleaning, coating, etching and modification, equipment)
- Biological applications
- Miscellaneous

Committees

International Scientific Committee

Ronny Brandenburg (Germany)
Mirko Černák (Czech Republic) -chair
Tomáš Hoder (Czech Republic)
Nicolas Gherardi (France)
Tony Herbert (Ireland)
Haruo Itoh (Japan)
Masuhiro Kogoma (Japan)
Kirill V. Kozlov (Russia)
Štefan Matejčík (Slovakia)
Jerzy Mizeraczyk (Poland)
Cristina Paradisi (Italy)
Henryka D. Stryczewska (Poland)
Hans-Erich Wagner (Germany)
Koichi Yasuoka (Japan)
Indrek Jõgi (Estonia)
Matti Laan (Estonia) - honorary member
Chobei Yamabe (Japan) - honorary member

Reading and Advisory Committee

(Masaryk University, Czech Republic)

Zdeněk Bonaventura
Jan Čech
Pavel Dvořák
Tomáš Hoder
Vít Kudrle
Zdeněk Navrátil
Jozef Ráhel'
Petr Synek
David Trunec
Jan Voráč

Local Organizing Committee

Lu Duan
Shui-Qing Li (co-chair)
Qing Liu
Hai-Yun Luo
Yi-Kang Pu (chair)
Yun Wu

Important information

1. Check in

Time: Sep 02 (Sunday) 14:00 – 22:00 Location: Lobby of Jin Chunyuan Hotel

2. Reception desk

Time: Sep 02 (Sunday) 14:00 – 22:00; Sep 03-07 (Monday-Friday) 8:00 -17:00;

Location: Lobby of Jin Chunyuan Hotel

3. Accommodation

Accommodation in Jin Chunyuan Hotel from Sep 02 evening to Sep 07 morning is included in the registration fees.

4. Oral presentation

All oral presenters are requested to copy your PPT into the computer, at least 10 minutes before the start of each session. The time for each paper in the oral session is 20 minutes, including 5 minutes for questions, answers and comments.

5. Poster presentation

Each poster should be printed in A0 portrait format, 1189 mm high × 841 mm wide (46.8" x 33.1"). Please submit it at collection point located by the registration desk during check-in. All the entries are to be mounted in the numbered space that has been reserved for it.

6. Meal

Breakfast for guests of Jin Chunyuan Hotel: 7:00-9:00

Location	Sep 02-Sun	Sep 03-Mon	Sep 04-Tus	Sep 05-Wed	Sep 06-Thu	Sep 07-Fri
Lunch	--	Jia Suo	Jia Suo	JinChunyuan	Jia Suo	JinChunyuan
Dinner	**Reception**	JinChunyuan	JinChunyuan	JinChunyuan	**Banquet**	--

Lunch: 12:00-13:30, Sep 03-07

Dinner: 18:00-19:30, Sep 03-04; 18:30-20:00, Sep 05

7. Welcome reception

18:00-19:30, Sep 02 (Sunday), Jin Chunyuan Hotel

8. Excursion

14:00-18:00, Sep 05 (Wednesday), The Summer Palace

Bus: depart from Jin Chunyuan Hotel at 14:00

9. Banquet

17:30-20:00, Sep 06 (Thursday), Quanjude Restaurant

10. Group Photo:

10:00-10:30, Sep 03 (Monday), Weather dependent

11. Committee meeting (ISC)

20:00-21:00, Sep 04 (Tuesday)

Meeting room 203, Department of Energy and Power Engineering

Scientific program

• Sep 03, Monday morning — Chair: M Černák

8:00-9:00	**Registration**
9:00-9:20	**Opening**
9:20-10:10	**Ulrich Kogelschatz Lecture Award** **Akira Mizuno** Electrostatics and Non-Thermal Plasma for Health and Environment
10:10-10:40	**Coffee break / Group Photo**
10:40-11:20	**Aart W. Kleijn** Plasma Catalytic Conversion of CO_2 and Small Hydrocarbons
11:20-11:40	**Hai-Xing Wang** An Investigation of Carbon Dioxide Splitting Using Microhollow Cathode Discharge
11:40-12:00	**Dušan Kováčik** Atmospheric-Pressure Plasma Treatment of Float Glass as Surface Cleaning and Activation Procedure Prior to Coating
12:00-13:30	**Lunch, Jia Suo**

• Sep 03, Monday afternoon — Chair: A Mizuno

14:00-14:50	**Invited lecture** **Anne Bourdon** Barrier Discharge and Pulsed Discharge Modelling
14:50-15:10	**Fumiyoshi Tochikubo** Simulation of Atmospheric-Pressure Glow Discharge Electrolysis for Silver Nanoparticle Synthesis in Silver Nitrate Solution
15:10-15:30	**Clémence Tyl** Experimental and Numerical Study of Memory Effect in Homogeneous Atmospheric Pressure Dielectric Barrier Discharges in N_2/O_2 and N_2/NO Mixtures
15:30-16:00	**Coffee break**
16:00-16:20	**Marc van der Schans** The Memory Effect of Pulsed Plasma Jets: Temporal and Spatial Behavior of Guided Streamers in N_2, He and Ar
16:20-16:40	**Xi Lin** Study of Memory Effect in A Townsend Discharge: Quantification of Species by Laser Induced Fluorescence Spectroscopy
16:40-17:00	**Yifei Zhu** Modeling of Streamer-to-Spark Transition of a Nanosecond Pulsed Discharge for Kinetics Parameters
17:00-17:20	**Veronika Medvecká** Atmospheric Pressure Low-Temperature Plasma in Agriculture and Food Processing
18:00-19:30	**Dinner, Jin Chunyuan**

• Sep 04, Tuesday morning — Chair: A Bourdon

9:00-9:50	**Invited lectures** **Giorgio Dilecce** Laser Induced Fluorescence in Nanosecond Pulsed Discharges
9:50-10:10	**Koichi Sasaki** Observation of 1d-1s Forbidden Optical Emission of Atomic Oxygen in Atmospheric-Pressure N_2/O_2 Plasma Jet
10:10-10:30	**Jintao Sun** Kinetic Contribution of Vibrational States in Plasma Assisted CH_4 Reforming
10:30-11:00	**Coffee break**
11:00-11:20	**Abdeldjalil Reguig** Comparison of Electrical Breakdowns Produced by High Voltage Pulses Applied to Anodes Made of Copper and Highly Resistive Composite Material
11:20-11:40	**Matej Klas** Discharge Breakdown Studied under Extreme Conditions
11:40-12:00	**Xingqian Mao** Hybrid Repetitively-Pulsed Nanosecond Discharge and DC Discharge Enhanced Low Temperature H_2/O_2/He Ignition by Non-equilibrium Excitation
12:00-13:30	**Lunch, Jia Suo**

• Sep 04, Tuesday afternoon — Chair: M Simek

14:00-14:50	**Invited lecture** **Lifang Dong** Pattern Formation in Dielectric Barrier Discharge
14:50-15:10	**Kirill V. Kozlov** Filamentary and Diffuse Barrier Discharges in Noble Gases with Admixtures of Molecular Gases
15:10-15:30	**Tetsuya Abe** Production of An Ammonia Storage Material by Atmospheric Dielectric Barrier Discharge at Room Temperature
15:30-16:00	**Coffee break**
16:00-16:20	**Nicolas Naudé** Influence of barrier material on the Atmospheric Pressure Townsend Discharge
16:20-16:40	**Marina V. Sokolova** Influence of Barrier Properties on Dielectric Barrier Surface Discharge Driven by Microsecond Voltage Pulses
16:40-17:00	**Indrek Jõgi** Ozone Assisted NOx Oxidation and Adsorption on Metal-oxides
17:00-17:20	**Sina Jahanbakhsh** Correlation Between Electrical and Spatio-Temporal Development in a One-Sided, Single Filament DBD in Pin-To-Hemisphere Configuration
18:00-19:30	**Dinner, Jin Chunyuan**
20:00-21:00	**ISC Meeting** Meeting room 203, Department of Thermal and Power Engineering

• Sep 05, Wednesday morning — Chair: L Dong

9:00-9:50	**Invited lectures** **Felipe Iza** Chemical Probes and Plasma Synthesis
9:50-10:10	**Mirko Černák** Micro-Hollow Surface Discharge for Bacterial Decontamination
10:10-10:30	**Bartosz Michalczuk** Ultrasensitive Method of Monitoring of VOC's Decomposition in Corona Discharge Based on Ion Mobility Spectrometry
10:30-11:00	**Coffee break**
11:00-11:20	**Jozef Rahel** The Use of DBD Plasma Activated Powders in Ceramic Processing
11:20-11:40	**Bingxuan Lin** Multi-Channel Plasma Igniter and Plasma Fuel Injector for Aero Engine
11:40-12:00	**Qiang Chen** The Generation of Aqueous Hydrogen Peroxide in DC Plasma-Liquid System with Liquid as Cathode
12:00-13:30	**Lunch, Jin Chunyuan**

• Sep 05, Wednesday afternoon

14:00-18:00	**Excursion** The Summer Palace The bus will depart from Jin Chunyuan Hotel at 14:00 pm
18:30-20:00	**Dinner, Jin Chunyuan**

Sep 06, Thursday morning — Chair: G Dilecce

9:00-9:50	**Invited lectures** **Milan Simek** Processing of Solid and Liquid Materials by Atmospheric-Pressure Surface DBD-Based Jet
9:50-10:10	**Jan Voráč** Quantum States Distribtuion in OH(X) Radical Produced by Streamer Discharges at Liquid Water Interface
10:10-10:30	**Tomáš Hoder** Microampere Currents in Barrier Discharges at Water Interface in Atmospheric Pressure Air
10:30-11:00	**Coffee break**
11:00-11:20	**Han Xu** Comparison Between the Water Activation Effects by Cold Plasma Jets in Different Working Conditions
11:20-11:40	**Yunqiu Cui** Experimental Study in Removal of Tetracycline in Simulant Water by Dielectric Barrier Discharge Plasma
11:40-12:00	**Qing Xiong** Time-Behavior of Plasma-Activated Aqueous Chemistry and its Indications to Inactivation of Candida Glabrata
12:00-13:30	**Lunch, Jia Suo**

Sep 06, Thursday afternoon

14:00-16:30	**Poster session** Posters will be displayed at the same conference room (Xi Jie)
17:30-20:00	**Banquet** Quanjude Restaurant: Peking Roast Duck

Sep 07, Friday morning

Chair: F Iza

9:00-9:20	**Masuhiro Kogoma** The Surface Treatment of Liquid Cristal Polymer Using Atmospheric Pressure Glow Discharge.
9:20-9:40	**Piotr Krupski** Cooling System of RF Plasma Jet for Temperature Non-resistant Surface Treatment
9:40-10:00	**Naoki Osawa** Distribution of Surface Potential on Dielectric Barrier Under Different Discharge Modes in Atmospheric-Pressure Air
10:00-10:20	**Coffee break**
10:20-10:40	**Ana Sobota** Plasma-Surface Interaction: The Influence of The Surface on the Electron Properties and Electric Fields in A Plasma Jet
10:40-11:00	**Yihua Ren** Complex Flame Control Using Electric Field / Plasma
11:00-11:20	**Cheng Zhang** Formation of Runaway Electrons Preionized Pulsed Diffuse Discharge at Elevated Pressure
11:20-11:40	**Haiyun Luo** Primary Research on Plasma Biosafety Using Atmospheric-Pressure Plasma in Air
11:40-12:00	**Closing**
12:00-13:30	**Lunch, Jin Chunyuan**

Sep 07, Friday afternoon

14:00-16:00	**Lab tour**

Poster session

P-1	**Chongshan Zhong**	Non-Thermal Plasma Enhancement of Drying Process
P-2	**Chengdong Kong**	Translational Temperature Measurement of a Pin-To-Pin Discharge Disturbed by a Turbulent Jet Flow in Atmospheric Pressure Air
P-3	**Simon Dap**	Development of a 0d Model to Investigate the Plasma Chemistry in a Townsend Discharge in the Mixture N2/O2: Role of the Associative Ionization Mechanisms in the Memory Effect
P-4	**Jan Voráč**	Massiveoes: Pushing the Limits – Disentagling Thermal N2(C-B) and Non-Thermal OH(A-X) Rotational Distribution by Combined State-By-State and Boltzmann Simulation Approach
P-5	**Paweł A. Mazurek**	Analysis of Electric Field Strength and Magnetic Flux From Plasma Reactor Installations
P-6	**Linsheng Wei**	Temperature Distribution in Ozone Generator with Parallel-Plate Configuration and Forced Air Cooling
P-7	**Rasmus Talviste**	Investigation of a He Micro Plasma-Jet for Distilled Water Treatment
P-8	**Clémence Tyl**	Diagnostics of Local Electrical Parameters in Atmospheric Pressure Dielectric Barrier Discharges
P-9	**Joanna Pawłat**	DBD Plasma Jet for Inactivation of Yeast Pathogens
P-10	**Fumiaki Mitsugi**	Observation of Reactive Oxygen Species Emitted by Plasma Jets Using Ki-Starch Method
P-11	**Dai Atsuta**	Ozone Generation and Gas Temperature Characteristics by Pulse Modulated Air Dielectric Barrier Discharge Device
P-12	**Nicolas Naudé**	Spatially-Resolved Electrical and Optical Study of Homogeneous Dielectric Barrier Discharges in Presence of Hexamethyldisiloxane and Nitrous Oxide
P-13	**Tomáš Hoder**	Simulation of Electron Interactions with Liquid Water and Processes Related to Sub-Nanosecond Electrical Breakdown
P-14	**Ekaterina Abramovskaia**	The Barrier Discharges in the Binary Gas Mixtures of Argon and Volatile Organic Compounds
P-15	**Justyna Jaroszyńska-Wolińska**	Biosensor Constructed by SPP Plasma Technique for Determination of Dihydroxybenzene Isomers
P-16	**Szymon Malinowski**	Quantum-Chemical Analysis of Laccase Bio-Coating Formation in Corona Plasma Jet
P-17	**Ján Dugáček & Pavel Sťahel**	Investigation of Atmospheric Pressure Surface Modified Zirconium Dioxide Nanopowder By Thermal Desorption Spectroscopy

P-18	**Bartosz Michalczuk**	Detection of Phthalates Using Corona Discharge Ion Mobility Spectrometry – Mass Spectrometry (CD IMS-MS)
P-19	**Zhongshu Zhang**	Interface reactions between water and drift positive ions
P-20	**Henryka Danuta Stryczewska**	Review of Developments in Application of Ozone in Agriculture
P-21	**Susana Espinho**	The Effect of O_2 Admixture on The Electron Density and Electron Temperature of Argon Microwave Discharges
P-22	**Shungo Zen**	Effects of Reactive Species on Low-temperature Annealing for Dye-sensitized Solar Cells
P-23	**Yong Tang**	Flow Fluctuation Induced by Coaxial Plasma Device at Atmospheric Pressure
P-24	**Wei Cui**	Lean Flammability Characteristics of Plasma-actuated Swirl Flames under Pulsating Flow Disturbances
P-25	**Yihua Ren**	Electrohydrodynamic flame instability under manipulations of AC and DC electric fields
P-26	**Yihua Ren**	Phase-selective Laser-induced Breakdown Spectroscopy

Social Program

- **Excursion：The Summer Palace**

The Summer Palace (Chinese: 颐和园; pinyin:Yi He Yuan), is a vast ensemble of lakes, gardens and palaces in Beijing. It was an imperial garden in Qing Dynasty. Mainly dominated by Longevity Hill and Kunming Lake.Longevity Hill is about 60 m (200 ft) high and has many buildings positioned in sequence. The front hill is rich with splendid halls and pavilions, while the back hill, in sharp contrast, is quiet with natural beauty. The central Kunming Lake, covering 2.2 square kilometers (540 acres), was entirely man-made and the excavated soil was used to build Longevity Hill.

In December 1998, UNESCO included the Summer Palace on its World Heritage List. It declared the Summer Palace "a masterpiece of Chinese landscape garden design. The natural landscape of hills and open water is combined with artificial features such as pavilions, halls, palaces, temples and bridges to form a harmonious ensemble of outstanding aesthetic value".

Hint: we recommend that participants wear sunscreen during the excursion.

Transportation: Airport-Tsinghua

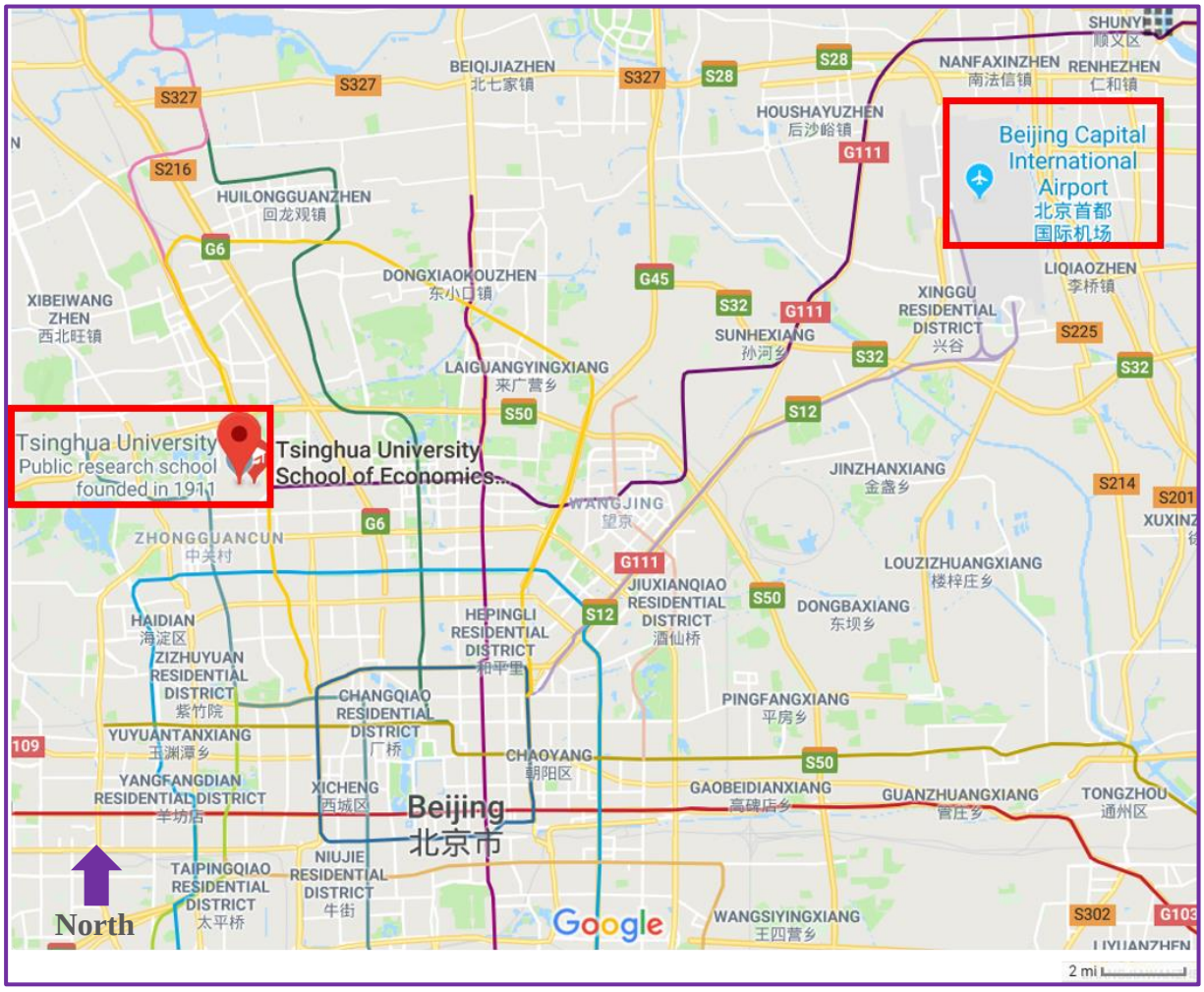

How to go to the symposium?

Beijing Capital International Airport (BCIA) – Tsinghua University: ~ 35 km away

- **Shuttle bus:** Take the shuttle bus from the airport to Tsinghua Science park
- **Subway:** Take Airport Express from Terminal 2 or Terminal 3 to SANYUANQIAO, take subway line 10 from SANYUANQIAO to HAIDIANHUANGZHUANG, and then take subway line 4 from HAIDIANHUANGZHUANG to YUANMINGYUAN. Then you can walk to the Tsinghua west gate.
- **Taxi:** It costs about 120 RMB (daytime 5:00-23:00) or 200 RMB (23:00-5:00)

Tips: You can show the information below to your taxi driver:

Please Take Me to Jin Chunyuan Hotel, Tsinghua University. Thank you!

请您送我到清华大学近春园宾馆，谢谢您！

How to leave there?

Tsinghua University – Beijing Capital International Airport (BCIA): ~ 35 km away

- **Shuttle bus:** Take the shuttle bus from Tsinghua Science park to the airport
- **Subway:** Walk to the YUANMINGYUAN station, then take subway line 4 from YUANMINGYUAN to HAIDIANHUANGZHUANG, then take subway line 10 from HAIDIANHUANGZHUANG to SANYUANQIAO, then take Airport Express from SANYUANQIAO to Terminal 2 or Terminal 3.
- **Taxi:** It costs about 120 RMB (daytime 5:00-23:00) or 200 RMB (23:00-5:00)

Tips: You can show the information below to your taxi driver:

Please Take Me to Beijing Capital International Airport Terminal 1/2/3. Thank you!

请您送我去首都国际机场 T1 /T2 /T3 航站楼，谢谢您！

Airport Shuttle

Web: http://en.bcia.com.cn/traffic/airbus/index.shtml

Route: BCIA-Zhongguancun (Airport → Tsinghua)

Line 5: Wanghe Bridge [RMB 20] -- Xiaoying[RMB 20] -- Asian Games Village (Anhui Bridge) [RMB 25] -- Xueyuan Bridge[RMB 30] -- North of Baofusi Bridge [RMB 30] -- Tsinghua University Science Park (TusPark) [RMB 30]

Time: 6:50-24:00 Every 30 minutes. Buses depart when fully seated.

Route: Zhongguancun-BCIA (Tsinghua → Airport)

Line 5: Tsinghua University Science Park (TusPark) [RMB 30] -- Zhongguancun (Fourth Bridge) [RMB 30] -- Beihang University (north gate) [RMB 30] -- Huixin West Street (Under the Bridge of Huixin West Street, East of Anhui Plaza) [RMB 20] -- **T2 -- T1 -- T3**

Time: 5:10 ~ 22:00 Every 30 minutes. Buses depart when fully seated.

Tips: It takes around 1.5 hours. Please note, the traffic in Beijing will become heavy during morning or evening peaks.

Beijing subway map

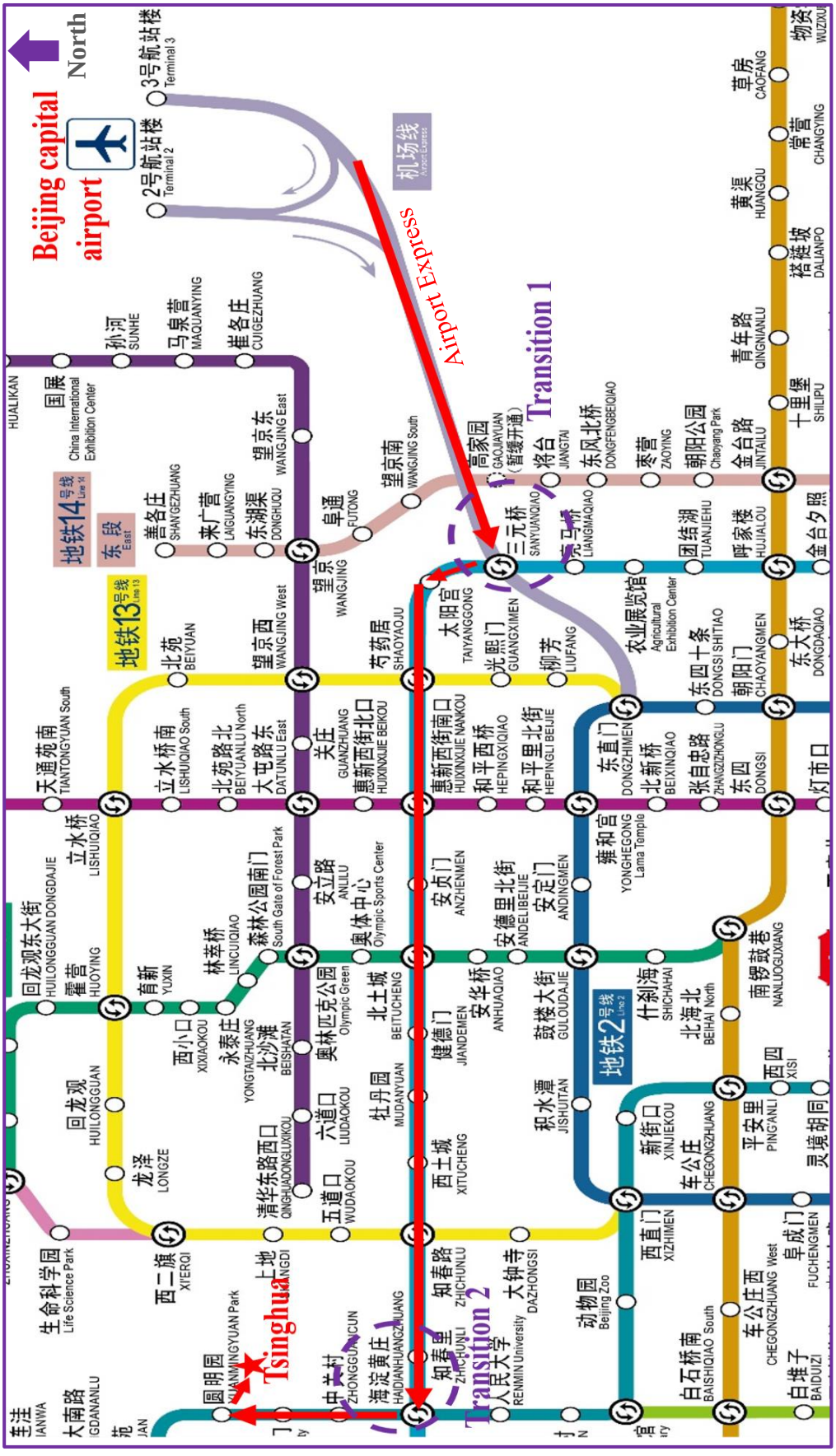

Website: https://www.bjsubway.com/en/

The nearest station to Tsinghua University is YUANMINGYUAN park station (100 meters away from Tsinghua west gate)

Tsinghua map

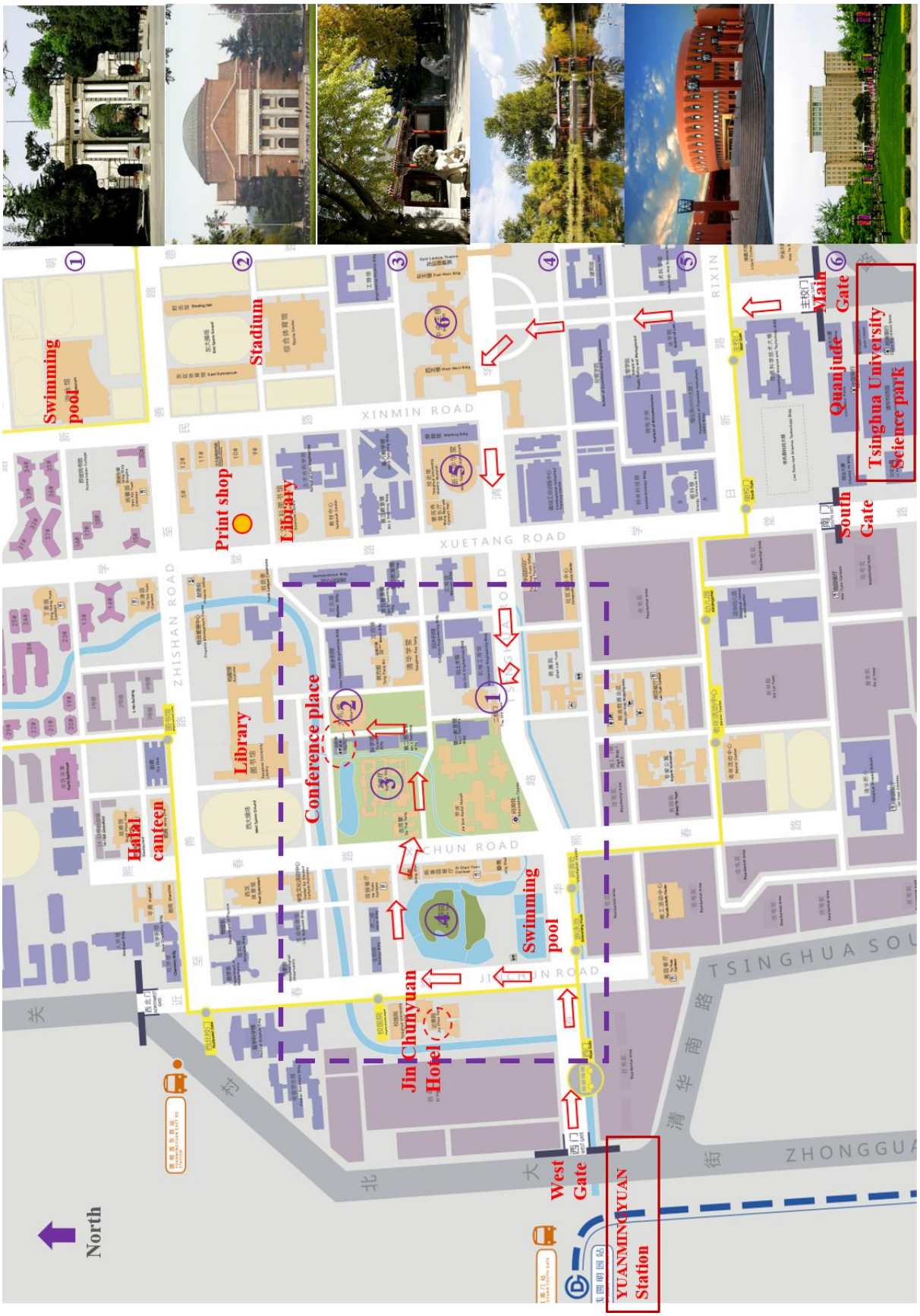

Tsinghua map (zoom in)

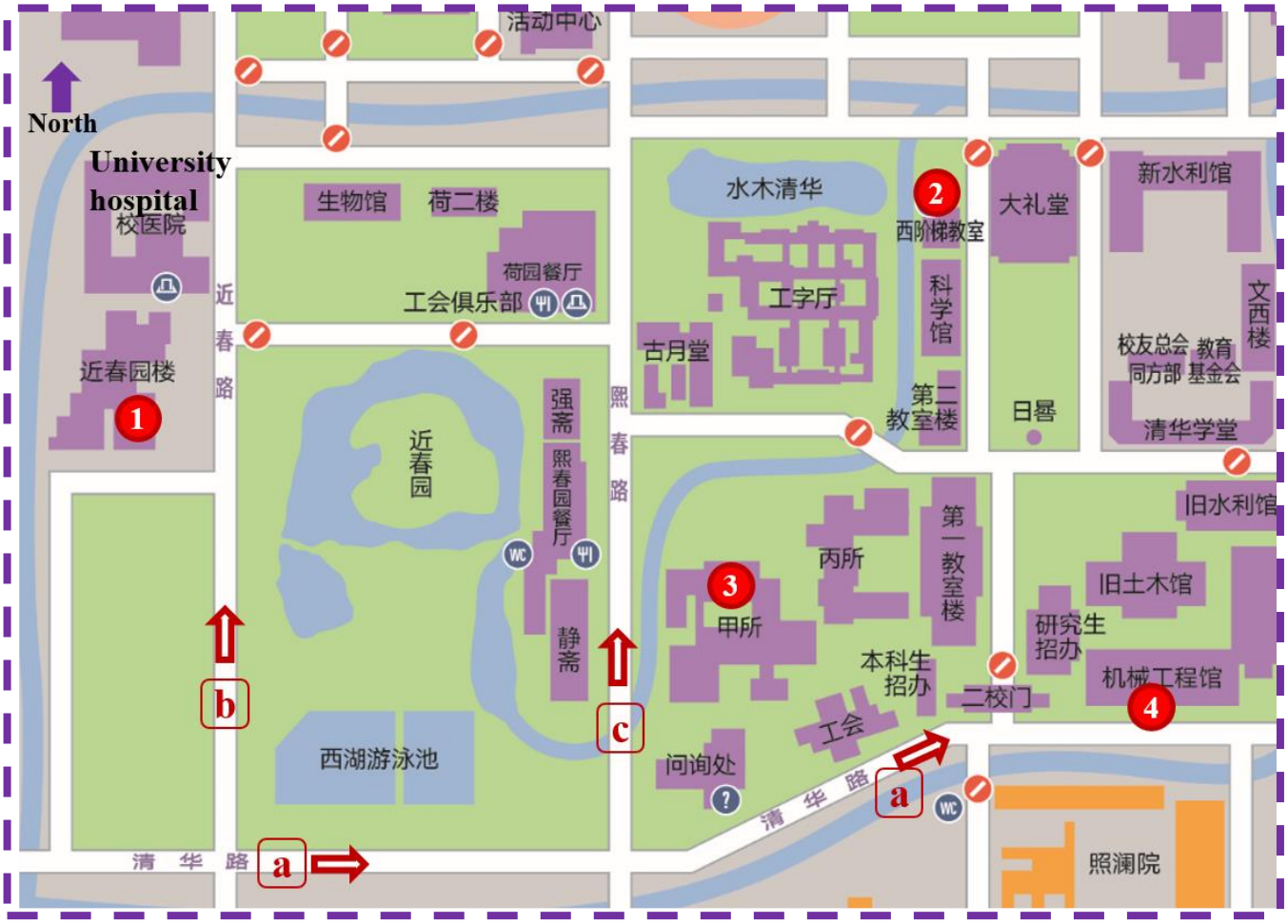

1. Jin Chunyuan Hotel (近春园宾馆)
2. Conference room: Xi Jie (主会场，西阶教室)
3. Jia Suo (甲所)
4. Department of Energy and Power Engineering (机械工程馆：能源与动力工程系系馆)

a. Tsinghua Avenue (清华路)
b. Jin Chun Avenue (近春路)
c. Xi Chun Avenue (熙春路)

Tips

Public Transportation in Beijing

1. Public Buses

Buses are the main means of transportation in Beijing. Please prepare changes before taking a bus. Buses may be very crowded during peak times at 07:00 - 09:00 and 17:00 - 20:00.

2. The Subway

There are currently 17 subway lines and an Airport Express in Beijing. The fare is between RMB 2 and RMB 12 based on the distance. The fare for the Airport Express is RMB 25. It is very convenient to transfer from one subway line to another.

3. Taxis

Taxis in Beijing have several colors. All of them show a taximeter inside. You can easily find them in every part of Beijing. All Taxis will charge RMB 2.3 per kilometer with a base rate or minimum charge of RMB 13 within 3 kilometers.

4. Uber

Help Lines

Police: 110
Traffic Police: 122
Local Telephone Number Inquiry: 114
Domestic Long Distance Inquiry: 116
Weather forecast: 121
Time Inquiry: 117
Medical emergency call: 120
Fire Alarm: 119

Electricity

The electric current used in China is 220V 50Hz. Please note that plug adapters and converters might be required. The picture on the right shows

Printing shop

There is a big printing shop (Wendingwenbo, 文鼎文博) on the first floor of Qingfen Canteen (清芬园), opening from 09:00 to 21:00

Notes

ELECTROSTATICS and NON-THERMAL PLASMA for HEALTH and ENVIRONMENT

Akira Mizuno
Toyohashi University of Technology, Toyohashi, Japan

E-mail: mizuno@ens.tut.ac.jp

Electrostatic precipitation and Dielectric barrier discharge are very useful for cleaning air and promoting low temperature plasma chemical reactions such as ozone generation and gaseous pollution control[1-3]. ESP uses corona discharge generated in non-uniform field in a relatively large volume. DBD uses uniform field in short gap distance. Both are categorized as Non-thermal plasma. Dr. Kogelschatz and his colleagues made significant contribution in understanding fundamentals of DBD and proposing various plasma chemical processes including treatment of flue gas, toxic gas, VOCs and surface treatment, etc. Especially cleaning air and sterilization are the most important characteristics of ESP and DBD, and due to these characteristics, those process can be used for prevention of airborne diseases. These NTP processes has recently been actively investigated for medical treatment.

In this presentation, brief review of ESPs, especially back corona problem for treating high resistivity dusts, is made since NTP technology in my research has been derived from the idea to cope with this problem[4, 5]. For instance, pulse energization is effective for high resistivity dusts. Using short pulse voltage, especially positive pulse, streamers propagate longer distance and ionization can be made in large gas volume. This can be used for gas treatment[6]. At the meantime, energy efficiency and selectivity of the NTP process should be high enough to compete with the existing technologies. Therefore, combination of low-temperature plasma with absorbing surface or catalysts is effective[7]. Generation of NTP combined with catalyst are introduced, and several examples of the NTP process are presented[8].

NTP generates reactive radicals which migrate the medium and penetrate into biological particles such as microbes and viruses, and destroy them. Recently pathways of these processes have been investigated in more details and more knowledge have been obtained. Some of these understandings are introduced[9, 10].

ESP and DBD are matured technology, yet still important improvements are possible to meet novel requirements such as to be more efficient, long maintenance period, and less usage of electric power. These requirements are important for NTP to be applied in control of bio-particles and prevention of infection. In this presentation, several improvements on ESP process will be reported[11-13]

References

[1] U. Kogelschatz, "Dielectric-Barrier Discharges: Their History, Discharge Physics, and Industrial Applications," *Plasma Chemistry and Plasma Processing,* vol. 23, pp. 1-46, 2003// 2003.

[2] H. J. White, "Industrial Electrostatic Precipitation, Addison-Wesley Publishing Co," 1962.

[3] B. Eliasson and U. Kogelschatz, "Nonequilibrium volume plasma chemical processing," *Plasma Science, IEEE Transactions on,* vol. 19, pp. 1063-1077, 1991.

[4] S. Masuda and A. Mizuno, "Initiation Condition and Mode of Back Discharge," *Journal of Electrostatics,* vol. 4, p. 35 ~ 52, 1977.

[5] S. Masuda and A. Mizuno, "LIGHT MEASUREMENT OF BACK DISCHARGE," *J Electrostatics,* vol. 2, pp. 375-396, 1977.

[6] A.Mizuno, J.S.Clements, and R.H.Davis, "A Method for the removal of sulfur dioxide from exhaust gas utilizing pulsed streamer corona for electron energization," *IEEE Trans. On Ind. Appl.,* vol. 22, pp. 516-522, 1986.

[7] A. Mizuno, "Generation of non-thermal plasma combined with catalysts and their application in environmental technology," *Catalysis Today,* vol. 211, pp. 2-8, Aug 1 2013.

[8] A. Mizuno, "Environmental Application of Nonthermal Plasma, Industrial Plasma Technology," in *Applications from Environmental to Energy Technologies*, Y. Kawai, H. Ikegami, N. Sato, A. Matsuda, K. Uchino, M. Kuzuya*, et al.*, Eds., ed: WILEY-VCH, 2010, pp. 7-18.

[9] A. Mizuno, "Destruction of biological particles using non-thermal plasma," *Journal of Clinical Biochemistry and Nutrition,* vol. 60, pp. 12-24, 2017.

[10] A. Mizuno and H. Yasuda, "Damages of Biological Components in Bacteria and Bacteriophages Exposed to Atmospheric Non-thermal Plasma," in *Plasma for Bio-Decontamination, Medicine and Food Security (NATO Science for Peace and Security Series A: Chemistry and Biology)*, Z. Machala, K. Hensel, and Y. Akishev, Eds., ed: Springer, 2012, pp. 79-92.

[11] A. KATATANI, H. HOSONO, H. MURATA, H. YAHATA, and A. MIZUNO, "Electrostatic Precipitator without Using Corona Discharge − State of Collected Particles on Pole-plates −," *Journal of Institute of Electrostatics Japan,* vol. 39, pp. 27-32, 2015.

[12] Y. KISANUKI, Y. MAKISHIMA, S. KATSUSHIMA, K. TAKASHIMA, and A. MIZUNO, "Study on the discharge electrode of an electrostatic precipitator," presented at the Proc. Annual meeting of Institute of Electrostatics Japan, 2015.

[13] A. Mizuno, "For further development of ESPs," presented at the International Conference on Electrostatic Precipitation, Wroclaw, Poland, 2016.

Barrier discharges and Pulsed Discharge Modelling

Anne Bourdon[1]
[1]*LPP, CNRS, UMR7648, Ecole Polytechnique, Route de Saclay, 91128 Palaiseau Cedex, France*

E-mail: anne.bourdon@lpp.polytechnique.fr

Recently, many experimental and numerical studies are carried out on atmospheric pressure plasma jets. These discharges are of particular interest for biomedical applications. It was shown by G. Naidis [1] and JP Boeuf [2] that AC driven of pulsed helium plasma jets are “guided streamers” propagating first in a dielectric tube and then in a helium flow mixing with air, before impacting a target. Many experiments have shown discharge conditions in which plasma jets are stable, repeatable, without branching. Therefore, these discharges offer a very interesting opportunity to better understand the fundamentals of atmospheric pressure discharges, compared to air streamer discharges.
In this talk, I will present some recent results on the fluid modeling of atmospheric pressure plasma jets and their interaction with different targets (metallic or dielectric). Particular interest will be put on the comparison with experiments. First, the influence of N_2 or O_2 admixtures in helium on the discharge structure in the dielectric tube will be presented. Comparisons with measurements of the discharge front propagation velocity in the tube will be shown [3]. Then, recent comparisons with time resolved measurements of the components of the electric field on two configurations will be presented. First, an electric probe is used to measure the electric field outside of the discharge. In this case, we show that the good/experiment modeling agreement outside of the discharge allows to use the simulations to know the electric field in regions where a probe can not be used. Second, we show a comparison of electric field measurements carried out by Mueller polarimetry on a dielectric target with electric fields derived from simulations. The comparison between experiments and simulations allows a better understanding of the interaction of a plasma jet with a target, which is crucial for biomedical applications.

[1] G. Naidis, Journal of Physics D: Applied Physics, 43(40) 402001, 2010

[2] J.P. Bœuf, L. L. Yang and L. C. Pitchford, Journal of Physics D: Applied Physics, 46 (2013) 015201, 2012

[3] A. Bourdon, T. Darny, F. Pechereau, J.-M. Pouvesle, P. Viegas, S. Iséni and E. Robert, Plasma Sources Science and Technology 25, 035002, 2016

Chemical Probes and Plasma Synthesis

A. Wright[1,2], A. Shaw[1], F. Montazersadgh[1], M. Shaban[1], H. Bandulasena[2], B.R. Buckley[3], F. Iza[1]
[1]*Wolfson School of Mechanical, Electrical and Manufacturing Engineering*
[2]*School of Aeronautical and Automotive, Chemical and Materials Engineering*
[3]*Department of Chemistry, School of Science*
Loughborough University, UK

E-mail: f.iza@lboro.ac.uk

In recent years, advances in the generation of nonthermal gas plasmas at atmospheric pressure and their interaction with liquids have revolutionized the field of plasmas, opening up a host of new applications in biology, medicine, food and agriculture. [1,2] These plasmas have the potential to provide novel solutions to some of the most important societal challenges of today, including the growing threat of antimicrobial resistance[3] and the need to sustainably increase the productivity of agricultural land to double crop production by 2050. [4] In these emerging applications, plasmas are brought in contact with liquids (e.g. body fluids, water and organic solvents) but our current understanding of the plasma-liquid interaction and the transport of reactive species from the gas to the liquid phase remain very limited. Not only they entail complex plasma and fluid dynamics (see Fig 1), but the lack of readily-available detection methods to quantify reactive species in plasma-treated liquids further hinders progress.[5]

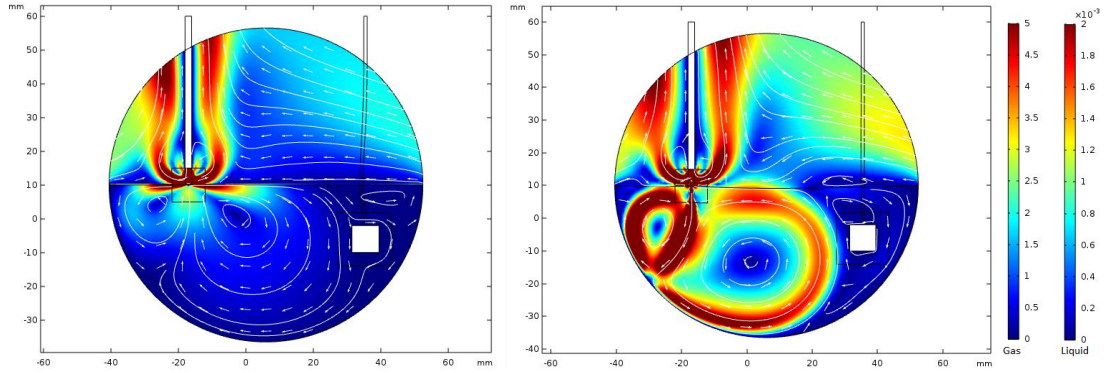

Fig. 1: Flow pattern induced by a DC helium plasma striking onto (a) water and (b) water + 1% PVA. Note the reversal of the flow in the liquid as well as the change in speed as a result of a small change in the liquid composition.

Unrelated to the developments in the plasma field, detection and quantification of reactive oxygen/nitrogen species (RONS) has been an area of intense interest for the biological and biochemistry communities due to the ubiquitous involvement of RONS in a wide range of biological processes. This has triggered the development of sensitive mechanisms by which to monitor and detect RONS and small molecule fluorescent probes have become increasingly applied.[6] This is due to their high levels of sensitivity, simplicity in terms of data collection, and high spatial resolution. Hence we believe small molecule fluorescent probes present a viable tool to be applied in the detection/quantification of the actual flux of ROS in nonthermal plasmas systems. However, despite the increasing number of fluorescent probes that are becoming commercially available, most (all) of them have not been developed for use in plasma

systems and therefore there is an urgent need for chemists and plasma physicists to work together to determine the suitability of existing probes for different plasma systems and where this is not the case, to development plasma-specific probes. We have recently used Pittsburgh Green, a selective fluorescent probe, for the quantification of the ozone dose delivered by a remote plasma system to a liquid sample[7] and compared its performance against electron paramagnetic resonance (EPR) spectroscopy.

Despite their complexity, non-thermal plasmas operating at atmospheric pressure also open the possibility of novel processing of liquids that were not possible in conventional vacuum systems due to vapour pressure limitations; and these can be used for novel chemical synthesis processes. For example, existing oxidation processes often generate large waste streams (e.g. the widely used oxidant oxone produces ~25 kg of waste per kg of oxygen transferred), whilst plasma-driven oxidation has the potential to completely eliminate waste streams (see Fig 3).

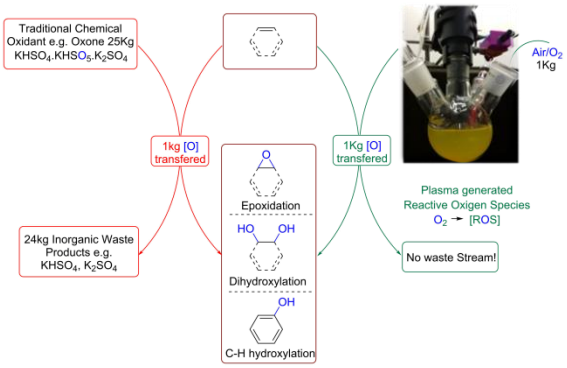

Fig 3: Schematic comparing traditional chemical oxidation and a plasma-enabled oxidation process.

In particular, we are interested in epoxidation, i.e. the formation of epoxides from alkenes. Epoxides are key building blocks in organic synthesis and important intermediates in the preparation of many natural products[8]. Conventionally, these are prepared by reacting alkenes with sacrificial mono-oxygen donors, such as peracids. Upon donating the atomic oxygen, the sacrificial donor then becomes a waste stream. Notwithstanding recent advances in the field of catalytic epoxidation, the ultimate scheme for synthesizing epoxides would be the direct reaction of alkenes with atomic oxygen as this would require no sacrificial material and produce no waste stream. It is well-known that oxygen containing plasmas can produce significant amounts of atomic oxygen and we can show that not only oxygen readily dissolves into aqueous solutions where it reacts with organic substrates,[9] but also that its reaction with an alkene produces epoxide.

[1] Lu, X et al. 2016 Phys. Rep. 630,1–84
[2] Park, DP et al. 2013 Curr. Appl. Phys. 13,S19-S29
[3] Abreu, AC et al. 2013 J Antimicrob. Chemother. 68,2718–2732
[4] Godfray, HCJ et al. 2010 Science 327,812–818
[5] Bruggeman, PJ et al. 2016 Plasma Sources Sci. Technol. 25,053002
[6] Wardman, P 2007 Free Radic. Biol. Med. 43 995–1022
[7] Wright, A 2018 Plasma Chem. Plasma Process. https://doi.org/10.1007/s11090-018-9923-1
[8] Page, PCB 2015 J. Org. Chem. 80, 16, 8036-8045
[9] Benedikt J 2018 Phys. Chem. Chem. Phys. 20 12037–42

Laser Induced Fluorescence in nanosecond pulsed discharges

G Dilecce[1,2], L M Martini[2,1] M Ceppeli[2], P Tosi[2,1]
[1]*P.Las.Mi Lab NANOTEC - CNR, via Amendola 122/D, Bari, ITALY*
[2] *Dipartimento di Fisica Università di Trento, via Sommarive 14, Povo, Trento, ITALY*

E-mail: giorgio.dilecce@cnr.it

Laser Induced Fluorescence (LIF) is nowadays a well established and widely used technique in gas discharges research, but still there is something left to understand and investigate about it. The need for further deepening of the knowledge about LIF basically comes from its application to atmospheric pressure discharges, that is to highly collisional conditions. LIF, intended as a way to measure the concentration of transient species, is in principle an absorption technique with a different observable, the fluorescence from an electronically excited state prepared by absorption of resonant laser light:

$$M + h\nu_{las} \rightarrow M^* \rightarrow M^{**}\_ + h\nu_{fluo} \qquad (1)$$

In a molecular case, M* can be a single ro-vibronic state. M**, the final state after radiative decay, may or may not be M itself. Collision processes between M* and the background gas, have an influence on the fluorescence outcome. Three collisional processes are possible: RET - rotational energy transfers; VET - vibrational energy transfers (often called vibrational relaxation); electronic quenching. When the frequency K of collision processes starts to be competitive, larger or much larger than the radiative rate A of M*, we enter a collisional regime in which the LIF outcome is more or less heavily influenced by these non-radiative losses/transfers.

Nanosecond repetitively pulsed (NRP) discharges, especially in a purely molecular gas like CO_2, represent a true challenge for LIF application. In the spark regime, a hot filament is suddenly created, with gas temperatures exceeding 2000 K, followed by an expansion and cooling in the tens of μs time scale. The collisional environment of LIF is then dramatically difficult to characterize. Both gas density and mixture composition rapidly change in time, affecting the LIF outcome in an unpredictable way.

In this talk, we shall first overview the basic principles of LIF in a collisional environment, through its application to the hydroxyl radical OH measurement in atmospheric pressure discharges [1], and review the actual knowledge of the rate coefficients for collision processes involving the OH(A, v=0,1) states (the actual M* of the LIF scheme (1)) [2]. We then introduce the concept of Collision Energy Transfer (CET) LIF, in which the focus is not more on the concentration of M (OH), but the M* fluorescence characteristics and how they are influenced by the background gas composition. By CET-LIF, and provided the relevant collision rate coefficients are known, it is possible to measure the background gas composition of simple mixtures. The application to He plasma jets (APPJ) impinging on liquid targets is recalled as a first application of the CET-LIF concept [3,4].

We shall then deal with LIF application to NRP discharges, both for OH concentration and kinetics measurements, in He-CO_2 discharges [5], and in pure CO_2 discharges in which CET-LIF has been applied, as a valuable tool even in harsh environmental conditions, for the

time-resolved measurement of the carbon dioxide dissociation degree [6]. The necessary knowledge of collision rate coefficients in conditions of high rotational non-equilibrium will be addressed, together with our most recent efforts devoted to their measurement.

References

[1] Dilecce G, Martini L M, Tosi P, Scotoni M and De Benedictis S 2015 Plasma Sources Sci. Technol. **24** 034007
[2] Martini L M, Gatti N, Dilecce G, Scotoni M and Tosi P 2017 J. Phys. D: Appl. Phys. **50** 114003
[3] Riés D, Dilecce G, Robert E, Ambrico P F, Dozias S and Pouvesle J M 2014 J. Phys D: Appl. Phys. **47** 275401
[4] Martini L M, Maranzana A, Tonachini G, Bortolotti G, Scapinello M, Scotoni M, Guella G, Dilecce G and Tosi P 2017 Plasma Process Polym. **14** e1600254
[5] Martini L M, Gatti N, Dilecce G, Scotoni M and Tosi P 2018 Plasma Phys. Controlled Fusion **60** 014016
[6] Martini L, Lovascio S, Dilecce G and Tosi P 2018 Plasma Chem Plasma Process **38** 707–718

Pattern Formation in Dielectric Barrier Discharge

Lifang Dong[1], Fucheng Liu[1], Weili Fan[1], Yuyang Pan[2]
[1]*College of Physics Science and Technology, Hebei University, Baoding 071002, China*
[2]*College of Quality and Technical Supervision, Hebei University, Baoding 071002, China*

E-mail: donglfhbu@163.com

Pattern formation is a self-organized phenomenon in nonlinear systems, which not only can be widely observed in natural systems such as animal coat markings, cloud formations and so on, but also can be studied in laboratory systems including thermal convection, nonlinear optics, chemical reactions, gas discharge, and so on. It is believed that the study of the pattern formation in gas discharge would advance the nonlinear science and plasma physics. Besides, there are plenty of potential applications about pattern formation, such as the plasma photonic crystal, the localized material growth, and so on.

There are two water-electrodes in the experimental setup sealed with glass plates. A metallic ring is immersed in each container and connected to a sinusoidal ac power supply. A glass frame is clamped between the two parallel glass plates, serving as a lateral boundary. The whole cell is placed in a big chamber, where the gas parameters can be changed. An intensified charge-coupled device (ICCD) camera (HSFC pro) is applied to record frames from the end view of the electrodes. The camera has three similar, intensified photographing channels. An optical beam splitter is placed between the input lens and the intensified channels. An input beam is split into three similar beams by the beam splitter and then received by each intensified channel. Through the computer-controlled software, the exposure time of each channel can be changed, and the delay times between channels can also be set to snap frames at different times.

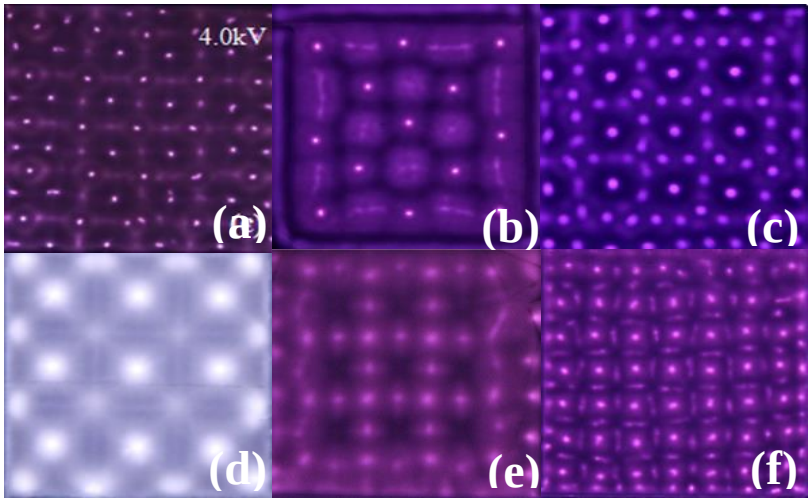

Figure.1 Some square superlattice pattern. (a) White-eye square superlattice pattern (b) Cluster square superlattice pattern, U = 3.08 kV, d = 4.2 mm, p = 30 kPa (c) White-eye square grid state pattern (d) Dot-line square super-lattice pattern with surface discharge, U = 2.68 kV, d = 4 mm, p = 40 kPa (e) Square superlattice pattern with discharge, U = 4.02 kV, d = 4.1 mm, p = 25 kPa (f) Antisymmetric stretching-vibration square superlattice pattern, U = 4.00 kV, d = 3.6 mm, p = 29 kPa

With this setup, about 50 types of patterns have been observed for the first time, some square superlattice patterns have been illustrated in Figure 1. By using high speed cameras it is found that the pattern in dielectric barrier discharge is a spatial-temporal pattern. Usually it is an interleaving of several sublattices, which discharge at different time.

These results should greatly advance the science of pattern formation and plasma physics

Processing of solid and liquid materials by atmospheric-pressure surface DBD-based jet

Milan Šimek
Institute of Plasma Physics of the Czech Academy of Sciences,
Za Slovankou 3, 18200 Prague, Czech Republic

E-mail: author.first@e-mail.address (Times New Roman, 12 pt)

Most of the non-LTE atmospheric pressure plasma jets, which are currently investigated for novel applications, are based on electrode configurations promoting generation of active plasma region in the volume of working gas. However, as in the case of volume discharges, highly reactive environment produced by atmospheric-pressure surface dielectric barrier discharges (SDBDs) can be used for pollution control, sterilization, ozone generation and surface processing/modification.

Recently, we have proposed and developed a concept of a surface DBD-based jet for processing solid and liquid materials. The electrode geometry is formed by a pair of concentric ring electrodes. Smaller discharge exposed high-voltage electrode is deposited on the surface of MACOR® glass-ceramic disk with a hole drilled in its centre. Grounded back electrode is embedded inside the disk and separated from the powered electrode by approximately 0.5 mm thick dielectric layer. The dielectric surface with powered electrode is closed inside cylindrical chamber containing two tangential gas inlets and one quartz window. Working gas is injected symmetrically through the two tangential inlets. Resulting whirlwind influences microdischarges propagating on the ceramic surface above the back electrode towards the central orifice (see figure 1). Induced vertex flow passes the discharge zone expelling discharge transients and products out of the chamber through an axial orifice in the form of the jet spinning around its axis [1].

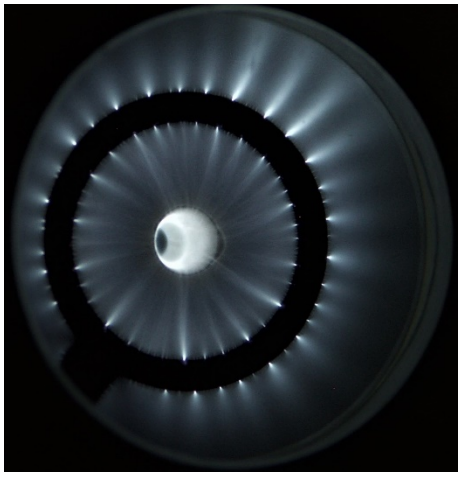

Fig. 1: Typical image of the surface DBD-based jet.

Compared with the concepts based on the volume discharge geometry, important advantages of the surface-based configuration include use of nearly arbitrary working gas composition, simple scale-up and serial operation of several jet units (stacked configuration). The discharge effluents can be easily utilized for the batch treatment of samples placed downstream. Furthermore, solid or even liquid samples can be directly injected into the spinning jet in order to interact with the discharge transients and products. Configurations suitable for both in-line and batch processing has been tested for various applications. Up to now, the most promising applications seem to be those related to the surface cleaning and activation, deposition of plasma polymers, organic farming, treatment and modification of nanocrystals/nanofibers, and activation of liquid water.

Concerning deposition of plasma polymers, the applicability of the SDBD-based jet for deposition of PEO-like plasma polymers in cavities was investigated using argon as carrier gas with di(ethylene) glycol vinyl ether used as a precursor [2]. The chemical composition of the films was found to be independent of the flowrate, duty cycle, and the distance from the jet orifice.

Concerning organic farming, one important issue is connected with the seed-borne microorganisms infecting or contaminating seeds either in the field or during storage. Seed-borne pathogens significantly affect quality of seeds and cause severe yield losses. Recently, it has been demonstrated that the SDBD is very efficient in reduction of microbial contamination and improvement of germination with a subsequent increase of vigor and growth of the derived seedlings [3]. Seeds were treated at various exposure conditions avoiding however direct contact of seeds with SDBD filaments. After the treatment, the reduction of overall microbial content, surface chemical modifications, and the response of seeds through seedling growth behavior were evidenced. Other running experiments include batch/in-line treatment of fruits, vine grapes and barley.

Feasibility of the in-line treatment of nanomaterials is actually under investigation using cellulose nanocrystals and nanofibers. The SDBD-based jet setup was modified to allow continuous delivery and passage of cellulose nanocrystals/nanofibers through the jet orifice with subsequent collection of treated samples in the downstream region. In-line treatment times of tens of seconds appear to be sufficient to modify surface of nanocellulose materials for further processing and use.

Acknowledgement
This work was supported by the Czech Science Foundation under project No. 15-04023S.

References
1. M.Šimek and V.Prukner, paper under preparation
2. I. Gordeev et al., Plasma Process. Polym. 13, 823, (2016)
3. P. F. Ambrico et al., J.Phys.D: Appl.Phys. 50, 305401 (2017)

COMPARISON OF ELECTRICAL BREKDOWNS PRODUCED BY HIGH VOLTAGE PULSES APPLIED TO ANODES MADE OF COPPER AND HIGHLY RESISTIVE COMPOSITE MATERIAL

Abdeldjalil Reguig[1], Karl Chatelain[1], Jason Damazo[2], Eddie Kwon[2], Deanna Lacoste[1]
[1]*King Abdullah University of Science and Technology, Clean Combustion Research Center, Thuwal 23955-6900, Saudi Arabia*
[2]*The Boeing Company, Research and Technology Department, Chicago, Illinois, USA*

E-mail: abdeldjalil.reguig@kaust.edu.sa

With the replacement of aluminum parts by composite materials, aircraft faces a change in ignition threat, due to the potential charge of dielectric surfaces by static electricity. The electrostatic charge accumulates through various processes including air friction during the flight, triboelectric charging as occurs while filling of the fuel tanks or lightning events. These phenomena tend to build up electrical potentials that can become high enough to cause electrical shock to persons or ignition of flammable gas mixtures or burnable surfaces [1]. According to the current regulations, for example by following the ARP-5416 from SAE Aerospace (Aircraft Lightning Test Methods), if the energy deposition into an electrical discharge is less than 200 μJ the ignition hazard is below the hazardous threshold for aviation fuel tanks. This energy threshold should not be reached if the stored electrical energy on the surface is below one millijoule [2]. A way to control the density of electrostatic charge is to use the electrical properties of materials, such as their resistivity, to tune the discharge characteristics. The electrical discharges generated when using such unconventional materials as electrodes are known as resistive barrier discharges (RBD). In 2002, Laroussi et al. [3] described RBD generated through porous or high-resistivity material. However, a quantitative understanding of RBD is not achieved yet, and the effect of various parameters such as the resistivity and capacitance of the material on the properties of the electrical discharges and the energy deposition in the gas are yet to be investigated. This is the purpose of the present study.

Experiments are carried out in a chamber filled with dry synthetic air at atmospheric pressure. The electrodes are in a pin-to-plane configuration, the pin being the anode, and the grounded electrode being a 3-cm diameter tungsten plate. The pins are made of wires of about 1.9-mm diameter. Three different wires are used: a copper wire of 50-mm length, a resisitive wire braid of 50-mm length and 6-kΩ resistance, and a resistive wire braid of 500-mm length and 58-kΩ resistance. The gap distance between the tip of the wires and the grounded plate is kept fixed for all the experiments at 2-mm. For each experiment, a square pulse of 500 ns is applied. It is generated by an Eagle Harbor Technologies pulse generator (model NSP-120-20-P).

The current and voltage waveforms are recorded using an oscilloscope (Tektronix, model DPO5204B, 2 GHz bandwidth) connected to dedicated probes. The current probe is a fast current transformer (Pearson, model 6585, 200 MHz bandwidth). The voltage across the inter-electrode gap is measured with a high voltage probe (Tektronix, model P6015A, 75 MHz bandwidth) at 2 mm before the extremity of the tested wire. In parallel to the electrical characterization, phase-locked imaging of the temporal evolution of the discharges is performed, using an Intensified-CCD camera (Princeton Instruments, PIMAX).

Typical voltage and current waveforms obtained with a resistive wire of 50-mm length are shown in Fig. 1. The corresponding deposited energy is determined by integrating the product of the voltage and current over the discharge duration. For an applied voltage of 15 kV, the breakdown occurs at 6.5 kV, then the voltage decreases to a plateau of about 1 kV. The maximal discharge current is 3 A and remains at about 2.5 A until the end of the pulse. The corresponding deposited energy is 2 mJ. Electrical characterization of the two other electrodes has been performed and the highest energy deposition (about 8 times higher than for the resistive wires) is obtained for the copper electrode, with a maximal current of 25 A.

Figure 2 illustrates phase-locked images of the discharge obtained with a resistive wire of 50-mm length. Two discharge phases can be observed: at the beginning of the voltage pulse (up to 22 ns), multiple filaments bridge the inter-electrode gap, while for longer times a single filament is promoted. This behavior has been observed for all configurations tested. The green line in Fig. 1 refers to the transition time from multiple to single filament phase. The average light emission from the discharges has been compared with the instantaneous power and a qualitative good correlation has been obtained for all the configurations tested. Finally, an explanation is proposed interpreting the significantly lower energy and light intensity of the RBD relative to the discharges obtained with the copper electrode.

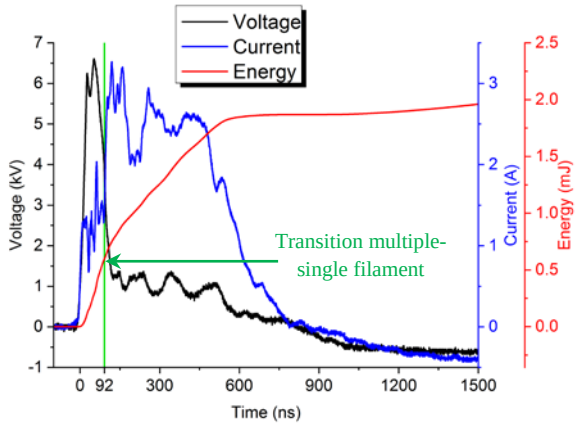

Fig. 1: Typical temporal evolution of voltage and current, and the corresponding deposited energy into the gas; length of the resistive wire L = 50 mm, V = 15 kV, pulse duration τ = 500 ns.

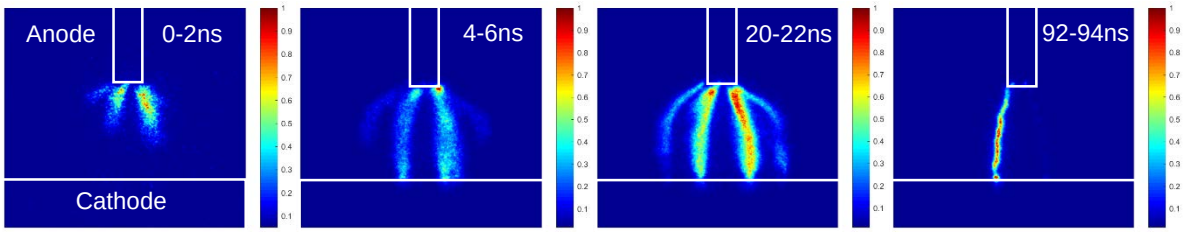

Fig. 2: Phase-locked images of the discharge propagation in the gap; length of the resistive wire L = 50 mm, pulse duration τ = 500 ns and V = 15 kV.

References

[1] W. C. Hall, "Electrostatic Dischargers for Aircraft," *J. Appl. Phy.*, vol. 18, pp. 759–765, Aug. 1947.

[2] J. Cierva, H. J. Gillis, and P. B. Wilson, "*Theoretical Analysis of Aircraft Electrostatic Discharge*," USAAVLABS Technical Report 65-53., U. S. Arm. Avi. Mat. Lab. Sci., Fort Eustis, Virginia, Aug. 1965.

[3] M. Laroussi, I. Alexeff, J. P. Richardson, and F. F. Dyer, "The Resistive Barrier Discharge," *IEEE Trans. Plasm. Sci.*, vol. 30, no. 1, pp. 158–159, Feb. 2002.

EXPERIMENTAL AND NUMERICAL STUDY OF MEMORY EFFECT IN HOMOGENEOUS ATMOSPHERIC PRESSURE DIELECTRIC BARRIER DISCHARGES IN N_2/O_2 AND N_2/NO MIXTURES

C. Tyl[1], X. Lin[1], M.C. Bouzidi[1], S. Dap[1], P. Ségur[1], N. Gherardi[1], N. Naudé[1]
[1]*LAPLACE, Université de Toulouse, CNRS, Toulouse, France*

E-mail: clemence.tyl@laplace.univ-tlse.fr

Dielectric Barrier Discharges (DBDs) are a robust way to obtain a non-equilibrium plasma at atmospheric pressure. Depending on various parameters, the discharge can operate in the classic filamentary mode, or in the homogeneous regime with a Townsend breakdown, which is more suitable for some applications such as thin film deposition [1]. For a Townsend breakdown to occur, a production source of seed electrons is necessary when the electric field is low enough to trap them in the gas volume, *i.e.* between two discharges. It leads to a memory effect, visible on the electrical characteristics of the discharge, with a discharge current jump between two successive discharges. In pure nitrogen, the literature suggests that the memory effect mainly comes from the collision of metastables $N_2(A^3\Sigma_u^+)$ on the charged dielectric surfaces, enhancing the secondary electron emission between two discharges [2]. In the presence of small concentrations of oxidizing gases, despite the metastable species quenching by oxygen, the memory effect increases [3]. This suggests that other phenomena occurring in the gas volume must be taken into account. The aim of this work is to adopt an experimental and a numerical approach to study the influence of oxidizing gas on the memory effect in the gas bulk and on the surfaces, by correlating optical an electrical measurements with a 1D numerical model.

The experimental set-up has already been described in a previous publication [4]. The discharge is performed with a plane-to plane DBD configuration, with two 635µm alumina plates metallized backside on a $3\times3cm^2$ square, with a 1 or 2mm gas gap, in N_2/NO and N_2/O_2 gas mixtures. Previously, Bouzidi *et al.* have highlighted the importance of the contribution of species in the gas volume to the memory effect by using the same experimental set-up but with one of the electrodes divided into 8 strips along the gas flow to measure the evolution of the electrical characteristics of the discharge as a function of position [5]. They observed that the current jump increases from the gas input to the gas output position, as well as the surface power density. It explains why the discharge becomes filamentary at the entrance whereas it remains stable at the gas output, for NO concentrations higher than 45ppm. Optical diagnostics have also been performed, with the measurement of the light intensity emitted by N_2-HIR, NOγ and $O(^1S)$-N_2 systems along the position of the discharge. These excited states are populated by $N_2(A^3\Sigma_u^+)$ metastables [6,7,8] and can give information on the concentrations of $N_2(A^3\Sigma_u^+)$, NO(A) and $O(^1S)$. The comparison of the emissions with the current jump and the surface power at the gas output position as a function of O_2 concentration shows that the current jump increase from 0 to 50ppm of O_2 is not related to $N_2(A^3\Sigma_u^+)$ because of its quenching by O_2 as N_2-HIR decreases. As NOγ and $O(^1S)$-N_2 emissions increase despite the decrease of the $N_2(A^3\Sigma_u^+)$, it indicates that the densities of NO and $O(^3P)$ increase. It suggests that this memory effect involves both $N_2(A^3\Sigma_u^+)$ and $O(^3P)$, and the associative ionization reaction between $N(^2P)$ and $O(^3P)$ could be a good candidate which can generate seed electrons in the gas volume.

If the memory effect in the presence of oxidizing species is related to phenomena in the gas bulk, it should increase by increasing the gas gap for the same power density, contrary to a memory effect related to surface mechanisms. Consequently, a comparison of the current jump in the presence of oxidizing gases for two different gas gaps have been performed. Figure 1(a) shows that the current jump is twice to ten times bigger at 2mm than with a gap of 1mm in N_2+O_2. However, some impurities remain in the gas even at 0 ppm of O_2 added, with oxidizing species influencing the memory effect. To overcome this issue, we use a 1D numerical model developed by C. Khamphan *et al.* [9] in pure nitrogen with the possibility to produce secondary electrons by $N_2(A^3\Sigma_u^+)$ collisions on the dielectric surfaces. Figure 1(b) shows that the metastables flow on the dielectrics is the same for gas gaps of 1 and 2mm before the breakdown, suggesting that the secondary electron emission due to the metastable species collision on the dielectrics does not depend on the gas gap. Consequently, the increase of the current jump with the gas gap in the presence of oxidizing specie is due to a memory effect arising in the gas volume involving oxidizing species.

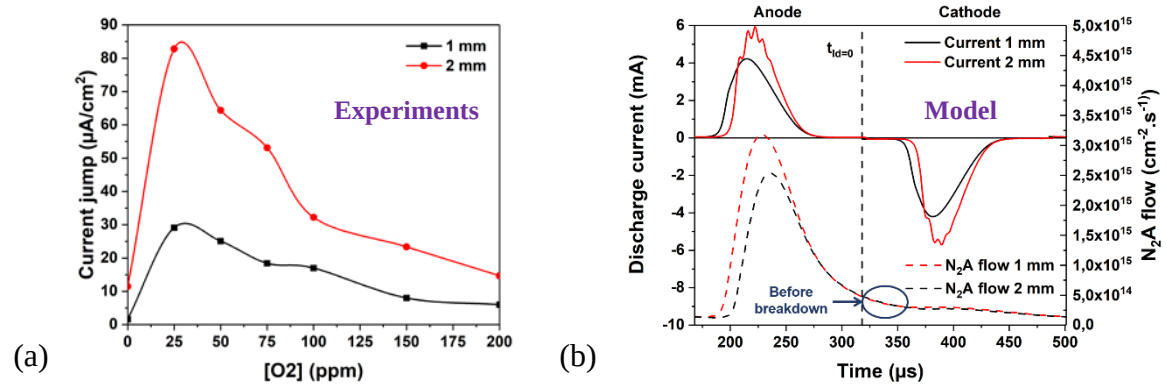

Fig. 1: **(a)** Current jump comparison in N_2+O_2 from the experiments and **(b)** comparison of the $N_2(A^3\Sigma_u^+)$ flow on one dielectric surface and the discharge current in the model in N_2, at 1 and 2mm (f=3kHz, P_{vol}=5W/cm^3)

The observation of the electrical and optical characteristics of the discharge in N_2 with oxidizing species and its comparison for different gas gaps and with a 1D model in pure nitrogen suggests that the memory effect in the gas volume is predominant compared to the memory effect related to the dielectric surfaces. The associative ionization reaction could explain the observed behavior. However, absolute measurements of the involved species such as O(^{3}P) and further modelling including oxidizing species are required to confirm this hypothesis [10,11].

[1] R. Brandenburg, *Plasma Sources Sci. Technol.* **26(5)** (2017) 053001.
[2] F. Massines *et al.*, *Eur. Phys. J. Appl. Phys.* **47(2)** (2009) 22805.
[3] N. Naudé *et al.*, *Proc. of the 31th ICPIG* (2013) Granada, Spain
[4] N. Naudé *et al.*, *J. Phys. D: Appl. Phys.* **38(4)** (2005) 530-538.
[5] M.C. Bouzidi *et al.*, *Proc. of HAKONE XIV* (2014) Zinnowitz, Germany
[6] I.A. Kossyi *et al.*, *Plasma Sources Sci. Technol.* **1(3)** (1992) 207-220
[7] M. Simek *et al.*, *J. Phys. D: Appl. Phys.* **34(21)** (2001) 3185-3190
[8] B.F. Gordiets *et al.*, *IEEE Transactions on Plasma Sci.* **23(4)** (1995) 750-768
[9] C. Khamphan *et al.*, *Proc. of the 16th Int. Symp. on Plasma Chem.* (2003) Taormina, Italy
[10] X. Lin *et al.*, *Proc. of HAKONE XVI* (2018) Beijing, China
[11] S. Dap *et al.*, *Proc. of HAKONE XVI* (2018) Beijing, China

FORMATION OF RUNAWAY ELECTRONS PREIONIZED PULSED DIFFUSE DISCHARGE AT ELEVATED PRESSURE

Cheng Zhang[1, 2], Tao Shao[1, 2], Ruexue Wang[1], Ping Yan[1, 2],
[1] *Institute of Electrical Engineering, Chinese Academy of Sciences, Beijing 100190*
[2] *University of Chinese Academy of Sciences, Beijing 100039*

E-mail: zhangcheng@mail.iee.ac.cn

By using a small–curvature radius cathode and a flat anode, diffuse discharges sustained by high-voltage nanosecond pulses with short rise time could be achieved in atmospheric pressure air in point-to-plane or point-to-point gaps. The diffuse discharge in the gap is ignited by electrodes of small radius of curvature and bridge the electrodes by overlapped plasma channels, appearing large-area volume at elevated pressure. The mechanism of the diffuse discharge has attracted much attention. Researches has been found beams of high-energy electrons can be generated in the pulsed diffuse discharge.

Since 2008, the characteristics of pulsed diffuse discharge and the behavior of the high-energy electrons has been conducted to understand the formation of the pulsed diffuse discharge at elevated pressure. The high-energy electrons are investigated by collecting the high-energy electron beams and detecting the X-ray radiation. The experimental show that the electron beam current with a time resolution of ~100 ps occurs at the rising edge of the applied voltage in pulsed diffuse discharge, indicating the generation of the high-energy in the early stage of the streamer formation. The spectra of the electron beams reconstructed from attenuation in foils with different thicknesses shows that the high-energy electrons range from the 20 keV to 80 keV when the applied voltage is 105 kV. Furthermore, the X-ray radiation shows the highest X-rays density occurred in the diffuse discharge in repetitive pulse mode, then the spark discharge with a small air gap, and then the corona discharge with a large air gap. The X-rays density increases with the atom number of the anode foil, indicating the detected X-rays are bremsstrahlung between the dense plasma front and the anode foil.

The structure and dynamics of pulsed diffuse discharge are simulated by using two-dimensional fluid and fluid-EMCS model. The simulation results show that electron beam with initial energy of 20 keV result in a pulsed diffuse discharge while the 20 eV beam has negligible influence on the discharge evolution. To sum up, the high-energy electrons play essentially role on the formation of the pulsed diffuse discharge at atmospheric pressure.

Key words: Pulsed diffuse discharge; high-energy electrons; electron beam current; X-ray radiation
Project: National Natural Science Foundation of Chin under contracts 50707032, 51222701 and 51207154.

OBSERVATION OF REACTIVE OXYGEN SPECIES EMITTED BY PLASMA JETS USING KI-STARCH METHOD

Fumiaki Mitsugi[1], Toshiyuki Kawasaki[2]
[1]*Kumamoto University, 2-39-1 Kurokami Chuo-ku Kumamoto 860-8555, Japan*
[2]*Nishinippon Institute of Technology, 1-11 Aratsu Kandamachi Fukuoka 800-0394, Japan*

E-mail: mitsugi@cs.kumamoto-u.ac.jp

Irradiating reactive oxygen and nitrogen species in the form of atmospheric pressure plasma jets has been expected for microbe treatment, bacteria inactivation, protein destruction, wound healing, plasma medicine, cancer treatment, and plant's growth. When the plasma jets are used for the aforementioned applications, the distribution of ROS (reactive oxygen species) on the surface of liquid or gel targets and the movement of ROS inside liquid should be investigated to distinguish region where the plasma jets work effectively. KI-starch method, which uses a mixture of potassium iodide and starch, is available in the form of gel agar as well as liquid to visualize ROS. The KI-starch reagent changes its color from transparent to blue by reacting with oxidative species which have oxidation potential higher than 0.54 V. In this work, ROS emitted from plasma jets was visualized with the KI-starch method and obtained results were evaluated by other different techniques of particle image velocimetry and an optical wave microphone.

Figure 1 shows an experimental setup to visualize ROS emitted by plasma jets. The plasma jet device is composed of a glass tube and two electrodes. Pure He gas was supplied into the glass tube with a flow rate of 1 L/min. KI-starch liquid reagent was poured in a glass cup and the distance between the liquid surface and the glass tube was set at 10 mm.

Figure 2 shows a series of typical behavior of the colored reagent during plasma irradiation observed in the liquid reagent. Colored KI-starch reagent started to be observed below the plasma jets after plasma irradiation, falling down to the bottom of the cup. After that, a transparent circular hole appeared on the surface at the center of the colored KI-starch where the colored reagent was push away to outside by a plasma induced force. The circular hole disappeared when the plasma jet was turned off. However, it appeared again when plasma jet was turned on again. The behavior of KI-starch reagent strongly depended on the initial surface condition of the reagent before the irradiation of plasma jets.

References

[1] F. Mitsugi, T. Nakamiya, Y. Sonoda, and T. Kawasaki, "Time-resolved observation of plasma jets synchronized with fibered optical wave microphone measurement," IEEE Trans. Plasma Sci., vol. 44, pp. 2759-2765, 2016.

[2] F. Mitsugi, S. Kusumegi, T. Kawasaki, T. Nakamiya, and Y. Sonoda, "Detection of pressure waves emitted from plasma jets with fibered optical wave microphone in gas and liquid phases," IEEE Trans. Plasma Sci., vol. 44, pp. 3077-3082, 2016.

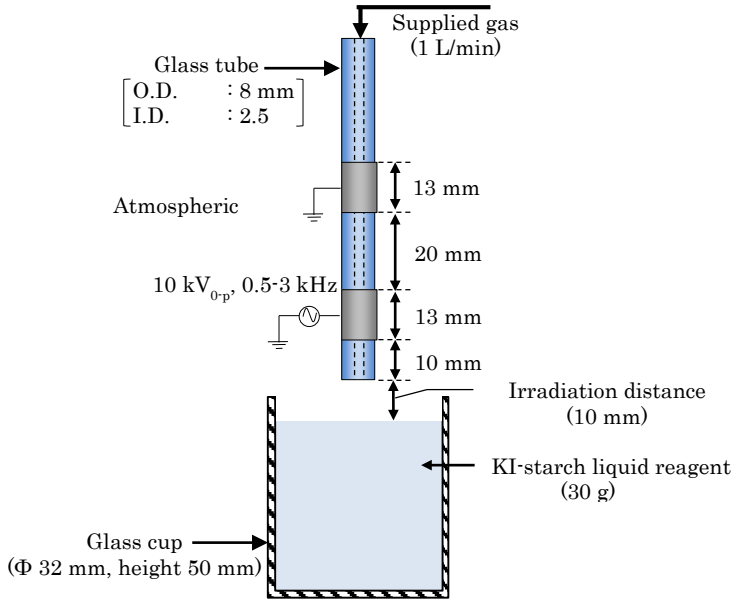

Fig. 1: Experimental setup of plasma jets and KI-starch reagent.

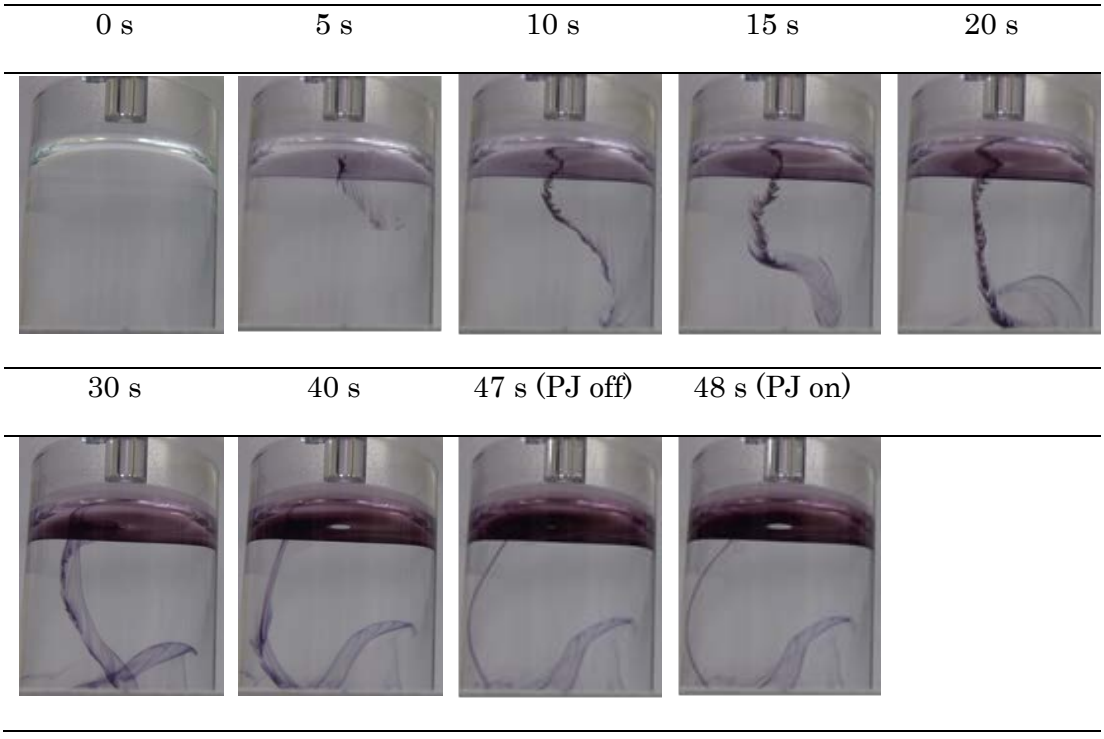

Fig. 2: Observation of colored KI-starch during He plasma jets irradiation (3 kHz, 10 kV, 1 L/min.).

FILAMENTARY AND DIFFUSE BARRIER DISCHARGES IN NOBLE GASES WITH ADMIXTURES OF MOLECULAR GASES

Kozlov K.V., Abramovskaia E.A.
Moscow State University, Department of Chemistry, Leninskie Gory 1/3, Moscow, Russia

E-mail: kozlov@kge.msu.ru

For the most of the surface plasma treatment technologies, the diffuse mode of the barrier discharges seems to be more desirable than the filamentary one. That is why the knowledge of the discharge operation parameters to control the transition between these modes is of great importance. Recently we reported the results of the plasma diagnostics of the barrier discharges in argon with admixtures of acetone [1]. These discharges were found to be diffuse only in the gaps wider than 4 mm and for a limited range of acetone concentration, the latter corresponding to the local minimum of the burning voltage. In the present paper, we propose a semi-empirical physical model for the barrier discharges in inert gases with small admixtures of molecular gases, that accounts for the experimental findings mentioned above, and that provides a simple method to prognosticate the possibility of the diffuse mode appearance for any chosen combination “noble gas + molecular gas (admixture)”.

The model is based on the assumption of the Townsend mechanism of initial (pre-breakdown) phase of the microdischarge development and of the validity of the Paschen law for the breakdown voltage. Certain additional assumptions concerning electron energy distribution functions in the gas mixtures under consideration should be made. Then qualitatively, our model is able to explain the experimentally observed dependencies of the burning voltage upon the content of molecular admixture, as well as a transition of the discharge to the diffuse mode within a certain concentration range of molecular gases.

In order to test our model and method, we carried out a series of experiments to investigate the barrier discharges in argon with the admixtures of the following organic compounds: methanol, ethanol, isopropanol, cyclohexanone, ethyl acetate, acetonitrile. For all these compounds excepting acetonitrile, the barrier discharges were found to demonstrate a continuous transition from the filamentary mode to the diffuse mode caused by the variation of the content of an admixture (see fig.1 as a typical example), similarly to the case of the admixtures of acetone [1]. In the mixtures of argon and acetonitrile, this effect was not observed, i.e. the discharge was filamentary in the entire range of concentrations.

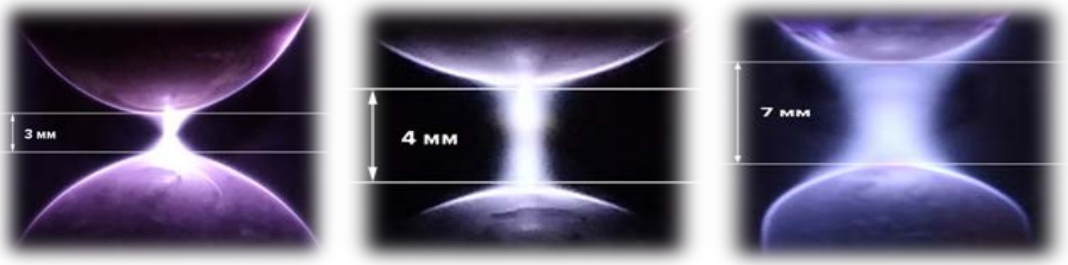

Fig. 1: Transition from the filamentary mode to the diffuse mode of the barrier discharges in argon with admixtures of ethanol. Concentrations of ethanol: 0.005% (left), 0.06% (center), 0.5% (right).

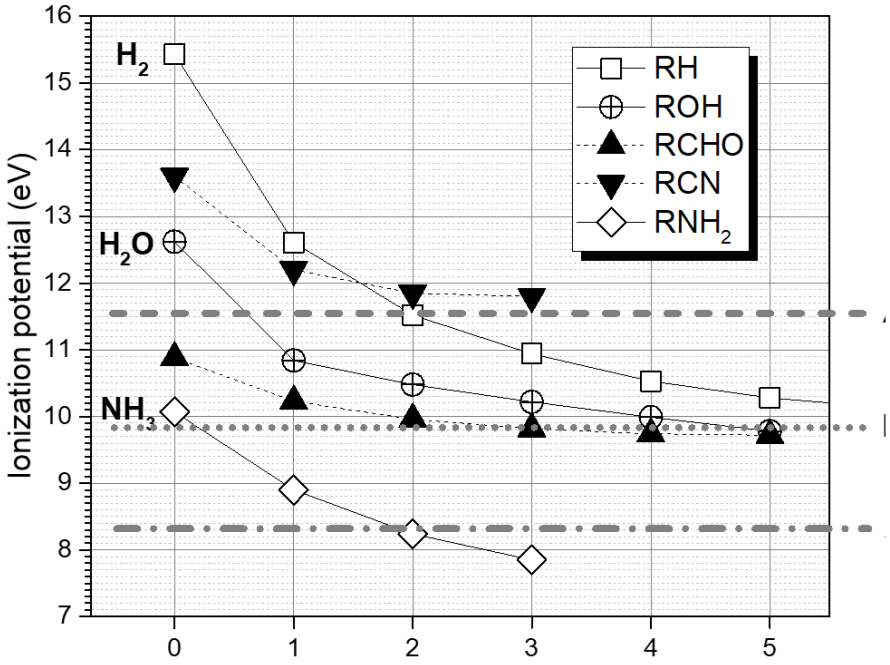

Fig. 2: Comparison of the ionization potentials of selected inorganic and organic compounds with the energies of the lowest metastable excited states of argon, krypton and xenon. See explanations in the text. All reference data were taken from the NIST databases [2].

This simple approach to the problem of the prognosis of the diffuse mode of barrier discharges in argon caused by small admixtures of a chosen molecular gas, can be applied to the barrier discharges in krypton and xenon (see fig.2). Unfortunately, barrier discharges in krypton and xenon are used relatively rarely and, as far as we know in the literature, there are no experimental data on the influence of molecular gases admixtures upon the discharge mode. As regards the barrier discharges in helium and neon, they are well-known to be diffuse in pure gases, and in the most of cases, admixtures of molecular gases result in their transition to the filamentary mode.

References.

1. Kozlov K.V., Abramovskaia E.A. Plasma diagnostics of the barrier discharges in the binary gas mixtures of argon and acetone. Proc. 15 Int. Symp. on High Pressure Low Temperature Plasma Chemistry (HAKONE-XV), Brno, Czech Republic, 2016, p.184-187.
2. https://www.nist.gov/data; https://webbook.nist.gov/chemistry/.

THE MEMORY EFFECT OF PULSED PLASMA JETS: TEMPORAL AND SPATIAL BEHAVIOR OF GUIDED STREAMERS IN N2, HE AND AR

M. van der Schans[1], J.H. Savenije[1], L.C. van Mouche[1], M. van Ommeren[1], R.G.J. Jongen[1], W.L. IJzerman[2] and S. Nijdam[1]
[1]*Eindhoven University of Technology, Eindhoven, The Netherlands*
[2]*Philips Lighting, Eindhoven, The Netherlands*

E-mail: m.van.der.schans@tue.nl

Atmospheric pressure plasma jets excited by kHz pulsed voltages typically generated so-called plasma bullets. Plasma bullets are guided streamer discharges that appear like a propagating bullet when short exposure images of the emission are taken. The most notable property of these discharges is that they are reproducible, i.e. the discharge produced by every voltage pulse is the same. This repeatable behavior is generally attributed to a memory effect. In this contribution we assess the reproducibility of guided streamer discharges produced in a pulsed plasma jet using N_2, He and Ar as feed gas flowing into open air, and we show how the memory effect develops during the first several discharges.

There are two aspects of the memory effect to be considered, the temporal memory and the spatial memory. The first one is related to the reproducibility of the moment of inception within the pulsed voltage cycle (the 'temporal memory'). To investigate the development of the temporal memory, a synchronized fast photomultiplier and high voltage probe are used to measure the emission and applied voltage for the first several discharges. This allows the determination of the moment of inception within the voltage pulse. It is found that the very first discharge can occur at any time during the voltage pulse. This likely happens whenever there is a background electron available at the right location that successfully develops into a streamer during the voltage pulse. The remnants of this first discharge can subsequently provide a source of electrons for the next discharge. Our measurements show that this process leads to a moment of inception that is reproducible to approximately within a nanosecond from the 2nd-3rd discharge onwards. This is the case for each of the three investigated feed gases

The second aspect of the memory effect is related to the reproducibility of the discharge path in space (the 'spatial memory'). To investigate the development of the spatial memory effect, the trajectories of the discharges during the first few voltage pulses are recorded. This is done by photographing the optical emission with a high frame-rate camera with image intensifier, which makes it possible to record the trajectories of consecutive individual discharges up to several kHz repetition rates. When using He as feed gas, the trajectories of all discharges are the same, with the exception of the very first one. The discharges travel along and are guided by the gas mixing layer where He mixes with ambient air. The length of the first discharge varies, depending on when during the voltage pulse the first discharge ignites.

In contrast, when N_2 is used as feed gas, a development phase of about 10 cycles is observed. In these first 10 discharges the trajectory of the guided streamer discharge grows along the axis of the jet until it reaches its final length and becomes reproducible. By numerical simulation of the gas flow, it is found that the length of a trajectory corresponds to the distance particles have travelled in the flow starting from the first discharge. This implies that in this case the guiding mechanism is not just related to the presence of the outflowing feed gas, but rather to the presence of discharge remnants that are transported in the gas flow.

The situation for Ar as feed gas depends on the applied voltage. For relatively low applied voltages, the discharges resemble those in the case of N_2: a guided streamer discharge propagates along the axis of the jet and it is observed that the length of the discharge develops during the first about 10 discharges. For higher applied voltage, the discharges in Ar start to propagate in the gas mixing layer, as in the case for He. However, whereas the discharges fill the entire gas mixing layer in the case of He, the discharges in Ar are branching streamer discharges that are confined in the gas mixing layer and are hence not reproducible in space.

Discharge breakdown studied under extreme conditions

Matej Klas[1], Štefan Matejčík[1], Marija Radmilovic[2], Branislav Radjenovic[2]
[1]*Department of Experimental Physics, Comenius University - Mlynská dolina F2, 84248 Bratislava, Slovakia*
[2]*Institute of Physics, University of Belgrade - Pregrevica 118, 11080 Zemun, Serbia*
E-mail: matej.klas@gmail.com

Experimentally as well as theoretically was found, that Paschen's law is no longer valid in compressed gases in electric field in the order of 10-20MV/m [1-3]. This failure of Paschen's law is associated with the onset of pre-breakdown current attributed to the field emission of electrons from the cathode.

In this study, we focused on the electrical characterization of breakdown phenomena in microdischarges at high gas pressures. The dependence of the electric breakdown potential on such properties as electrode separation, working gas, frequency and pressure (up to 50 bar) were studied. The breakdown voltages measurements were carried out using high pressure chamber equipped with stainless steel sphere to plane geometry electrodes with electrode spacing from 5-100µm.

It revealed that field emission effect has a different impact in different gases. While in compressed air, we have observed a decrease of breakdown voltages with decreasing electrode distance, in argon, at 10µm and pd of 7 Torr.cm we have observed an increase of breakdown voltage compare breakdown voltage at 100µm and the same value of pd. (Fig. 1) [4]. We assumed this behavior is due to a different onset of the field emission at the different gases, however, further analysis has to be done to unfold this behavior under different conditions.

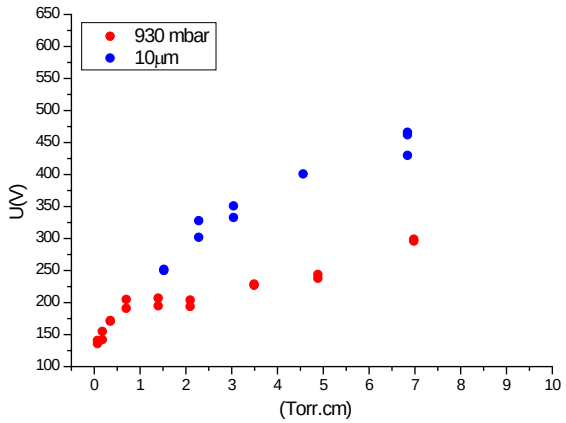

Fig. 1: DC Breakdown voltages for Ar at constant pressure of 930mbar and different electrode separation and for 10µm at pressure from 2 to 8bar.

Acknowledgements

This project has received funding from the European Union's Horizon 2020 research and innovation programme under grant agreement No. 692335. This work has been supported by

Development Agency Projects Nr. APVV-15-580, No. SK-SRB-2016-0035, and Ministry of Education and Science Republic of Serbia O171036 project.

[1] J.M. Meek, .I.D. Craggs,“Electrical Breakdown of Gases” Clarendon Press, Oxford, 1953
[2] G.Francis: Ionization Phenomena in Gases (Butterworths, London 1969
[3] P. Watson, H. Sharbaugh, “The Electric Strength of Nitrogen at Elevated Pressures and Small Gap Spacings”, Journal of Applied Physics, Volume 40, Issue 1, p.328-334, 1969
[4] M Klas, L Moravsky, Š Matejčik, M Zahoran, V Martišovitš, B Radjenović The breakdown voltage characteristics of compressed ambient air microdischarges from direct current to 10.2 MHz Plasma Sources Science and Technology 26 (5), 055023

DISTRIBUTION OF SURFACE POTENTIAL ON DIELECTRIC BARRIER UNDER DIFFERENT DISCHARGE MODES IN ATMOSPHERIC-PRESSURE AIR

Naoki Osawa, Yuto Mori, Naoki Hirose, Shun-ichi Motoyama,
Yoshio Yoshioka, Ryoichi Hanaoka
Kanazawa Institute of Technology, 7-1 Ohgigaoka Nonoichi Ishikawa, Japan

E-mail: n.osawa@neptune.kanazawa-it.ac.jp

1. Introduction

Diffuse dielectric barrier discharge (DBD) is promising technology for homogeneous surface treatment, ozone generation with less NOx emission from air, etc. So far, we succeeded in generating a diffuse DBD in atmospheric-pressure air using specific alumina barrier. From the analysis of discharge appearance, current waveform and gap voltage during discharge, we concluded that this diffuse DBD is a kind of atmospheric-pressure Townsend discharge (APTD). In order to elucidate decisive factors for generating APTD in air, we investigated the homogeneity of accumulated surface charge on alumina barrier and its temporal change by a plane type DBD device [1]. The result showed that surface potential distribution during APTD is homogeneous. However, since we could not control the points where streamer generates, the difference of surface potential distributions between filamentary DBD and APTD was not clear. In this work, we investigated discharge appearance and surface charge distribution of the discharge generated by a hemisphere rod electrode DBD device which can fix the streamer generation point.

2. Experimental setup

Fig. 1 shows an experimental setup. A hemisphere rod electrode type DBD device was set in atmospheric-pressure air. The radius of the hemisphere rod electrode tip was 5 mm. Alumina (Material code: A473 and A440, Kyocera) was used as dielectric material of the plane electrode. Gap length was set to 1 mm. The relative humidity was between 33.5% and 38.1%. AC high voltage of 50 Hz was applied to the DBD device by a high-voltage testing transformer and an AC power supply. The applied voltage was interrupted at various phases using a synchronous switching system. Photos of the discharge were taken by a high-speed camera with an image intensifier. The surface potential distribution on the alumina surface was measured by a non-contacting electrostatic voltmeter.

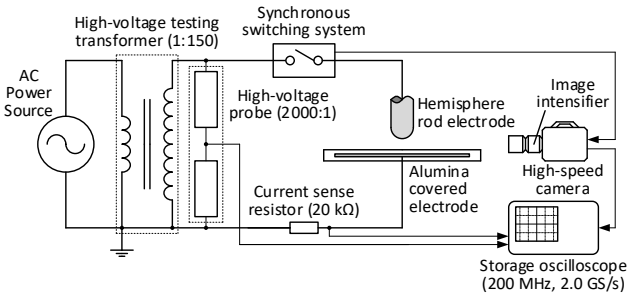

Fig. 1: Experimental setup

3. Results

Fig. 2 shows current waveform and discharge appearance of the hemisphere rod type DBD device. Voltage of 10 kV_p was applied to the hemisphere rod electrode. The current waveforms changed by barrier material. The current without pulses was recorded when A473 alumina barrier was a cathode. In this case, homogeneous light emission was recognized in the vicinity of the electrode tip. These features coincide with the characteristics of APTD in air [2]. On the other hand, streamer discharges generated in the vicinity of the electrode tip when the A440 alumina barrier became a cathode. From these observations, we confirmed that we succeeded in fixing the streamer generation place and that even with the hemisphere rod type DBD device, we can generate the APTD in air.

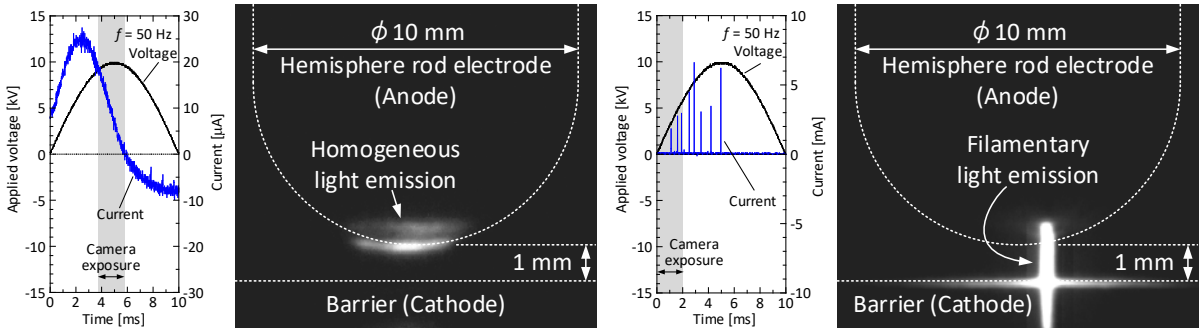

(a) A473 alumina barrier (APTD) (b) A440 alumina barrier (streamer discharge)

Fig. 2: Discharge appearance of hemisphere rod plane DBD on different alumina barrier plates.

Fig. 3 shows spatial distributions of surface potential on different alumina barriers. In both cases, surface potential under the hemisphere rod electrode increased with increasing applied voltage. At the same applied voltage, surface potential caused by APTD was higher and narrower than those caused by streamer discharge. These results suggested that to keep high surface potential on barrier is necessary for the generation of APTD.

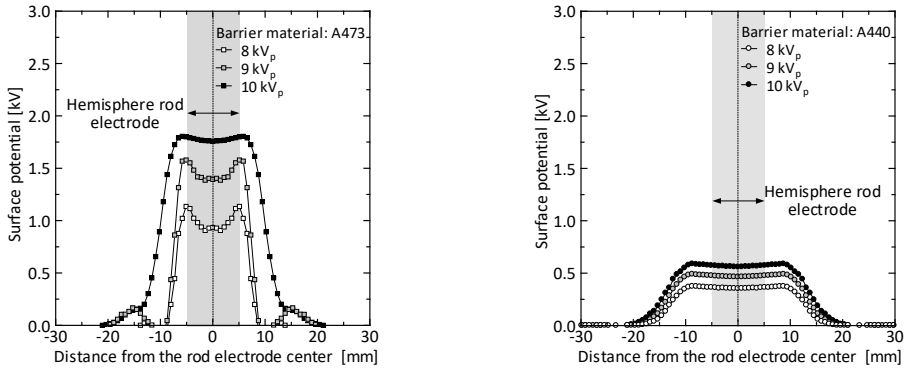

(a) A473 alumina barrier (APTD) (b) A440 alumina barrier (streamer discharge)

Fig. 3: Spatial distribution of surface potential on different alumina barrier plates.

We would like to thank KYOCERA Corporation for providing alumina barrier electrode and also thank Prof. Y. Kanamaru for providing the high-speed camera system.

Reference

[1] Y. Mori, M. Mori, N. Osawa, Y. Yoshioka, R. Hanaoka, *in Proc. of the ISPC 23, 2017*
[2] N. Osawa, Y. Yoshioka, IEEE Trans. Plasma Sci., **40**, 2 (2012)

The generation of aqueous hydrogen peroxide in DC plasma-liquid system with liquid as cathode

Qiang Chen, Xinyi He, Jiao Lin
[1] *Institute of Electromagnetics and Acoustics, Fujian Provincial Key Laboratory of Plasma and Magnetic Resonance, Department of Electronic Science, Xiamen University, Xiamen 361005, China*

E-mail: chenqiang@xmu.edu.cn

Atmospheric pressure discharge DC plasma is generated above a NaCl solution surface, and the solution acts as cathode. The formation pathways of aqueous hydrogen peroxide (H_2O_2) in this plasma-liquid system are investigated using a colorimetric method. Dimethyl sulfoxide is used as a hydroxyl (OH) radical scavenger to investigate the contribution of dissolved OH radicals to the aqueous H_2O_2. The results indicate that the aqueous H_2O_2 is mainly formed by the combination of the dissolved OH radicals and/or in situ liquid chemistry such as UV radiation, while the H_2O_2 formed in the gas phase has no contribution.

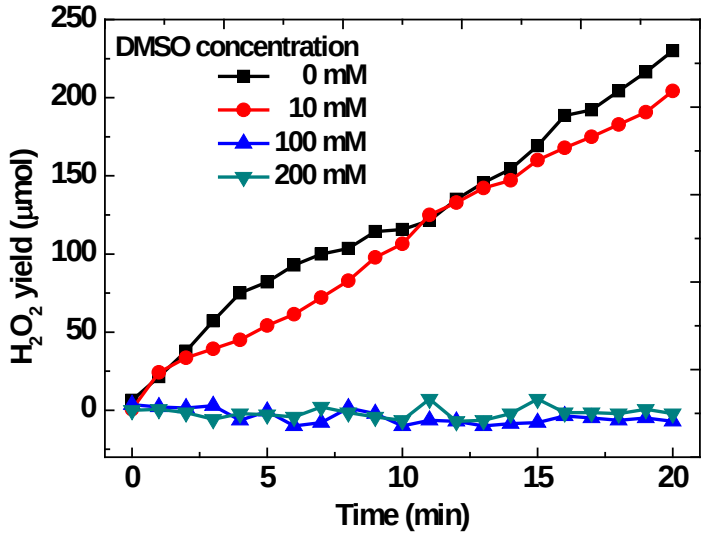

Fig. 1: Yields of aqueous hydrogen peroxide as a function of the plasma exposure time for the NaCl solutions with different DMSO concentrations of 0 mM, 10 mM, 100 mM, and 200 mM. The initial conductivity of treated NaCl solutions is 4800 μS cm^{-1}.

THE EFFECT OF O_2 ADMIXTURE ON THE ELECTRON DENSITY AND ELECTRON TEMPERATURE OF ARGON MICROWAVE DISCHARGES

S. Espinho[1,2], S. Hofmann[1], J. Palomares[3] and S. Nijdam[1]
[1]*Eindhoven University of Technology, Eindhoven, The Netherlands*
[2]*Instituto de Plasmas e Fusão Nuclear, Instituto Superior Técnico, Universidade de Lisboa, Lisboa, Portugal*
[3]*Dutch Institute for Fundamental Energy Research (DIFFER), Eindhoven, The Netherlands*

E-mail: s.m.espinho@tue.nl

The electron density and electron temperature of Ar-O_2 microwave discharges are studied as a function of the oxygen content in the mixture. The plasma source consists of a typical surface-wave-sustained discharge in a surfatron configuration [1]. The surfatron is connected to a microwave generator working at 2.45 GHz and with a maximum output of 500 W. The plasma is created inside a quartz tube with inner/outer radius of 3/4 mm, where the background gases are injected under laminar flow condition, using total gas flows of 100 or 200 sccm. A picture of a typical argon discharge with a small admixture of oxygen is shown in Fig. 1.

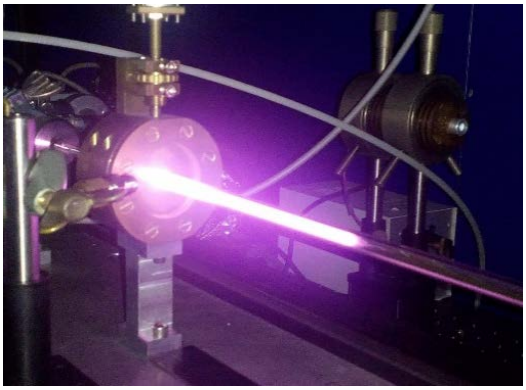

Fig. 1: Picture of a microwave driven surfatron discharge in argon with a small percentage of oxygen.

In order to determine the electron density and temperature, laser scattering measurements were performed using the triple grating spectrometer (TGS) available at the Eindhoven University of Technology [2]. This active spectroscopy method relies on the scattering of laser photons by the free plasma electrons, known as Thomson scattering [3, 4]. In the case of molecular gases, like mixtures of Ar–O_2, measured spectra include contributions not only from Thomson scattering but also from Raman scattering. The electron density and electron temperature are determined from the Thomson scattering contribution to the overall spectrum. A fitting procedure of the experimental Thomson scattering signal is performed to derive these parameters simultaneously, using the Matlab code by van Gessel *et al* [4]. Additionally, optical emission spectroscopy measurements are carried out as well in order to identify the main active species in the plasma.

The plasma electron density and electron temperature have been determined experimentally in Ar-O_2 discharges containing oxygen percentages up to 50% of the total gas flow, at a pressure of 38 mbar and applied microwave power of 100 W. A sharp drop in the plasma electron density is observed, with the values decreasing from 10^{20} m^{-3} to approximately 10^{18} m^{-3}, as the percentage of oxygen in the discharge is increased to 15% of the total gas flow. As the O_2 content is raised even more to 50%, the estimated electron density reaches approximately constant values of $1 – 2 \times 10^{18}$ m^{-3}. For small percentages of oxygen in the plasma, the electron temperature is estimated to be about 2 to 3 times higher than for a pure argon discharge in the same conditions ($T_e \sim 1$ eV). However, a decrease to about 0.5 eV is observed as the percentage of O_2 is raised to 50%. This is likely related to the higher ionization potential of argon compared to the one from molecular and atomic oxygen. As a result, higher electron temperatures are obtained as the Ar/O_2 ratio in the gas mixture increases. This in turn is expected to result in a higher dissociation degree of oxygen molecules, as predicted in previous theoretical investigations [5, 6].

For high O_2 contents, the drop in electron density and temperature, as well as the increase of the Raman scattering signal intensity, suggest that the power delivered to the plasma is mainly being channeled into the population of vibrational and rotational levels of O_2 molecules. It should be noted, however, that the position of the measurements relative to the plasma length influences the electron density and temperature results. In this sense, the measurements performed at higher O_2 percentages near the end of the plasma column result in lower electron density values. Furthermore, the pressure was varied from 15 to 38 mbar while keeping constant power (100 W) and both the electron density and temperature of discharges containing low percentages of oxygen were more sensitive to gas pressure variations.

As a final remark, the limitations of the diagnostics should be kept in mind for the interpretation of the results here presented. For O_2 percentages above 30%, the scattering spectra become Raman dominated, resulting in large uncertainties in the estimated electron densities and temperatures. The influence of photo-detached electrons from negative ions caused by the typical Thomson scattering laser fluences is also likely to contribute to the uncertainty in the measured electron densities for high oxygen percentages. Moreover, the detection limit of the system is reached for percentages of O_2 higher than 25%.

References

[1] Moisan M, Zakrzewski Z and Pantel R 1979 Journal of Physics D: Applied Physics 12, 219.
[2] van de Sande M J 2002 Laser scattering on low temperature - high resolution and stray light rejection, PhD Thesis Eindhoven, Technische Universiteit Eindhoven.
[3] Carbone E and Nijdam S 2015 Plasma Phys. Control. Fusion 57, 014026.
[4] van Gessel A F H, Carbone E A D, Bruggeman P J and van der Mullen J J A M 2012 Plasma Sources Sci. Technol. 21, 15003.
[5] Gudmundsson J T and Thorsteinsson E G 2007 Plasma Sources Sci. Technol. 16, 399–412.
[6] Kutasi K, Sá P A and Guerra V 2012 J. Phys. D: Appl. Phys. 45, 195205.

CORRELATION BETWEEN ELECTRICAL AND SPATIO-TEMPORAL DEVELOPMENT OF SINGLE FILAMENTS BETWEEN A METAL PIN AND A DIELECTRIC-COATED HEMISPHERIC ELECTRODE

Sina Jahanbakhsh[1], Hans Höft[1], Volker Brüser[1], and Ronny Brandenburg[1, 2]
[1]*INP Greifswald, Felix-Hausdorff-Str. 2, 17489 Greifswald, Germany*
[2]*Institute of Physics, University of Rostock, A.-Einstein-Str. 23-24, 18051 Rostock, Germany*

E-mail: sina.jahanbakhsh@inp-greifswald.de

An experimental investigation of microdischarges (MDs) in a one-sided dielectric barrier discharge (DBD) arrangement with a metal pin electrode is presented. This arrangement combines features of barrier and corona discharges. An electric field enhancement is obtained at the tip of the pin, and deposition of charge on the dielectric surface can limit the discharge duration, and avoid transition to thermal regime. Experimental investigation of single MD development in such arrangements are still rare. A better understanding of the discharge physics is a key to optimize these discharges for plasma chemical applications [1, 2]. A photo of the electrodes and the plasma is shown in Fig. 1a. A sinusoidal voltage with the frequency of 7.5 kHz is applied to the dielectric-coated hemisphere electrode (Al_2O_3, 2 mm curvature radius) while the metallic pin electrode (0.2 mm curvature radius) is grounded. The gap between the electrode tips is 1 mm. The diagnostic tools employed in this study are electrical probes (current probe: Tektronix CT1, voltage probe: Tektronix P6015A), which are connected to an oscilloscope (Tektronix DPO4104), and time-correlated single photon counting (TCSPC) with a temporal and spatial resolution of about 12 ps and 25 µm, respectively [3, 4]. The TCSPC measurements are conducted for the 0-0 transitions of the molecular bands of the second positive system (SPS) (wavelength: 337 nm, excitation energy: 11 eV) and first negative system (FNS) (wavelength: 391 nm, excitation energy: 19 eV) of nitrogen.

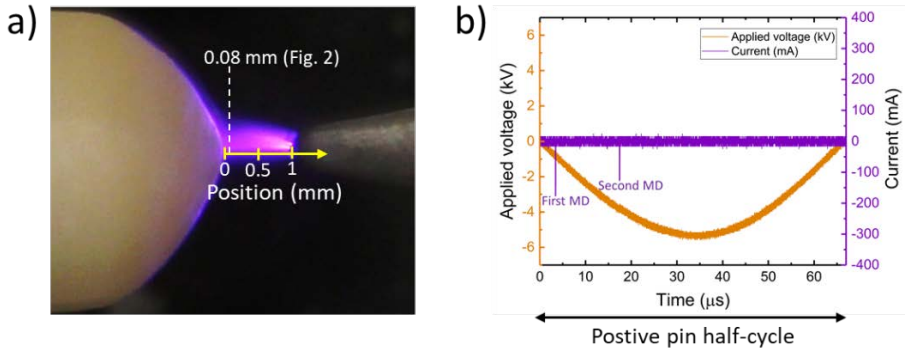

Fig. 1: a) Picture of the electrodes and plasma, b) a sample positive pin half-cycle with two current pulses

Here, only the results for the negative half-period of applied voltage (i.e metal pin acts as the anode) are discussed. As shown in Fig. 1b, two MDs appear in each applied voltage half-period. The MDs inception phase jitters within several microseconds, resulting in appearing as two groups of MDs. MD channels bridge the whole gap and spreads over the dielectric surface,

similar to conventional DBDs [4]. The first MDs changes the surface charge on the dielectric. Residual volume and surface charges influence the streamer propagation in the gap [5] and on the dielectric surface [6]. Similar effects are investigated here and describe differences between the first and second MDs.

The average current pulses of first and second group MDs are shown in Fig. 2. The current pulse of the first group has a fast increase with a sharp maximum. The current pulse of the second group also forms a first sharp, local maximum, but with smaller amplitude compared to the first group MDs. Then, current decreases for few nanoseconds, and increases again to reach a second broader, but global maximum. The average current pulses are correlated to the TCSPC measurements. Therefore, the starting time for the current pulse is set to 11 ns and normalized profiles of the TCSPS measurements at selected positions are compared.

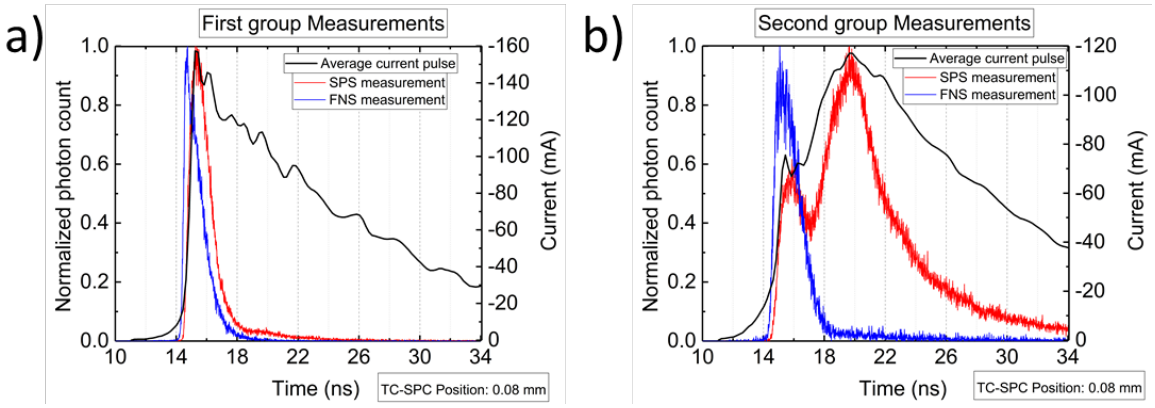

Fig. 2: Average current pulse, and SPS and FNS profiles at 0.08 mm for a) first, and b) second group MDs.

For the first group MDs (Fig. 2a) the SPS profile maximum at 0.08 mm (i.e. close to the dielectric surface which acts as cathode) coincides with the average current pulse maximum. However, the maximum of the FNS profile proceeds the first maximum of current pulse by approximately 400 ps. Fig. 2b shows the same trend for the first maximum of current and emission for second group MDs. On the other hand, the SPS signal follows the increases of the current pulse after 17 ns, while the FNS signal does not follow the current pulse in this part. The results give insights into the streamer head arrival on the dielectric surface and the formation of the bulk plasma in the following glow-like phase. This will be discussed in the contribution in detail.

References

[1] K.H. Becker, U. Kogelschatz, K.H. Schoenbach, R.J. Barker *Non-equilibrium air plasmas at atmospheric pressure* Institute of Physics Publishing, Bristol, Philadelphia, 2005
[2] Y. S. Akishev, A. V. Dem'yanov, V. B. Karal'nik, A. E. Monich, and N. I. Trushkin, *Plasma Physics Reports* **29** (2003) 1
[3] K.V. Kozlov, H.-E. Wagner, R. Brandenburg, P. Michel, *J. Phys. D: Appl. Phys.* **34** (2001) 21
[4] T Hoder, R. Brandenburg, R. Basner, K.-D. Weltmann, K. V. Kozlov, and H.-E. Wagner, *Journal of Physics D: Applied Physics* **43** (2010) 12
[5] H. Höft, M. M. Becker, and M. Kettlitz, *Plasma Sources Science and Technology* **27** (2018) 3
[6] T. Hoder, P. Synek, D. Chorvát, J. Ráhel, R. Brandenburg, and M. Černák, *Plasma Physics and Controlled Fusion* **59** (2017) 7

GENERATION AND CHARACTERIZATION OF THE WIRE-SHAPED PLASMA FROM FILAMENTARY ELECTRIC DISCHARGE IN ATOMSPHERIC PRSSURE AIR

Zhongshan Li, Chengdong Kong, Jinlong Gao and Andreas Ehn
Division of Combustion Physics, Lund University, S221 00 Lund, Sweden
E-mail: Zhongshan.li@forbrf.lth.se

In this presentation, we report the characterization of the wire-shape thin plasma channel generated in filamentary electric discharges in air [1]. With a proper design to restrict the peak current, electric discharge in air can be operated in the non-thermal regime by avoiding the conversion to thermal arc [2]. Shown in the figure are photos of a gliding arc discharge taken with different exposure times [3]. With a short exposure gate, a discharge channel can be found connecting the two electrodes. Temperature in the thin filament conduction channel was measured for the transitional, rotational and vibrational and electron motions [4], indicating a nonthermal condition. Both the glowing and spark discharge have been observed along the same plasma channel, which shows a lifetime of hundreds of μs [5]. A preliminary model [6] has been proposed to describe and promote this extraordinary property for novel applications.

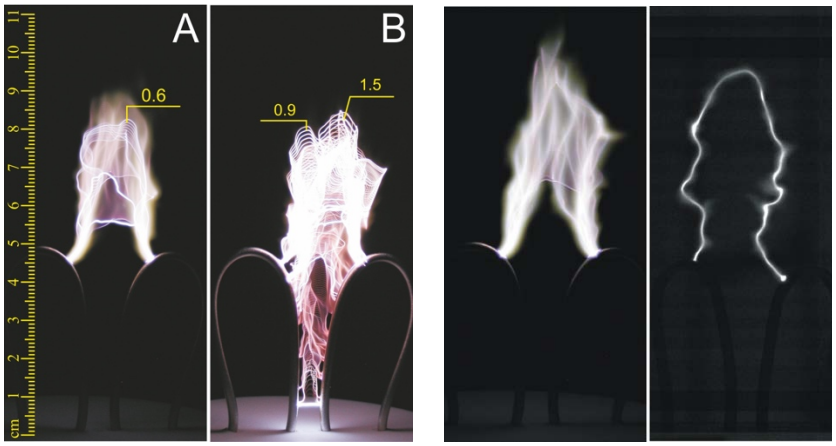

Fig. Photos of a nonthermal plasma of a gliding arc discharge generated in open air with different exposure times.

Reference

[1] Sun ZW, Zhu JJ, Li ZS, Alden M, Leipold F, Salewski M, et al. Optical diagnostics of a gliding arc. Opt Express 2013;21(5):6028-44.
[2] Zhu J, Gao J, Li Z, Ehn A, Aldén M, Larsson A, et al. Sustained diffusive alternating current gliding arc discharge in atmospheric pressure air. Applied Physics Letters 2014;105(23).
[3] Zhu J, Sun Z, Li Z, Ehn A, Aldén M, Salewski M, et al. Dynamics, OH distributions and UV emission of a gliding arc at various flow-rates investigated by optical measurements. Journal of Physics D: Applied Physics 2014;47(29).
[4] Zhu J, Ehn A, Gao J, Kong C, Alden M, Salewski M, et al. Translational, rotational, vibrational and electron temperatures of a gliding arc discharge. Opt Express 2017;25(17):20243-57.
[5] Zhu JJ, Gao JL, Ehn A, Alden M, Larsson A, Kusano Y, et al. Spatiotemporally resolved characteristics of a gliding arc discharge in a turbulent air flow at atmospheric pressure. Phys Plasmas 2017;24(1).
[6] Kong CD, Gao JL, Zhu JJ, Ehn A, Alden M, Li ZS. Characterization of an AC glow-type gliding arc discharge in atmospheric air with a current-voltage lumped model. Phys Plasmas 2017;24(9).

PLASMA-SURFACE INTERACTION: THE INFLUENCE OF THE SURFACE ON THE ELECTRON PROPERTIES AND ELECTRIC FIELDS IN A PLASMA JET

A Sobota[1], M Hofmans[1,2], E Slikboer[1,2,3], BLM Klarenaar[1], R Engeln[1], O Guaitella[2], E Garcia-Caurel[3]

[1]*Eindhoven University of Technology, The Netherlands*
[2]*LPP, CNRS, Ecole Polytechnique, UPMC, Universite Paris-Saclay, 91128 Palaiseau, France*
[3]*LPICM, CNRS, Ecole Polytechnique, Universite Paris-Saclay, 91128 Palaiseau, France*

E-mail: a.sobota@tue.nl

Atmospheric pressure non-thermal plasmas are relevant for biomedical applications, surface functionalization, plasma catalysis, atomic layer deposition. The restrictions on the plasmas can be rigorous – they have to be at room temperature and not transfer significant amount of charge to the target, while still providing a mixture of reactive species, charge, electric field. In those intended applications, plasmas interact with a surface. In ALD the aim is to design and create a surface layer, in medicine or catalysis it is to modify the target or to use the surface to promote a chemical reaction enabled by a plasma. In any case, the interaction of the plasma and the surface is complex and bi-directional – the surface often modifies plasma properties just as much as the plasma modifies the surface. The investigation of the plasma surface interaction is therefore crucial for the understanding of the processes that take place.

This work focuses on the effect the target has on the plasma with regards to the fundamental properties such as the electric field, charge density and electron temperature. The system under investigation is a He plasma jet operated under kHz excitation, in a regime where it produces exactly one ionization wave per voltage pulse. The discharge was characterized in its freely expanding mode as well as when interacting with targets of different electrical properties, from low-permittivity dielectrics such as glass, to water, to metal. The measurements were performed in the plasma plume, but also in a target when a high-permittivity dielectric ($\varepsilon_r = 56$) was used.

The results bring one of the first sets of data concerning the E field, electron density and electron temperature, which are relatable to each other through the fact that they were all obtained on the same discharge. The work shows not only that the presence of the target influences the plasma, but that the properties of the target determine the plasma parameters, also in the gas phase.

EFFECTS OF SURROUNDING GASES OF A PLASMA JET ON PLASMA-INDUCED LIQUID FLOWS

T. Kawasaki[1], M. Kawaguchi[2] , K. Nishida[2], Y. Hazama[2], F. Mitsugi[3]
[1]Nishinippon Institute of Technology, 1-11 Aratsu, Kanda-machi, Fukuoka 800-0394, Japan
[2]Nippon Bunri University, 1727 Ichigi, Oita 870-0397, Japan
[3]Kumamoto University, 2-39-1 Kurokami, Chuo-ku, Kumamoto 860-8555, Japan

E-mail: tkawasak@nishitech.ac.jp

The safe and effective use of plasma technology in applications such as plasma medicine, plasma agriculture, and water treatment requires understanding of the mechanisms for the transport of reactive species in the depth direction through a liquid layer. Several recent reports have highlighted the importance of plasma-induced liquid flows and mixing effects in various plasma-liquid systems. Interestingly, plasma-liquid interactions can enhance the specific plasma-induced effects in applications involving liquids. In previous studies, we observed interesting plasma-induced liquid flow linearly extending in the depth direction and discussed the relationship between the flow and the transport of reactive oxygen species in the liquid [1-3]. The plasma-induced liquid flow in the depth direction is considered an important parameter for the transport of reactive species in liquids. However, a detailed understanding of the mechanisms of these processes is currently unavailable.
In the present work, we found that the plasma-induced liquid flow linearly extending in the depth direction is remarkably influenced by the surrounding gas of a plasma jet. Understanding this phenomenon is speculated to be a key factor in elucidating of the mechanisms underlying the driving forces for the flow. We here report and discuss the effects of the surrounding gas on plasma-induced liquid flows.

Acknowledgment
This work was supported by JSPS KAKENHI Grant Number JP17K05100.

References

[1] T. Kawasaki, W. Eto, M. Hamada, Y. Wakabayashi, Y. Abe, and K. Kihara, Jpn. J. Appl. Phys. 54, 086201 (2015).
[2] T. Kawasaki, S. Kusumegi, A. Kudo, T. Sakanoshita, T. Tsurumaru, A. Sato, G. Uchida, K. Koga, and M. Shiratani, J. Appl. Phys. 119, 173301 (2016).
[3] T. Kawasaki, S. Kusumegi, A. Kudo, T. Sakanoshita, T. Tsurumaru, and A. Sato, IEEE Trans. Plasma Sci. 44, 3223 (2016).

DIAGNOSTICS OF LOCAL ELECTRICAL PARAMETERS IN ATMOSPHERIC PRESSURE DIELECTRIC BARRIER DISCHARGES

C. Tyl[1], H. Höft[2], X. Lin[1], S. Dap[1], M. Kettlitz[2], R. Brandenburg[2], N. Naudé[1]
[1]*LAPLACE, Université de Toulouse, CNRS, Toulouse, France*
[2]*Leibniz Institute for Plasma Science and Technology (INP Greifswald), Greifswald, Germany*

E-mail: clemence.tyl@laplace.univ-tlse.fr

Dielectric Barrier Discharges (DBDs) are a robust way to obtain a non-thermal plasma at atmospheric pressure and have many applications in the fields of surface treatment, sterilization, treatment of flue and toxic gases, etc. [1,2] Depending on various parameters such as gas nature or power supply conditions, the DBD can operate on the common filamentary mode or in the homogeneous regime [3], which is preferable for some applications such as thin-film deposition. To characterize the discharge, electrical measurements are widely used because of their simple implementation and the various information they provide: discharge current and voltage, power dissipated in the discharge, gas temperature etc. [4] The current measured is usually integrated over the whole discharge surface. However, even in the homogeneous mode, the discharge properties are not necessarily the same all over the discharge surface, because of the gas flow circulation, but also in case of material with a gradient of properties. The aim of this work is to study the local electrical parameters in a DBD in nitrogen with oxidizing gas addition.

In order to be able to measure the local currents in a DBD, a new electrical diagnostic tool has been developed. The experimental set-up has already been described in a previous publication [5]. The DBD is kept in an enclosed vessel to perform experiments in a well-controlled atmosphere. The reactor is pumped down to 10^{-3} mbar before being filled up at atmospheric pressure with nitrogen (99,999% purity) delivered by Air Liquide. The discharge cell consists of two 635 µm thick alumina plates (96% Al_2O_3, 115×70 mm^2, relative permittivity of 9.6) separated by a gap of 1 or 2 mm, which are metallized backside on a square of 3×3 cm^2. The innovative feature is that one of the electrodes is divided into 64 square zones of 3.4×3.4 mm^2, separated from each other by 400 µm. A gas flow of 2-4 slm is injected longitudinally, and a pumping system maintains the atmosphere at 1 bar. A low frequency sinusoidal voltage is applied to the primary winding of a transformer in series with a 4 Ω resistor, and the secondary of the transformer is connected to the discharge cell. The local discharge currents are measured through 64 shunt resistors (1.6 kΩ) in series with each segment on the ground side. The gas voltage and discharge current are calculated from an equivalent circuit as described in [6]. A data acquisition system with high enough sampling rate (4 MS/channel/s) has been developed. The overall behavior of the discharge is not affected as the space between each segment is very small. An electrostatic simulation using COMSOL© software shows that the electric potential is not affected by the division of the electrode. A first prototype with a division along the gas flow into 8 strips (3.4 mm×30 mm) has already been tested [7], demonstrating its feasibility.

The segmented electrode was first tested in nitrogen with addition of small concentrations of oxygen, with a gas gap of 2 mm. The overall behavior of the discharge is the same as in the classical configuration i.e. with a non-segmented electrode (total current, frequency and voltage domains of the homogeneous and filamentary regimes). The local measured current distribution as a function of time and position confirms that the discharge behavior is not the same over the whole electrode surface in the homogeneous regime, along the gas flow but also on the edges of the discharge. Figure 1 shows the surface power density as a function of position in nitrogen (a), N_2+50 ppm O_2 (b) and N_2+150 ppm O_2 (c). In each case, the power density increases from the gas input to the gas output and reaches a plateau. One explanation is that at the gas outlet position, the residence time of the gas particles is higher with more reactive species contributing to the memory effect and thus the breakdown voltage is lower, increasing the discharge power. The power density is lower along the edges and at the corners because of the discharge spreading. When oxygen is added to nitrogen, the discharge power is higher than in pure nitrogen as a small quantity of oxidizing gas improves the stability of the discharge and the memory effect leading to a homogeneous regime [8], and the power density maximum is reached closer to the gas input.

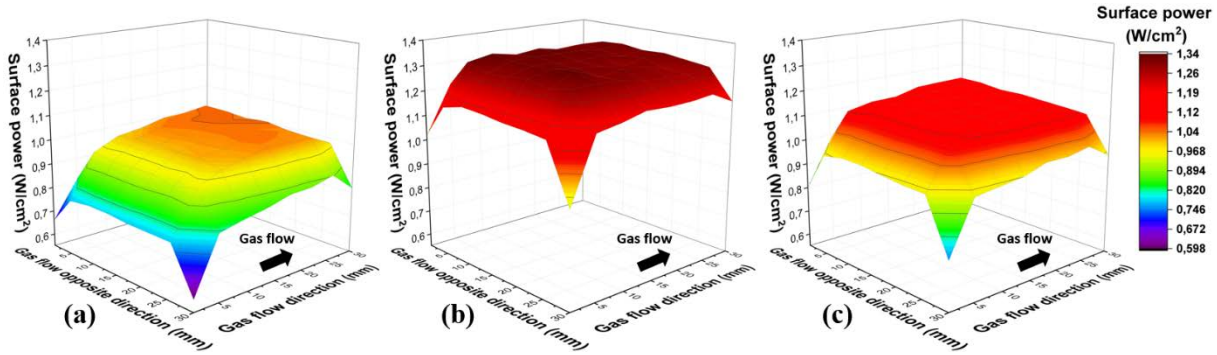

Fig. 1: Surface power as a function of position in the discharge in N_2 (a), N_2 + 50 ppm O_2 (b) and N_2 + 150 ppm O_2 (c), gap = 2 mm, f = 2 kHz, applied voltage = 16 kV_{pp}

The implementation of a new electrical diagnostic tool to measure the local currents in a dielectric barrier discharge allows to get more accurate mapping of the electrical parameters of the discharge. A correlation of this tool with optical diagnostics in space and time such as optical emission spectroscopy and ICCD camera imaging will help to better understand the influence of different parameters on the physics of homogeneous and filamentary discharges.

[1] U. Kogelschatz, *Plasma Chem. Plasma Process*. **23(1)** (2003) 1-46.
[2] F. Massines *et al*, *Plasma Process. Polym.* **9(11-12)** (2012) 1041–1073.
[3] R. Brandenburg, *Plasma Sources Sci. Technol.* **26(5)** (2017) 053001.
[4] F. Massines *et al*, *Eur. Phys. J. Appl. Phys.***47(2)** (2009) 22805.
[5] F. Massines *et al*, *Plasma Phys. Control. Fusion* **47(12B)** (2005) 577-588.
[6] N. Naudé *et al*, *J. Phys. D: Appl. Phys.* **38(4)** (2005) 530-538.
[7] N. Naudé *et al., Proc. of the 15th High Pressure Low Temp. Plasma Chemistry Symp.* (HAKONE XV) (2016) Brno, Czech Republic
[8] N. Naudé *et al., Proc. of the 31th Int. Conf. on Phenomena in Ionized Gases* (2013) Granada, Spain

Translational temperature measurement of a pin-to-pin discharge disturbed by a turbulent jet flow in atmospheric pressure air

Chengdong Kong[1], Andreas Ehn[1], Zhongshan Li[1], Marcus Aldén[1]
[1]*Division of Combustion Physics, Lund University, P.O. Box 118, S-221 00 Lund, Sweden*

E-mail: chengdong.kong@forbrf.lth.se

The plasma can be categorized into two-types, thermal and non-thermal plasma, depending on the difference of electronic, vibrational and translational temperatures. Detection of translational temperature (T_g) provides valuable input for the understanding of thermal properties of plasma. Here laser induced Rayleigh scattering thermometry was applied to visualize the T_g profiles across the plasma column of a pin-to-pin discharge in atmospheric pressure air. **Fig. 1** illustrates the experimental setup schematically. This discharge is driven by a 40 kHz AC power supply (Generator 9030 E, SOFTAL Electronic GmbH). In principle, the intensity of scattered light depends on the number density of molecules and their Rayleigh scattering cross sections in the probed volume. However, the plasma column has unknown gas compositions, which will induce systematic errors for temperature estimate. In order to overcome this issue, a quasi-equilibrium approximation model which assumes the chemical compositions of the plasma can be approximated by the chemical equilibrium compositions corresponding to an effective temperature of 4500K, was used to estimate the error from uncertainty of gas composition. The result indicates a maximum overestimate of temperature by 20% when the gas composition is assumed invariant. The underlying reason is mainly due to the dissociation of O_2 to atomic O in the plasma column. Furthermore, the T_g profiles at different flow rates were measured, as shown in **Fig. 2** and **Fig. 3**. With the flow rate increase, the area of hot zone shrinks and meanwhile the peak T_g value in the plasma column drops. It is possibly due to the decrease of residence time of gas in the plasma column.

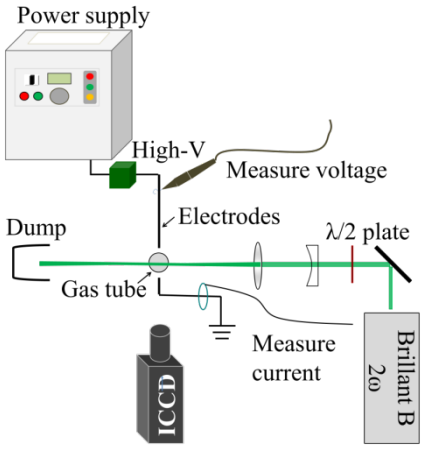

Fig. 1 schematics of the experimental setup

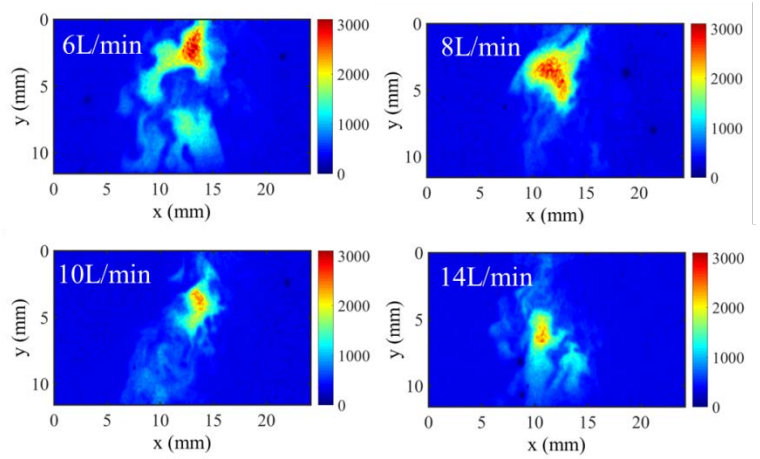

Fig. 2 Translational temperature profiles across the plasma column with different flow rates

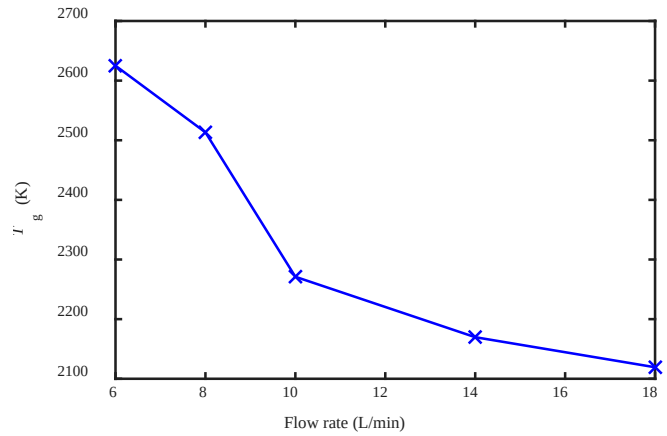

Fig. 3 Peak translational temperature across the plasma column (T_g) with respect to the flow rate.

ATMOSPHERIC PRESSURE TOWNSEND DISCHARGE: INFLUENCE OF BARRIER MATERIAL ON THE MEMORY EFFECT IN NITROGEN

Christopher Laurent, Clémence Tyl, Xi Lin, Simon Dap, Nicolas Gherardi, Nicolas Naudé
LAPLACE, Université de Toulouse, CNRS, Toulouse, France

E-mail: nicolas.naude@laplace.univ-tlse.fr

Dielectric Barrier Discharges (DBD) can be used for a lot of applications. The most promising among them concerns surface treatments like thin-film coating. Indeed, the use of atmospheric pressure plasma allows (i) to realize continuous treatment of large surface substrates, (ii) to reduce the equipment costs by avoiding the need for expensive pumping systems of conventional low-pressure plasma devices, and (iii) to use open systems [1]. However, depending on the gas, electrical parameters, and electrode configuration, these discharges can operate in the classical filamentary mode or in a homogeneous mode. The filamentary mode can be very restrictive for surface coatings. On the other hand, conditions to get a homogeneous DBD can also be restrictive. Homogeneous DBD at atmospheric pressure have been obtained in noble gases, nitrogen and air [2-4]. In air and nitrogen, the electrical field is quasi-uniform over the discharge gap, like in low-pressure Townsend discharge, and the obtained discharge is called Atmospheric Pressure Townsend Discharge (APTD) [2]. For a Townsend breakdown to occur, a production source of secondary electrons is necessary when the electric field is low. This effect is visible on the electrical characteristics (discharge current and voltages) [2]. The discharge current never reaches zero between two discharges. Hence, a current jump can be measured when the gas voltage polarity reverses. This current is due to seed electrons generated in between two discharges, when the field is low enough to “trap” them in the gas volume, and this is a clear signature of the memory effect from one discharge to the other. The importance of this memory effect is also pointed out by the evolution of the first discharges after ignition [2]. The first two discharges are different from the following ones showing that one DBD pulse depends on the previous one and that some discharges are necessary to reach the equilibrium. The first discharge is filamentary, the second one is a mix of a Townsend discharge and micro-discharges and the third one is a fully Townsend one. In nitrogen-based discharges the creation of seed electrons is correlated with the presence of $N_2(A^3\Sigma_u^+)$ metastable molecules created during the previous discharge and persisting between two discharges [5]. These seed electrons could come from secondary electron emission by $N_2(A^3\Sigma_u^+)$ impact on the dielectric surface [2] or from gas reactions like associative ionization [6].

However, these mechanisms cannot explain the APTD obtained in air or in nitrogen when the frequency is much lower than 1 kHz. In these conditions, experimental study shows that a memory effect is also present and that the discharge could be homogeneous with an *off time* up to 30 ms [7] *i.e.* for a time larger than the $N_2(A^3\Sigma_u^+)$ lifetime and also higher than the residence time of the gas in the discharge area [7-8]. A hypothesis is that the seed electrons can come from a spontaneous electron desorption [9]. This mechanism is often considered of minor importance [10]. However, in nitrogen at low frequency and in air it could be the major process

for the creation of seed electrons. This could explain why a homogeneous discharge in air is only obtained at low frequency.

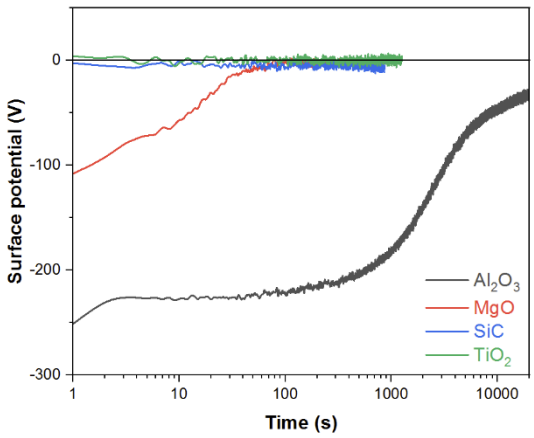

Fig. 1: Time evolution of the surface potential after a discharge when the material was on the anode for different barrier materials (Al_2O_3, SiC, MgO and TiO_2)

The aim of this work is to better understand the mechanism(s) that could be at the origin of the production of seed electrons in pure nitrogen at low frequency (from few Hz to 1 kHz) and in air. For this, we will compare the discharge behavior for different dielectric materials. We will use Al_2O_3 (ε_r=9.6-9.9, $\rho_S>10^{15}$ Ω/sq), MgO (ε_r=9-10), SiC (ε_r=113, $\rho_S=10^{10}$-2.10^{15} Ω/ sq) and TiO_2 (ε_r=140, $\rho_S>2.10^7$ Ω/ sq). For the SiC and TiO_2 cases only one electrode is covered whereas the second electrode is covered by alumina to obtain a barrier capacitance compatible with the obtaining of a homogeneous discharge. According to the first surface potential measurements (figure 1), the retention time of charges on the dielectric surfaces depends on the surface resistivity. The higher is the surface resistivity, the higher is the retention time. Thus, changing the surface resistivity should modify the creation of seed electrons and then the discharge behavior (*e.g.* homogeneity).

References

[1] Massines F *et al.*, *Plasma Processes and Polymers*, **9** (2012) 1041–1073
[2] Massines F *et al.*, *The European Physical Journal Applied Physics*, **47** (2009) 1–10
[3] Kanazawa S *et al.*, *Journal of Physics D: Applied Physics*, **21** (1988) 838–840
[4] Osawa N *et al.*, *IEEE Trans. Plasma Sci.*, **40** (2012) 2-8
[5] Naudé N *et al.*, in *Proc. Int. Conf. on Phenomena in Ionized Gases ICPIG*, 2013, Granada, Spain
[6] Bouzidi M *et al.*, in *Proc. Int. Symp. on High Pressure Low Temperature Plasma Chemistry (HAKONE)*, 2014, Zinnowitz, Germany
[7] Naudé N *et al.*, in *Proc. Int. Conf. on Phenomena in Ionized Gases (ICPIG)*, 2015, Iasi, Romania
[8] Dilecce G *et al.*, *Plasma Sources Sci.*, **16** (2007) 511-522
[9] Golubovskii Y B *et al.*, *J. Phys. D: Appl. Phys.*, **35** (2002) 751
[10] Brandenburg R *et al.*, *J. Phys. D: Appl. Phys.*, **38** (2005) 2187

NUMERICAL SIMULATIONS OF PERIOD-DOUBLING BIFURCATION AND CHAOS IN AN ATMOSPHERIC DIELECTRIC BARRIER DISCHARGE WITH COAXIAL ELECTRODES

Fucheng Liu, Zhixiang Zhou, Xue Guo, Yafeng He and Xiaofei Wang

College of Physics Science and Technology, Hebei University, Baoding 071002, China

E-mail: hdlfc@hbu.cn

As a typical nonlinear dynamical system with a large number of degree, dielectric barrier discharges (DBDs) can exhibit a variety of nonlinear phenomenon, such as self oscillation, bifurcation, chaos, self-organization etc. These nonlinear dynamics play a profound role in the transport of charged particles and energy and hence change the plasma structures and affect the stabilities of the discharges. Additionally, they are harmful and should be avoided for many applications. Therefore, it is essential to have a better understanding of these nonlinear phenomena not only from a fundamental but also from a practical point of view.

In the past ten years, different types of nonlinear phenomena have been reported in DBDs at atmospheric pressure. However, most of the studies of nonlinear behaviors concentrated on DBDs with plane-parallel electrode configurations. The effects of electrode curvature on DBDs have been unexplored, and this is of the current study.

A self-consistent one-dimensional fluid model consisting of electrons and ions is applied to a cylindrical DBD reactor consisting of two coaxial electrodes with a 1 mm thick dielectric on the inner side of the outer electrode. A sine shaped high voltage with 1.5 kV amplitude and 20 kHz frequency is applied on the inner electrode and the outer electrode is grounded. In order to investigate the effects on electrode curvature, the gas gap width is kept at 5mm while the radius of the inner bare electrode R can be varied ranging from 0.2mm to 100mm.

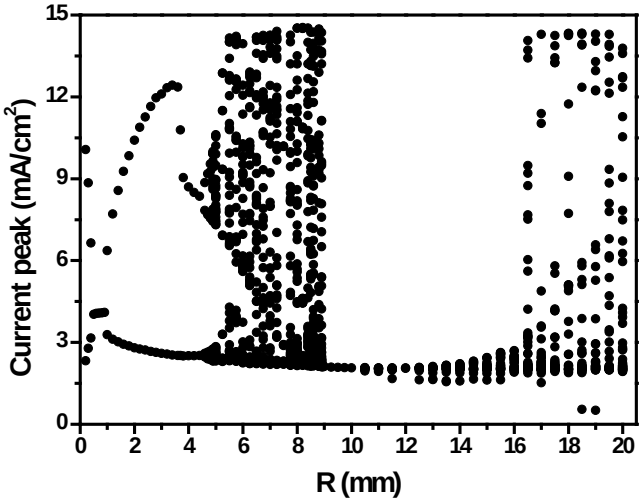

Fig. 1: Bifurcation diagram of positive current peak value as a function of the electrode radius R.

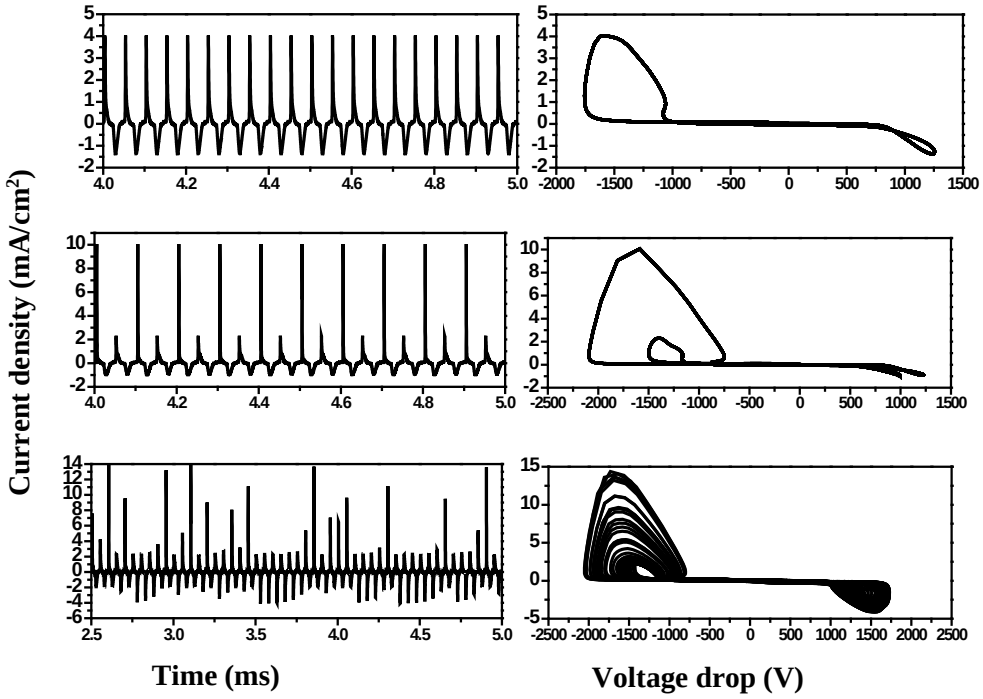

Fig. 2: Time evolutions of current densities (left) and their corresponding phase plots (right) at different electrode radius R, 0.5mm (upper), 0.2mm (middle), 8.9mm (lower).

Figure1 shows the bifurcation diagram from period-1 discharge to chaos with the increasing of electrode radius R. When the electrode radius *R* is 0.5mm, the discharge operates in a typical asymmetric discharge mode, as shown in Fig. 2(a). In this mode, there is only one discharge current pulse in each half cycle of the applied voltage. The amplitude of the current pulse at the positive half cycle is much larger than that at the negative half cycle. Different from the parallel-plate configuration, the asymmetry of the discharge current originates from the asymmetric electrode configuration. It is found that the period-1 discharge mode exists only in a very narrow range. It becomes unstable and transits into a period-2 discharge mode when the electrode radius is increased or decreased. Further increasing the electrode radius, the discharge transits into period-4 and period-8, and finally into a chaotic discharge, as shown in fig.2(c).The results indicate that period- doubling bifurcation is an intrinsic feature of the plasmas produced in the atmospheric pressure glow discharge with coaxial electrodes.

Acknowledgements

This work was supported by the National Natural Science Foundation of China (Grant Nos. 11405042), Hebei Natural Science Fund (Grant Nos. A2017201099), the Research Foundation of Education Bureau of Hebei Province, China (Grant No. ZD2015025), and China Postdoctoral Science Foundation (Grant No. 2015M570232).

Simulation of Atmospheric-Pressure Glow Discharge Electrolysis for Silver Nanoparticle Synthesis in Silver Nitrate Solution

Fumiyoshi Tochikubo[1], Yusuke Nakagawa[1], Satoshi Uchida[1]
[1]*Department of Electrical Engineering and Computer Science, Tokyo Metropolitan University, 1-1, Minami-Osawa, Hachioji, Tokyo 192-0397, Japan*

E-mail: tochi@tmu.ac.jp

Recently, atmospheric-pressure dc glow discharge with liquid electrode is applied for material processing in liquid, such as metallic nanoparticles (NPs) synthesis [1, 2]. This system is considered as glow discharge electrolysis (GDE) [3] at atmospheric pressure. Liquid-phase reactions in GDE will be different from those in conventional electrolysis since electrons/ions/radicals from the glow discharge induce the primary liquid-phase reaction at plasma-liquid interface. In GDE with $AgNO_3$ solution, Ag NPs will be synthesized in the following process; electrons from the glow discharge are hydrated at liquid surface, the hydrated electrons reduce Ag^+ to form Ag, nucleation is induced by the oversaturated Ag atoms in the solution, and finally Ag NPs are synthesized. To examine this hypothesis and also to understand the material processing using GDE, it is necessary to investigate the liquid-phase reaction process just below the plasma-liquid interface quantitatively. In this work, we carried out numerical simulation of atmospheric-pressure GDE with $AgNO_3$ solution for Ag NPs synthesis.

Fig. 1 shows the simulation model. DC glow discharge in atmospheric-pressure He/H_2O mixture with 1 mm gas-gap is connected with $AgNO_3$ solution with 1 mm depth in series. Both the dc glow discharge and the electrolysis were calculated based on one-dimensional fluid model using continuity equations for charged/neutral species coupled with Poisson equation. In liquid, we considered 6 anions, hydrated electrons, OH^-, NO_3^-, NO_3^{2-}, HNO_3^-, O_2^-, 6 cations, H^+, Ag^+, Ag_2^+, Ag^{2+}, Ag_4^{2+}, $AgOH^+$, and 8 neutral species, Ag, Ag_2, OH, H, O_2, H_2O_2, HO_2, NO_2. The liquid-phase reactions and their rate coefficients were mainly collected from NIST Solution Kinetics Database. As boundary conditions at plasma-liquid interface, we assumed that electrons and negative ions from the glow discharge are immediately changed into hydrated electrons, and neutral species are dissolved in the solution. The calculation condition in this work is as follows. Gas is atmospheric pressure He/H_2O(0.1%), the concentration of $AgNO_3$ solution is 0.1, 1.0 and 10 mM, and the applied voltage is 500 V.

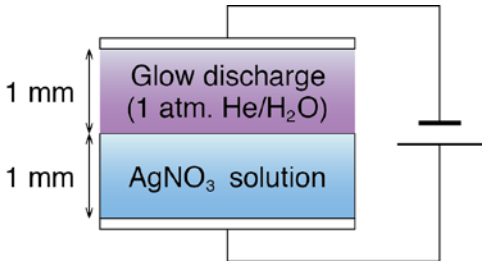

Fig. 1: Simulation model of glow discharge electrolysis at atmospheric pressure for Ag nanoparticles synthesis.

The calculated structure of atmospheric-pressure dc glow discharge in Fig. 2(a) is very similar to that between two metal electrodes. Although the mole fraction of H_2O is only 0.1%, the negative ion density is roughly ten times higher than the electron density. However, the electron flux onto liquid surface is still higher than the negative ion flux.

Spatial distributions of chemical species in 1 mM $AgNO_3$ aqueous solution near the plasma-liquid interface is shown in Fig. 2(b). The hydrated electrons, which are assumed to be transformed from incident electrons and negative ions from the glow discharge at liquid surface in our model, react with other species. Thus, the hydrated electrons exist in very narrow region from the liquid surface. This result qualitatively supports the experimental observation by Rumbach et al.[4]. The fastest reaction of hydrated electrons is the reduction of Ag^+, the reaction time of which is approximately 35 ns in 1.0 mM $AgNO_3$ solution and 3.5 ns in 10 mM $AgNO_3$ solution. Therefore, Ag has higher concentration with thinner profile near the plasma-liquid interface at higher $AgNO_3$ concentration. This profile will influence the nucleation and growth for Ag particle synthesis. Another interesting property is solution pH. The hydrated electrons also react with H_2O to form OH^-. Therefore, the solution near the plasma-liquid interface is alkalified, and the pH value locally exceeds 10. The local distribution of species near the plasma-liquid interface will strongly influence the liquid-phase reaction in GDE.

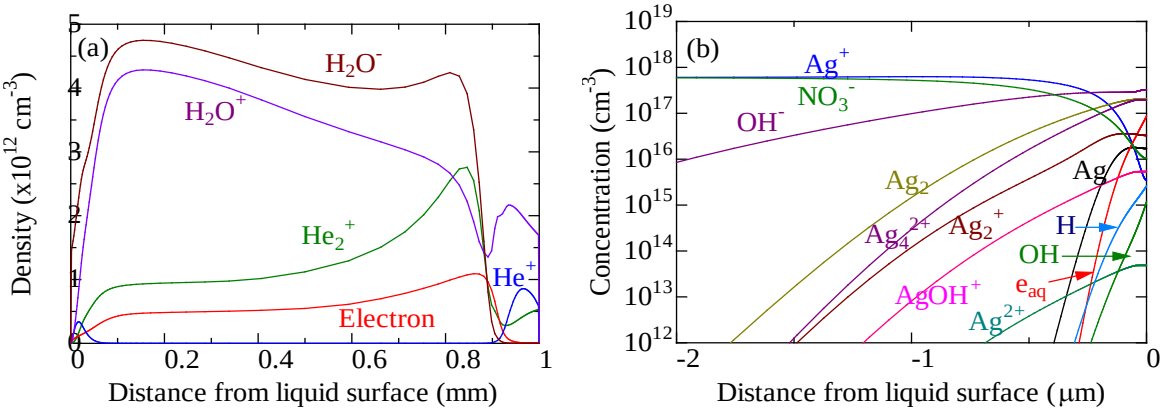

Fig. 2: Spatial distribution of (a) charged species in $He/H_2O(0.1\%)$ atmospheric-pressure dc glow discharge and (b) chemical species near plasma-liquid interface in 1 mM $AgNO_3$ aqueous solution, at 50 μs after starting GDE.

This work is partly supported by Grant-in-Aid for Scientific Research (B) from JSPS (No.15H03584).

References

[1] D. Mariotti and R. M. Sankaran, J. Phys. D **43**, 323001 (2010).
[2] N. Shirai, S. Uchida, and F. Tochikubo, Jpn. J. Appl. Phys. **53**, 046202 (2014).
[3] A.Hickling and M.D.Ingram, J. Electroanal. Chem. **8**, 65 (1964).
[4] P. Rumbach, D. M. Bartels, R. M. Sankaran and D. B. Go, Nat. Commun. **6**, 7248 (2015).

QUANTUM STATES DISTRIBUTION IN OH(X) RADICAL PRODUCED BY STREAMER DISCHARGES AT LIQUID WATER INTERFACE

Jan Voráč [1], Petr Synek [1], Pavel Dvořák[1], Tomáš Hoder [1]
[1]*Masaryk University, Faculty of Science, Czech Republic*

E-mail: vorac@mail.muni.cz

Streamer discharges originating from liquid water interface show interesting properties from fundamental point of view [1] as well as for applications [2]. One of the important fundamental aspects is the distribution of rotational quantum states in both ground (X) and excited (A) electronic states, as this is often used for spectroscopic thermometry, particularly for discharges in noble gas atmosphere lacking other molecular spectra. From the application point of view, concentration of reactive radicals produced in the plasma is crucial as these are the main cause of improved properties of the plasma treated materials or inactivation of potentially dangerous microorganisms. To address both these matters, the ground state (X) of OH generated in a streamer discharge in contact with liquid water interface was probed by laser-induced fluorescence (LIF) with high spectral, spatial and temporal resolution.

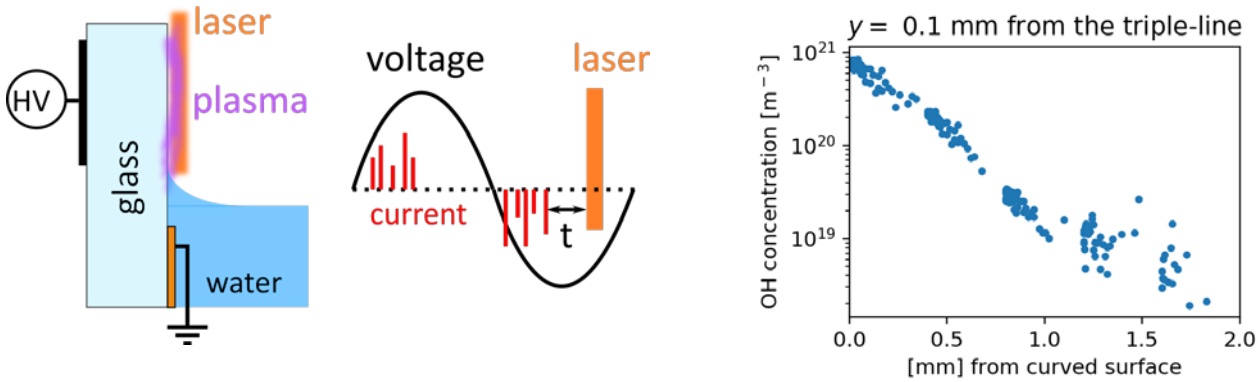

Fig. 1: The sketch of the experimental setup and timing (left) and the profile of OH (X) concentration versus the horizontal distance from the dielectric (right).

In this work a special case of a surface barrier discharge in contact with water level was used, see figure 1 (left) for a sketch of experimental arrangement. The point where water, solid dielectric and gas meet is called the triple line. Driven by alternating voltage, both negative and positive streamers arise in the respective half cycles, always starting from the water level. Since the mechanisms of breakdown and plasma development are fundamentally different, it can be expected that the effect on the OH concentration and its quantum states distribution will be also different. This was partially confirmed in the active discharge phase by optical emission spectroscopy, when the OH (A) excited electronic state was thoroughly examined [1]. The fluorescence measurements revealed the dynamic of OH (X) total concentration is much slower than the period of the driving voltage (65 μs), leaving the concentration spatial profiles constant during the whole cycle. The whole discharge region was mapped with planar

LIF to obtain profiles of the OH (X) concentration versus the vertical distance from the water level and the horizontal distance from the dielectric barrier. The maximal concentration of OH (X) in the order of 10^{21} m^{-3} was found at the dielectric barrier and decreased gradually with the distance from the dielectric barrier, by two orders of magnitude over the distance of 1.5 mm, see figure 1 (right).

To tackle the problem of non-equilibrium rotational distributions, the population of four different rotational states was examined OH (X, v'' = 0, J'' = 1, 2, 3, 7) and evaluated by the absorption Boltzmann plot method. This revealed a quasi-Boltzmann distribution, i.e. a distribution following the Boltzmann law but with unrealistically high temperature parameter, even 10 μs after the active discharges. This was a surprising result, as the long lifetime of OH(X) and the long delay after the active discharge phase are orders of magnitude longer than the characteristic time for rotational energy transfer in OH, which is known to be in the order of nanoseconds at atmospheric pressure. This also shows that even the ground electronic state of OH (X) may be unsuitable for spectroscopic thermometry of discharges in contact with liquid water.

Further, the concentration of hydrogen atoms was measured by TALIF. The absolute concentration was found to be in the order of 10^{21} m^{-3} at the water level gradually decreasing to 60% of the maximum at 4 mm above the water level.

Acknowledgement
This contribution was supported by the Czech Science Foundation projects 16-09721Y and 17-04329S and LO1411 (NPU I) funded by the Ministry of Education, Youth and Sports of the Czech Republic.

References
[1] Voráč, J., Synek, P., Procházka, V., & Hoder, T. (2017). State-by-state emission spectra fitting for non-equilibrium plasmas: OH spectra of surface barrier discharge at argon/water interface. *Journal of Physics D: Applied Physics*, *50*(29), 294002.

[2] Pavliňák, D., Galmiz, O., Zemánek, M., Brablec, A., Čech, J., & Černák, M. (2014). Permanent hydrophilization of outer and inner surfaces of polytetrafluoroethylene tubes using ambient air plasma generated by surface dielectric barrier discharges. *Applied Physics Letters*, *105*(15), 154102.

MASSIVEOES: PUSHING THE LIMITS – DISENTAGLING THERMAL N_2(C-B) AND NON-THERMAL OH(A-X) ROTATIONAL DISTRIBUTION BY COMBINED STATE-BY-STATE AND BOLTZMANN SIMULATION APPROACH

Jan Voráč [1], Petr Synek [1]
[1]*Masaryk University, Faculty of Science, Czech Republic*

E-mail: vorac@mail.muni.cz

massiveOES is a free open source spectroscopic software with unique features of batch processing and state-by-state fitting for high-precision and high-speed construction of molecular Boltzmann plots recently developed at Masaryk University [1-3]. Handling high number of overlapping spectra with thermal distribution was achieved in diagnostics of power modulated microwave surfatron plasma jet [2]. Non-thermal distribution of OH(A-X) spectra in a surface barrier discharge in argon atmosphere in contact with liquid water was revealed by the novel approach of state-by-state fitting [3], allowing observation of features like iso-energetic vibrational energetic transfer [3]. The state-by-state fitting method utilizes the linear nature of the problem, allowing the evaluation of the populations of quantum states with rotational and fine-structure resolution in a fraction of a second. This approach requires an overdetermined problem, i.e. the number of measured spectral positions (e.g. pixels) needs to be greater than the number of states to be evaluated. There are, however, cases, when this assumption is not met, such as in discharges ignited in argon with water vapor, containing nitrogen admixtures.

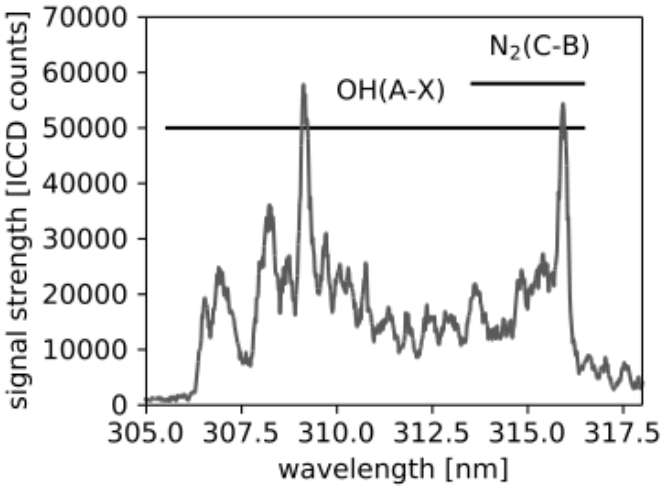

Fig. 1: An example of the emission spectra around 310 nm where the (0.0) and (1,1) bands of non-thermal OH(A-X) clearly overlap with the (v, v-1) bands of N_2(C-B).

In this contribution we introduce spectra from a volume barrier discharge developed originally for atomization of hydrides and subsequent atomic absorption spectroscopy [4,5] for analytical purposes. The plasma is ignited in humidified argon and mixes with ambient air,

introducing both excited hydroxyl OH(A) and nitrogen N2(C). The measured spectrum has 1024 pixels, and 2588 possible quantum states affecting this wavelength range by at least one spectral line. This is consequently an underdetermined problem that cannot be solved by conventional least-squares fitting. The proposed solution is measuring the N2(C) rotational temperature separately in another spectral window (e.g. around 337 nm) and treating the whole N2(C, $T_{rot|}$) as a single quantum state, reducing the number of quantum states to be evaluated to 226. This procedure is applied to spectra measured along the discharge axis from points with different concentration of air admixture.

Acknowledgement
This contribution was supported by the Czech Science Foundation projects 17-04329S and 16-09721Y and LO1411 (NPU I) funded by the Ministry of Education, Youth and Sports of the Czech Republic.

References
[1] massiveOES available at https://bitbucket.org/OES_muni/massiveoes

[2] Voráč, J., Synek, P., Potočňáková, L., Hnilica, J., & Kudrle, V. (2017). Batch processing of overlapping molecular spectra as a tool for spatio-temporal diagnostics of power modulated microwave plasma jet. *Plasma Sources Science and Technology*, 26(2), 025010.

[3] Voráč, J., Synek, P., Procházka, V., & Hoder, T. (2017). State-by-state emission spectra fitting for non-equilibrium plasmas: OH spectra of surface barrier discharge at argon/water interface. *Journal of Physics D: Applied Physics*, 50(29), 294002.

[4] Kratzer, J., Boušek, J., Sturgeon, R. E., Mester, Z., & Dědina, J. (2014). Determination of bismuth by dielectric barrier discharge atomic absorption spectrometry coupled with hydride generation: method optimization and evaluation of analytical performance. *Analytical chemistry*, 86(19), 9620-9625.

[5] Dvořák, P., Talába, M., Obrusník, A., Kratzer, J., & Dedina, J. (2017). Concentration of atomic hydrogen in a dielectric barrier discharge measured by two-photon absorption fluorescence. *Plasma Sources Science Technology*, 26(8).

INFLUENCE OF BARRIER PROPERTIES ON DIELECTRIC BARRIER SURFACE DISCHARGE DRIVEN BY MICROSECOND VOLTAGE PULSES

M.V. Sokolova[1], V.V. Voevodin[1], V.R. Soloviev[2], Ju.I. Malachov[1]
[1]*National Research University "Moscow Power Engineering Institute", Russia*
[2]*Moscow Institute of Physics and Technology, Russia*

E-mail: mvsokolova@mail.ru

The aim of the work was to analyze the type of the influence of the dielectric barrier properties on characteristics of dielectric barrier surface discharge (DBSD) in atmospheric air. The experimental values of the ignition voltages U_0 and dimensions of discharge area L of DBSD that can be found in publications for identical barriers differ much and it prevents their usage in modeling and calculations. For instance, interesting results given in [1] are for different ε values of different barrier material, whereas the barrier thickness and other experimental conditions are not indicated. Influence of each of these properties separately on DBSD for equal other features was the aim of the present investigation. All results given below were achieved in accurately defined following conditions. The electrode configuration seen in fig. 1 includes two electrodes 50 μm of thickness placed on both sides of a dielectric plate 48x60 mm in dimensions.

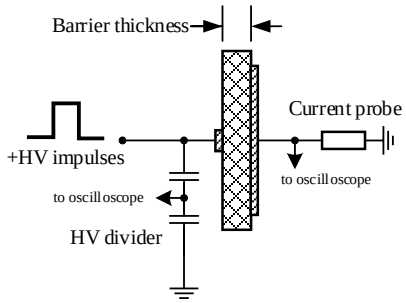

Fig. 1: Experimental setup

Fig. 2: Dust figure of the positive charge left on the ceramic barrier after impulse discharge

Electrode exposed to high voltage is a strip of copper foil pasted to the barrier surface. The copper foil electrode at the reverse side of the barrier consists of three parts: the central one was grounded through a current probe to measure the discharge current. Two outer strips were grounded directly. The outer edges of all electrodes were covered by epoxy compound to exclude parasite discharges that can occur during the measurements. The high voltage impulse amplitude was up to 10 kV with front duration in the range of 30-50 ns and impulse duration 5 μs. The P6015 voltage divider, 50-Ohm current probe and DPO7354C oscilloscope were used to measure the voltage and the discharge current. The dust technique was used to visualize the charge formed on the barrier surface during the discharge (fig. 2).

Two kinds of barrier material were used: Plexiglas plates of different thickness (d = 0.85 – 5.08 mm) and ε = 3 and ceramics on base of MgO with different additives (SiO_2, TiO_2, TiO_3, $SrTiO_3$) with ε values from 7 to 35 and d = 0.9 – 1,7 mm. The impulse voltage generator has been described previously in [2]. The value of the ignition voltage U_0 for all cases was obtained using the curves of the applied voltage and discharge current for the moment of the first sharp increase of the current as it is seen in fig. 3 A. The current in oscillograms is the total current that includes the displacement current and the discharge current. They were not

divided as only the moment of sharp increase of the total current was used to obtain the ignition voltage. Such method has one serious disadvantage in case when the discharge appears at very early stages, has a diffusive form and develops into a channel form much later. The ignition voltage value in this case is not easy to distinguish as it is seen in fig.3 B.

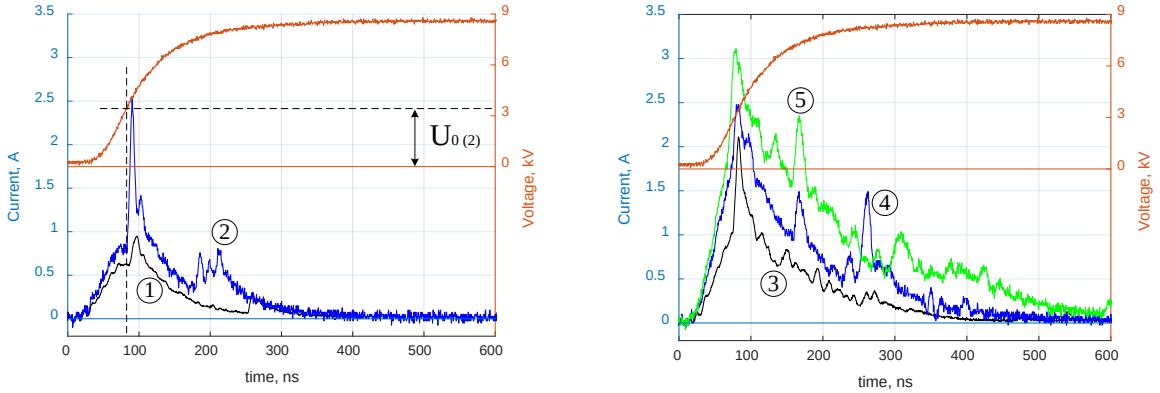

Fig. 3: Examples of voltage and current oscillograms for a set of ceramic barriers. **1** – ε = 7; **2** – ε = 10; **3** – ε = 15; **4** – ε = 25; **5** – ε = 35.

An increase of the barrier thickness of Plexiglas with the same ε value leads to an increase of U_0. The current curves for ceramic plates of different chemical composition are very different. It is easy to distinguish the moment of the discharge ignition for barriers with ε values less than 15 (fig. 3 A) as the sharp increase of the discharge current is seen. Less obvious transition to discharge current is seen for the discharge over ceramic barrier with ε > 15. It can be supposed that one of probable causes of such effect is connected with a decrease of volume resistance of the barrier material. It must be mentioned that ceramic material of the barriers with high ε consists additionally of molecules of TiO_2 or TiO_3. It is known [3] that such material can produce high electron emission ability even in relatively low electric fields.

Analytical estimation for a discharge length dependence on the dielectric barrier parameters and the applied voltage has been carried out for a case of discharge development as a set of single 3D near-surface streamers. The results are in a qualitative agreement with experimental data: the discharge length is proportional to applied voltage, decreases with dielectric relative permittivity ε rising up, and slowly logarithmically increases with the increase of dielectric barrier thickness. Thus, it is possible to state that in a whole the ignition of surface discharge driven by impulse voltage can depend on a range of barrier characteristics, such as: the barrier material, its chemical composition, ε value, barrier thickness, the roughness and the profile of the barrier surface. One of important factors that can influence the discharge ignition is the presence of charges on the barrier surface left after previous discharges or being the result of occasional rubbing of the barrier surface near the electrode edge.

References.

[1] V.I. Gibalov, G.J. Pietsch. *J. Phys. D: Appl. Phys.* **2000,** 33, p. 2618
[2] Khomich, V.Yu., Malashin, M.V., Moshkunov, S.I., Rebrov, I.E., Shershunova, E.A. *In proceedings of 21st SPEEDAM, Anacapri 2012, p. 1512.*
[3] Zs. Szalay, Z. Machala & al. *HAKONE XII, Trencianske Teplice, Slovakia 2010, p.502*

Acknowledgements. This work was partly supported by Russian Ministry of Science and Education (project No 3.9279.2017). The authors would like to thank Central Bureau of Special Radio Materials (CKBRM) for provided ceramic samples.

SPATIALLY-RESOLVED ELECTRICAL AND OPTICAL STUDY OF HOMOGENEOUS DIELECTRIC BARRIER DISCHARGES IN PRESENCE OF HEXAMETHYLDISILOXANE AND NITROUS OXIDE

N. De Mejanes[1,2], K. Guemmache[1,2], L. Maechler[1], J. Profili[2], L. Stafford[2], N. Naudé[1]

[1]*LAPLACE, Université de Toulouse, CNRS, Toulouse, France*
[2]*Département de Physique, Université de Montréal, Montréal, Québec, Canada*

E-mail: nicolas.naude@laplace.univ-tlse.fr

Keywords: Dielectric Barrier Discharge (DBD), homogeneous discharge, atmospheric pressure (AP), local current measurement, time resolved optical emission spectroscopy

1 Introduction

During the past decades, deposition of novel thin-film materials and nanomaterials using Dielectric Barrier Discharges (DBD) at atmospheric pressure has been widely studied. However, many challenges remain for large-scale industrial applications. Among these challenges, a precise control of the deposition rate and chemical composition of plasma-deposited coatings are of great importance. In this work, spatially-resolved electrical and optical measurements are used to examine the influence of the gas residence time on the physics and chemistry of DBD in presence of hexamethyldisiloxane (HMDSO) precursor and oxidizing gas (N_2O) for plasma-enhanced chemical vapor deposition of functional SiOCH coatings [1]. Two types of homogeneous regimes are studied: an Atmospheric Pressure Glow Discharge (APGD) in He and an Atmospheric Pressure Townsend Discharge (APTD) in N_2 [2]. Details on the set-up are presented elsewhere [1,3]. All experiments are performed in a plane-to-plane DBD configuration (1 mm gap) with a laminar gas flow in a controlled environment.

2 Spatially-resolved analysis of plasma-deposited coatings

Figure 1 shows the influence of the gas residence time t_{res} on the deposition rate of SiOCH coatings along with the corresponding O/C and O/Si atomic ratios obtained by X-ray photoelectron spectroscopy (XPS). These values were obtained by spatially-resolved measurements on the sample surface along the gas flow lines.

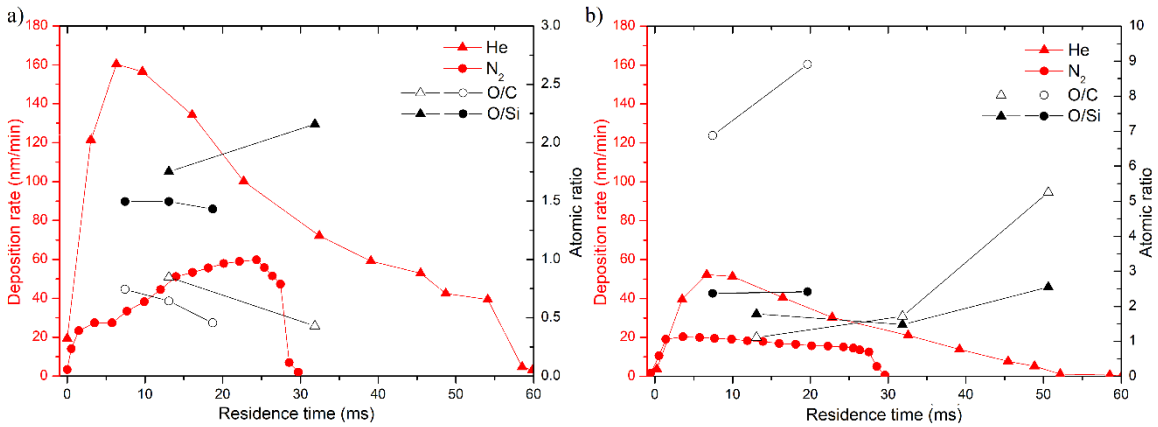

Figure 1 - Deposition rate and atomic ratio as a function of t_{res} **a)** without and **b)** with oxidizing gas (N_2O).

In both APGD and APTD in presence of HMDSO with and without N_2O, significant variations of the deposition rate and film composition are observed along the gas flow lines. The addition of the oxidizing gas also modifies the film stoichiometry (resulting in O/Si ratio closer to 2) and significantly reduces the deposition rate. The latter can be related to the lower amount of carbon embedded in the layer (translated by a higher O/C ratio).

3 Spatially-resolved analysis of the discharge characteristics

In order to establish links between the characteristics of plasma-deposited coatings observed in Figure 1 and those of the gaseous phase, spatially-resolved electrical measurements were performed. This technique recently developed at LAPLACE (Toulouse, France) relies on a structured electrode to obtain local current density measurements [3]. A schematic of the system is presented in Figure 2 along with a typical example of a local surface power density evolution as a function of position along the gas flow lines.

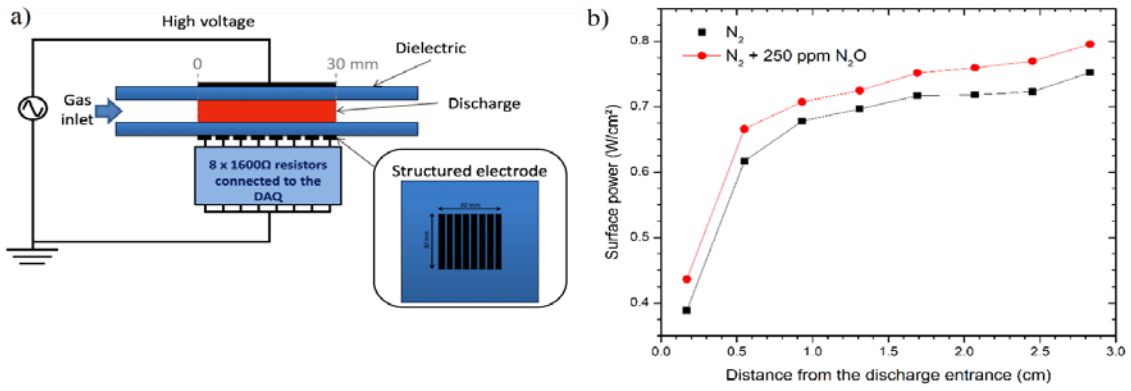

Figure 2 - a) Schematics of the discharge cell proving spatially-resolved measurements using a structured electrode with 8 strips. **b)** Typical surface power density evolution as a function of position from the discharge entrance (1D measurements). The applied voltage is 12 kV and the excitation frequency is 3 kHz [2]

The increase of the surface power density with the distance from the discharge entrance presented in Figure 2 is likely to play an important role on the fragmentation kinetics of HMDSO and thus on the evolution of the film composition and deposition rate. These electrical properties will be coupled with spatially-resolved optical emission spectroscopy (OES) measurements. Preliminary results obtained without N_2O show that the emission intensities of organic species (CN for the APTD, CH and C_2 for the APGD) increase with the residence time. Additional measurements with and without oxidative species will also be realized. In the case of APGD, OES measurements of He n=3 lines will also be coupled to a recently-developed collisional-radiative model to analyze the spatial distribution of the electron temperature, electron number density, and number density of He metastable (n=2) atoms [4].

4 References

[1] O. Levasseur, L. Stafford, N. Gherardi, N. Naudé, P. Blanchet, B. Riedl, and A. Sarkissan, Surface and Coatings Technology 234, 42 (2013)

[2] F. Massines, N. Gherardi, N. Naudé, P. Ségur, Eur. Phys. J. Appl. Phys. **47**, 22805 (2009)

[3] N. Naudé, M.C. Bouzidi, V. Roustit, C. Tyl, S. Dap, A. Belinger, N. Gherardi, Investigation of the local current in homogeneous dielectric barrier discharge, HAKONE XV (2016)

[4] R K Gangwar *et al.* Plasma Sources Sci. Technol. 25 015011 (2016).

SIMULATION OF ELECTRON INTERACTIONS WITH LIQUID WATER AND PROCESSES RELATED TO SUB-NANOSECOND ELECTRICAL BREAKDOWN

Petr Bílek[1], Milan Šimek[2], Tomáš Hoder[1], Zdeněk Bonaventura[1]
[1]*Department of Physical Electronics, Faculty of Science, Masaryk University, Brno, Czech Republic*
[2]*Department of Pulse Plasma Systems, Institute of Plasma Physics, Academy of Sciences of Czech Republic, Prague, Czech Republic*

E-mail: petrbilek248@gmail.com

Initiation of electric discharge in dielectric liquids such as water can be caused either by formation of gaseous bubbles (when the system is driven by high-voltage waveforms of microsecond duration) or due to creation of cavitation voids in case of very-steep high-voltage pulses with sub-nanosecond rise times. Presence of these deformations prolong mean-free path of electrons, which can then gain enough energy for excitation/ionization/dissociation of water molecules.

We propose to use Geant4-DNA [1, 2] toolkit for studies of elementary processes related to interaction of accelerated electrons with liquid water. The Geant4-DNA provides a complete set of models describing the step-by-step physical electromagnetic interactions of electrons with liquid water. These models describe both the cross sections and the final states of the physical interactions, with a full description of the interaction products, taking into account the molecular structure of liquid water. Geant4-DNA electron models for the calculation of ionization and excitation cross sections are based on the Emfietzoglou model [3] of the dielectric function of liquid water. The dielectric function approach is currently the state-of-the-art technique for modeling the energy-loss of electrons in the condensed phase [4].

The aim of our work will be to study elementary processes related to interaction of accelerated electrons with liquid water. Geant4-DNA provides appropriate tools for simulations of different liquid-water characteristics during electrical breakdown such as: electron-penetration-range computation [5] and others. These tools enable us determination of electrical-breakdown characteristics of liquid water, which will be confronted with experimental data acquired in point-plane electrode geometry [6, 7].

Acknowledgements

This contribution was supported by the Czech Science Foundation projects 18-04676S and 16-09721Y and LO1411 (NPU I) funded by the Ministry of Education, Youth and Sports of the Czech Republic.

References

1. M.A. Bernal et al., Physica Medica: European Journal of Medical Physics 31.8, (2015) 861–874.
2. S. Incerti et al., Medical physics 37.9, (2005).
3. D. Emfietzoglou Radiat. Phys. Chem., 66, 373 (2003).
4. Emfietzoglou et al., Int. J. Radiat. Biol., 88, 22 (2012).
5. Z. Francis et al., Applied radiation and isotopes 69.1, (2011) 220–226.
6. M. Šimek et al., Book of Contributed Papers of 15th International Symposium on High Pressure Low Temperature Plasma Chemistry (HAKONE XV) p. 405-407 (2016).
7. M. Šimek, et al., Plasma Sources Science and Technology 26.7, (2017) 07LT01.

Visualization of Active OH and H Species in A Water-Contacting Discharge

Qing Xiong[1], Lin Xiong[1], Qinghua Huang[1], Zhan Shu[1]
[1]*State Key Laboratory of Power Transmission Equipment & System Security and New Technology, Chongqing University, Chongqing 400044, PR China*

E-mail: qingugent@gmail.com

Plasma interacting with liquids attracts widely interests from both points of plasma fundamental research and novel plasma applications such as in fields of bio-medicine and water-pollution control. In this work we will present a detailed studying on the reactive species of OH and H above the water surface in a water-contacting micro-discharge, with emphasis on their spatially resolved distributions by advance laser diagnostic approaches. The studied discharge is generated in a helium atmosphere with NaCl solution working as the anode. Gas temperature in the vicinity of plasma-water interface was determined through analysis of excitation LIF spectra and space-resolved OES of OH. The H_2O distribution above the water surface was estimated from the time decay characteristics of OH fluorescence. And fluorescence calibrations were done individually by Rayleigh scattering and TALIF of Kr atoms for determining the absolute concentrations of both OH and H species. Density patterns of this two important species, and their production and loss mechanisms were discussed.

Development of a 0D model to investigate the plasma chemistry in a Townsend discharge in the mixture N_2/O_2: role of the associative ionization mechanisms in the memory effect

S.Dap[1], X. Lin[1], C.Tyl[1], N.Naudé[1], N.Gherardi[1]
[1]*Laboratoire LAPLACE, Université de Toulouse, France*

E-mail: simon.dap@laplace.univ-tlse.fr

Dielectric barrier discharges (DBD) are non-equilibrium discharges, generally working at atmospheric pressure. Their low cost and ease to use ensure DBDs a wide range of applications such as thin-film deposition, wastewater treatment, sterilization… Depending on the experimental conditions, DBDs can work in filamentary or homogeneous regimes. For the latter to be obtained, it has been shown that a memory effect is needed *i.e.* a mechanism able to produce seed electrons in between two successive discharges, under low electric field. In nitrogen, it results in a homogeneous discharge called Townsend discharge. Experimentally, it can be evidenced and quantified by looking at the discharge current: a current jump is observed when the polarity reverses.

In pure nitrogen atmosphere, previous studies have pointed out the major role of $N_2(A)$ metastable which can be responsible for the production of seed electrons by secondary emission as they diffuse towards the dielectric surfaces. Nevertheless, we observed that a small addition of oxygen enhances the current jump and thus the memory effect [1]. At first sight, it seems contradictory since O_2 and its products such as atomic oxygen $O(^3P)$ or NO are efficient quenchers of $N_2(A)$. A possible explanation is that reactions susceptible to produce electrons take place in the discharge volume. One possible candidate is the associative ionization reaction (1):

$$N(^2P) + O(^3P) \rightarrow NO^+ + e^- \qquad (1)$$

where $N(^2P)$ is produced by reaction (2):

$$N(^4S) + N_2(A^3\Sigma_u^+) \rightarrow N(^2P) + N_2 \qquad (2)$$

To verify this hypothesis, one and two photons laser induced fluorescence (LIF and TALIF) measurements have been performed to quantify the density of atomic nitrogen $N(^4S)$ and oxygen $O(^3P)$ and nitric oxide NO. The corresponding results are presented in the work of Xi Lin *et al*. [2]. The aim of the present work is to identify the main chemical paths responsible for the creation of these species, to provide estimations of the densities of unmeasured species such as $N_2(A)$ and $N(^2P)$ and to estimate the rate of reaction (2) in our experimental conditions. For this purpose, a 0D model has been developed and is presented here.

The general principle of the model is similar to the one proposed by Tsyganov et al. [4]. Since it is a 0D model, it is not self-consistent. To overcome this limitation we use electrical experimental measurements of the applied voltage and total current to calculate the gas gap voltage V_g and the discharge current I_d, following the method detailed in [3]. Then, the time-varying electron density and the electric field between the

dielectric surfaces are deduced using equations (3) and (4) assuming that all the discharge current is due to electrons and the electric field is uniform.

$$E(t) = \frac{|V_g(t)|}{d} \quad (3)$$

$$n_e(t) = \frac{|j_d(t)|}{e\mu_e(E)E(t)} \quad (4)$$

Using these data, the electron induced reaction rates can be determined. The main reactions considered in this work are taken from [5]. To validate the model, its results are compared to experimental measurements coming from [2] or from the literature. Once the model is validated, the numerical results are compared to experimental measurements and discussed. Figure 1(a) shows the evolution of the densities of the main important species as a function of the oxygen concentration. The corresponding rate of reaction (1) is given figure 1(b).

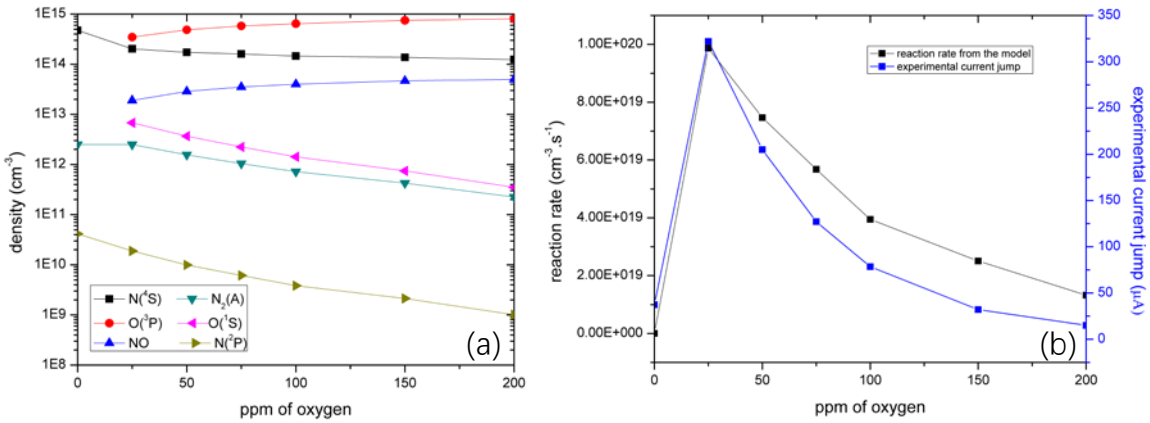

Fig. 1: (a) species density provided by the model and (b) rate of associative ionization reactions from the model compared to experimental measurements of the current jump. Simulations where performed for different oxygen concentrations at a constant applied voltage of 17.12 kV.

A qualitative agreement is found between the evolution of the calculated densities and the measured ones regarding the oxygen concentration. The evolution of the associative ionization reaction rate for different oxygen concentrations is quite similar to the evolution of the current jump indicating that this mechanism can play a significant role in the memory effect.

[1] Tyl, C., *et al.* Memory effect in a Dielectric Barrier Discharge in N2: phenomena in the gas bulk versus phenomena on the dielectrics surfaces in XXXIII ICPIG, July 9-14, 2017, Estoril/Lisbon, Portugal.
[2] Lin, X., *et al.* Study of memory effect in a Townsend discharge: quantification of species by laser induced fluorescence spectroscopy, Proc. HAKONE 2018, September 2-7, 2018, Beijing China.
[3] Naudé, N., et al., Journal of Physics D: Applied Physics, 2005. **38**(4): p. 530-538.
[4] Tsyganov, D. *et al.*, Plasma Sources Science & Technology, 2012. **21**(6).
[5] Kossyi, I.A., *et al.*, Plasma Sources Science & Technology, 1992. **1**(3): p. 207-220.

MICROAMPERE CURRENTS IN BARRIER DISCHARGES AT WATER INTERFACE IN ATMOSPHERIC PRESSURE AIR

Tomáš Hoder and Petr Synek
Masaryk University, Department of Physical Electronics, Brno, Czech Republic

E-mail: hoder@physics.muni.cz

The barrier discharge in atmospheric pressure air is relatively well understood phenomenon [1,2]. While its spectroscopic, macroscopic electrical or plasma-chemical properties have been investigated by various means [3], the microscopic electrical current recording with sub-nanosecond time resolution and sensitivity reaching several units of microamperes was challenged only recently [4].

In this contribution, we present unique electrical current measurements with self-assembled current probe of coaxial arrangement with large bandwidth and dynamical range [4]. The probe consists of the four resistors connected concentrically around the inner wire of a coaxial cable. It works on principle of measurement of a voltage drop partly on the outer resistors and input resistance of the oscilloscope.

In [4], the probe was quantitatively compared to the typically used commercial ones and its performance was shown on the volume barrier discharge in air at atmospheric pressure. Under few simplifying assumptions, the electronic and ionic components of the measured current have been separated. The amplitude of the ionic current was few tens of microamperes while its decay lasted for several microseconds. Using statistical methods, changes in the ionic current features (amplitude, decay time) were detected for sub-sequent discharges within one half-period. It has been hypothesized that observed changes are due to the variation of the plasma conductivity which is a consequence of the gradual gas heating and/or discharge mechanism deviations.

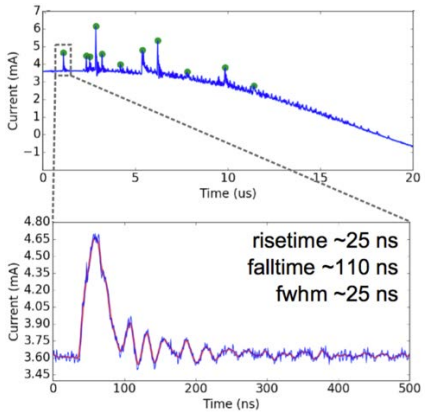

Fig. 1: Electrical current measured on surface barrier discharge at the water interface in atmospheric pressure air.

In figure 1, measurements using the same current probing system are shown for the surface barrier discharge in contact with water. These fast and high-sensitivity measurements reveal the previously experimentally unknown diversity of the discharging phenomena at the triple-line.

Trains of current pulses with very low amplitude has been theoretically reported by Lagmich et al. [5] and the technical complications connected with their direct measurement described in [6]. In this contribution, we report on the precise detection of various current pulses in surface barrier discharge and analyze them statistically in detail. Based on the recent knowledge, we hypothesize about their possible mechanisms and about the origin of these various currents.

Acknowledgement:
This contribution was supported by the Czech Science Foundation projects 16-09721Y and 18-04676S and by LO1411 (NPU I) funded by the Ministry of Education, Youth and Sports of the Czech Republic.

References:
[1] Kozlov et al. 2007 Contrib. Plasma Phys. 47, 26
[2] Hoder et al. 2010 J. Phys. D: Appl. Phys. 43, 124009
[3] Brandenburg et al. 2013 J. Phys. D: Appl. Phys. 46, 464015
[4] Synek et al. 2018 Plasma Sources Sci. Technol. accepted
[5] Lagmich et al. 2008 J. Phys. D: Appl. Phys. 41, 095205
[6] Grosch et al. 2010 Eur. Phys. J. D 60, 547

Study of memory effect in a Townsend discharge: quantification of species by laser induced fluorescence spectroscopy

X.Lin[1], C.Tyl[1], N.Naudé[1], N.Gherardi[1], S.Dap[1]
[1]*LAPLACE, Université de Toulouse, CNRS, Toulouse, France*

E-mail: xi.lin@laplace.univ-tlse.fr

Dielectric barrier discharge (DBD) is one kind of nonequilibrium gas discharge, generally working at atmospheric pressure. For most gases and discharge conditions, the DBD consists in a multitude of microdischarges corresponding to the so called filamentary regime. Under certain conditions, the discharge is homogenous along the electrodes surfaces [1]. For example, in N_2, the discharge is characterized by an uniform light located close to the anode and is called Townsend discharge because its electrical features are similar to those of the dark Townsend discharge at low pressure [2]. To obtain a Townsend discharge, a source of seed electrons between two successive discharges at low electric field is required, which is called Memory Effect. In pure nitrogen, the mechanism of secondary electron emission induced by the impact of $N_2(A)$ on the charged dielectric surfaces was found to be the most probable source of seed electrons [2]. However, we found that the addition of few oxygen (<100ppm) makes the homogeneous discharge more stable, in spite of the high destruction rate of $N_2(A)$ due to their quenching by the oxidizing species, which leads to a filamentary discharge for higher oxygen rates (>400 ppm). Hence, to explain this phenomena, we propose another mechanism that generates seed electrons in volume, based on the following associative ionization reaction [3,4]:

$$N(^2P)+O(^3P)\rightarrow NO^+ + e^- \quad (1)$$

where $N(^2P)$ is produced by the reaction:

$$N(^4S)+N_2(A)\rightarrow N(^2P)+N_2(X) \quad (2)$$

The aim of this work is to verify this hypothesis. For this propose, we need to determine the absolute density of $N(^4S)$ and $O(^3P)$ using Two-photon Absorption Laser Induced Fluorescence (TALIF). Besides, the absolute density of NO(X) is also determined by Laser Induced Fluorescence (LIF) because it is known to efficiently quench $N(^2P)$ and $N_2(A)$. Finally, with the help of a 0D model (not described here, see [5]), we can estimate the amount of seed electrons produced by associative ionization reactions in between two discharges, and the corresponding current jump occurring when the polarity reverses. By comparing with the experimental results, we can verify the role of the reactions contributing to the memory effect.

The general principle of the aforementioned LIF/TALIF spectroscopy is to use a laser beam to excite the species of interest to a resonant level, then the subsequent fluorescence allow to infer the ground-state population. The experimental set-up is similar to the one described in reference [6], except that in our measurements, the dielectrics used are alumina with 635µm thickness spaced by a 2mm gas gap.

Figure 1 shows the absolute densities of $N(^4S)$, $O(^3P)$ and NO as a function of O_2 concentration for the same discharge power. The decrease of $N(^4S)$ with the addition of O_2 in the discharge,

can be attributed to its strong destruction by the reactions with oxidizing species, mainly NO and O(^{3}P) through the following reactions:

$$N(^4S)+NO \rightarrow N_2+O(^3P,^1D) \quad (3)$$

$$N(^4S)+O(^3P)+N_2 \rightarrow NO+N_2 \quad (4)$$

The production of N(^{4}S) mostly occurs during N_2 dissociation by electron impact, hence it can be considered rather constant for similar discharge power.

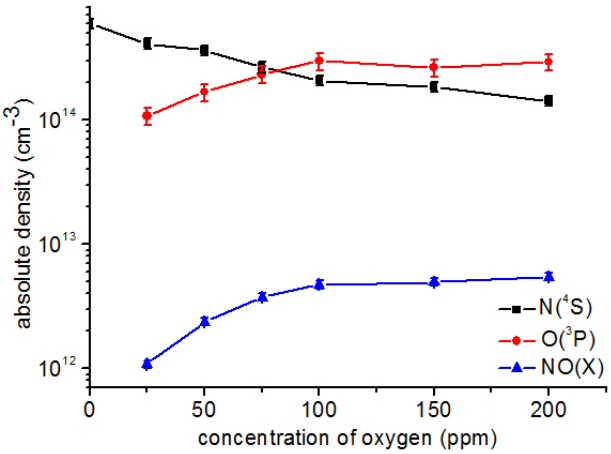

Fig. 1 Absolute density of the species as a function of concentration of O_2 for the same discharge power 0.9W/cm^2 and at the exit of discharge. Common conditions: f=2kHz, flux=1.0l/min

The density of O(^{3}P) increases with the addition of O_2 and then remains constant above 100 ppm. In our conditions, the main production of O(^{3}P) is found to be the dissociation of O_2 by N_2(A), and NO reduction by N(^{4}S). O(^{3}P) destruction is also related to N_2(A) through the reaction:

$$N_2(A)+O(^3P) \rightarrow NO+N(^2D) \quad (5)$$

Consequently, the observed behavior of O(^{3}P) density with respect to O_2 ppm can be explained as follows: for lower concentration of O_2, the addition of O_2 favors the production of O(^{3}P); while for higher concentration, the decrease of N_2(A) restricts O(^{3}P) production and its density varies very slightly. Finally, the evolution of the NO(X) density shows a similar trend and considering that the production of NO mainly occurs by the reaction (5), a similar explanation could be argued. It means that N_2(A) molecules keep playing a major role in discharge chemistry even in the presence of a small amount of oxygen.

References:

[1] R. Brandenburg, *Plasma Sources Sci. Technol.*, vol. 26, no. 5, 2017.
[2] F. Massines *et al*, *Eur. Phys. J. Appl. Phys.*, vol. 47, no. 2, p. 22805, 2009.
[3] N. Popov, *Plasma Phys. Reports*, vol. 35, no. 5, pp. 436–449, 2009.
[4] I. A. Kossyi *et al*, *Plasma Sources Sci. Technol.*, vol. 1, pp. 207–220, 1992.
[5] S.Dap *et al*, *Proc. of the 16th High Pressure Low Temp. Plasma Chemistry Symp.* (HAKONE XVI) (2018) Beijing, China
[6] E. T. Es-Sebbar *et al*, *Appl. Phys.*, vol. 106, no. 7, 2009.

Hybrid repetitively-pulsed nanosecond discharge and DC discharge enhanced low temperature H_2/O_2/He ignition by non-equilibrium excitation

Xingqian Mao, Qi Chen*, Shoufa Huang
School of Mechanical, Electronic and Control Engineering, Beijing Jiaotong University, Beijing 100044, China

E-mail: qchen@bjtu.edu.cn

Introduction

Non-equilibrium plasma has shown a great potential to enhance the combustion in the past decades. Many researchers have studied plasma assisted combustion of the small molecule fuels, such as H_2, CH_4, C_2H_4, as well as large hydrocarbons, like n-pentane and n-heptane [1-2]. Recently, researchers found that plasma could enhance combustion efficiently at low temperatures [3]. The enhancement mainly comes from the kinetic effect by non-equilibrium excitations, such as vibrational excitation and electronic excitation. The excited species, for example, vibrationally excited species ($H_2(v)$, $O_2(v)$, $N_2(v)$) and electronically excited species ($O_2(a^1\Delta_g)$, $O(^1D)$, He^*) [4], could be produced by different types of discharge. In the previous studies, most researches focused on the kinetic enhancement of the excited species on combustion by using a certain discharge type alone, such as DC, AC, microwave, RF, gliding arc, repetitively-pulsed nanosecond discharge. Few studies worked on the development of the new discharge types to achieve the optimized enhancement on combustion.

As shown in Fig.1, in a stoichiometric H_2/O_2 mixture with 85% He dilution, most energy goes to the excitation of $H_2(v)$, $O_2(v)$ and $O_2(a^1\Delta_g)$ at relatively low *E*/*N* (electric field/gas density, below 20 Td), however, the electronic excitation, dissociation and ionization reactions dominate electron impact kinetics at higher *E*/*N*. In this work, a hybrid repetitively-pulsed nanosecond discharge and DC discharge is developed and applied to assist the low temperature H_2/O_2/He ignition. The NSD is used to supply the high *E*/*N*. During the two pulses, a low *E*/*N* is maintained by the DC discharge. Firstly, a H_2/O_2/He plasma-combustion mechanism is developed based on HP-mech and validated by the plasma assisted low temperature oxidation experiment. Secondly, the ignition delay time is calculated by a time splitting Hybrid ZDPlasKin-CHEMKIN model at different temperatures and discharge conditions. Finally, the kinetic effect of the $H_2(v)$, $O_2(v)$ and $O_2(a^1\Delta_g)$ by non-equilibrium excitation and the gas heating effect by plasma on ignition are studied.

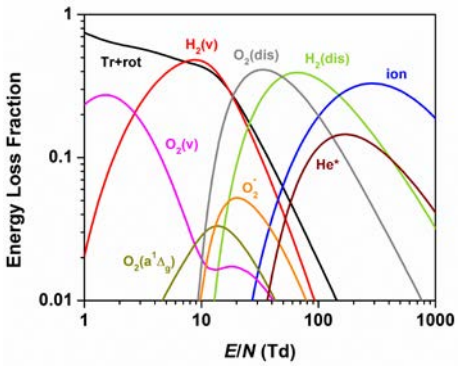

Fig. 1: Energy fractions dissipated into different excitation modes in H_2/O_2/He ($0.10H_2$/ $0.05O_2$/ 0.85He) mixtures as a function of *E*/*N*.

Results and discussion

Experiments of NSD plasma enhanced low temperature H_2 oxidation are conducted to validate the H_2/O_2/He plasma-combustion mechanism. The experiments are conducted in a $0.10H_2$/ $0.05O_2$ /0.85He combustible mixture with an initial temperature of 296 K and a pressure of 60 Torr. The flow rates of the gases are controlled by the mass flowmeters with a total flow rate of 0.174 m/s. The central part of the flow reactor is a rectangle quartz cell,

which is 220 mm in length, 20 mm in width and 10 mm height. Two copper electrodes are placed on top and bottom sides of the reactor forming a plane-to-plane DBD with barrier thickness of 2 mm. The length of the discharge region is 5 mm. A repetitively-pulsed nanosecond power supply is applied to generate the plasma. The discharge frequency ranges from 1 kHz to 30 kHz. An average square wave voltage of 6500 V with 200 ns pulse width is used for all experiments. The mole fractions of the components are measured by a gas chromatograph (GC) coupled with a thermal conductivity detector (TCD). The temperature is measured by a thermal couple placed at the end of the discharge region.

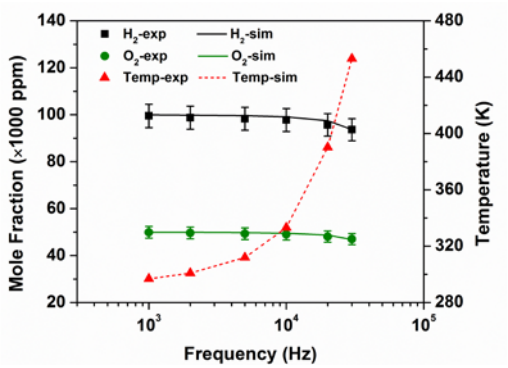

Fig. 2: Comparison of the species between the experiment and the prediction in a continuous plasma ranging from 1 to 30 kHz at 60 Torr.

A time splitting Hybrid ZDPlasKin-CHEMKIN model is used to calculate the species concentrations of the low temperature H_2 oxidation in a NSD. The measured temperature is used as the input parameter. A good agreement of the species concentration between the experiment and the prediction validates the model and numerical methods, as shown in Fig. 2.

In order to study the effects of the non-equilibrium excitation by hybrid plasma on ignition enhancement, the ignition delay times are calculated under auto-ignition, thermal ignition, NSD and hybrid plasmas respectively between 400 and 800 K at atmospheric pressure, as shown in Fig. 3. The *E*/*N* during the nanosecond discharge is 100 Td, when the dissociation of H_2 and O_2, electronical excitation and ionization occur efficiently. In the hybrid plasma, 2 Td, 9 Td and 14 Td are chosen when most plasma energy goes to the excitation of $O_2(v)$, $H_2(v)$ and $O_2(a^1\Delta_g)$ respectively in the DC part. It is clearly to see the effective enhancement of hybrid NSD/DC discharge on H_2/O_2 ignition, especially at low temperatures. When the same amount of the energy deposited in the plasma is used to provide the thermal energy, the enhancement is not as effective as the discharge conditions. It indicates that the ignition enhancement by plasma mainly comes from the kinetic effects. The excited species $H_2(v)$ and $O_2(a^1\Delta_g)$ mostly generated in the DC discharge enhance the ignition via kinetic pathways, such as $O + H_2(v1) \rightarrow H + OH$ and $H + O_2(a^1\Delta_g) \rightarrow O + OH$. During the NSD discharge, the electronically excited $O(^1D)$ kinetically enhances ignition via $O(^1D) + H_2 \rightarrow H + OH$.

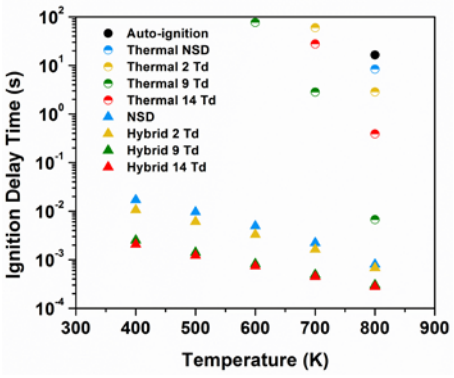

Fig. 3: Ignition delay time of auto-ignition, thermal ignition, NSD and hybrid discharge conditions with different temperatures at 1 atm.

References

[1] Starikovskiy, A., and Aleksandrov, N., *Progress in Energy and Combustion Science*, Vol. 39, No. 1, 2013, pp. 61-110.
[2] Ju, Y., and Sun, W., *Progress in Energy and Combustion Science*, Vol. 48, 2015, pp. 21-83.
[3] Ju, Y., Lefkowitz, J. K., Reuter, C. B., Won, S. H., Yang, X., Yang, S., Sun, W., Jiang, Z., and Chen, Q., Vol. 36, No. 1, 2016, pp. 85-105.
[4] Popov, N. A., *Plasma Sources Science Technology*, Vol. 25, 2016, p. 043002.

Modeling of Streamer-to-Spark Transition of a Nanosecond Pulsed Discharge for Kinetics Parameters

Yifei ZHU[1], Yun WU[2]
[1]*Laboratory of AeroPlasma Dynamics, Xi'an, China*
[2]*School of mechanical engineering, Xi'an Jiaotong University, Xi'an, China*
E-mail: Yifei.zhu.plasma@gmail.com

Pulsed nanosecond discharges are characterized by a short duration and a high peak voltage on the electrodes. They produce strongly nonequilibrium plasma at high pressures before arc formation, resulting in high chemical reactivities. Recently, the interest to nanosecond discharges at atmospheric pressure and higher increases significantly due to their potential use for plasma assisted aerodynamics, plasma assisted biology and medicine, plasma assisted combustion, etc. In spite of wide and physically different range of applications conducted in different geometric configurations, there are common features in physics and chemistry of nanosecond discharges to study, vitally important for any of mentioned applications.

A systematic experimental study of high pressure (100 Torr) nanosecond pulsed discharge has been conducted in a sphere-to-sphere configuration recently with the help of picosecond Coherent Anti-Stokes Raman Spectroscopy (CARS), Optical Emission Spectroscopy (OES) and electrical measurements[1-3]. The well defined experimental condition allows further diagnostics technologies, and the consistent set of experimental data, provides a good basis for theoretical analysis with the help of numerical modeling.

0D/1D kinetics models were built for the experiments, a good agreement was achieved for N_2 vibrational levels and temperature evolution. Despite the ability to resolve detailed chemistries, the kinetics models depend strongly on experimental input and some assumptions, especially the E/N value, electron density and the spatially uniform assumption. To allow predicting conditions using kinetics model when experimental data are incomplete, and to further study the dynamics of plasma for complex geometries, self-consistent 2D models are required.

A two dimensional code PASSKEy (PArallel Streamer Solver with KinEtics) was used in this work. The code couples the solution of species and photon transport, electric potential, fluid dynamics and circuits. In this work, the local field approximation and a simplified cathode boundary condition were used to achieve numerical efficiency and accuracy simultaneously. Details of the numerical scheme and air kinetics for 2D modeling can be found in [4]. Some initial results will be presented in this abstract.

The schematic configuration of the studied sphere-to-sphere nanosecond pulsed discharge [1-3] can be found in Fig.1(a). The pressure was 100 Torr. Two sphere electrodes with diameter of 7.5 mm were placed 10 mm apart. The applied voltage was shown in Fig.1 (b). As can be seen in Fig.1 (a), during the first 100 ns, the streamer forms and propagates from both electrodes. The negative streamer propagates much quicker during expansion. Once two streamers merge, a quasi-neutral discharge channel is formed and spark starts, the rise of electric field leads to a significant increase of electron density and electric current, as is

shown in Fig.1 (b) and Fig.2 (a). The calculated current agrees well with the measured one, indicating the validity of the code and the model.

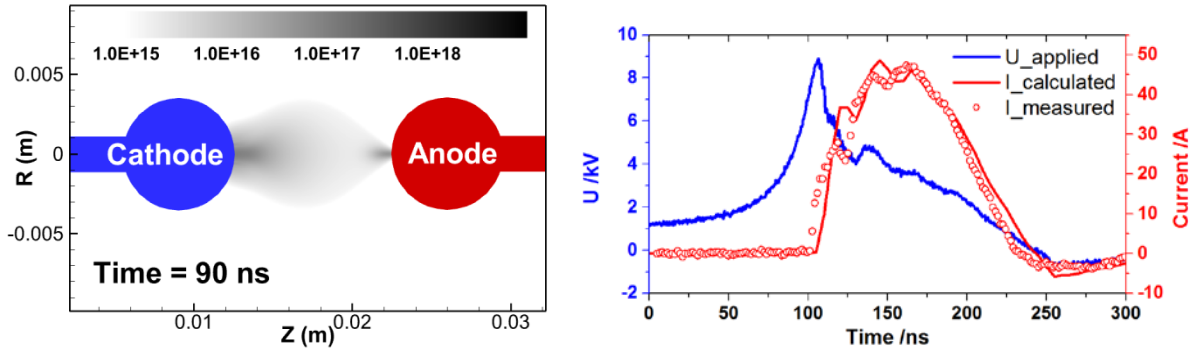

(a) (b)

Fig. 1: Distribution of electron density in streamer propagation (a) and in spark phase (b), unit in m^{-3}. The experimental voltage and current are taken from [1].

One of the key input parameters for kinetics models to study the detailed plasma chemistry is the E/N value. By probing half way from the electrodes in the 2D model, one can plot the calculated E/N over time. Assuming spatial uniformity of spark discharge at this condition, a 0D calculation was also done to recover the E/N value from measured current. As can be seen in Fig.2 (b), the E/N obtained from two models agrees well with each other.

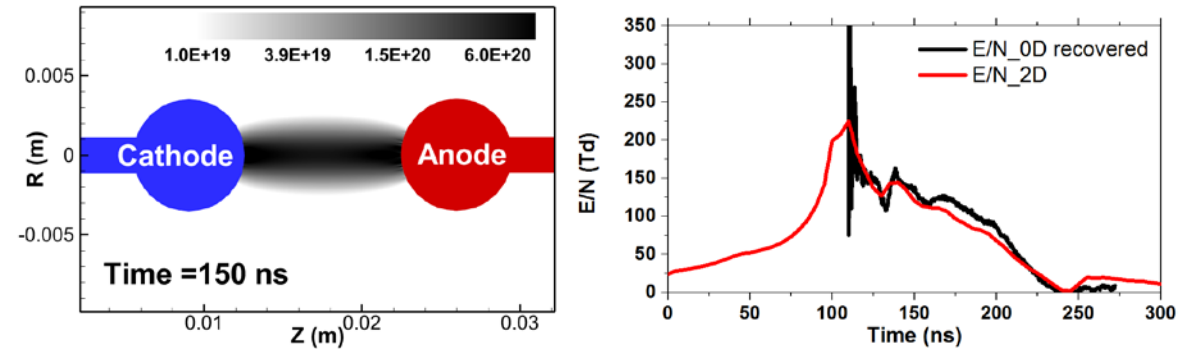

(a) (b)

Fig. 2: Distribution of electron density in spark (a), unit in m^{-3}. Comparison between calculated and measured values of E/N (b).

This validated, self-consistent model based on PASSKEy code can be easily scaled to other geometries or pressures, to capture the dynamics of discharges, to provide key parameters for kinetics investigations, and to help the design of E/N for applications. The extended discussions will be presented in the conference.

Acknowledgement:
This work is supported by National Natural Science Foundation of China (NSFC, 91541120).

Reference:

[1] A Montello *et al* 2013 *J. Phys. D: Appl. Phys.* **46** 464002
[2] D Burnette *et al* 2014 *Plasma Sources Sci. Technol.* **23** 045007
[3] Ivan Shkurenkov and Igor V Adamovich 2016 *Plasma Sources Sci. Technol.* **25** 015021
[4] Yifei Zhu *et al* 2017 *Plasma Sources Sci. Technol.* **26** 125004

NON-THERMAL PLASMA ENHANCEMENT OF DRYING PROCESS

Chongshan Zhong[1], Alex Martynenko[2], Kazimierz Adamiak[3]
[1] *Dept. of Electrical Eng., China Agricultural Univ., China*
[2] *Dept. of Eng., Fac. of Agriculture, Dalhousie Univ., Truro, Nova Scotia, Canada B2N 5E3*
[3] *Dept. of Electrical and Comp. Eng., Univ. of Western Ontario, London, Ontario, Canada N6A 5B9*

E-mail: kadamiak@eng.uwo.ca

Non-thermal plasmas, produced by variety of electrical discharges, have recently found many industrial and research applications due to their ability to promote numerous chemical reactions at low temperatures. One more effect of these discharges, the electrohydrodynamic (EHD) flow, was for long time treated as a curiosity, or even a harmful effect. Recently, EHD flows are considered as beneficial effects in different applications. One of them is EHD drying. In the food industry this technique offers many important advantages: it doesn't increase temperature, so food preserves its quality, and it is very energy efficient, as power needed to generate EHD flow is much lower than that needed by conventional devices [1].

The presented paper deals with numerical simulation of drying process. A regular array of sharp needles is supplied with a high negative voltage and dried material is placed on a flat ground plate. Corona discharge is generated near needle tips due to very high electric field intensity in this area. Different ion species are generated and some of them drift across the air gap towards the ground plate. The momentum transfer between moving ions and neutral molecules results in the secondary electrohydrodynamic flow, also called the ionic wind.

EHD flow generated by each needle has a form of an impinging jet, which helps to transport humidity from the surface of dried material to the ambient gas [2]. This effect alone wouldn't substantially accelerate drying, as the gas would be quickly saturated with humidity. The drying rate depends on the humidity diffusion, so it is necessary to maintain a high humidity concentration gradient. This can be achieved with help of an external gas flow, parallel to drying material, which removes humidity from the drying chamber.

The whole process was simulated numerically and the computational model involved: 1) electric field between the high voltage needles and the ground plane, which also considers the presence of ionic charges, 2) generation and transport of ionic charges, affected by electric field and moving gas, 3) EHD flow produced by corona discharge, 4) external gas flow and 5) humidity transport from the surface of dried material to the chamber outlet.

A regular infinite array of identical needles was assumed, so only one 3D cell can be considered with proper symmetry and periodic boundary conditions. The Finite Element Method was used to solve Poisson equation for the electric field, drift-diffusion equations for the space charge density and humidity concentration, and Navier-Stokes equation for the gas

flow. The most important input parameters affecting the process were drier geometry, supply voltage and the external velocity of moving gas. The EHD flow may also affect the evaporation rate from the substrate, but this effect was not included.

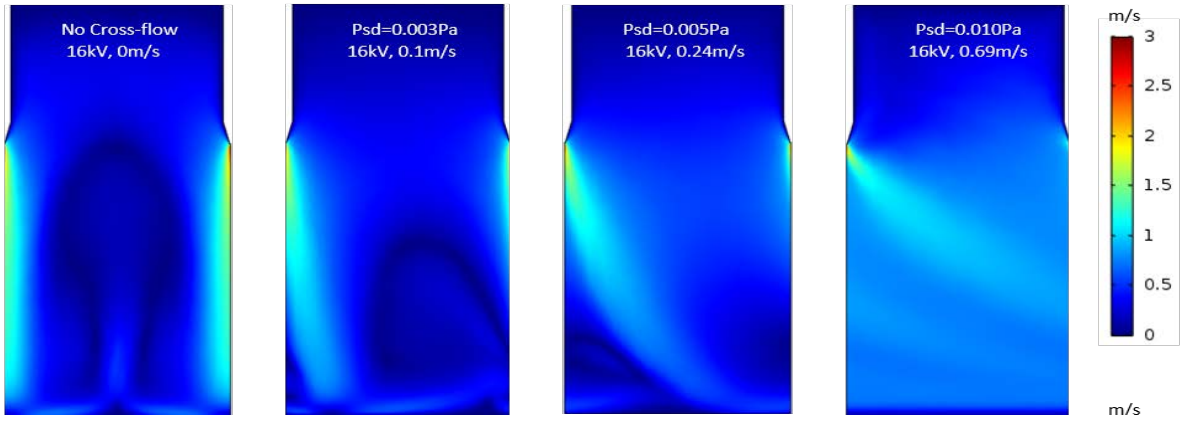

Fig. 1: Gas velocity distribution in the central plane of the drier between two adjacent needles for different velocities of the external flow.

The gas flow has practically no effect on the discharge characteristics. The electric body force, driving the gas motion, has the maximum value near the discharge tip, where ions are very fast and the flow velocity is small. A minor distortion of ion trajectories near the ground plate has a negligible effect on the overall flow pattern, as this happens in the area of a very low electric field and, consequently, a minimal body force.

Without the external gas flow the EHD flow forms jets from the discharge needles towards a ground plate (Fig. 1). The flow velocity has a maximum value near the needle tips and its magnitude strongly depends on the voltage level. For the highest voltage levels, this velocity can reach a value close to 10 m/s in the area just below the discharge electrode. The jets are rebounded by the solid ground plates and closed vortices are formed. The external flow distorts this pattern, bending EHD jets in the flow direction. At high external flow velocities, the EHD jets practically don't reach the ground plate.

The gas flow velocity distribution is the major factor affecting the humidity transport. The spatial distribution of the humidity concentration was used to evaluate the drying rate. At corona needle voltages below the onset level this rate increases with the external gas velocity. At low external flows, the EHD effects slightly enhance the drying rate. This rate significantly improves with the increasing velocity of the external flow. However, too high external velocities eliminate the effect of the EHD flow. Therefore, for each voltage level there is an optimum velocity of the external gas flow, which guarantees the highest rate of drying.

References

1. T. Kudra and A. Martynenko, Energy aspects in electrohydrodynamic drying. Drying Technol., vol. 33 (13), pp.1534-1540, 2015.
2. C.A. Shi, A. Martynenko, T. Kudra, P. Wells, K. Adamiak and G.S.P. Castle, Electrically-induced mass transport in a multiple pin-plate electrohydrodynamic (EHD) dryer. J. Food Eng., vol. 211, pp.39-49, 2017.

Plasma catalytic conversion of CO_2 and small hydrocarbons

Aart W. Kleyn and Qiang Huang
Center of Interface Dynamics for Sustainability, Institute of Materials, CAEP, Chengdu
E-mail: a.w.kleijn@contact.uva.nl

Endothermic catalytic reactions require operation at elevated temperatures. The heating required is usually obtained by combustion of hydrocarbons and in this way contributes to CO_2 emission. Instead electricity obtained in a sustainable fashion should drive the reaction. In addition, it is desirable that the energy transfer involved is done in a bond specific manner. Plasma excitation and dissociation of molecules can serve this purpose. In low temperature plasma, all molecular degrees of freedom are not in equilibrium and dissociation of CO_2 can be realized much more efficiently than in thermodynamic equilibrium [1].
In CIDS, Chengdu we use mass spectroscopy, infrared spectroscopy, optical emission spectroscopy and a Langmuir probe to study the characteristics of the Radio Frequency or Micro Wave plasma, reaction products and the catalyst [2]. The most simple reaction studied in the plasma reactor is the dissociation of CO_2 into CO and O_2. We find energy efficiencies higher than 45%, indicating that the system is not in thermodynamic equilibrium and plasma favors vibrational excitation to translational heating. Adding a catalyst like AgO or NiO on Al_2O_3 does not enhance the yield. However, a purely metallic catalyst does significantly enhance the yield. The role of the catalyst, such as Co-MgO, is subject of our current research. The yield of the conversion shows a strong correlation with electron temperature, measured by a Langmuir probe. The highest yield is seen at lowest electron temperature. Optical emission spectroscopy shows a similar correlation and can serve as a signature for efficient conversion. A typical result is shown in Figure 1.

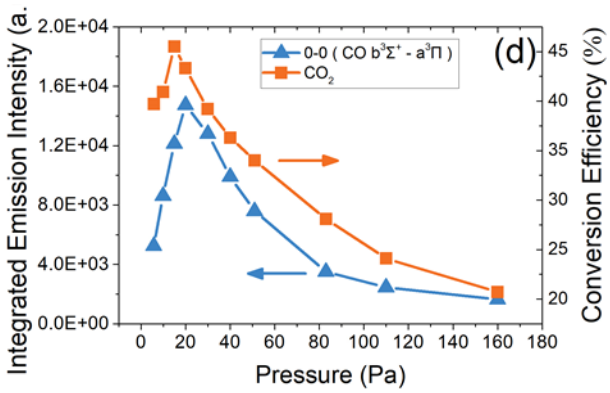

Figure 1: Dependences of conversion efficiency and Σ emission intensity of the CO (b $^3\Sigma^+$ - a $^3\Pi$) 0-0 transition on reactor pressure. The CO_2 flow was fixed at 100 sccm. Power was fixed at 150 W.

The figure shows a very similar dependence of optical emission and CO_2 conversion on pressure. Distinct peaks are observed in both datasets. Plotting the electron temperature versus pressure gives a similar, but opposite result. A distinct minimum is observed. This demonstrates that there is a strong anti-correlation between electron temperature and emission or conversion.

Very high non-thermal vibrational excitation is seen in the emission spectra. This indicates that non-thermal processes are occurring in these conversion plasmas.

Plasma excitation can also be carried out under fully thermal conditions. A plasma torch is used [3]. Problem is that the reverse reaction ($CO + O \Rightarrow CO_2$) removes most reaction products that are leaving the cooling plasma. Using chemical quenching this back reaction can be suppressed. In this way very high CO yields and electrical energy efficiencies can be obtained. Efficiencies exceeding 70% can be obtained with a conversion exceeding 95%, world record numbers.

In the case of dry reforming of CH_4 or butane with CO_2 in the plasma reactor we find that addition of an oxidic catalyst does not enhance the yield of $CO + H_2$. However, conversion and energy efficiency of the pure plasma reaction is high.

The work shows that the combination of classical catalysis and low temperature plasma enables a novel kind of chemical conversion, which can be explored by a compination of plasma physical and catalytical tools.

1. Snoeckx, R. and A. Bogaerts, *Plasma technology - a novel solution for CO2 conversion?* Chemical Society Reviews, 2017. **46**(19): p. 5805-5863.
2. Huang, Q., D.Y. Zhang, D.P. Wang, K.Z. Liu, and A.W. Kleyn, *Carbon dioxide dissociation in non-thermal radiofrequency and microwave plasma.* Journal of Physics D-Applied Physics, 2017. **50**(29): p. 6.
3. Li, J., et al., *Dissociation of CO2 by thermal plasma with contracting nozzle quenching.* Journal of CO2 Utilization, 2017. **21**: p. 72-76.

Ultrasensitive method of monitoring of VOC's decomposition in corona discharge based on Ion Mobility Spectrometry

B. Michalczuk, L. Moravský, M. Sabo and Š. Matejčík

Comenius University, Faculty of Mathematics, Physics and Informatics, Bratislava, Slovakia

E-mail: matejcik@fmph.uniba.sk

The problem of fast detection of trace amounts of volatile organic compounds (VOCs) has become an important issue in the last decades. One of the most suitable techniques in this field is Ion Mobility Spectrometry (IMS), which offers fast and ultrasensitive detection [1-6]. In present paper we demonstrate the ability of IMS to detect the dimethyl phthalate (DMP) and its isomers with vapor pressure of 0.304 Pa at 25°C with fast response time (<1s) and sufficient spectral resolution. These parameters make IMS a suitable instrument for online monitoring of these compounds. The DMP vapors were mixed with ambient air at atmospheric pressure and this mixture was introduced in small experimental corona discharge (CD) reactor. Decomposition of DMP was carried out in CD reactor of wire to cylinder geometry, in positive polarity and U = 6.7 kV, I = 350-650 μA. The flow rate of the sample gas was 5 sccm. We have applied IMS technique for monitoring the decomposition of DMP. In Figure 1 we present the first results. Application of CD decomposition on the DMP vapors resulted in decrease of the DMP signal in IMS spectrum from the original amplitude for nontreated vapors (black) to lower amplitudes (red and green) for CD treated gas. The amplitudes correspond to the relative DMP concentrations in the range from 1 ppm to 100 ppb.

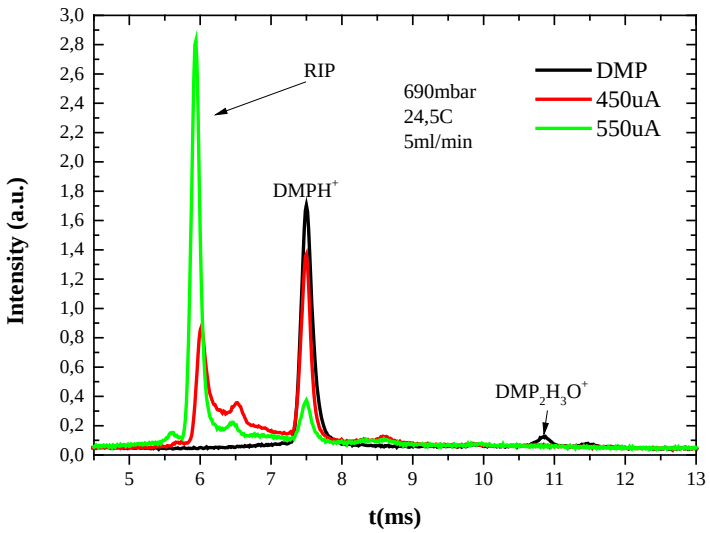

Fig. 1: IMS spectra of DMP after degradation by corona discharge at various discharge current, RIP – reactant ion peak – ions responsible for chemical ionisatoin of the sample.

Acknowledgements

This work has been supported by European Union's Horizon 2020 research and innovation programme under the Marie Skłodowska-Curie grant agreement No 674911 and innovation programme under grant

agreement No 692335, additionally Slovak Research and Development Agency Project Nr. APVV-15-0580 and the grant agency VEGA, project Nr. VEGA-15-089 support is acknowledget.

[1] S. J. Valentine, X. Y. Liu, M. D. Plasencia, A. E. Hilderbrand, R. T. Kurulugama, S. L. Koeniger, D. E. Clemmer, Expert Rev. Proteom. 2 (2005) 553–565.
[2] S. L. Koeniger, S. J. Valentine, S. Myung, M. Plasencia, Y. J. Lee, D. E. Clemmer, J. Proteome Res. 4, (2005) 25–35.
[3] R. A. Sowell, S. L. Koeniger, S. J. Valentine, M. H. Moon, D. E. Clemmer, J. Am. Soc. Mass Spectrom. 15, (2004) 1341–1353
[4] C. Wu, W. F. Siems, J. Klasmeier, H. H. Hill,. Anal. Chem. 72, (2000) 391–395
[5] J. A. McLean, B. T. Ruotolo, K. J. Gillig, D. H. Russell, Int. J. Mass Spectrom. 240, (2005) 301–315
[6] M.F. Jarrold, Annu.Rev.Phys. Chem. 51, (2000) 179–207

Kinetic Contribution of Vibrational States in Plasma Assisted CH_4 Reforming

Jintao Sun, Qi Chen*
School of Mechanical, Electronic and Control Engineering, Beijing Jiaotong University, No.3 Shangyuancun Haidian District, Beijing 100044 P. R. China

E-mail: qchen@bjtu.edu.cn

Introduction

Traditional CH_4 conversion is normally conducted under high reaction temperature or high pressure conditions. In comparison, non-equilibrium plasma assisted low temperature CH_4 reforming can take the advantage of higher electron energy with low neutral gas temperature in a plasma [1-2]. Non-equilibrium plasmas have the potential of in situ production of reactive species to accelerate the reaction processes at low temperature. Many past studies have been made to demonstrate the effectiveness of plasma assisted methane reforming in DC, AC, microwave, radio frequency, and nanosecond plasmas [3-6].

The reduced electric field *E/N* controls the direction of species production and the energy deposited in a plasma. The energy from electric field will be dissipated into different molecular degrees of freedom at different value of *E/N*, as shown in Fig.1. Vibrationally excited species have been proven effective on chemical reactions because their reaction rates are significantly higher than the ground state counterparts. Nevertheless, the kinetic impacts of the excited species on the overall pyrolysis process of methane fuel have not been investigated thoroughly due to the measurement and modeling complexities, and need further study.

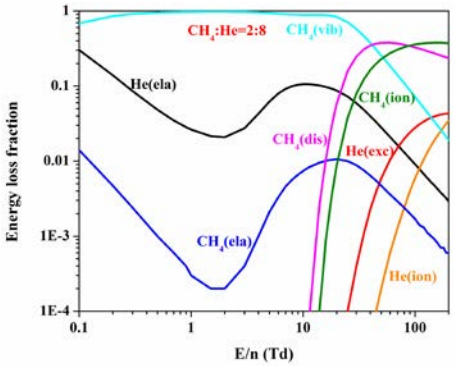

Fig. 1: Energy fractions dissipated into different excitation modes in CH_4/He (0.2CH_4/ 0.8He) mixtures as a function of *E/N*.

Motivated by the above, the objective of this work is to study computationally the kinetic process involving vibrational excitations of CH_4 molecules, as well as main product molecules in a CH_4/He mixture activated by RF plasmas.

Numerical methods

The present numerical model solves time evolution of species production and consumption in a constant pressure well-mixed reactor with non-equilibrium plasma processing on CHEMKIN Plasma-PSR module. Thus the kinetic model consisted of two different stages: DBD streamer discharge and chemistry reactions, the first stage is used to solve non-equilibrium plasma kinetics and the second stage is used to calculate the chemistry reactions. The rate coefficients of the electron impact elementary reactions were calculated on Bolsig+ by solving Boltzmann equation [7]. The deposition energy was treated as an adjustable parameter to fit the methane conversions obtained in experiments.

A set of elementary reactions was modeled for methane pyrolysis in a RF discharge plasma. The comprehensive combustion model, HP-Mech [8], modeled the rate coefficients of radical/ion reactions, which governed the kinetic process of plasma assisted low and high temperature chemistry. Other reactions were integrated for describing the kinetic model of a plasma reforming system, including electron impact reactions involving vibrationally-excited species, ion-ion exchange reactions, electron-ion recombination reactions and reactions involving excited particles. The rate coefficients of electron impact reactions were calculated

from a set of impact cross sections compiled from the online LXCAT database and literatures [9,10]. The reaction rate constants involving vibrationally excited species were calculated by using Fridman-Macheret α–Model. The numerical model included 81 species, 970 elementary reactions. Vibrational species included in numerical modeling are listed in Table 1.

Table.1 Excited species included in numerical modeling.

Excited States	He(2^3S) CH_4(v24) CH_4(v13) C_2H_6(v24) C_2H_6(v13) C_2H_4(v1) C_2H_4(v2) C_2H_2(v1) C_2H_2(v2) C_2H_2(v31) C_3H_8(v1) C_3H_8(v2) H_2(v1) H_2(v2) H_2(v3)

Results and Discussion

Fig.2 presents the reaction path flux for C_2H_4 and CH involved by vibrationally excited molecules of CH_4(v) and H_2(v). As can be seen in Fig.2, the vibrational molecules play significant roles in the CH_4 reforming. Among the main production pathways, 31.4% of C_2H_4 comes from the reaction $CH_4(v)+CH \rightarrow C_2H_4+H$. For the higher vibrational levels, the energy of excitation is sufficient to reduce the activation energy barrier and further affect radical formation, such as CH radical formation shown in Fig.2, H_2(v) lead to 7.9% of the CH radical formation. It follows that the concentrations of CH is crucial for determining the formation of major product C_2H_4. The predicted pathway shows that CH is dominantly consumed to produce C_2H_4 via the reactions $CH+CH_4 \rightarrow C_2H_4+H$ (13.1%) and $CH+CH_4(v) \rightarrow C_2H_4+H$ (67.4%).

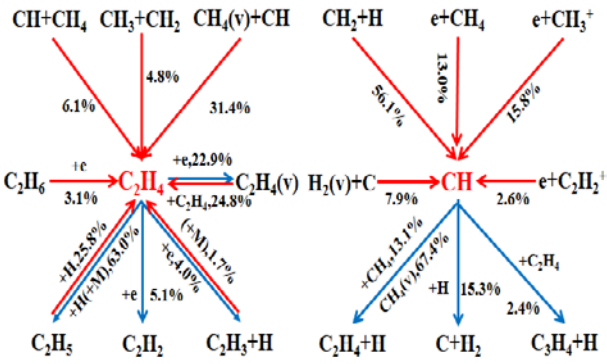

Fig. 2: Path fluxes of C_2H_4 and CH

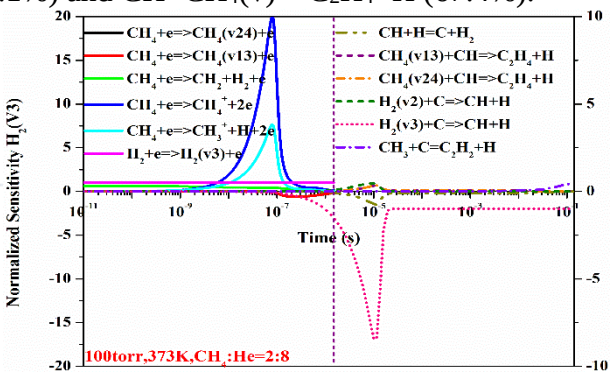

Fig. 3: Sensitivity analysis of H_2(v3)

A sensitivity analysis is conducted for a stoichiometric mixture (CH_4 0.2/ He 0.8) at pressure of 100 torr and temperature of 373K. Fig.3 shows the time evolution of sensitivity coefficients for the production of excited species H_2(v3). Sensitivity analysis coefficients presents the promotive effects of the responding reactions on species production and vice versa. The sensitivity plots of H_2(v3) reveals that the CH_4 impact ionization and dissociation by electrons as well as the excitation reactions in a RF plasma discharge, $H_2+e \rightarrow H_2(v3)+e$ play a sensitive role in H_2(v3) production, while the CH_4 impact excitation by electrons depress the formation of H_2(v3). On the other hand, the reactions $CH_4(v24)+CH \rightarrow C_2H_4+H$ and $H_2(v2)+C \rightarrow CH+H$ help to promote H_2(v3) production in the discharge afterglow. However, according to sensitivity analysis, these two pathways do not affect H_2(v3) production significantly. Additionally, the chain reaction, $H_2(v3)+C \rightarrow CH+H$, is found sensitive for H_2(v3) consumption. This is mainly because this reaction is a major consumption pathway for H_2(v3).

Reference

[1] S M Starikovskaia, *Journal of Physics D: Applied Physics*. 2006, 39(16):265-299.
[2] G. Petitpas, et al., *International Journal of Hydrogen Energy*. 2007, 32(14):2848-2867.
[3] C.S.Kalra, A.F.Gutsol, et al., *IEEE Transactions on Plasma Science*. 2005, 33(1):32-41.
[4] Hidetoshi Sekiguchi, Yoshihiro Mori, *Thin Solid Films*. 2003, 435(1):44-48.
[5] Changsheng Shen, Dekun Sun, Hongsheng Yang, *Journal of Natural Gas Chemistry*. 2011, 20(4):449-456.
[6] Wenting Sun, Mruthunjaya Uddi, et al., *Combustion and Flame*. 2012, 159(1):221-229.
[7] Qi Chen, Xiaofang Yang, et al., *Plasma Chemistry and Plasma Processing*. 2017, 37(6):1551-1571.
[8] X. Shen, X. Yang, J. Santner, J. Sun, Y. Ju, *Proceedings of the Combustion Institute*. 2015, 35(1):721-728.
[9] R. K. Janev and D. Reiter, *Physics of Plasmas*. 2002, 9(9):4071-4081.
[10] R. K. Janev and D. Reiter, *Physics of Plasmas*. 2004, 11(2):780-829.

REFORMING OF ETHANOL IN HYBRID PLASMA-CATALYTIC SYSTEM

O.A. Nedybaliuk[1], V.Ya. Chernyak[1], I.I. Fedirchyk[1], V.P. Demchina[2]
[1]*Taras Shevchenko National University of Kyiv, 64/13 Volodymyrska Street, 01601, Kyiv, Ukraine*
[2]*Gas Institute of National Academy of Sciences of Ukraine, 39 Degtyarivska Street, 03113, Kyiv, Ukraine*

E-mail*: oanedybaliuk@gmail.com*

Hybrid plasma-catalytic approach provides an opportunity to conduct chemical transformation of complex raw materials at the non-equilibrium conditions and low temperatures. This method is appealing for creating technologies that are compliant with the green chemistry requirements. The aforementioned approach is the foundation of hybrid plasma-catalytic reforming. Studies have shown that hybrid plasma-catalytic reforming is an effective method of synthesis gas production from hydrocarbons. Nevertheless, many aspects of this process as well as the ways it is affected by the external factors are still lacking sufficient research coverage. The influence of the reaction chamber material on the reforming process and its products is one of such dark areas that require investigation.

Fig. 1 shows the scheme of the plasma-catalytic system and the setup used for the hybrid plasma-catalytic reforming of ethanol into synthesis gas during the experiments. Reforming system comprised connected discharge and reaction chambers. 96% food-grade ethanol was used as model hydrocarbon and atmospheric air was used as model oxidant. Air flow was divided between the discharge chamber and reaction chamber. Air introduced into the discharge chamber was activated by the discharge and became a source of active species. Activated air was injected into the reaction chamber as a torch. The mixture of ethanol and air was introduced into the system through the top of reaction chamber. Interaction between ethanol-air mixture and activated air led to partial oxidation of ethanol and production of synthesis gas. Reforming was conducted using steel and quartz cylindrical reaction chambers 100 mm high and with 36 mm inner diameter.

During the experiment, the air flow into discharge chamber was 10 $l \cdot min^{-1}$ and the air flow into reaction chamber was 5 $l \cdot min^{-1}$. Ethanol flow was set to 486 $ml \cdot h^{-1}$, which results in molar ratio between C_2H_5OH and O_2 in reactants equal to 1. Sampling of gaseous reforming products was conducted at reaction chamber temperature set to 200 ^oC. Required temperature of the reaction chamber was maintained by increasing input air flow and combusting part of introduced ethanol. Discharge current and voltage characteristics were measured using digital oscilloscope. Optical emission spectra from inside the reaction chamber were obtained during the experiments with quartz reaction chamber. Two thermocouples measured reaction chamber temperatures 10 mm from its top and bottom. Reforming was evaluated based on

reforming efficiency η, ratio between chemical energy of reforming products and electrical energy spent on plasma generation α and hydrogen energy yield $E_Y(H_2)$.

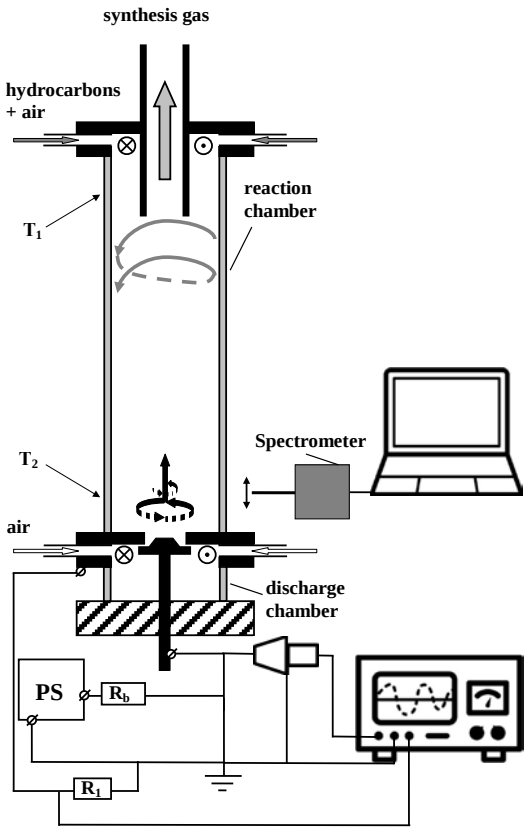

Fig. 1: Scheme of hybrid plasma-catalytic system with rotating gliding discharge for reforming of liquid hydrocarbons into synthesis gas

The research showed that addition of ethanol into the reaction chamber caused the vanishing of the NO bands from the emission spectra of the torch. The disappearance of NO may be caused by its reduction with the help of H_2 produced during ethanol reforming. Study showed that reaction chamber material influences the composition of gaseous reforming products. Ethanol reforming inside steel reaction chamber had higher volumetric concentrations of H_2 and CO in its products in comparison to reforming inside quartz chamber. Concentration of other reforming components remained on similar levels in both cases. Changes in reforming products composition resulted in the changes of reforming parameters. The move from quartz reaction chamber to steel reaction chamber resulted in 12% increase of reforming efficiency from 60% to 72% and increase of ratio α from 20 to 28. In addition, changing reaction chamber material from quartz to steel provided a 40% increase of hydrogen energy yield from 102 $g \cdot kWh^{-1}$ to 147 $g \cdot kWh^{-1}$. However, the H_2/CO ratio in the reforming products decreased from 1.5 during reforming inside the quartz reaction chamber to 1 during reforming inside the steel reaction chamber.

This work was funded via grant 0116U002531 issued by the Ministry of Education and Science of Ukraine, and in part by the National Academy of Sciences of Ukraine, the Ministry of Education and Science of Ukraine, and Taras Shevchenko National University of Kyiv.

AN INVESTIGATION OF CARBON DIOXIDE SPLITTING USING MICROHOLLOW CATHODE DISCHARGE

Qi Shi, Tao Ma, Hai-Xing Wang
[1]*School of Astronautics, Beihang University, China*

E-mail: whx@buaa.edu.cn

In recent years, there is increasing interest in CO_2 dissociation using low-temperature plasma techniques. Micro-hollow cathode discharge (MHCD) can be sustained at high pressure with low input power, which also features high power density, providing a highly reactive environment for chemistries. In this study, Micro-hollow cathode discharge (MHCD) used as a micro-reactor for dissociating CO_2 at atmospheric pressure has been experimentally investigated. The main structure of MHCD consists of two copper electrodes covered by a mica dielectric layer on both sides, through which a cylindrical hole is drilled.

In the experiments, pure CO_2 was fed through the MHCD hole, and the self-pulsing regime was observed in most of the situations through voltage and current measurements. Experiments within different operating parameters such as applied voltage and flow rate were conducted. It was found that the maximum of conversion yield exceeds 10% and a maximum of energy conversion efficiency is close to 10% for the MHCD dissociation of CO_2. It was also found that the self-pulsing regime plays a vital role in CO_2 dissociation compared to the normal glow discharge mode. Based on the experimental results, a preferable hole diameter was chosen to operate arrays of several MHCDs which can enlarge the plasma volume. Appropriate combination of the key operational parameters allows for good performance of the MHCDs functioning as a CO_2 dissociation reactor. The results of this study provide further insights to operating MHCD for efficient gas dissociation at atmospheric pressure.

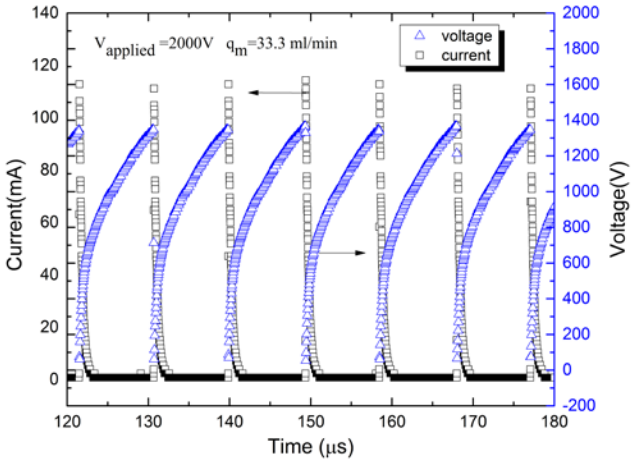

Fig. 1: Typical electrical characteristics of the MHCD in the self-pulsing regime

Acknowledgements: This work was supported by the National Natural Science Foundation of China (Nos. 11575019, 11735004)

OZONE GENERATION AND GAS TEMPERATURE CHARACTERISTICS BY PULSE MODULATED AIR DIELECTRIC BARRIER DISCHARGE DEVICE

Dai Atsuta[1], Naoki Osawa[1] and Yoshio Yosioka[1],
Yoshizou Ito[2], Hirotsugu Yamada[2]
[1]*Kanazawa Institute of Technology, 7-1 Ohgigaoka Nonoichi, Ishikawa, Japan*
[2]*RB Controls Co.,ltd., Ro71, Kannondou, Kanazawa, Ishikawa, Japan*

E-mail: b1350146@planet.kanazawa-it.ac.jp

1. Introduction

Ozone is strong oxidizing agent and used for sterilization of *E. coli* and deodorization [1]. Generally, the ozone yield by air-fed dielectric barrier discharge (DBD) without cooling system decreases drastically with increasing discharge power. This is because ozone is decomposed by heat and/or reduced by reacting with nitrogen oxides [2, 3]. Generally, the ozone generator operates with a continuous AC power supply. If we operate by applying intermittent AC voltage to the air-fed ozone generator without cooling system, the decrease of ozone yield will expected to be suppressed. In this paper, we investigated whether the ozone generation characteristics change or not by continuous and intermittent voltage application.

2. Experimental setup

Figure 1 shows an experimental setup. This system consists of a high voltage amplifier, a cylindrical DBD type ozone generator and measuring devices. 4.5 kV_p of sinusoidal voltage was applied to the ozone generator. The frequency (*f*) was changed between 20 and 30 kHz. Duty ratio (*d*) was changed between 10 and 50%. Discharge power was calculated from multiplying the area of *V-q* Lissajous figure by power frequency and duty ratio. A rod shaped electrode (outer diameter: 3 mm) wound with a stainless steel wire (diameter: 0.33 mm) was placed in the center of a grass tube (inner diameter: 5 mm, outer diameter: 7 mm). A grounded electrode was wound around the glass tube (length: 60 mm). Flow rate of dry-air was set to 4 L/min by a mass flow controller. Ozone concentration was measured by an UV absorption type ozone monitor. Plasma zone temperature was measured by a fiber optic thermometer.

Figure 2 shows an example of applied voltage waveform with f = 20 kHz and d = 50%.

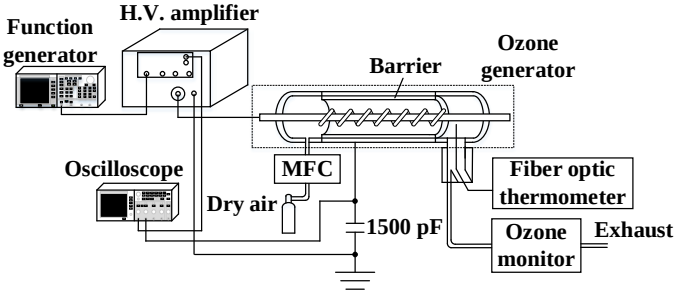

Fig. 1: Experimental setup

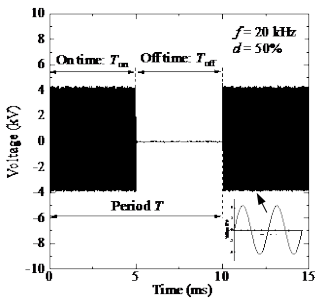

Fig. 2: Applied voltage

3. Results

Figure 3 shows time change of ozone concentration by continuous and by intermittent application of AC voltage. The discharge power of both cases was adjusted as same. The

maximum ozone concentration by continuous application of AC voltage was higher than that of by intermittent application. However, as the operating time increased, the ozone concentration by continuous application decreased faster than that by intermittent application.

Figure 4 shows ozone concentration and ozone yield at the operating time of 300 s. In this experiment, the frequency of the applied voltage was changed to 20, 25 and 30 kHz. At any frequency, the ozone concentration increased with increasing specific input energy (SIE). On the other hand, the ozone yield was almost constant (78 g/kWh) below 40 J/L. However, it decreased with further increase of SIE.

Figure 5 (a) shows the relation between ozone yield and plasma zone temperature at 300 s. Although ozone yield decreased with increasing plasma zone temperature, the maximum plasma zone temperature was below 80°C, which is lower than the decomposition temperature of ozone molecule (120°C). In order to clarify the influence of the generation of nitrogen oxides to the ozone yield decrease, the ozone generation characteristics by pure oxygen was investigated. In this case, nitrogen oxides are not generated. Figure 5 (b) shows the result. The ozone yield decreased with increasing temperature although nitrogen oxides do not exist. Therefore, we concluded that ozone yield decrease was due to the thermal decomposition of ozone molecule.

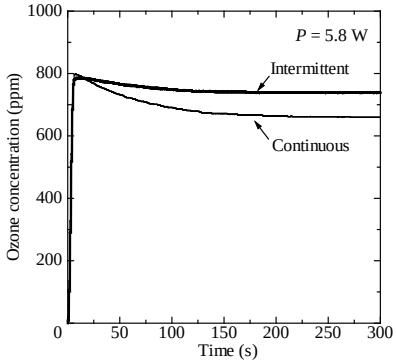

Fig. 3: Time change of ozone concentration.

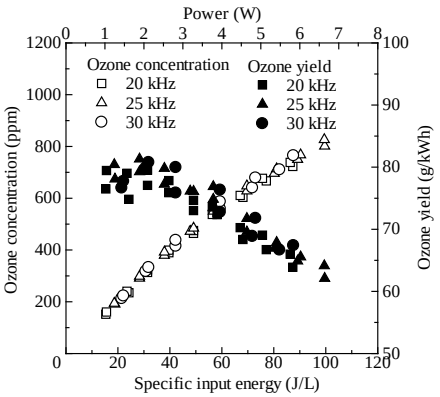

Fig. 4: Ozone concentration and ozone yield.

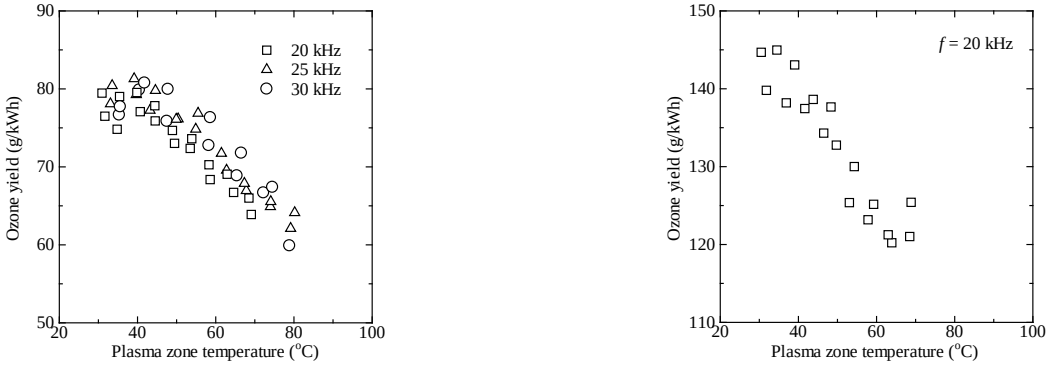

(a) air (b) oxygen

Fig. 5: Ozone yield as a function of plasma zone temperature.

References

[1] C. Yamabe, J. Plasma Fusion Res., Vol.74, No.2, pp.134-139 (1998)

[2] M. Taguchi, IEEJ Trans. FM, Vol.134, No.11, pp.585-590 (2014)

[3] D. Braun, U. Kuchler, and G. Pietsch, Pure & Appl. Chem., Vol.60, No.5, pp.741-746 (1988)

TEMPERATURE DISTRIBUTION IN OZONE GENERATOR WITH PARALLEL-PLATE CONFIGURATION AND FORCED AIR COOLING

Linsheng Wei, Haizhong Deng, Xin Liang, Yafang Zhang, Shukai Sun
School of Resources, Environmental and Chemical Engineering, Nanchang University, Nanchang 330031, China

E-mail: weilinsheng@ncu.edu.cn

In the process of ozone generation in low temperature plasma, most of electric energy more than 80% is emitted in the form of heat energy. Furthermore, the process is significantly impacted by temperature distribution particularly in discharge gap. However, there is no report about the temperature distribution in ozone generator because it is extremely difficult to obtain experimentally temperature distribution in discharge gap. In this work, the temperature distribution in a traditional parallel-plate ozone generator with forced air cooling is investigated numerically using software FloEFD. The ozone generator (size: 320mm×190mm×400mm) mainly consists of an AC power supply with frequency of 7.47 kHz, a discharge reactor with two cooling fins, a controller, and two ventilating fans. The discharge reactor with 90mm×120mm in valid area includes two parallel-plate electrodes, a dielectric barrier ceramic of 1mm in thickness attached to high voltage electrode, and a discharge gap of 1mm in thickness. The discharge gap is fed with pure oxygen (99.99%). Its flow rate and pressure are fixed at 1 slm and 760±5Torr, respectively. The discharge power is assumed to be deposited evenly on two electrodes. The effective coefficient of energy utilization can be determined based on the total reaction $3O_2 \rightarrow 2O_3$+144.8 kJ/mol and ozone concentration obtained by experiment. The results show that gas temperature in discharge gap gradually increases from room temperature to about 315 K along gas flow direction but has a slight decrease near outlet, and gradually decreases from high voltage electrode to grounding electrode owing to ceramic dielectric adjacent to high voltage electrode. Cooling fins make an important contribution to reduce the gas temperature in discharge gap. The power supply and controller only has small influence on temperature distribution because of their small power dissipation, the forced air cooling through two fans as well. The influence of important parameters on temperature distribution is also investigated, and the flow field is also obtained simultaneously. These results can be used to optimize the arrangement of ozone generator.

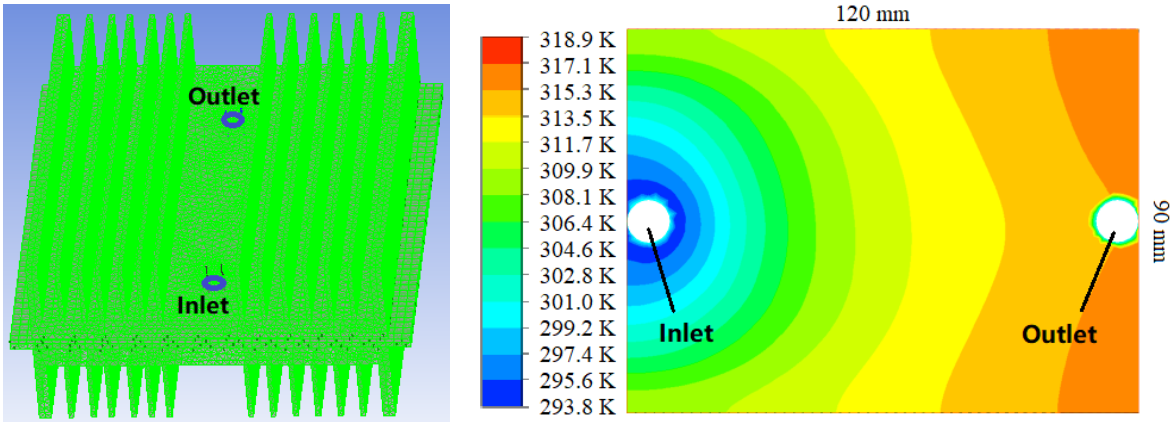

Fig. 1: The configuration of the discharge reactor (left) and the temperature distribution in discharge gap (right)

OBSERVATION OF ^1D-^1S FORBIDDEN OPTICAL EMISSION OF ATOMIC OXYGEN IN ATMOSPHERIC-PRESSURE N_2/O_2 PLASMA JET

Koichi Sasaki, Shusuke Nishiyama, and Naoki Shirai
Division of Quantum Science and Engineering, Hokkaido University, Japan

E-mail: sasaki@qe.eng.hokudai.ac.jp

Various types of atmospheric-pressure plasma jets, which employ rare gases for the discharges, have been developed to date. However, it is quite difficult to realize the ejection of a plasma jet from the nozzle when employing nitrogen for the discharge. We recently developed an atmospheric-pressure nitrogen plasma jet. In this work, we report an interesting change of the optical emission spectrum from the plasma jet by adding a small amount of oxygen into nitrogen.

The plasma source was composed of a quartz tube with an inner diameter of 4 mm, a tungsten rod electrode with a diameter of 1 mm, and a copper ring electrode which was attached on the outside of the quartz tube. The tungsten rod was placed at the center of the quartz tube, and was connected to a high-voltage ac (10 kHz) power supply. The rod electrode was not covered with dielectrics. The length of the copper ring electrode was 20 mm, and it was electrically grounded. Nitrogen was fed through the quartz tube at a flow rate of 7 l/min. In this discharge geometry, we observed the production of an asymmetric dielectric barrier discharge inside the quartz tube in the region corresponding to the length of the copper ring electrode. We observed the ejection of a jet with optical emission from the end (the nozzle) of the quartz tube. The optical emission from the jet part was collected using a lens and it was guided to spectrographs with different wavelength resolutions using optical fibers.

Figure 1(a) shows a photograph of the plasma jet which was operated using pure nitrogen. As shown in the figure, the active discharge zone inside the quartz tube emitted pink optical radiation. This is the normal color of nitrogen plasmas. On the other hand, the color of the jet part ejected from the nozzle was different and was yellow or orange. The optical emission spectrum of the yellow optical emission is shown in Fig. 2(a), indicating that the optical emission was mainly composed of the first and second positive systems of molecular nitrogen. Note that this spectrum was measured using a low-resolution spectrograph (USB2000), and we did not calibrate the wavelength dependence of the sensitivity in this spectrum. By referring intensive works carried out using flowing afterglows of medium-pressure ($0.1<P<10$ Torr) discharges [1,2], the jet part is considered to be a spatial afterglow and the optical emission is due to the energy transfer via vibrational excited states of molecular nitrogen (V-V pumping up).

Figure 1(b) was observed when we added oxygen at a flow ratio of 0.7%. The discharge color of the active discharge zone was not affected by the addition of oxygen, whereas the color of the jet part was changed from yellow to green dramatically. The optical emission spectrum of

the green plasma jet is shown in Fig. 2(b). As shown in the figure, we observed the disappearance of the first and second positive systems of molecular nitrogen, and the optical emission in the UV region was occupied by the β and γ systems of NO. The green optical emission shown in Fig. 1(b) is due to the emission around 558 nm which is indicated by an arrow in Fig. 2(b). A fine-resolution spectrum of the green emission is shown in Fig. 2(c). As shown in the figure, the green emission was composed of a sharp line at a wavelength of 557.73 nm and a broadband emission around it. The line emission was assigned as the ^1D-^1S transition of atomic oxygen. This is a forbidden line with a small transition probability of 1.26 s^{-1}, but it is well known that this line is the source of the green color of an aurora. The broadband tail component is the collision induced emission by the formation of the ON_2* excimer [3]. It is known that the collision with N_2 enhances the transition probability of the forbidden line [4].

As described above, in this work, we observed the ^1D-^1S forbidden optical emission from an atmospheric-pressure nitrogen plasma jet with the addition of a small amount of oxygen. We believe that the observation of the forbidden optical emission from the spatial afterglow of a small atmospheric-pressure plasma source is surprising and interesting.

[1] N. Sadeghi, C. Foissac, and P. Supiot, J. Phys. D: Appl. Phys. **34**, 1779 (2001).
[2] V. Guerra, P. A. Sa, and J. Loureiro, Eur. Phys. J. Appl. Phys. **28**, 125 (2004).
[3] I. P. Vinogradov and K. Wiesemann, Plasma Sources Sci. Technol. **6**, 307 (1997).
[4] G. Black, R. L. Sharpless, and T. G. Slanger, J. Chem. Phys. **63**, 4546 (1975).

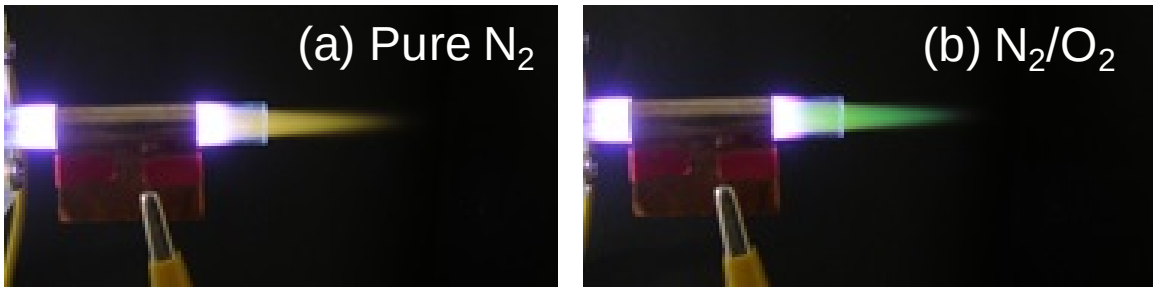

Fig. 1: Photographs of plasma jets employing (a) pure N_2 and (b) N_2/O_2 (0.7%) for discharges.

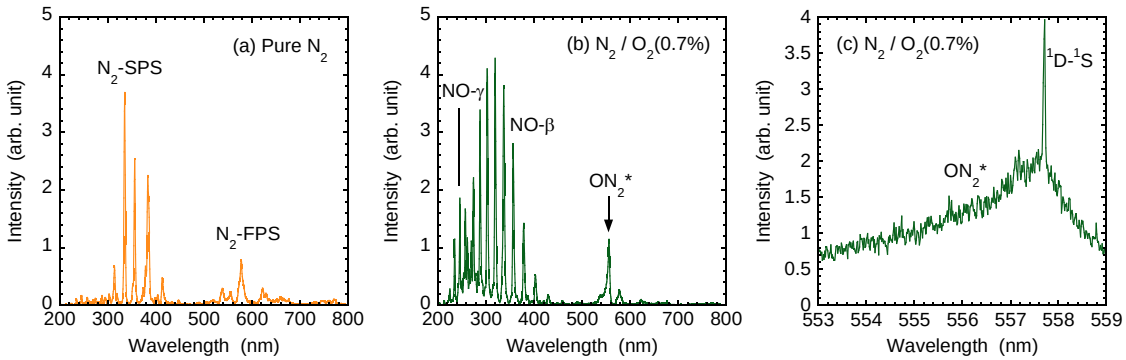

Fig. 2: Spectra of plasma jets employing (a) pure N_2 and (b) N_2/O_2 (0.7%) for discharges. (c) is a fine-resolution spectrum of a part of (b).

ANALYSIS OF ELECTRIC AND MAGNETIC FIELDS FROM PLASMA REACTOR INSTALLATIONS

Paweł A. Mazurek[1], Joanna Pawłat[1], Michał Kwiatkowski[1], Piotr Terebun[1]
[1] *Institute of Electrical Engineering and Electrotechnologies, Lublin University of Technology, Nadbystrzycka Street 38A, 20-618 Lublin, Poland*

E-mail: p.mazurek@pollub.pl

Plasma reactors for the production of low-temperature plasma are technological devices of great popularity as they have many applications. They are used in environmental protection - purification of air, water, sewage and soil, in biomedical engineering - for sterilization of surface, wounds and tools not resistant to high temperatures and in material technology, where they are used to change physico-chemical properties of the surface of materials [1-5].
Implementation of plasma reactor installations requires a good design with an optimized power supply. This is due to the fact, that plasma reactors are typical energy receivers with non-linear characteristics, and their operation requires high voltages, also at high frequencies. In practice, power circuits can be reduced to solutions based on transformers or systems with power electronics elements [1-5].
From the operator's point of view, continuity of work and stability of plasma parameters are desirable. Reactors are subjected to high quality and safety requirements. Information about the radiation of electric and magnetic fields is important. Reactors and their installations are the source of electrical and magnetic fields because they convert electricity for plasma generation. Electromagnetic fields in the environment of the reactor installation can cause undesirable effects. The basic parameters that characterize this environment in relation to human exposure are the intensity of electric fields (E), the intensity of magnetic fields (B), the energy absorption coefficient (SAR) and the frequency of the sinusoidal fields in time.
In the Institute of Electrical Engineering and Electrotechnologies there are several constructions of plasma reactors. Four installations have been tested: three-electrode construction, with two ignition electrodes (3-phase GlidArc reactor); compact, single-phase plasma reactor with gliding arc discharge, “plasma jet” reactor with DBD barrier discharge and installation of a reactor powered by radio frequency (RF) power supply.
The Mashek ESM100 meter was used to test plasma reactors mentioned above. ESM100 is a hand-held measuring instrument which allows easy measuring of alternating electric and magnetic fields at the same time. It is equipped with an isotropic electromagnetic field sensor. It has a measuring range 1 nT – 20 mT, 0.1 V/m – 100 kV/m, and frequency 5 Hz – 400 kHz.
Because the reactors work for scientific purposes, the working gases during their operation were nitrogen, argon, oxygen and the air mixture. All gases were compressed in cylinders, and through the gas delivery and regulation system they were directed to the discharge chamber. Emission measurements concerned analysis in the immediate vicinity of the discharge chamber. Electromagnetic interactions must be analyzed in the low and high frequency range. This is the effect of the permissible human exposure and EMC requirements.

Presented measurements were carried out in the low frequency range (5 - 2000 Hz). Typical field values in the laboratory environment are approximately 40 nT and 20 V/m in that frequency range. When the reactor installation is switched on, field values increase significantly. For example, the results of the tests from the “plasma jet” reactor with DBD barrier discharge installation were presented. The photograph presents the installation with measuring points. Around reactor, it was found that the magnetic fields were several dozen μT and the values of electric field strength were several dozen kV/m. Small magnetic field values were observed at the plasma head.

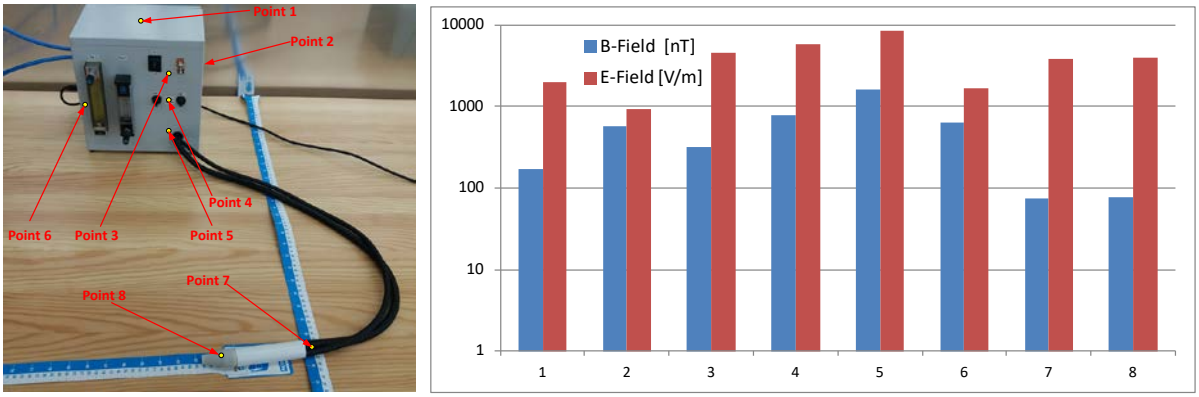

Fig. 1: DBD reactor installation with measuring points and the results of field strength values at several points around the reactor installation

Electric and magnetic fields in the environment can cause undesirable effects. National and European regulations are the basis for monitoring the strength of that fields and exposure limits. The fields values were different for different reactor installations and different working gases. Monitoring is needed where danger could arise - incompatible work of electric devices or dangerous exposure for humans. The measured values are compared with the limits of standards. Research results show that electric and magnetic fields are safe for personnel.

Bibliography

[1] Stryczewska H., Technologie plazmowe w energetyce i inżynierii środowiska, Politechnika Lubelska, 2006

[2] Mazurek P.A., Pawłat J., Badania natężeń pól elektrycznych i magnetycznych generowanych przez instalację reaktorów plazmowych, Rocznik Ochrona Środowiska 2016, nr 2, vol. 18, s. 567-578

[3] Mazurek P.A., Pawłat J., Kwiatkowski M., Terebun P., Analysis of electrical and magnetic fields in ELF band from plasma reactor installations, International Conference on Electromagnetic Devices and Processes in Environment Protection with Seminar Applications of Superconductors (ELMECO & AoS) 2017, WOS; New York: IEEE, 2017

[4] Pawłat J., Starek A., Sujak A., Kwiatkowski M., Terebun P., Budzeń M., Effects of atmospheric pressure plasma generated in GlidArc reactor on Lavatera thuringiaca L. seeds’ germination, PLASMA PROCESSES AND POLYMERS 2017, nr 2, vol. 15

[5] Pawłat J., Starek A., Sujak A., Terebun P., Kwiatkowski M., Budzeń M., Andrejko D., Effects of atmospheric pressure plasma jet operating with DBD on Lavatera thuringiaca L. seeds' germination, PLOS ONE - 2018, nr 4, vol. 13

[6] Impact of radio-frequency atmospheric-pressure plasma on water contact angles of high-impact polystyrene / Terebun Piotr, Kwiatkowski Michał, Mazurek Paweł, Pawłat Joanna // SENSORS AND MATERIALS - 2018, nr 5, vol. 30, s. 1213-1220

Detection of phthalates using Corona Discharge Ion Mobility Spectrometry – Mass Spectrometry (CD IMS-MS)

B. Michalczuk[1], L. Moravský[1], M. Sabo[2] and Š. Matejčík[1]

[1]*Comenius University, Faculty of Mathematics, Physics and Informatics, Bratislava, Slovakia*

[2] *MaSa Tech, s.r.o.*

E-mail: matejcik@fmph.uniba.sk

In recent years phthalates have been accused of showing negative impact on human health. Breast cancer in females or mental and motor development in children can be caused by long term exposure on phthalates [1]. Therefore it is important to have a fast, sensitive and high resolution technique for their detection. The most common techniques for detection of phthalate esters are gas chromatography coupled with mass spectrometry (GC-MS) and high-performance liquid chromatography (HPLC) [2][3].

In our laboratory we have developed Corona Discharge Ion Mobility Spectrometry combined with orthogonal acceleration time of flight spectrometry technique (IMS-oaTOF) [4] for high resolution separation of complex samples and isomeric compounds. This technique we have applied also for studies of phthalates

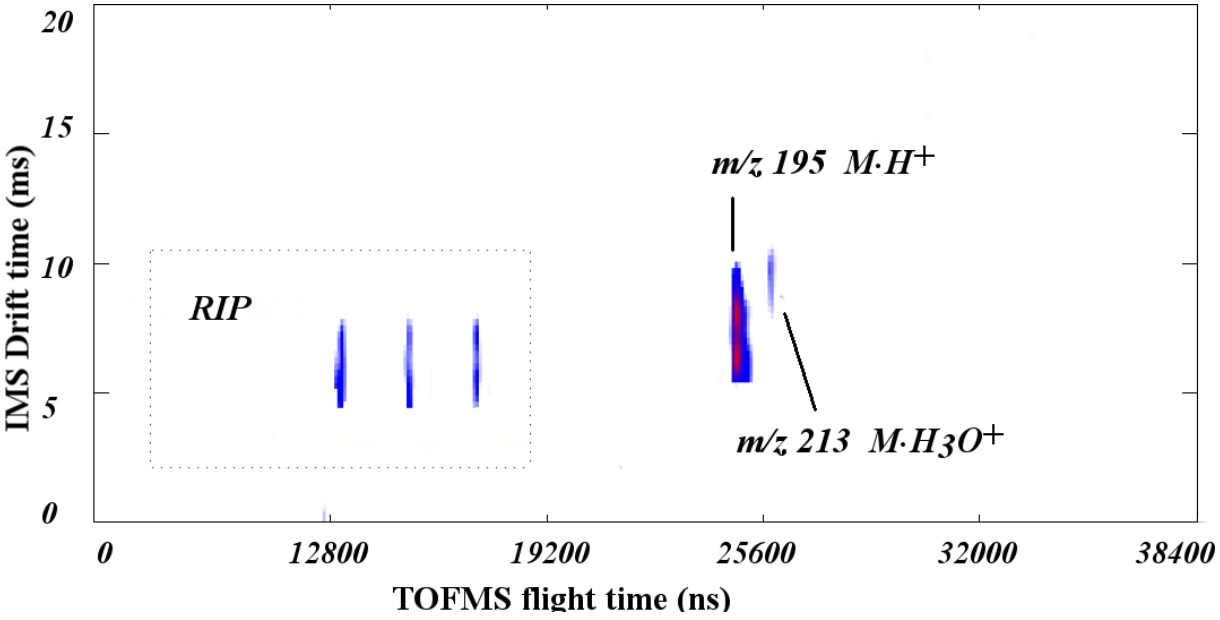

Fig. 1: Two dimensional spectrum of dimethyl phthalate.

We have investigated several phthalates (dimethyl phthalate (DMP), diethyl phthalate (DEP) and dipropyl phthalate (DPP)) using the IMS-oaTOF technique. The ionisation of the phthalates was on the basis of Atmospheric Pressure Chemical Ionisation. The reactant ions formed in CD ($H_3O^+.(H_2O)_n$, n=2,3) reacted via proton transfer reaction with phthalates resulting in formation protonated and hydronium attached monomer $M.H^+$, $M.H_3O^+$ and dimer ions $M_2.H^+$, $M_2.H_3O^+$ (M represents the phthalates molecule). In the Figure 1 we present 2-

dimensional (2D) IMS (y-axis) and MS (x-axis) spectrum of dimethyl phthalate. In this case only the protonated and hydronium attached ions are formed.

Acknowledgements

This work has been supported by European Union's Horizon 2020 research and innovation programme under the Marie Skłodowska-Curie grant agreement No 674911 and innovation programme under grant agreement No 692335, additionally Slovak Research and Development Agency Project Nr. APVV-15-0580 and the grant agency VEGA, project Nr. VEGA-15-089 support is acknowledged.

References

[1] T. Schettler, Int. J. Androl., 29 (2006) 134-139,

[2] A.O. Earls et al., J. Chromatogr. A 983 (2003) 237–246,

[3] J. Fisher et al., Chromatographia 37 (1993) 47-50,

[4] A.J. Midey et al., Analytica Chimica Acta 804 (2013) 197–206,

Ozone assisted NO_x oxidation and adsorption on metal-oxides

Indrek Jõgi[1], Kalev Erme[1], Jüri Raud[1]
[1]*Institute of Physics, University of Tartu, W. Ostwaldi str. 1, Estonia*

E-mail: indrek.jogi@ut.ee

NO_x (NO and NO_2) are important pollutants emitted during fossil fuel burning. The main constituent of the NO_x is NO which is difficult to remove by purely absorption- or adsorption-based methods. One possible solution for this problem is the ozone oxidation of NO to NO_2 and then further to N_2O_5. We have shown that the efficiency of NO_2 oxidation to N_2O_5 can be improved by the presence of metal oxides which can act both as catalysts and adsorbents [1-2]. The aim of the present study was to further investigate the catalytic properties of TiO_2, Fe_2O_3 and Al_2O_3 and to compare the adsorption of NO_x on these materials at varying experimental conditions.

The concentration of NO in the mixture of N_2 and O_2 was varied between 200-800 ppm. The flow rates of N_2 and O_2 were both 0.5 L/min. Ozone was produced from the pure O_2 by a dielectric barrier discharge reactor and was directed through the reaction chamber which contained the metal-oxide powder and could be heated up to 140°C. The concentrations of gas-phase reaction products were measured at the outlet of the reaction chamber by UV absorption spectroscopy.

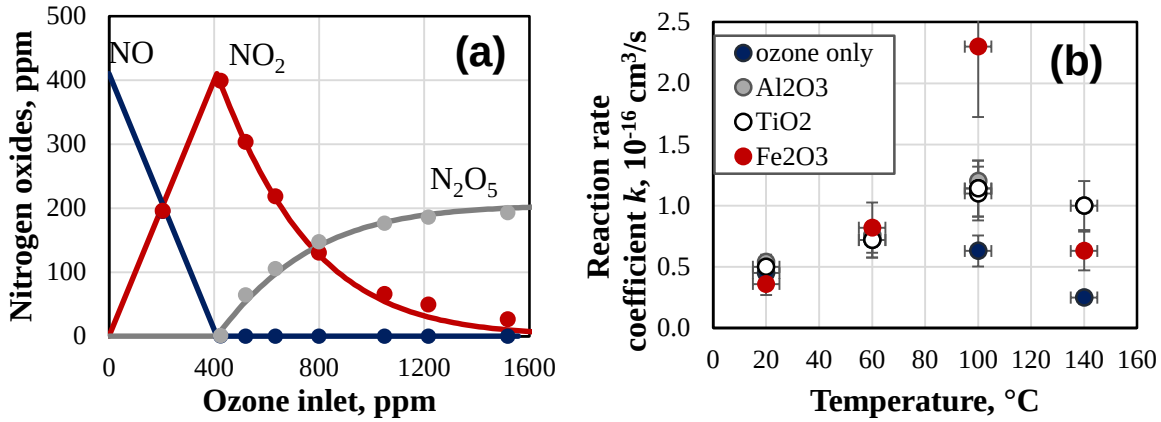

Fig. 1: (a) - outlet concentrations of nitrogen oxides as a function of inlet ozone concentration at NO inlet concentration of 400 ppm and reactor temperature 20°C. Circles denote experimental points and lines the theoretical fit by equation (1). (b) - efficient reaction rate coefficient *k* for NO_2 oxidation to N_2O_5 as a function of reactor temperature.

At all experimental conditions, NO was initially oxidized to NO_2 and N_2O_5 started to form from NO_2 only when all NO was removed (Fig. 1a). The oxidation of NO to NO_2 was linear function of ozone concentration whereas the oxidation of NO_2 to N_2O_5 could be described by equation

$$[NO_2] = [NO]_0 \frac{2\frac{[O_3]_0}{[NO]_0} - 3}{\left(2\frac{[O_3]_0}{[NO]_0} - 2\right) e^{\left(2\frac{[O_3]_0}{[NO]_0} - 3\right)[NO]_0 kt} - 1} \qquad (1)$$

where $[NO]_0$ and $[O_3]_0$ are the inlet NO and ozone concentrations, t is the residence time in the reactor and k is the effective reaction rate coefficient [3]. The value of k describes the ozone oxidation efficiency of NO_2 to N_2O_5 and allows to compare various metal-oxides when all other experimental conditions remain the same. Figure 1b shows the value of k as a function of temperature for TiO_2, Fe_2O_3 and Al_2O_3. The values are obtained in the absence of metal-oxide are also shown for comparison. All metal-oxides started to improve the oxidation at reactor temperatures above 60°C. Highest improvement was obtained with Fe_2O_3. The experiments with TiO_2 showed that the change of metal-oxide mass in the range of 0.3-0.9 g had no effect on the catalytic activity.

The adsorption of NO_x on the surface of metal-oxides increased with increasing inlet ozone concentration and there was an abrupt increase of adsorption capacity when all NO was oxidized to NO_2 and N_2O_5 appeared in the outlet (Fig. 2a). At even higher inlet ozone concentrations, the absorbed amount of NO_x saturated. The adsorbed amount of NO_x was proportional with the mass of metal-oxide in the limits of measurement uncertainty.

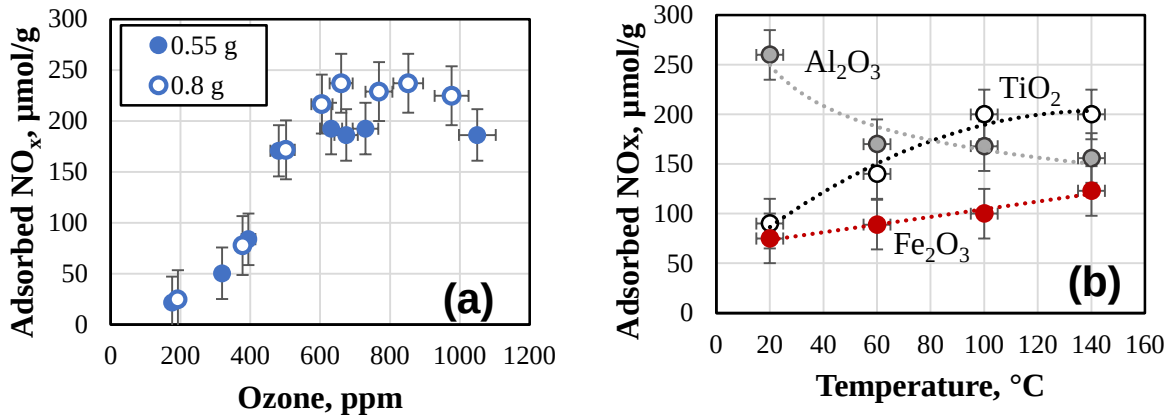

Fig. 2: (a) – nitrogen oxide adsorption on the TiO_2 surface as a function of ozone inlet concentration for TiO_2 powder with different total mass. NO inlet concentration was 400 ppm and reactor temperature 100°C. (b) – highest amount of adsorbed nitrogen oxides as a function of reactor temperature for different metal-oxides.

The maximum adsorption capacities of metal-oxides reached at high inlet ozone concentrations are shown on figure 2b. In the case of TiO_2 and Fe_2O_3, the adsorption capacity increased with temperatures whereas the adsorption capacity of Al_2O_3 was highest at room temperature. At the temperature of 100°C, the adsorption capacity of TiO_2 was almost two times higher than Fe_2O_3 and the adsorption capacity of Al_2O_3 remained between the values of other materials.

[1] I. Jõgi, K. Erme, J. Raud, M. Laan, Fuel **173**, 45 (2016)
[2] I. Jõgi, K. Erme, A. Haljaste, M. Laan, Eur. Phys. J. Appl. Phys. **61**, 24305 (2013)
[3] I. Jõgi, K. Erme, E. Levoll, J. Raud, E. Stamate, Plasma Sources Sci. Technol. **27**, 035001 (2018)

Experimental study in removal of tetracycline in simulant water by dielectric barrier discharge plasma

Yunqiu Cui, Jiushan Cheng, Qiang Chen
Laboratory of Plasma Physics & Materials, Beijing Institute of Graphic Communication, Beijing, China

E-mail: jscheng@bigc.edu.cn; lppmchenqiang@hotmail.com

In this paper, the tetracycline in the simulant water is moved by a dielectric barrier discharge (DBD) plasma. We focus on the power parameters. The three power sources are employed in DBD plasma. The effect of the pulsed power and the high frequency sinusoid power on removal efficiency of tetracycline is then compared. The experimental results show that pulsed DBD plasma can much effectively remove tetracycline in stimulant water. The tetracycline is nearly completely decomposed by the pulsed DBD plasma in a short time. When the pulsed power supply is working in 50ns rising/falling edge, the removal rate is up to 90% ($k=0.15min^{-1}$) in 10min, and the energy efficiency is over 0.5g/kWh. The process follows the first-order kinetics. It is found that the degradation of tetracycline is prefer to argon/air plasma mainly due to the increasing concentration of •OH in this plasma based on the optical emission spectra diagnostic. With the liquid chromatography-mass spectrometry (LC-MS) analysis, we notice that the tetracycline is destroyed and small molecules are formed after 2 min plasma treatment, and the small substances are increased after 10min. The path of degradation of tetracycline in the pulsed plasma is then presumed.

Interface reactions between water and drift positive ions

Zhongshu Zhang, Tao Wang, Scott MacGregor, Igor Timoshkin
Electronic and Electrical Engineering, University of Strathclyde, Glasgow, United Kingdom, G1 1XW

E-mail: zhongshu.zhang@strath.ac.uk

The interface reactions between plasma and water have been studied extensively. Hydroxyl radicals are produced via water dissociation by electrons, positive ions and active species etc. The dimerization of hydroxyl radicals is a major pathway of hydrogen peroxide formation in water under streamer discharge on water surface. This work focused on the reactions between water and drift positive ions generated by corona discharge, and the mechanisms of reactive species formation in water. Corona discharge from a multi-needle anode in nitrogen produced positive ions drifting towards the water surface with a constant DC current of 30 uA.

The number ratio of hydrogen peroxide formed in water under atmospheric pressure to the drift positive ions was measured to be 0.26. The hydrogen peroxide was formed via two pathways: one is the direct reaction of positive ions and water molecules, which contributed 50% of the hydrogen peroxide formation; the remaining 50% was produced from the corona-produced neutral reactive species reacting with water.

The amount of hydrogen peroxide increased as the nitrogen pressure decreased from 760 to 100 Torr. At 100 Torr, the number ratio of hydrogen peroxide to the drift positive ions was increased to 0.44, of which 0.29 was contributed by the direct reactions between positive ions and water. The increase in ion contribution is thought due to the increase of the kinetic energy of ions, leading to a change in reaction mechanisms between positive ions and water. Hydrogen peroxide produced by the neutral reactive species is almost unchanged with pressure drop.

The hydrogen peroxide was found to be formed directly from the interactions between water and positive ions and neutral reactive species, rather than the dimerization of hydroxyl radicals.

ATMOSPHERIC-PRESSURE PLASMA TREATMENT OF FLOAT GLASS AS SURFACE CLEANING AND ACTIVATION PROCEDURE PRIOR TO COATING

Dušan Kováčik[1], Slavomír Sihelník[1], Jakub Kelar[1], Zlata Tučeková[1], Richard Krumpolec[1], Miroslav Zemánek[1], Monika Stupavská[1], Jozef Ráheľ[1], Oliver Beier[2], Jost Wittwer[3], Andreas Pfuch[2], Bernd Grünler[2], Mirko Černák[1]
[1]*Masaryk University, Faculty of Science, CEPLANT, Department of Physical Electronics, Kotlářská 2, 61137 Brno, Czech Republic*
[2]*Innovent e.V. Technology Development Jena, Prüssingstraße 27B, 07745 Jena, Germany*
[3]*Polartherm Flachglas GmbH, Eichenallee 2, 01558 Großenhain, Germany*

E-mail: dusan.kovacik@mail.muni.cz

Cleaning and preparation of solid surfaces such as of glass or metals are one of the most crucial stages of material processing. Surface cleaning is the preliminary stage of almost every surface treatment and preparation process including surface printing, painting or coating with protective or other functional layers that makes products useful for industrial applications. It should be noted that the majority of glass products would not have the properties that make them so useful without coatings. Therefore, applications of coatings are an essential part of glass manufacturing. Currently, cleaning of glass surfaces prior to coating or further glass processing (e.g. laminated safety glasses) is primarily done by the combination of mechanical and wet chemical processes. Tight restrictions on hazardous waste disposal and workplace safety regulations have made wet cleaning increasingly expensive and unpractical. Atmospheric-pressure plasma processes offer several advantages compared to conventional chemical cleaning methods such as low-temperature environment, elimination of the problems associated with wet chemistry, favourable environmental impact without liquid waste and hence without the need for expensive waste disposal. Moreover, using plasmas is a simple process usually requiring only little supervision.

In this contribution, we present the results of a bilateral project on the surface activation and cleaning of soda-lime sheet glasses using atmospheric-pressure plasmas. For surface treatment of areal glass sheets provided by Polartherm Flachglas GmbH (Großenhain, Germany) different atmospheric-pressure plasma sources shown in Fig. 1 with further potential for large area up-scaling were used: *Diffuse coplanar surface barrier discharge (DCSBD), volume dielectric barrier discharge (VDBD), multi-hollow surface dielectric barrier discharge (MHSDBD), plasma beam and jets, and glide arc.* As a working gas either ambient or pressurized air was used. For each plasma source, we tried to determine the optimal treatment conditions such as treatment time, power, working gas or distance of glass sheet from electrode system. The effect of glass cleaning by plasmas in dependence on plasma parameters was evaluated by water contact angle measurement, atomic force microscopy AFM and spectroscopic methods

FTIR, UV/Vis, and XPS. The stability of the treatment was examined in relation to the flowing time after the treatment (8 hours, 1 day, 3 days and 1 week).

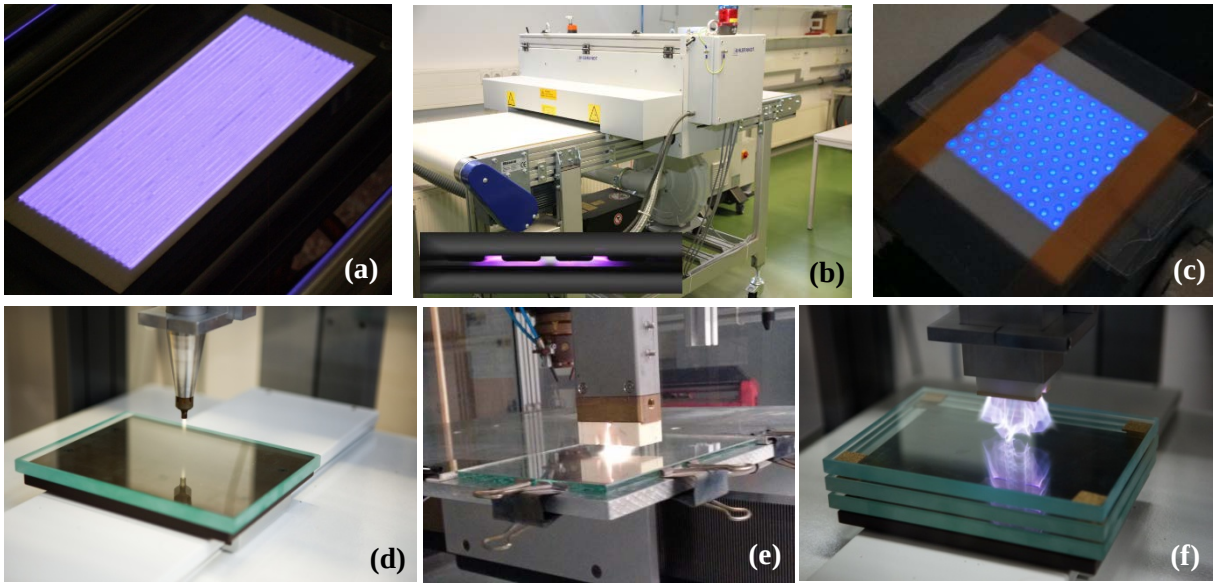

Fig. 1: Illustrative photos showing the individual atmospheric-pressure plasma sources used for float glass treatment: DCSBD (a), VDBD – Ahlbrandt System GmbH Panel Treater (b), MHSDBD (c), plasma beam – Diener electronic GmbH + Co. KG (d), plasma jet – Tigres GmbH Plasma CAT (e), glide arc - Diener electronic GmbH + Co. KG (f).

For all plasma sources used in the present study of glass cleaning, a significant decrease of water contact angle values was achieved. However, the treatment of glass by glide arc led to inhomogeneous treatment. Due to the thermal damage of glass during the treatment by plasma beam this method has proved to be inappropriate also. The significant decrease of water contact angle with satisfactory surface homogeneity was achieved by the MHSDBD but we observed the immediate ageing effect of the plasma treatment. The most effective treatment of glass was observed after plasma treatment using DCSBD when the lowest values of water contact angle (5.5° ± 0.5°) as well as the most homogeneous and the most durable effect of treatment were achieved. For such high-quality plasma treatment it is crucial to keep the glass sheet at a precise effective distance ~ 0.3 mm from the ceramic plate of DCSBD without any contact. For this purpose, the contactless method of glass leading termed as “DCSBD Air Pillow” was developed and successfully verified.

This research has been supported by the project CZ.01.1.02/0.0/0.0/16_053/0007132 funded by European Regional Development Fund and by the German BMWi under project No. ZF 4028609AG6.

INVESTIGATION OF ATMOSPHERIC PRESSURE PLASMA SURFACE MODIFIED ZIRCONIUM DIOXIDE NANOPOWDER BY THERMAL DESORPTION SPECTROSCOPY

Ján Dugáček[1], Lubomír Prokeš[1], Pavel Sťahel[1], Jozef Ráheľ[1], Martina Ilčíková[1]
[1]*CEPLANT – R&D Centre For Low-cost Plasma and Nanotechnology Surface Modifications, Masaryk University, Kotlářská 2, 611 37 Brno, Czech Republic*

E-mail: jan.dugacek@gmail.com

Zirconium dioxide nanopowder is a chemically stable, in water insolvable and non-toxic white powder material commonly used for removing dissolved materials from water and sintering into ceramics with attractive mechanical properties. Atmospheric pressure plasma was used for improve its wetting properties. To resolve created hydration state which play important role during wet process the thermal desorption spectroscopy was used as a well sensitive indicator. Thermal desorption technique is able to give us information about bonding energy of particular hydratation states according to their thermal stability.

Keywords: DCSBD, thermal desorption, zirconium dioxide nanopowder

Nanopowders are a group of materials with unique characteristics owing to the small grain size that makes their surface properties not negligible compared to their bulk properties [1]. Zirconium dioxide nanopowder has many applications in removing dissolved contaminants like phosphate or arsenic from water. Zirconium dioxide itself is trivial to remove from water because of its low solubility [2][3]. Additionally, the nanopowder can be sintered into ceramic materials with attractive mechanical properties [4]. We have studied the modification of its properties after treatment in atmospheric plasma generated by Diffuse Coplanar Surface Barrier Discharge (DCSBD), a type of atmospheric discharge with open geometry and high plasma density [5] at power 500W with frequency 30 kHz for 30s using thermal desorption spectroscopy (TDS) method. This method analyses the dependence of thermally desorbed materials as a function of temperature [6]. Thermal desorption spectra of plasma treated zirconium dioxide nanopowder are completely different in comparison with untreated nanopowder TDS spectra which is shown in Figure 1. Example of TDS spectra measured for the plasma treated nanopowder is shown in Figure 2. Both samples contain major desorption peaks around temperature 150°C, mainly at masses 18 amu. and 44 amu.

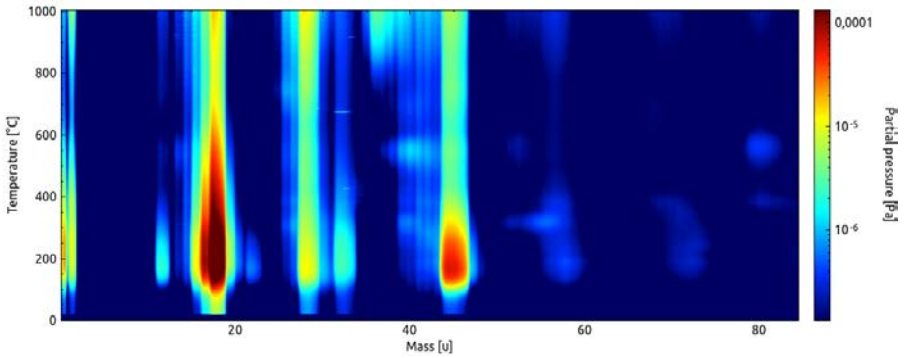

Fig. 1: Thermal desorption from the untreated nanopowder

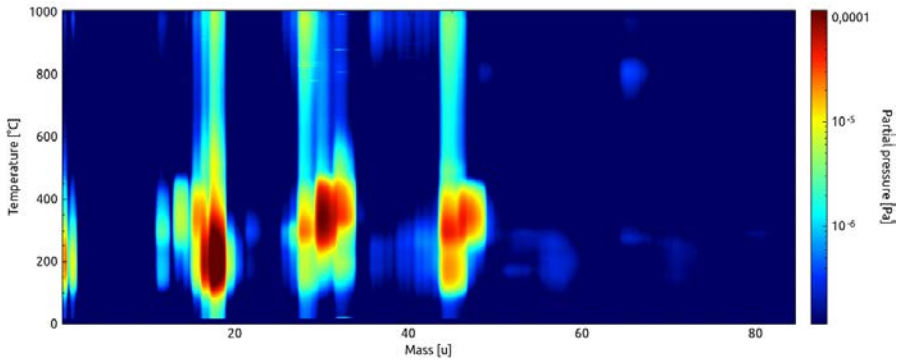

Fig. 2: Thermal desorption from the nanopowder after treatment in DCSBD

A major difference between the plasma treated and untreated sample is observed around temperature 300°C, where additional desorption peaks appeared in the spectra for the plasma treated sample. This difference is well visible in thermal desorption spectra measured at 300 °C see Figure 3.

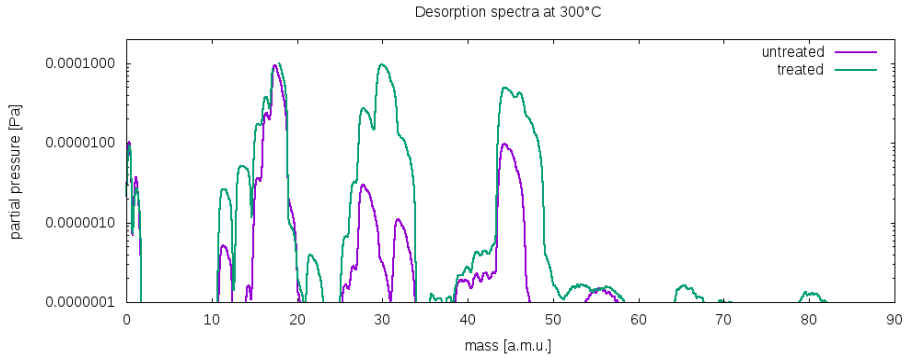

Fig. 3: Comparison of thermal desorption spectra at temperature 300 °C

This study proved that TDS is useful tool for detection of plasma induced changes of powder materials. It provides information about bonding energy of particular hydratation states according to their thermal stability. Correlation of thermal desorption peaks with chemical composition of plasma treated and untreated powders was analyzed using FTIR and will be included in the presented paper.

References

[1] D. Mondelaers et al., Mater. Res. Bul., 37 (2002)
[2] Yu Su et al., Water Res., 47 (2013)
[3] Hang Cui., J. Ind. Eng. Chem., 18 (2012)
[4] Martin Trunec, Karel Maca, J. Am. Ceram. Soc., 90 (2007)
[5] M. Černák et al., Eur. Phys. J. Appl. Phys., 47 (2009)
[6] L. Zábranský et al., Surf. Coat. Tech., 267 (2015)

Acknowledgement

The work was financially supported by the Czech Science Foundation, contract No. GA17-05620S, project CZ.1.05/2.1.00/03.0086 funded by European Regional Development Fund and project LO1411 (NPU I) funded by Ministry of Education, Youth and Sports of Czech Republic.

THE USE OF DBD PLASMA ACTIVATED POWDERS IN CERAMIC PROCESSING

Jozef Rahel[1], Martina Ilcikova[1], Jan Dugacek[1], Daniel Drdlik[2,3], Vaclav Pouchly[2,3]
[1]*Dept. of Physical Electronics, CEPLANT, Masaryk University, Brno, Czech Republic*
[2]*CEITEC BUT, Brno University of Technology, Brno, Czech Republic*
[3]*Faculty of Mechanical Engineering, Brno University of Technology, Brno, Czech Republic*

E-mail: rahel@mail.muni.cz

Fine Al_2O_3 and ZrO_2 submicron powders were activated in atmospheric pressure air by a coplanar dielectric barrier discharge (DBD) and studied for its impact on ceramic wet processing. As expected, DBD activated powders exhibited an improved stability in water dispersion. Less expected was the positive effect on the porosity of slip casted green-body, and microstructure of final sintered ceramics, which had shown more than 2-fold smaller grains in comparison to the reference samples. The coplanar DBD treatment had a dramatic effect on the process of electrophoretic deposition (EPD) of powders dispersed in non-aqueous organic solvent. The treatment resulted in a substantial improvement of surface roughness of deposit (Fig. 1), smaller mean grain size and slightly higher relative density. The dynamics of EPD was affected significantly, as the process had switched to the opposite polarity electrode. Performed thorough analysis of activated surfaces (FTIR, XPS, thermoluminescence TG and TDS) pointed out the importance of DBD originated molecular gases, adsorbed of the powders surface [1]. A critical factor in achieving the desired results is a proper handling of powders within the active plasma zone.

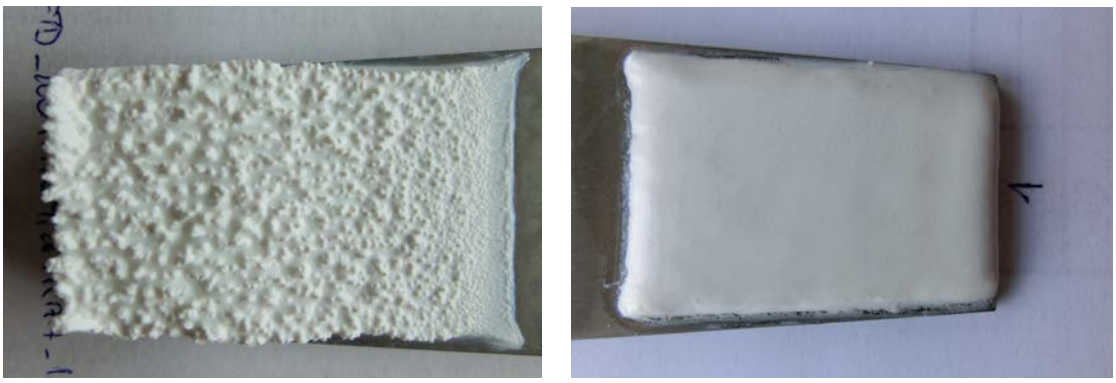

Fig.1: Surface roughness of EPD layer from untreated (left) and DBD treated submicron Al_2O_3 powders

Acknowledgement: The work was financially supported by the Czech Science Foundation, contract No. GA17-05620S, project CZ.1.05/2.1.00/03.0086 funded by European Regional Development Fund and project LO1411 (NPU I) funded by Ministry of Education, Youth and Sports of Czech Republic.

[1] Drdlik, D et al., Ceramics International, doi: 10.1016/j.ceramint.2018.02.215

THE SURFACE TREATMENT OF LIQUID CRYSTAL POLYMER USING ATMOSPHERIC PRESSURE GLOW DISCHARGE

Kunihito Tanaka, Kazuo Takahashi, Masuhiro Kogoma
Department of Materials and Life Sciences, Faculty of Science and Technology, Sophia University, 7-1 Kioi-cho, Chiyoda-ku, Tokyo 102-8554, Japan

E-mail: m-kogoma@sophia.ac.jp

1. Introduction

The Liquid Crystal Polymer (LCP) exhibits low water absorption, low gas permeability, low dielectric loss at high frequency, high temperature tolerance and the cost lower than other super engineering polymers. LCP has many advantages to be applied for the electric devices such as flexible print circuit board, normal solid circuit board, connector and so on. In case of the film, the extruded LCP films by melted polymer (Sumika Super LCP) shows higher shear failure strength than that of the general industrial plastics such as PEEK.

The LCP has a hydrophobic nature, because of the full aromatic chemical structure that composed with three part of chemical clusters, *p*-hydroxybenzoic acid, *p, p'*-biphenol, and terephthalic acid. Normaly, the surface oxidation is needed to add the adhesive ability with adhesive. On the other hand, for the multiple layer production of LCP films to produce the flexible print circuit, we need self-adhesion ability with thermocompression for the high temperature application. The first target of present study is to make the adhesive surface by epoxy glue on the composite LCP plate that reinforced by short staple glass fiber. And the second target is to refine the self thermocompression bonding ability of LCP films to produce the multiple layer film.

2. Experimental

Two types of the discharge systems were used for the surface oxidation and the surface activation. The first one was the parallel plate electrodes reactor in the glass chamber to take the oxidation of the surface using He-O_2 as shown in figure 1. In the case, the sample was set on the lower electrode. The second one was the scanning type discharge system using transfer

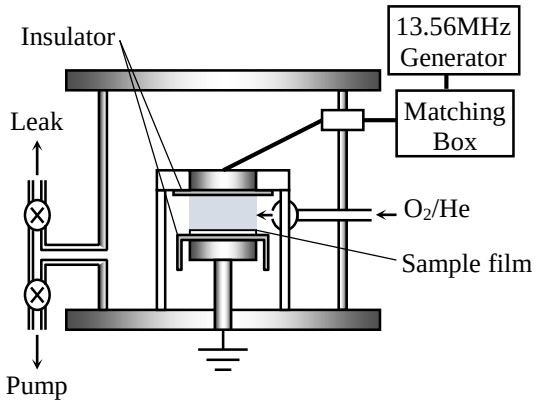

Fig. 1 Parallel plate electrodes dischrage system (type 1).

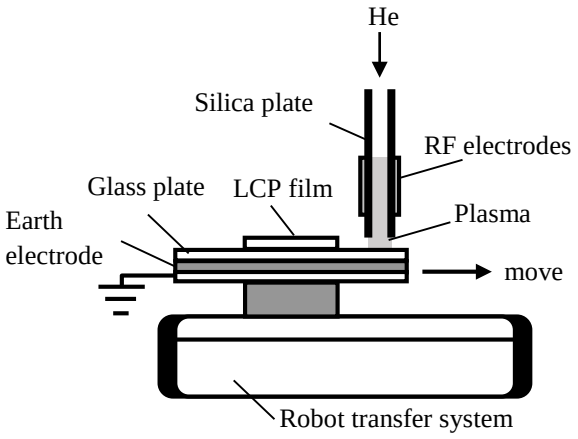

Fig. 2 Transfer robot discharge system (type 2).

robot to irradiate the film surface in the atmospheric ambience as shown in figure 2. The upper

electrode that connected to RF high voltage was installed right angle to the treatment surface. The inter space between the sample film and the plasma jetting port was 2 mm. RF (13.56 MHz) discharges were used in the both discharge systems.

3 Results and Discussion

3.1 Surface oxidation on the LCP-glass fiber composite plate.

For the surface oxidation to take the wettable surface in the type 1 system, He-O_2 mixture gas (10 - 30 sccm of O_2 mixed with 2 slm of He) was introduced and discharged with 200 W RF power. The sample size was 2cm × 1cm × 1mm. The surface adhesibility of the treated samples were measured with epoxy glue and the tensile tester (Heidon,14D). In the figure 3, the water contact angles were decreased with increasing of the treatment times. After the surface treatment, we got extremely good results for all adhesion tests pieces.

3.2 Adhesion less adhesion (Thermocompression) of films.

From the reason of the liquid crystal structure, LCP is very easy to deform or melt come close to the softening temperature. It conduce strong difficulty of thermocompression for the self-adhesion of LCP films. M. Kogoma et al reported that different kind of polymer films could adhere by thermocompression using He plasma irradiation on the polymer surfaces [1]. So we will present the surface treatment of LCP film by irradiation of He plasma to refine the self-thermocompression property. In the case, a couple of LCP film (2.5cm × 12cm × 25μm), were irradiated both side by He plasma using type 2 system in the atmosphere. The each irradiated side of the films were super imposed and then 5 minutes thermo-compressed at 270 ℃ in 1 ton pressure. The peering force of the test piece (adhered film) was measured using tensile tester (Minebea, LTS 200NB). Figure 4 shows the peering force of the test piece as a function of the film treatment time. The peeling forces were increased with increasing of the treatment times. Increasing rate of the peeling force at the early time was very much depended on the discharge power. At the plateau in the figure, all peeled film surfaces show cohesive failure. We will discuss all about the results in the conference.

[1] M. Kogoma, A. Manabe, and K. Tanaka, P Proc. 19th Inter. Symp. Plasma Chem. (2009).

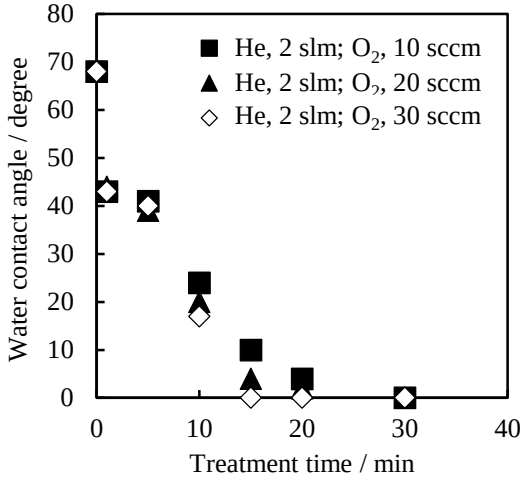

Fig. 3 Water contact angle of LCP composite plate as a function of the treatment time.

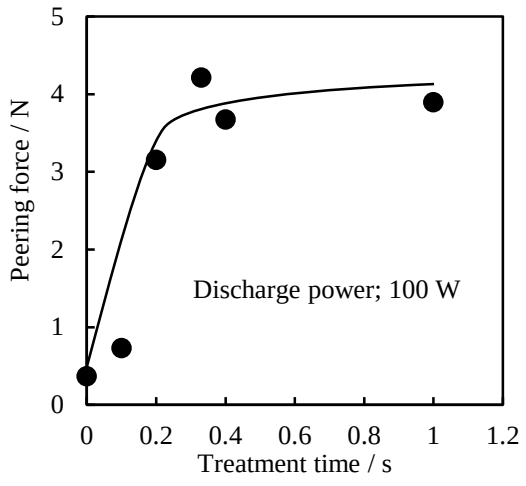

Fig. 4 Peering force of the test piece as a function of the He plasma treatment time.

COOLING SYSTEM OF RF PLASMA JET FOR TEMPERATURE NON-RESISTANT SURFACE TREATMENT

Piotr Krupski[1], Henryka Danuta Stryczewska[2]
[1]*Phd student of Faculty of Electrical Engineering and Computer Science, Lublin University of Technology, Nadbystrzycka 38A, 20-618 Lublin, Poland*
[2] *Faculty of Electrical Engineering and Computer Science, Lublin University of Technology, Nadbystrzycka 38A, 20-618 Lublin, Poland*

E-mail: piotr-jl <piotr-jl@o2.pl

Among the applications of non-thermal plasma in biomedicine, there occurs the subject of living structures' treatment in the purpose of influencing the pathogens existing on them. An important parameter, in this case, is the level of plasma temperature which is required to obtain the needed properties of plasma decontamination, and which also influences the stability of discharge products in gas, such as ozone and active gas oxides. At the same time, together which decreasing temperatures of the produced plasma, the negative thermal influence on living tissues is being minimalised. An increased temperature exposes both of the sensitive hydrogen and hydrophobic bonds, causing the protein to lose its spatial structure which is relevant for its function played in living tissues. An exemplary plasma jet reactor is shown in Figure 1.

A) B)

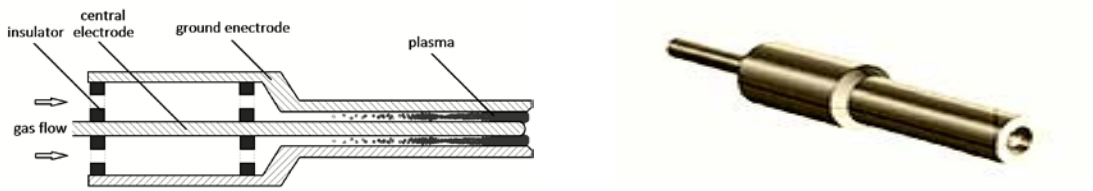

Fig. 1: Cross-section of an exemplary plasma jet and (A), and its picture created in COMSOL Multiphysics® Modeling Software

The paper shows an active cooling system involving process gas and plasma area. Non-thermal plasma properties are obtained inside a specially-constructed jet which is made from copper and has two functions at the same time: zero-potential electrode and evaporator in the cooling system. The cross section of the cooling jet is presented in the Figure 2.

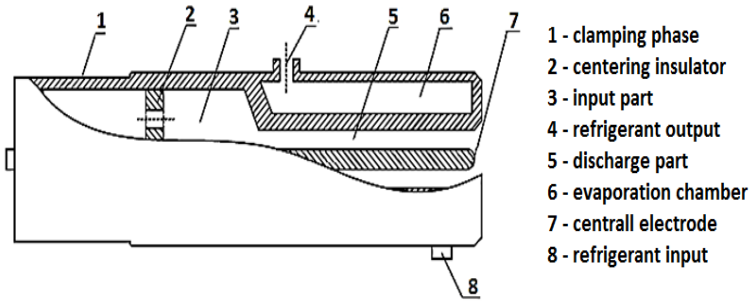

Fig. 2: A cross-section of the cooling jet.

Two materials were selected for plasma processing. In the first case it was a popular acrylonitrile butadiene styrene polymer (ABS) sample of thickness 2 mm. In the second case, the plasma treatment was carried out on 120g/mm^2 white paper. Thermal imaging was conducted with the use of camera VIGOcam V50 and the edition of images was conducted in a Therm 2.21.2 environment. Before the conduction of the measurement the camera had adjustments of emission factors set. This selection was made according to standard procedures: the temperature of the surface was heated in a homogenous way, next the surface temperature was measured with the use of thermocouple and the emission factor was adjusted so that the thermal image surface of temperature indication was the same as the one indicated by thermocouple.

Before the beginning of appropriate measurements, the air temperature was measured and it was in the range of 22 to 23 ºC. Humidity was also measured and it was equal to 63%. For the ABS material the emission factor was established on the level of 0.990 and for the paper - 0.945. The average distance between the surface and the camera lens was equal to 540 mm.

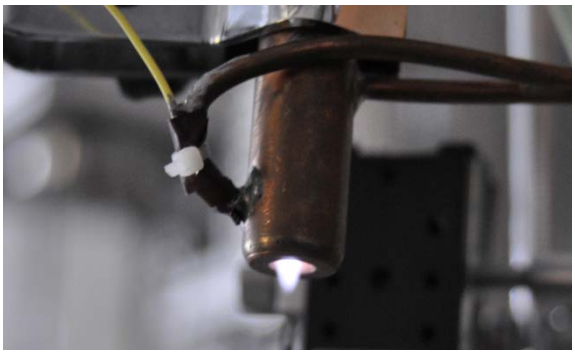

Fig. 3: Plasma jet working at 50 W of power and nitrogen - helium conditions.

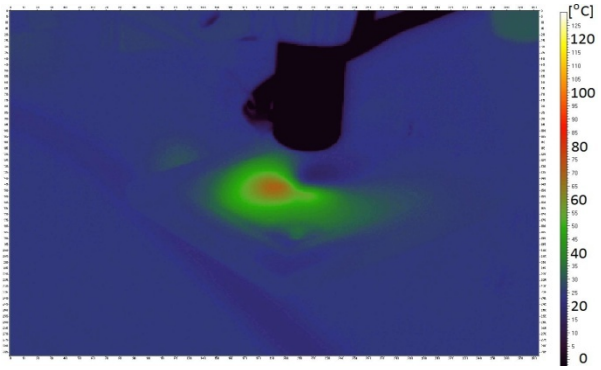

Fig. 4: Thermal image of plasma treated ABS surface with cooling system for nitrogen and helium conditions.

Presented on the Figure 3 reactor worked with helium and nitrogen gases with volume streams 7.1 m^3/min and 4.1 m^3/min. Thermal images were recorded for plasma treated surfaces of ABS and white paper with and without cooling system. Figure 4 presents obtained thermal image of the ABS surface treated by plasma jet with the cooling system. The research proved the cooling system to be highly efficient, which is visible on thermal images. The temperature of the treated plate was decreased up to 35 ºC degrees Celsius and the result is unobtainable for any other known cooling methods.

The proposed solution shows an applicatory potential not only in medical and biotechnological fields, but also during the treatment of high-temperature-susceptible materials which are represented by a low threshold of thermal plastification.

Effects of Reactive Species on Low-temperature Annealing for Dye-sensitized Solar Cells

Shungo Zen[1], Tsuneto Hujishima[2], Yuta Komatsu[2], Ryo Ono[2]
[1]*Department of Electrical and Electronic Engineering, Tokyo Institute of Technology, S3-3,2-12-1, Ookayama, Meguro-ku, Tokyo, Japan*
[2]*Department of Advanced Energy, the University of Tokyo, 5-1-5 Kashiwanoha, Kashiwa, Chiba 227-8568, Japan*

E-mail: zen@ee.e.titech.ac.jp

Plastic type of dye-sensitized solar cells (DSSC) can be manufactured at low cost and has the characteristics of lightweight and flexibility compared to glass types. Since high performance cells require 450 ℃ annealing and plastic limits the annealing temperature of up to 150 ℃, a low-temperature manufacturing technique is required. We have developed a low-temperature manufacturing technique using UV treatment (Hot UV annealing technique) and dielectric barrier discharge (DBD) treatment [1,2]. However, our low-temperature annealing technique requires long time annealing for 18 hours, while the annealing time at 450 ℃ was only 1 hour.

In this paper, we investigated the effects of O and O_3 produced in the low-temperature UV and DBD treatment on the production of DSSC. We showed that O radicals have the ability to eliminate the organic binder and strengthen the necking of TiO_2 nanoparticles. Then, we developed an indirect Hot DBD treatment, shown in figure 1, that can efficiently supply O radicals. As a result, we succeeded in reducing the annealing time from 18 to 4 hours.

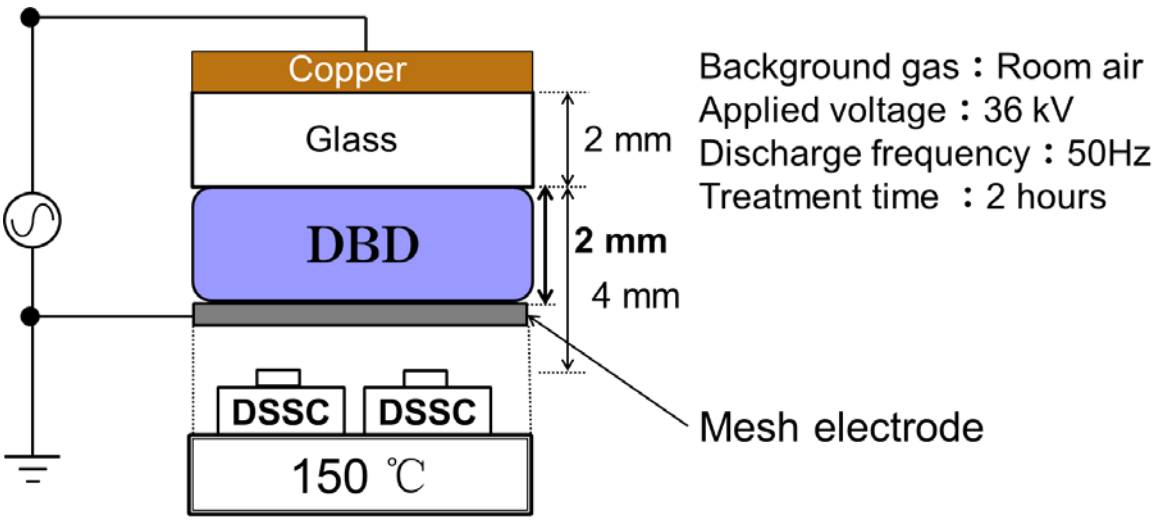

Fig. 1: Indirect Hot DBD treatment technique

5. References

[1] S. Zen, Y. Ishibashi and R. Ono, Appl. Phys. Lett., Vol. 104, 213904, 2014.
[2] S. Zen, Y. Inoue and R. Ono, J. Appl. Phys., Vol. 117, No. 10, 103302, 2015.

Production of an ammonia storage material by atmospheric dielectric barrier discharge at room temperature

Tetsuya Abe[1], Shungo Zen[1]
[1] *Department of Electrical and Electronic Engineering, Tokyo Institute of Technology, 2-12-1-S3-3, Ookayama, Meguro-ku, Tokyo, Japan*

E-mail: abe@hv.ee.e.titech.ac.jp

1. Introduction

There is no doubt that we need an energy storage system for the road to a low-carbon society. Recently, NH_3 has been considered as a promising energy storage material because NH_3 has high hydrogen storage density [1]. An indirect NH_3 synthesis method has been proposed by Zen et al., as shown in Fig. 1a [2]. Mg_3N_2 is a key material for the indirect NH_3 synthesis, and a circulation of Mg has been proposed. Zen et al. succeed in generating Mg_3N_2 by nitridation of MgO with nonthermal atmospheric-pressure dielectric barrier discharge (DBD) plasma in a N_2 atmosphere. In this paper, the improvement of MgO nitridation efficiency was investigated by using pure nitrogen and mixed gas of nitrogen and hydrogen as the background gas.

2. Experiment

Fig. 1b shows the experimental setup. A stainless steel pipe and water were used for the electrodes. Uniform discharge was achieved by using the water electrode. The discharge gap length from the stainless steel pipe to the quartz tube was 7.5 mm and the thickness of the quartz tube was 2.5 mm, respectively. At the bottom of the quartz test tube, 5 g of MgO nanoparticles (average diameter: 35 nm) were placed. When filling the background gas, the gas pressure was adjusted to be 1 atm. 500 Hz of sinusoidal high-voltage AC (V_{p-p} = 40 kV) was used as the applied voltage. After 10 min nitridation of MgO, 1.5 g of the nanoparticles were completely reacted with 15 ml of deionized water for 10 min to generate NH_3. After the sample solution was filtered, a commercially available indophenol blue colorimetric method was used to measure the total concentration of NH_4^+.

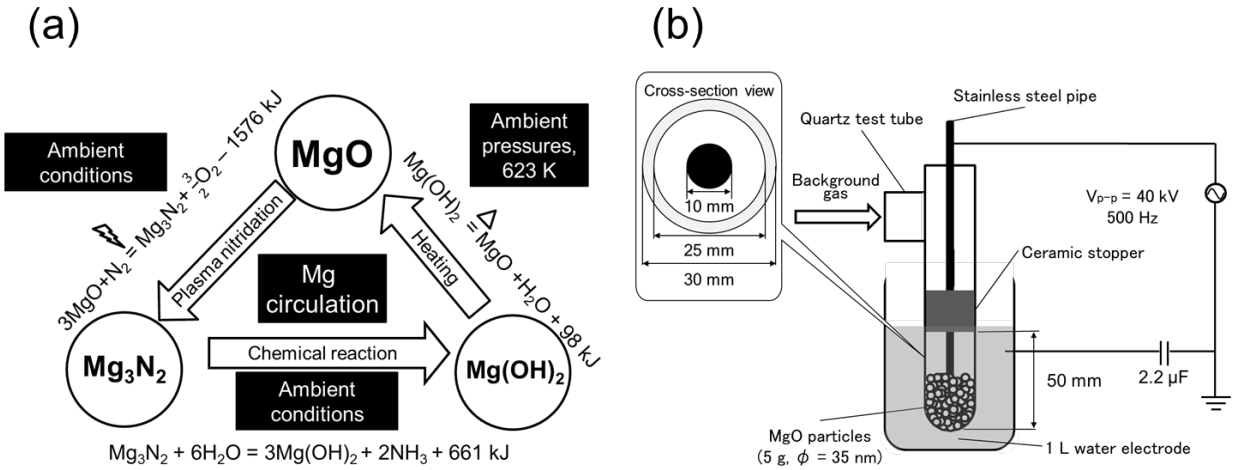

Fig. 1: Nitridation of MgO via DBD: **a** Changes in magnesium compounds with the indirect synthesis of ammonia [2], **b** Experimental setup

3. Experimental Results and Discussions

Fig. 2 shows the results of NH_4^+ concentrations via changing the hydrogen proportion of the background gas. It was found that the peak value of NH_4^+ was obtained when the hydrogen ratio was 35%. At this time, the NH_4^+ concentration was about 16.8 times higher than that of using pure nitrogen as the background gas. There are two possible reasons for the improvement of the MgO nitridation. First, ions and active species such as $NH_{(x)}^+$ and $NH_{(x)}$ play a major role in nitridation [3]. Second, H atoms generated by DBD contribute to reduction of MgO directly or indirectly. These H atoms collide on the surface of the MgO nanoparticles, and reduce oxides and clean the surface. As a result, diffusion of nitrogen into the MgO nanoparticles was promoted [3].

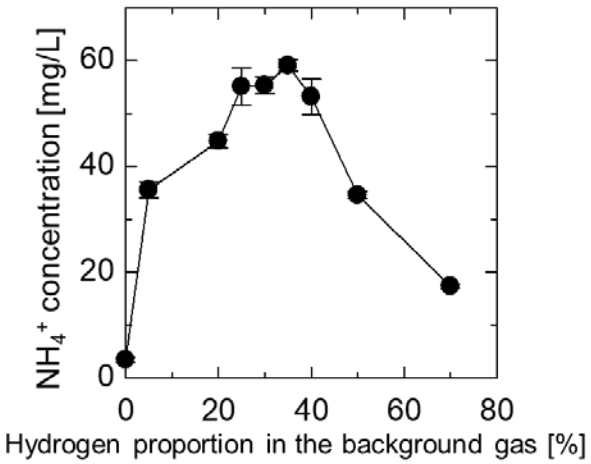

Fig. 2: Changes in the average NH_4^+ concentrations with different proportions of hydrogen in the background gas

4. Conclusions

In this paper, we investigated generation of Mg_3N_2 by using DBD via adding hydrogen to the background nitrogen gas. We succeeded in improving the nitriding effect at 35% of hydrogen ratio, the production amount was about 16.8 times higher than using pure nitrogen as the background gas. This research is still in its early stages, and the amount of nitriding treatment has not yet reached the practical level. However, we succeeded in remarkably increasing the effect of the nitriding treatment by changing the plasma generation condition. The possibility of reaching the practical level is fully conceivable by future development of this research.

5. References

1. Wang W, Herreros JM, Tsolakis A and York APE, “Ammonia as hydrogen carrier for transportation; investigation of the ammonia exhaust gas fuel reforming”, Int J Hydrogen Energy, 38(23), pp.9907–9917, 2013

2. S. Zen, T. Abe and Y. Teramoto, “Indirect Synthesis System for Ammonia from Nitrogen and Water Using Nonthermal Plasma Under Ambient Conditions”, Plasma Chem Plasma Process, 38(2), pp.347-354, 2018

3. T. Sato and K. Akashi, “Surface modification of Ti-6Al-4V alloy by plasma nitriding”, J. JILM, 42(11), pp.650-656, 1992

REVIEW OF DEVELOPMENTS IN APPLICATION OF OZONE IN AGRICULTURE

Fumiaki Mitsugi[1], Kenji Ebihara[2], Shin-ichi Aoqui[3], Henryka Danuta Stryczewska[4]
[1] *Kumamoto University, 2-39-1 Kurokami, Chuo-Ku, Kumamoto 860-8555 Japan*
[2] *Environment and Energy Laboratory, Kumamoto, Japan*
[3] *Sojo University, Kumamoto Japan*
[4] *Faculty of Electrical Engineering and Computer Science, Lublin University of Technology, Nadbystrzycka 38A, 20-618 Lublin, Poland*

E-mail: h.stryczewska@pollub.pl

Application of ozone produced by electrical discharges in agriculture becomes recently one of the most important techniques to ensure the safety of plant growing, soil treatment and food processing. The objective of agricultural soil sterilization is to destroy or eliminate microbial cells in the soil. Conventional agricultural methods based on chemical compounds, especially methyl bromide (CH3Br), have contributed to ozone layer depletion, the degradation of soil and chemical residues in food. Other methods, including autoclaving (moist heat), dry heat and microwaves have been attempted as alternatives to chemical fumigation. Soil treatment using pesticides is one of the effective ways to resist the spread of diseases in the soil. However, the pesticides' residues in the ground water, caused by the overuse of chemicals, has become a serious issue in agriculture. From the environmental point of view, the alternative methods of soil treatment are sought. Ozone is a powerful oxidising agent and much more effective disinfectant than chlorine compounds. A mixture of water-mist with ozone produces a very reactive intermediate, hydroxyl free radicals, which are much stronger oxidising agents than ozone itself, having the great potential in soil and plants treatment pest removing from agriculture soil.

Up to now, many studies on the application of ozone in agriculture have been carried out in the authors laboratories [1-5]. Paper presents the review of the recent progress in application the non-thermal plasma and ozone in agriculture. As the example, the ozone diffusion treatment system, composed of a surface barrier discharge reactor and chamber is presented on Figure 1. Studies on the effectiveness of such a system in promoting the growth of a plant, Chinese cabbage (Komatsuna) have been presented. The chamber is pull by a motor to treat long ridge. To avoid the leakage of ozone from the chamber, a stainless plate immersed inside soil and a pressing soil surface sheet are used. The surface barrier discharge has an ability to generate 38 g/m3 of ozone with a flow rate of 1 L/min of pure oxygen. Ozone is irradiated from an ejection pipe into the chamber, treating soil surface by following the mechanism of diffusion. The ridge size is 170 cm in length and 80 cm in width because this is laboratory-scaled experiment. After treating the ridge for 90 min, Komatsuna seeds are planted every 15 cm, therefore, the total number of Komatsuna cultivated at ozone treated ridge is 30. Another 30 seeds are planted at control ridge for comparison. The soil of the ridges is composed of the mixture of Andosol and compost.

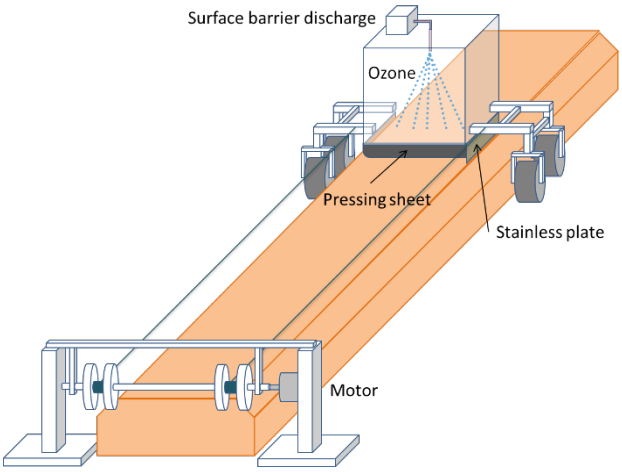

Fig. 1: Ozone diffusion treatment system

(a) Control

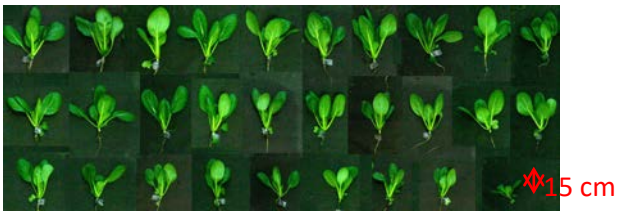

(b) Ozone

Fig. 2: Comparison of harvested Komatsuna leaves without (a) and with ozone soil treatment

Photographs presented on Figure 2 show the comparison of harvested Komatsuna leaves after 42 days passed from seeding. No negative influence of ozone is observed on the growth of Komatsuna. Detailed statistical analysis on the harvested Komatsuna leaves was done regarding the weight and the number of leaf.

Bibliograpy

[1] Stryczewska H. D., Application of non-thermal plasma in agriculture, Workshop on Application of Advanced Plasma Technologies in CE Agriculture, Ljubljana, Slovenia 2016
[2] Pawłat, J., Stryczewska, H. D., Ebihara, K., *J. Adv.Oxid. Technol.* Vol. 13, No. 2, 2010
[3] K. Ebihara, F. Mitsugi, T. Ikegami, Y. Yamashita, Y. Hashimoto, T. Yamashita, S. Kanazawa, H. D. Stryczewska, J. Pawłat, S. Teii, T-L. Sung, International Journal of Plasma Environmental Science and Technology, vol. 10, No. 1, pp. 11-15, 2016
[4] Stryczewska H. D., Ebihara K., Mitsugi F., Aoqui S., Muszański R., In proceedings *First* International Conference on Hybrid Agriculture (HYBRID 2016), 21-24 October 2016, Sojo University, Japan
[5] Ebihara K., et all, Ozone-mist spray sterilization for pest control in agricultural management, Contribution to the Topical Issue “13th International Symposium on High Pressure Low Temperature Plasma Chemistry (Hakone XIII)”, Edited by N. Gherardi, H. D. Stryczewska and Yvan Ségui, *Eur. Phys. J. Appl. Phys.* 61: 24318, 2013

SPORES INACTIVATION BY VUV EMISSION

G. Zvererva[1], I. Kirtsidely[2] and E. Machs[2]
[1]*State University of Civil Aviation, 38 Pilotov str., St.Petersburg, 196210, Russia*
[2]*Komarov Botanical Institute RAS, Professor Popov str.-2, St.Petersburg, 197376, Russia*
[3]*S.I.Vavilov State Optical Institute, Kadetskaya line-5-2, St.Petersburg, 199053, Russia*

E-mail: zvereva@soi.spb.ru

Vacuum ultraviolet (VUV) radiation (10 nm < λ < 190 nm) can occur in gas discharge plasma and in interstellar one. As VUV photon has high energy, it produces photochemical effects comparable to plasma-chemical ones by direct absorption or by indirect pathways due to ROS production. VUV emission play important role in plasma sterilization processes [1,2], in astrobiological studies related to origin of life on the Earth, conditions of microorganisms transfer in space, development of microflora in spacecraft[3] etc.
VUV irradiation of microorganisms is known to lead to their inactivation[4,5]. The mechanism of VUV inactivation differs from the UV ones and has not been sufficiently studied to the present day. The aim of our work was investigation of the role of DNA destruction and role of ROS in VUV inactivation of microorganisms.
As the sources of VUV radiation was used laboratory samples of xenon excimer barrier discharge lamps (wavelength λ=166-180 nm with maximum intensity at 172 nm, the surface VUV emission power I=1,25 mW/cm^2). The spores of various types of microfungi were irradiated by VUV radiation. Experimental conditions more detailed are described in[6].
VUV irradiation of DNA is known to induce single- and double-strand break[7]. In our work a study of the effect of VUV radiation on the DNA molecule has been carried out. The results of electrophoresis of DNA of VUV irradiated spores indicated its degradation. Figure 1 shows that: in the DNA of irradiated spores appear low molecular weight fragments (marked as I) and a peak corresponding to fragments with a length of about 20 000 pairs of nucleotides (marked as II). These results confirm VUV cutting effect on DNA.

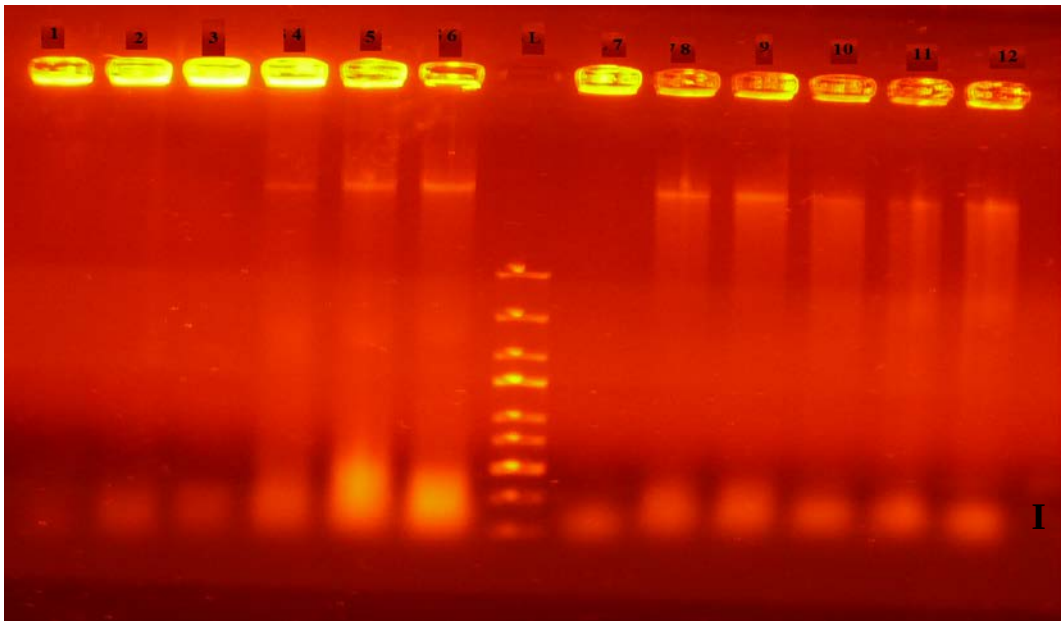

Fig. 1: DNA electrophoresis of *Rhodotorula* and *Aureobasidium* spores, 1,7- nonirradiated samples, 2,8- I=4 J/cm^2, 3,9- I=7 J/cm^2, 4,10- I=13 J/cm^2, 5,11-I= 25 J/cm^2, 6,12-I=50 J/cm^2.

VUV photolysis of H_2O and O_2 molecules leads to the formation of highly reactive oxygen-containing species (ROS): ·OH, $O(^1D)$ and others. To study the role of reactive radicals the experiments were made with the use of antioxidants. For these purposes iodine I_2 was added to cultivation media, as a result antioxidant I^- (iodide) appeared inside spores. Figure 2 dependencies show that ROS provide 10-15% decrease of the survival probability.

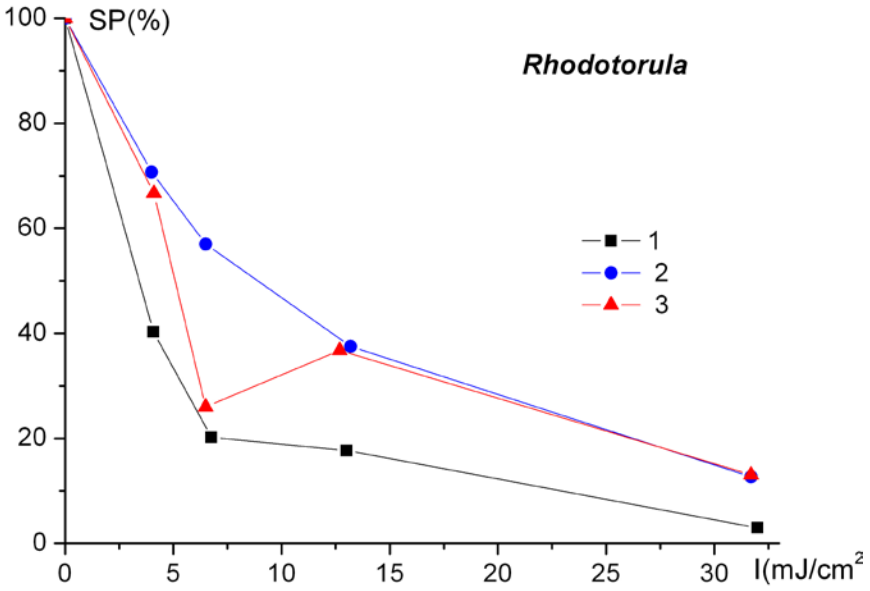

Fig. 2: Influence of iodine on survival probability of *Rhodotorula* cells. 1- control (cultivation medium without I_2), 2- cultivation medium with 5% iodine solution (1µl/mL), 3- medium with 5% iodine solution (1.5 µl/mL).

The results of the work indicate that VUV inactivation occurs both because of DNA destruction and because of the effect of ROS.

References

1. J Ehlbeck, U Schnabel, M Polak, J Winter, Th von Woedtke, R Brandenburg, T von dem Hagen and K-D Weltmann, J. Phys. D: Appl. Phys. 44, 013002 (18pp),(2011).
2. V. V. Tsiolko, pp.231-249, in Z. Machala et al. (eds.), Plasma for Bio-Decontamination, Medicine and Food Security, NATO Science for Peace and Security Series A: Chemistry and Biology, Springer Science+Business Media B.V.,(2012).
3. Horneck, G., Klaus, D.M. and Mancinelli, R.L., Microbiol. and Molec. Biol. Rev. 74(1), 121-156,(2010).
4. Ito, T., Ito, A., Hieda, K. and Kobayashi, K., Rad. Res. 96, 532-548, (1983).
5. Zvereva, G., Kirtsidely, I., Benken, K., Saifitdinova, A., Galkina, S. and Parfenov, V., Proc. SPIE 9810, 98101W, (2015).
6. G.Zvereva,I.Kirtsideli,A.Kovalenko, A.Vangonen, A.Saifitdinova and S.Galkina, Journal of Science and Technology in Lighting, 41,52-56, (2017).
7. Michael, B.D., Prise, K.M., Folkard, M., Vojnovic, B., Brocklehurst, B., Munro, I.H. and Hopkirk, A., Int. J. Radiat. Biol. 66(5), 569-572 (1994).
8. Winkler, R., Natural Science, 7, 548-557 (2015).

Primary Research on Plasma Biosafety Using Atmospheric-Pressure Plasma in Air

Haiyun Luo[1], Hao Wang[1], Zhe Ren[2], Jinfeng Tie[2], Lingyun, Wang[3], Hongwei Liu[3], JianqiangYuan[3], Xinxin Wang[1]

[1]*Dept. of Electrical Engineering, Tsinghua University, Beijing 100084, China*
[2]*Key Laboratory of Pulsed Power, Institute of Fluid Physics, CAEP, China*
[3]*Institute of Disease Control and Prevention of PLA, Beijing, China*

E-mail: lhy@tsinghua.edu.cn

Bacterial decontamination plays a great role in medical facilities, factory processing, food security, bio-safety[1], environmental application[2], etc. There are certain restrictions, like shape, structure, thermal damage and chemical corrosion, of traditional methods when processing different objects.

The main content of this research is that using atmospheric pressure plasma of different structure to decontaminate representative bacterial of different environment. We used DBD plasma to treat the Bacillus subtilis spore on biological indicator, and the Escherichia coli in liquid. And the results suggest that the effect of plasma treatment could achieve sterilization (The bacteria density is reduced more than six orders of magnitude) within 2 min. These experiments show that the plasma decontamination technology has the advantage of multiple structure, convenient operation, low loss processing and environmental protection.

The measurement of discharge current, applied voltage and electric field is to analyze the mechanism and effective agents of plasma treatment. The possible agents were reactive species from reactive oxygen species(ROS), heat, UV photons, charged particles, particle etching and electric fields[3]. We compared the role of these agents in processing. Many past research focused on surface morphological changes of microbe with scanning electron microscopy and Transmission electron microscope[4], which is of limitations to research the specific processing of plasma. We evaluate the plasma-induced effect using the fourier transform infrared spectroscopy[5] to quantitatively detect the biological activities besides traditional bacteria culture. With the exposure time increasing, the membrane and the proteins decompose to fatty acid chains and Amino acid.

Comparison between the water activation effects of cold plasma jets in different working conditions

Han Xu[1], Dingxin Liu[1], Chen Chen[1], Michael G Kong[1]
[1]*State Key Laboratory of Electrical Insulation and Power Equipment, Center for Plasma Biomedicine, Xi'an Jiaotong University, Xi'an 710049, P. R. China*

E-mail: liudingxin@mail.xjtu.edu.cn

Recent years cold atmospheric plasmas have attracted considerable attention thanks to their potential applications such as plasma biomedicine. Since many of these applications involve operation in humid environments and/or treatment of liquid substrates, the study and control of the liquid chemistry induced by the plasmas is of great importance. It is found that the liquid chemistry is sensitive to the plasma characteristics, while the plasma characteristics are dependent on the discharge conditions such as the electrode structure and the exctiation power. However, the correlation between the plasma-induced liquid chemistry and the discharge conditions has not been well understood. In this paper, the liquid chemistry induced by the plasma jets with two typical structures of cross-field and linear-field are compared[1], as well as three kinds of excitation powers with sinusoidal, pulsed and pulse-modulated RF woltages[2,3]. The results are of practical indicator to select better discharge conditions for the future medical application.

The results show that the plasma jets with two types of electrode structures produce substantially the same gaseous reactive species at the same discharge power, however the linear-field plasma jet can deliver reactive species more efficiently to the downstream liquid phase. Thus, the concentration of the aqueous reactive species induced by the linear-field plasma jet is higher than that of the cross-field plasma jet. Moreover, the characteristics of the aqueous reactive species induced by the plasma jets are different under different excitation powers. Taking the short-lived reactive species OH which considered to have important biomedical effect as an example (DMPO-OH is the resultant of the aqueous OH and its spin trap DMPO, measuring by an electron spin resonance spectrometer), its concentration induced by the sinusoidal plasma jet is slightly lowerer than that by the pulsed plasma jet, but much higher than that by the pulse-modulated RF plasma jet with the same discharge power. Besides, the bacterial inactivation results are also in accordance with the concentrations of aqueous reactive species induced by these plasma jets.

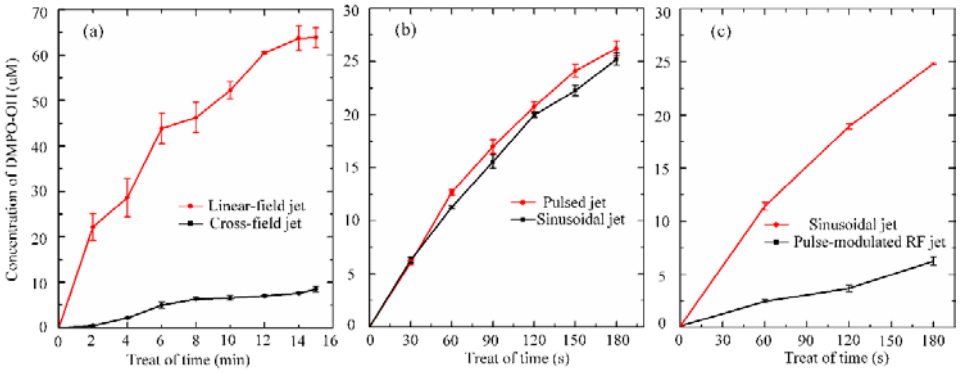

Fig. 1: The concentration of DMPO-OH in the liquid phase as a function of the discharge treatment time for different types of cold plasma jets.

[1] H. Xu, C. Chen, D. X. Liu, D. H. Xu, Z. J. Liu, X. H. Wang, M. G. Kong, *J. Phys. D: Appl. Phys.* **50**, 245201 (2017).
[2] H. Xu, D. X. Liu, W. J. Xia, C. Chen, W. T. Wang, Z. J. Liu, X. H. Wang, M. G. Kong, *Phys. Of Plasmas.* **25**, 013520 (2018).
[3] P. Olszewski, J. F. Li, D. X. Liu, J. L. Wslsh, *Journal of Hazardous Materials*, **279**, 60–66 (2014).

DBD PLASMA JET FOR INACTIVATION OF YEAST PATHOGENS

Joanna Pawłat[1], Barbara Chudzik[2], Piotr Terebun[1], Michał Kwiatkowski[1], Mariusz Gagoś[2], Paweł Mazurek[1]
[1]*Faculty of Electrical Engineering and Computer Science, Lublin University of Technology*
ul. Nadbystrzycka 38A, 20-618 Lublin, Poland
[2]*Department of Cell Biology, Maria Curie– Skłodowska University*
ul. Akademicka 19, 20-033 LublinLublin, Poland

E-mail: askmik@hotmail.com

Candida albicans, a yeast pathogen, is the most common causative agent of fungal infections in humans, which is especially dangerous in case of diabetes, pregnancy and immunocompromised patients. Treatment of fungal infections is difficult as many antifungal drugs have a fungistatic effect and may result in strain resistance. Atmospheric pressure plasma with generated oxygen and nitrogen-based active species can be utilized for various decontaminative purposes [1]–[8]. This paper presents a comparison of the fungicidal activity and the ability of induction of oxidative stress and cell membrane damage of non-thermal atmospheric pressure plasma against *C. albicans* cells in dependence on the geometry of the set-up and the presence of the culture medium. The *C. albicans* cell suspension was aliquoted to 1 ml portions and poured into 2-ml Eppendorf tubes and further treated with the plasma generated in dielectric barrier discharge (DBD) plasma jet for 0.5, 1, 3, 5, 10, 15, and 20 minutes, setting the nozzle 0.5 cm from the surface of the medium. The ceramic tube of jet had internal diameter of 1.4 mm, distance between two copper ring electrodes was 12 mm. Reactor was supplied by voltage of 3.7 kV with frequency of 17 kHz and mean power of 6 W [9]. Paralelly, *C. albicans* cell suspension was centrifuged, the supernatant was discarded, and the cell pellet was washed in deionized water and centrifuged again. After decanting the water, the wet cell pellet remaining on the bottom of the Eppendorf tubes in the first part of the samples was treated with plasma or, the wet cell pellet was spread using a sterile inoculating loop on the surface of Petri dishes and treated with the plasma. Controls consisted of plasma-untreated cells or cells treated for 20 min with a mixture of gases having the same partial pressure as gases used for producing the plasma. To determine the level of oxidative stress and membrane damage in the plasma-treated *C. albicans* cells, specific fluorescent probes such as Dihydrorhodamine 123 (DHR 123, Life Technologies, cat. no: D-23806), MitoSOX™ Red indicator for live-cell imaging, and a mixture of 20 µM propidium iodide (PI) and 3.34 µM SYTO®9 dye solution (LIVE/DEAD® FungaLight TM Yeast Viability Kit, Life Technologies, cat. no L34952 were used. Nikon Labophot 2 fluorescence microscope using a specific fluorochrome filter was further used. The number of DHR 123-positive (fluorescing green), MitoSox-positive (fluorescing red), and PI-positive (fluorescing red) cells, among 300 cells on each slide, was counted and microphotographs were taken using a Canon A 640 digital camera. Analysis of the microscopic slides also allowed determination of the ability of plasma-treated *C. albicans* cells to form hyphae and pseudohyphae, which are considered major invasive forms.

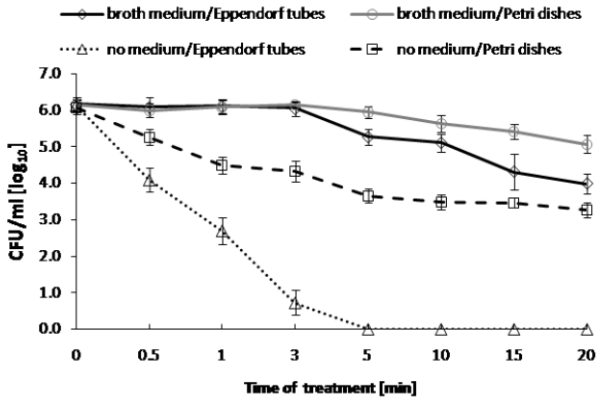

Fig. 1: Reduction of the number of *C. albicans* colonies (CFU/ml) under the non-thermal atmospheric pressure plasma (DBD He/O_2) treatment versus the time of the exposure, depending on the geometry of the set-up and presence of the broth medium in which the cells were suspended. The assays were performed in triplicate in two independent experiments; mean values with standard deviation (SD) are presented.

The results presented in Fig.1. showed that the antifungal activity of the non-thermal atmospheric pressure plasma was largely dependent on the presence of the organic medium surrounding the pathogenic microorganism cells and on the geometry of the experimental set-up. DBD plasma jet had a strong fungicidal activity, in the case of the medium-deprived *C. albicans* cells. In the experimental variant with Eppendorf tubes, a reduction of the CFU/ml number by about 2 $\log_{10}$ was observed after 0.5 minute of the treatment. After 1 minute, the number of CFU/ml decreased by 3.4 $\log_{10}$; after 3 minutes by 5.4 $\log_{10}$; and after 5 minutes of the treatment the colonies were completely eradicated. The presence of broth medium organic compounds significantly decreased the antifungal activity of the plasma (2 $\log_{10}$ after 20 minutes of the treatment). It was also found that the geometry of the experimental set-up was extremely important for the antimicrobial activity of the plasma.

Acknowledgment

This study has been supported by M-Era.net, Inkubator Innowacyjności+ found, networking action CEEPUS CIII-AT-0063.

References

[1] J.-L. Brisset and J. Pawlat, "Chemical Effects of Air Plasma Species on Aqueous Solutes in Direct and Delayed Exposure Modes: Discharge, Post-discharge and Plasma Activated Water," *Plasma Chem. Plasma Process.*, vol. 36, no. 2, pp. 355–381, Mar. 2016.

[2] P. J. Bruggeman *et al.*, "Plasma–liquid interactions: a review and roadmap," *Plasma Sources Sci. Technol.*,

[3] B. G. Dasan, B. Onal-Ulusoy, J. Pawlat, J. Diatczyk, Y. Sen, and M. Mutlu, "A New and Simple Approach for Decontamination of Food Contact Surfaces with Gliding Arc Discharge Atmospheric Non-Thermal Plasma," *Food Bioprocess Technol.*, vol. 10, no. 4, pp. 650–661, Apr. 2017.

[4] K. Hensel *et al.*, "Effects of air transient spark discharge and helium plasma jet on water, bacteria, cells, and biomolecules," *Biointerphases*, vol. 10, no. 2, p. 029515, May 2015.

[5] K. G. Kostov, A. C. Borges, C. Y. Koga-Ito, T. M. C. Nishime, V. Prysiazhnyi, and R. Y. Honda, "Inactivation of Candida albicans by Cold Atmospheric Pressure Plasma Jet," *IEEE Trans. Plasma Sci.*, vol. 43, no. 3, pp. 770–775, Mar. 2015.

[6] T. Maisch *et al.*, "Contact-Free Inactivation of Candida albicans Biofilms by Cold Atmospheric Air Plasma," *Appl. Environ. Microbiol.*, vol. 78, no. 12, pp. 4242–4247, Jun. 2012.

[7] L. Moravskỳ, M. Klas, E. Machová, K. Pisklová, and Š. Matejčík, "Influence of a plasma jet on the viability of Candida albicans," *Open Chem.*, vol. 13, no. 1, pp. 257–262, 2015.

[8] Y. Sun *et al.*, "Inactivation of Candida Biofilms by Non-Thermal Plasma and Its Enhancement for Fungistatic Effect of Antifungal Drugs," *PLOS ONE*, vol. 7, no. 7, p. e40629, Jul. 2012.

[9] J. Pawłat *et al.*, "Effects of atmospheric pressure plasma jet operating with DBD on Lavatera thuringiaca L. seeds' germination," *PLOS ONE* vol. 13, no. 4, p. e0194349 April, 2018.

BIOSENSOR CONSTRUCTED BY SPP PLASMA TECHNIQUE FOR DETERMINATION OF DIHYDROXYBENZENE ISOMERS

Justyna Jaroszyńska-Wolińska, Szymon Malinowski[1],Cecylia Wardak[2],
P. Anthony F. Herbert[3],

[1]*Lublin University of Technology, Civil Engineering and Architecture Faculty, Lublin Poland*
[2] *Department of Analytical Chemistry and Instrumental Analysis, Maria Curie-Sklodowska University, Maria Curie-Sklodowska Sq. 3, 20-031 Lublin, Poland*
[3] *Plasma Ireland, Cork, Ireland*

E-mail: j.wolinska@gmail.com

Biosensors are devices used in analytical chemistry for determination of many chemical compounds. They comprise two parts: (I) transducer and (II) bio-recognition element. Depending on the generation mechanism of the measurable signal, biosensors can be divided into amperometric, voltammetric, potentiometric or conductivity sensors. In biosensor construction different bio-recognition elements can be used, e.g. enzymes, whole cells, antibodies, nucleic acids. Recent research has been focused on enzymes, especially oxidoreductases, which have found wide application in environmental protection for determination of pollution. Therefore, in this work the Laccase enzyme was selected for biosensor construction, which enzyme catalyzes the oxidation of phenolic compounds with simultaneous reduction of molecular dioxygen into water. Laccase molecules are glycoproteins containing four copper atoms in their active center divided into three sites named T1, T2 and T3.

Currently many procedures are known for the construction of Laccase based biosensors involving so-called “wet” methods. These methods are complex and time-consuming generally needing many hours of storage of the basis electrode in biological precursor solution. Increasing demand for biosensors in practical applications has resulted in a need for new, faster and lower cost methods of their construction. One such method is SPP *(Soft Plasma Polymerization)* based on the polymerization/crosslinking of biological precursor inside a Corona plasma discharge generated in the conventional pin-to-plane electrode configuration. Our previous study [1] proved that the Corona SPP process can be successfully used in the deposition of Laccase bio-active coatings with preservation of the original redox properties of the biological precursor. These properties allow the application of these bio-coatings in construction of biosensors designed for determination of catechol in environmental samples. Catechol (1,2-dihydroxybenzene) is a phenolic compound with two hydroxyl groups placed at first and second carbon atoms of benzene rings.

A Laccase based biosensor designed for determination of catechol in environmental samples was constructed using an innovative, one-step Corona SPP method. The basis of this biosensor fabrication is the plasma deposition of polymerized and cross-linked Laccase molecules and their bonding onto a conductive solid support in the form of GCE (Glassy Carbon Electrode) carefully polished using 0.3 μm alumina slurry. The Corona SPP process of this Laccase recognition layer deposition was carried out by introducing liquid precursor enzyme solution at constant flow rate (200 μL/min) into a nebulizer (Burgener type T2100). The vapourised/atomized Laccase was subsequently introduced into a 10 L/min Helium carrier gas stream and carried into a plasma reaction zone generated by pin-to-plane low energy Corona Discharge generated at a voltage of 4

kV at room temperature and atmospheric pressure. These two last factors are critical for deposition of bio-recognition layers by plasma with minimum damage to the bio-active molecules.

A study of the analytical parameters of fabricated biosensors was performed by Electrochemical Analyzer EA-9 (MTM-ANKO, Poland) using the differential pulse voltammetric method. Measurements were carried out using an electrochemical cell with a conventional three electrode system where a Laccase-based biosensor was used as the working electrode, an Ag|AgCl (3M KCl) electrode as the reference electrode and a platinum electrode as an auxiliary electrode.

Determination of catechol by Laccase-based biosensors is based on the two-step redox reaction occurring between the Laccase bio-recognition element and catechol molecules. In the first step of the reaction catechol is oxidized to 1,2-benzoquinone. The reduced form of the Laccase bio-recognition element is subsequently oxidized by molecular oxygen, which is reduced to the water molecule.

As is seen in Figure 1, the linear range of the Laccase-based biosensor constructed by the Corona SPP method extends up to 60 µM of catechol with equation y = 0.0901x + 1,492 (R^2=0.996). The analytical peak of catechol oxidation appears at a voltage of 0.250 V and was identified from literature [2]. This analytical response by the fabricated biosensor confirms that the Corona SPP process does not significantly change or damage the active center of the Laccase molecule and allows it to retain its biological activity. Figure 1 shows also that the sensitivity of the fabricated biosensor, defined as the slope of its linear range, in determination of catechol is 0.0122 mA/mM. An important factor in the determination of catechol by this Corona SPP Laccase-based biosensor is the pH of the measurement environment. Study showed that this biosensor generates the highest analytical signal in acetate buffer at a pH=6.13.

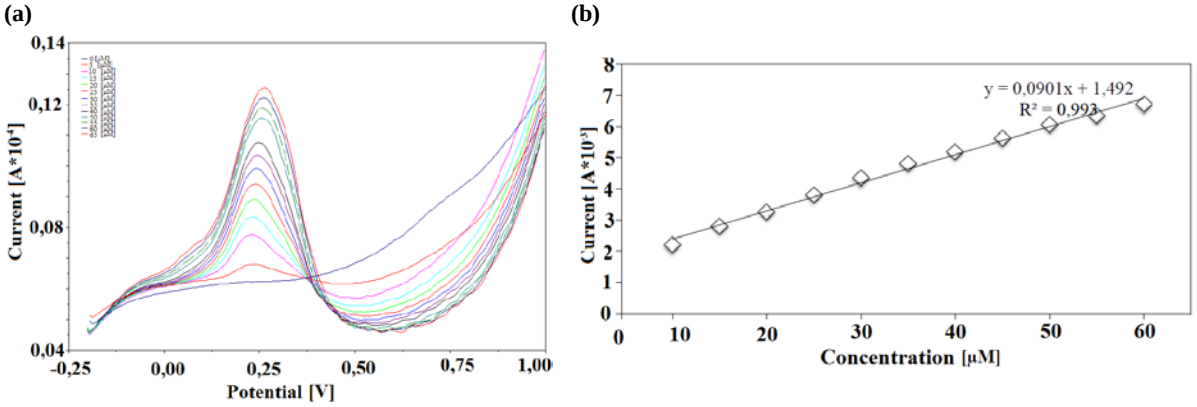

Figure 1: (a) Voltamperogram obtained during determination of catechol by Laccase-based biosensor constructed by Corona SPP method and (b) its linear range (I-oxidation peak current generated during enzymatic reaction).

The presented study shows that low energy density Corona discharge can be successfully applied in biosensor construction. Comparison of the analytical parameters of biosensors fabricated in this work with devices obtained from conventional "wet" methods shows that application of this Corona SPP method allows for the construction of devices with similar or better linear range and sensitivity in shorter times.

Acknowledgements

We acknowledge support from Polish Ministry of Science and Higher Education within the statutory work research number S/ 12/ II B/2018.

References

[1] Sz. Malinowski, P.A.F. Herbert, J. Rogalski, J. Jaroszyńska-Wolińska, Book of Contributed Papers HAKONE XV, 11-16 September 2016, Brno, Czech Republic

[2] M. Velmurugan, N. Karikalan, S.M. Chen, Y.H. Chem, Ch. Karuppiah, *Journal of Colloid ad Interface Science*, 500 (2017) 54-62

MICRO-HOLLOW SURFACE DISCHARGE FOR BACTERIAL DECONTAMINATION

Mirko Černák[1], Zlata Tučeková[1], Richard Krumpolec[1], Lukáš Vacek[2], Jakub Kelar[1], Filip Růžička[2]
[1]*CEPLANT, Department of Physical Electronics, Faculty of Science, Masaryk University, Kotlářská 2, 611 37 Brno, Czech Republic*
[2]*The Department of Microbiology, Faculty of Medicine, Masaryk University, St. Anne's University Hospital, Pekařská 53, 602 00 Brno, Czech Republic*

E-mail: cernak@physics.muni.cz

A proprietary type of surface discharge capable to generate diffuse plasma in flowing gas mixtures with concentration of water vapor above 50% without any admixture of inert gases will be presented.

The bactericidal effects of OH and H_2O_2 rich plasma activated gas flow on bacterial biofilm (*Escherichia coli*, methicillin-resistant *Staphylococcus aureus* and *Staphylococcus epidermidis*) contamination on polypropylene non-woven textile surface was investigated. The dependence of germicidal efficiency on exposure time and input power was evaluated by standard microbiological cultivation (CFU plate counting) and fluorescence analysis using fluorescence multi-well plate reader. The test was repeated at different distances of the contaminated PP non-woven sample from the plasma source. The reactive species in plasma activated gas flow were studied using the optical emission and laser induced fluorescence spectroscopy, thermal and electrical properties of used plasma source were measured also.

The bacterial biofilm decontamination efficiency increased with the rise of exposure time and the discharge input power. The log reduction of viable biofilm units varied with the increasing distance from the plasma surface.

This research has been supported by the project CZ.1.05/2.1.00/03.0086 funded by European Regional Development Fund and project LO1411 (NPU I) funded by Ministry of Education, Youth and Sports of Czech Republic. This work was also supported by the project TG02010067 funded by Technology Agency of the Czech Republic and by Grant No. 16–29916A funded by Ministry of Health of the Czech Republic.

Investigation of a He micro plasma-jet for distilled water treatment

Rasmus Talviste[1], Indrek Jõgi[1] and Jüri Raud[1]
[1]*University of Tartu, Institute of Physics, Ravila 14c, Tartu 50411, Estonia*

E-mail: rasmus.talviste@ut.ee

Atmospheric pressure plasma-jets (APPJs) have been the focus of extensive investigations over the past decade mainly due to possible applications in biomedicine as sources for production of reactive oxygen and nitrogen species (RONS) [1]. The simplest approach is to directly treat the cells or tissue with an APP. Alternatively, plasma can be utilized to activate a medium such as distilled water (PAM or PAW) [2] which could then be used for treatment of cells or tissue.
In case of plasma-jets the production rates of long-lived RONS such as NO_3^-, NO_2^- and H_2O_2 in water is known to depend on the mode of operation. The direct contact of the plasma-jet with the treated water surface and non-contact mode can be used to vary the composition and quantity of created RONS in the water [2]. Reducing the dimension of the plasma-jet influences the plasma parameters [3] and was shown to be more efficient at generating RONS in PAW than larger jets [5]. The aim of this work was to identify the plasma-water contact and non-contact modes for the micro plasma-jet and measure *in situ* the concentrations of NO_3^-, NO_2^- and H_2O_2 in distilled water during plasma treatment using UV absorption spectroscopy.

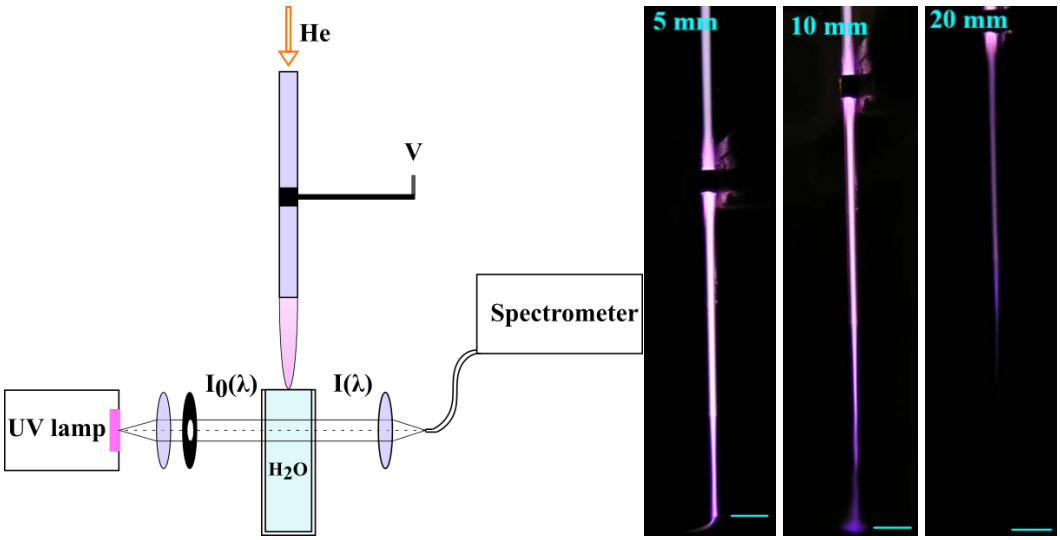

Figure 1. Experimental set-up (left). Photographs of the plasma jet at flow rate 500 sccm and various distance between the water surface and tube orifice (right). The water surface is marked with the horizontal line.

The experimental configuration used in this work is shown in figure 1 (left) and described in detail in our previous work [6]. Plasma was ignited inside a 500 µm quartz tube by applying a sinusoidal voltage with frequency of 6 kHz and amplitude of 5- 12 kV. A quartz cuvette (4 µl) was filled with distilled water and the water surface was placed at variable distances (5- 20 mm) from the tube orifice. Lenses were used to obtain a parallel beam between the UV source and Ocean Optics 4000 spectrometer. The beam diameter (10 mm) was determined by a diaphragm. The center of the light beam passing through the cuvette (optical path length of 10 mm) was centered 20 mm below the water surface. The concentrations of RONS in PAW were determined from the Beer-Lambert law similarly as in [4]. The measured UV absorption spectra were fitted using the method of least squares. The linear combination of the calibration spectra of individual species which assured the best fit was determined and the concentrations of species were calculated from determined fitting parameters.

Figure 1 (right) shows photos taken of the micro plasma-jet at various distances from the water surface and quartz tube orifice. The distance of 5 mm was identified as the contact mode for all flow rates as the bright plasma column clearly reached the water surface. At the distance of 10 mm and flow rate of 500 sccm a purple circle can be seen on the water surface while the bright plasma column tip is just above the water surface (for lower flow rates the purple tip was clearly above the water surface). At 20 mm the plasma did not reach the water surface at used voltages and flow rates. Additionally, at the distance of 20 mm the visual appearance of jet was the same as having no water surface and was clearly shorter than at the distance of 10 mm indicating that the presence of the water surface affects the intensity of the plasma jet.

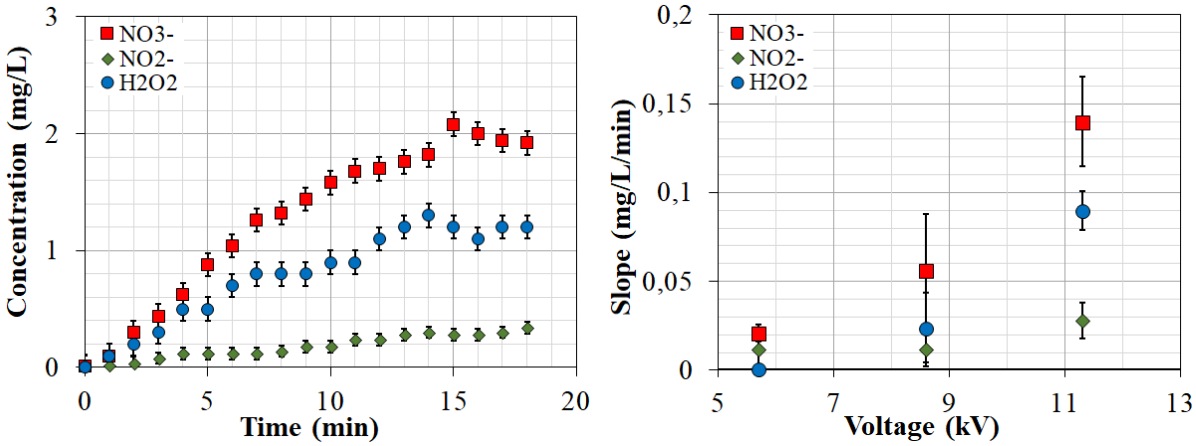

Figure 2. Temporal change of NO_3^-, NO_2^- and H_2O_2 concentration during plasma treatment (left). Note that plasma was switched off at 15 minutes. The effect of applied voltage on the slope (linear part up to 15min) of dependence between concentration and time (right). Contact mode (5 mm) at flow rate of 200 sccm and voltage of 11.3 kV. The values for H_2O_2 concentration and slope are both divided by 10 on the graphs for clarity.

Figure 2 (left) shows the temporal evolution of NO_3^-, NO_2^- and H_2O_2 concentrations during 15 min of plasma treatment. Nearly linear increase is observed for all species which is consistent with the observations of other authors who investigated larger plasma-jets [4]. Figure 2 (right) depicts the influence of applied voltage on the slope of the linear fit to the data presented in figure 2 (left). A linear increase of the species' concentration was observed with increased applied voltage amplitude.

In our previous study the increase of voltage resulted in an increased number of ionization waves occurring during one period [6]. In the present study it was confirmed that the same effect occurs in the case when the grounded electrode is replaced with water surface. The increased number of ionization waves reaching the water results in increased concentrations of NO_3^-, NO_2^- and H_2O_2 in the distilled water. This holds for both the contact and non-contact mode but in non-contact mode the distance variation has a greater effect on the species concentrations than the voltage variation. In addition, the concentrations of NO_3^- were also calculated from the pH of the distilled water treated for 15 min with plasma. The result agreed well with the values measured by UV absorption.

[1] X. Lu, G. V. Naidis, M. Laroussi, S. Reuter, D. B. Graves and K. Ostrikov. Phys. Rep. 630 (2016) 1-84
[2] G. Uchida, A. Nakajima, T. Ito, K. Takenaka, T. Kawasaki, K. Koga, M. Shiratani and Y. Setsuhara. J. Appl. Phys. 120 (2016) 203302
[3] I. Jõgi, R. Talviste, J. Raud, K. Piip and P. Paris. J. Phys. D. Appl. Phys 47 (2014) 415502
[4] J.-S. Oh, E. J. Szili, N. Gaur, S.-H. Hong, H. Furuta, H. Kurita, A. Mizuno, A. Hatta and R. D. Short. J. Phys. D. Appl. Phys. 49 (2016) 304005
[5] J.-S. Oh, M. Kakuta, H. Furuta, H. Akatsuka and A. Hatta. Jap. J. Appl. Phys. 55 (2016) 06HD01
[6] R. Talviste, I. Jõgi, J. Raud and P. Paris. Contrib. Plasma Phys. 56 (2016) 134-145

QUANTUM-CHEMICAL ANALYSIS OF LACCASE BIO-COATING FORMATION IN CORONA PLASMA JET

Szymon Malinowski[1], P. Anthony F. Herbert[2] & Justyna Jaroszyńska-Wolińska[1]

[1]*Lublin University of Technology, Civil Engineering and Architecture Faculty, Poland*
[2] *Plasma Ireland, Cork, Ireland*

E-mail: s.malinowski@pollub.pl

The mechanism of laccase biocoating formation by Soft Plasma Polymerisation using low energy pin-to-plane Corona jet is complex and involves cross-linking of laccase molecules in the plasma jet region and at the surface of the growing film. In addition, reactions between laccase and the glass substrate are needed to achieve bonding of coating to glass.

To evaluate the possible mechanisms of biocoating formation we assumed that cross-linking and bonding result from radical-radical reactions [1] induced by active plasma species, e.g. radicals, fast electrons, ions, and that only external amino acids in the laccase enzyme structure take part in such reactions. This allows retention in our model of the molecule's active center structure in unchanged form. On the basis of this assumption we selected (PDB ID: 3DIV) the seven amino acids in the external regions of the laccase molecule as potentially able to play a role in cross-linking and bonding reactions, namely arginine (ARG), aspartic acid (ASP), glutamine (GLN), serine (SER), threonine (THR), tyrosine (TYR) and lysine (LYS). Hartree Fock quantum-chemical modelling used B3LYP exchange-correlation functional with 6-311G (d,p) basis set. Calculations were performed by Parallel Quantum Solutions (PQS) suite ab initio programs and the PQSMol graphical interface package [2]. The structures of the chosen amino acids so optimized are presented in Figures 1(a)-(g). The form of the glass support used for the modeling was SiO_4 as presented in Figure 1h.

The structures modeled indicate that regions can be identified in these amino acids: (I) the regions responsible for creation of amide bonds between amine and carboxyl groups in the amino acids resulting in cross-linking between laccase molecules and (II) the regions responsible for bonding with the surface of the glass substrate. Important groups in cross-linking and bonding are identified by the modeling as amine groups in ARG, ASP, LYS and GLN, carboxyl groups in ASP, carbonyl groups in GLN and hydroxyl groups in SER, LYS, THR and TYR which latter can interact with the glass molecule to deliver bonding. Thus, bonding of laccase to the glass support involves functional groups such as $–NH_2$, -COOH, -C=O or –OH while multiple amine and carboxyl groups are seen to be available for cross-linking between laccase molecules. Regions II are regions of electrostatic charge imbalance with positive charge regions concentrated at hydrogen and silicon atoms and negative charge at oxygen atoms. Such charge concentrations give rise to electrostatic interactions between glass and amino acid molecules perhaps based on induction of local charges on the glass slides. Interactions between these opposite charges create bonds between protein and the glass surface causing the initial monolayers of the deposited laccase to adhere to the substrate.

(a) (b) (c)

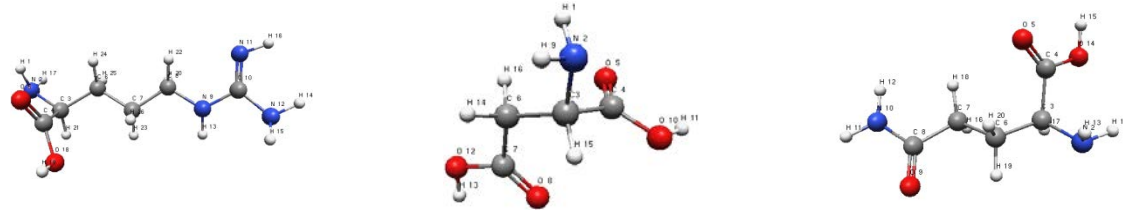

(d) (e) (f)

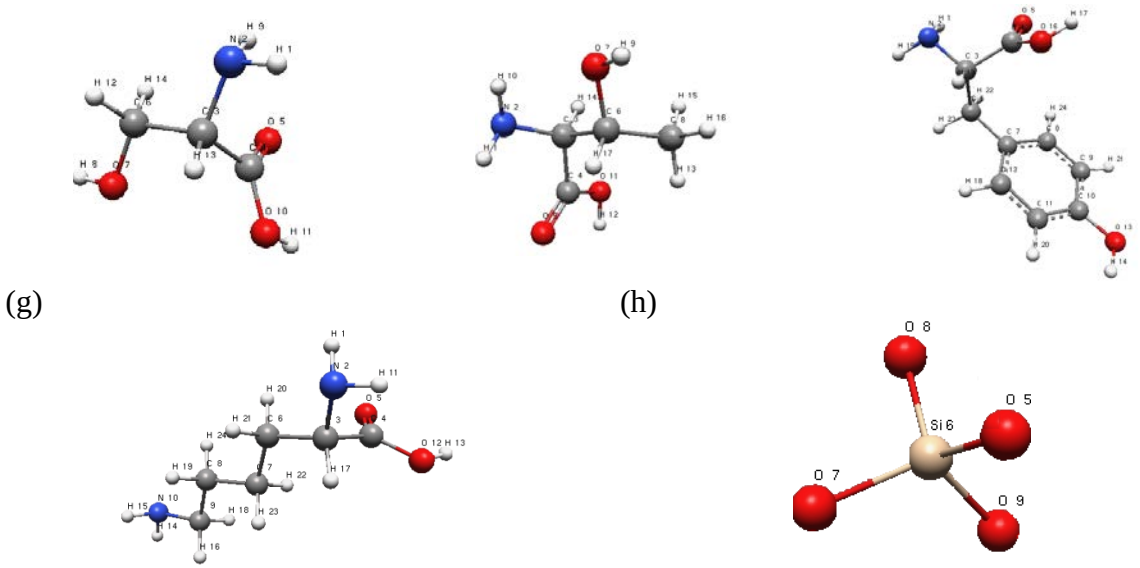

Fig. 1: Optimized molecular structures of (a) ARG, (b) ASP, (c) GLN, (d) SER, (e) TYR, (f) THR, (g) LYS and (h) SiO_4^{4-}.

Additionally, it is likely that the plasma plays a significant role in both cleaning the substrate surface and creating active, high energy sites in both glass and laccase molecule through bombardment with energetic plasma species.

Numerical analysis to evaluate the most probable mechanisms for creation of the glass to laccase bonding was done in two steps: calculation of the energy needed to create covalent bonding and estimation of electrostatic interactions between them. To calculate the energy of reaction in the creation of covalent bonds the following formula was used:

$$\Delta E = (E_{[SiO4]4-} + E_{aminoacid}) - E_{complex}, \text{ where}$$

ΔE = energy needed for covalent bond creation; $E_{[SiO4]4-}$ = energy of SiO_4^{4-};
$E_{aminoacid}$ = energy of selected amino acids (ARG, ASP, GLN, SER, TYR, THR or LYS);
$E_{complex}$ = energy of SiO_4^{4-} + amino acid complex cross-linked by covalent bond.

Estimations of the energy needed for covalent bond creation were performed between laccase and Si atom of SiO_4^{4-} and laccase and O atom of SiO_4^{4-}. Electrostatic interactions were evaluated based on local charges occurring in SiO_4^{4-} and amino acids molecules determined using Mulliken population analysis performed by the HF/6-311G (d,p) method.

Results showed different energies of creation of covalent bonds by Si and O atoms. Calculated ΔE values indicate that creation of covalent bonds by O atoms of SiO_4^{4-} is energetically more favourable. Quantum-chemical analysis showed that the lowest energy required for bonding is between O atoms of SiO_4 and N atoms in the $–NH_2$ group of LYS.

Local charges determined by Mulliken population analysis showed that O atoms are characterized by negative and Si atoms by positive local charges. Thus, we predict that electrostatic bonding interactions can occur between O atoms of SiO_4^{4-} and C atoms of amino acids and between Si atoms of SiO_4^{4-} and N or O atoms of amino acids.

Acknowledgements

We acknowledge support from Polish Ministry of Science and Higher Education within the statutory work research number S/ 12/ II B/2018.

Literature:

[1] D. Hegemann, M.M. Hossain, E. Korner, D.J. Balazs, *Plasma Process and Polymers*, 4 (2007) 229-238

[2] PQS version 3.1 Parallel Quantum Solutions, 2013 Green Acres Road, Fayetteville, Arkansas 72703

ATR-FTIR study of low-temperature atmospheric pressure plasma treated *Aspergillus* mycelia

Veronika Medvecká[1], Juliana Šimončicová[2], Dušan Kováčik[1], Anna Zahoranová[1], Mirko Černák[1]

[1]*Department of Experimental Physics, Faculty of Mathematics, Physics and Informatics, Comenius University, Mlynská dolina F2, 842 48 Bratislava, Slovakia*
[2]*Institute of Biochemistry and Microbiology, Faculty of Chemical and Food Technology, Slovak University of Technology, Radlinského 9, Bratislava 812 37, Slovakia*

E-mail: veronika.medvecka@fmph.uniba.sk

The low-temperature plasma is widely studied as prospective tool for decontamination and sterilization and has advantages of low-temperature operation, time-saving and non-toxicity over the conventional methods such as dry heat, steam autoclave, γ-ray irradiation and ethylene oxide [1]. The dominant position in this area have low pressure discharges, by which the suitable non-equilibrium plasma can be generated. However, vacuum equipment brings more complicated application in practice. Atmospheric pressure plasma sources provide advantages in practical side, design simplicity, low operational time and cost and others [2]. The important requirement for plasma is low temperature. The dielectric barrier discharges (DBD) have been widely studied for decontamination and sterilization of various surfaces [3,4].

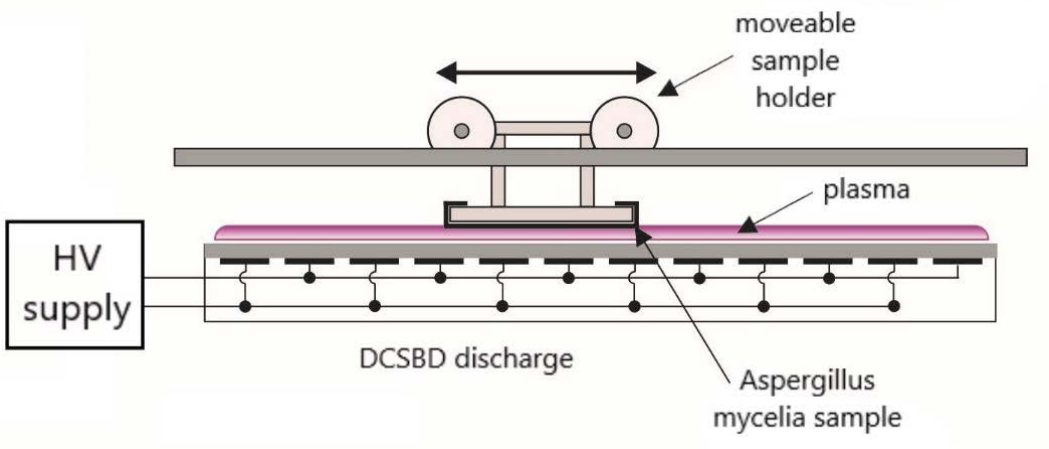

Fig. 1: Scheme of experimental set-up with DCSBD for treatment of *Aspergillus* spp.

In our work, a special type of DBD was studied for surface changes corresponding to growth inhibition of three fungal species of *Aspergillus* genus – *A. flavus*, *A. parasiticus* and *A. ochraceus*. The effect of plasma was studied on mycelia samples. Fungal samples were treated by Diffuse Coplanar Surface Barrier Discharge (DCSBD) [5] at atmospheric pressure in ambient air for 60 s and 180 s. Cell surfaces first come into contact with biologically active species generated by plasma and the key role play reactive oxygen species. The changes in chemical bonds on the surface of samples were detailed studied by Fourier Transform Infrared Spectroscopy (ATR-FTIR). The fungal cell walls are composed of polysaccharides and smaller

amounts of lipid and protein. Comparison of surface composition of all three fungal models and the possible plasmo-chemical and biological processes are discussed.

Acknowledgement: This work was supported by the Slovak Research and Development Agency under the contract No. APVV-16-0216. This project has received funding from the European Union's Horizon 2020 research and innovation programme under grant agreement No 692335.

References

[1] F. Rossi *et al., New Journal of Physics*, **11** (2009), 115017.
[2] J. Ehlbeck *et al., Journal of Physics D: Applied Physics*, **44** (2011), 13002.
[3] K.G. Kostov *et al., Surface and Coatings Technology*, **204** (2010), 2954.
[4] H. Miao, G. Yun, *Applied Surface Science*, **257** (2011), 7065.
[5] M. Černák *et al., Plasma Physics and Controlled Fusion*, **53** (2011), 124031.

THE BARRIER DISCHARGES IN THE BINARY GAS MIXTURES OF ARGON AND VOLATILE ORGANIC COMPOUNDS

Abramovskaia E.A., Kozlov K.V.
Lomonosov Moscow St. University, Chemical Dept., Leninskie gory 1/3, Moscow, Russia

E-mail: kat.abramovskaya@gmail.com

At present generators of low-temperature chemical active plasma, which use inert gases as a plasma-forming environment are particularly attractive for practical application in thin-film deposition, etching, and surface modification technologies for various materials. In gas discharges noble gases are chemically inert and possess high energy of electrons which initiate chemical transformations of reagents [1]. As is known, the barrier discharge can be operated in the filamentary mode or in the diffuse mode depending on the operation conditions [2 and references therein]. According to the authors' data [3, 4], a DBD can be diffuse in mixtures of argon with acetone depending on the conditions of the experiment which makes the system "argon + volatile organic compound" extremely attractive for a practical applications. In connection with this, we investigated the barrier discharge in mixtures of argon with certain organic substances of various classes such as methanol, ethanol, propan-2-ol, ethyl acetate and acetonitrile. Diagnostics of the plasma of the discharges in such gas mixtures was carried out by means of the technique of cross-correlation spectroscopy.

As a result of our the experiments it turned out that a barrier discharge can be operated in both filamentary mode and diffuse one in argon with an admixtures of all the organic compounds investigated with the exception of the argon-acetonitrile mixture (in this gas composition diffuse type of barrier discharge was not observed under any experimental conditions). Difference between two regimes is shown at fig. 1. Moreover, it was revealed that the operation mode of the barrier discharge depends primarily on the concentration of the organic impurity and on the discharge gap width.

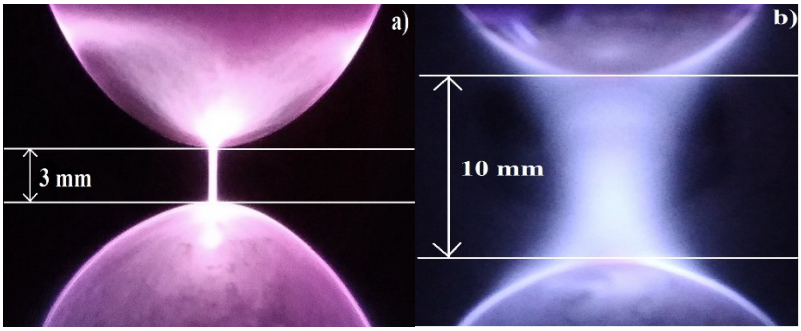

Fig. 1: Filamentary mode (a) and diffuse mode (b) on the example of DBD in gas mixtures of argon and ethanol. Concentration of EtOH: (a) 0.01%, (b) 0.3%. Feeding voltage frequency f = 6.2 kHz.

Typical dependencies of the discharge operation mode on the mentioned above conditions are shown at fig. 2.

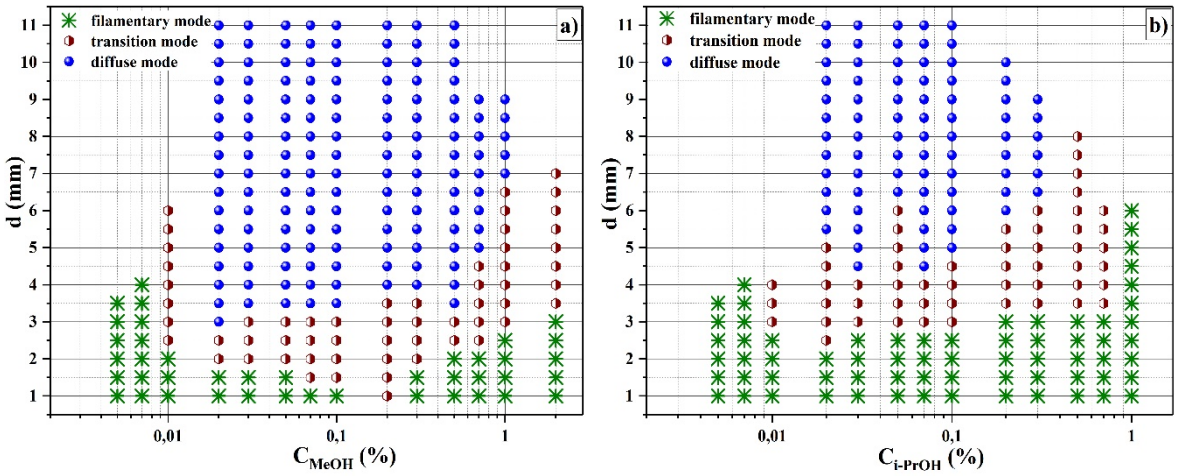

Fig. 2: Dependences of the barrier discharge operation mode on the methanol (a) and isopropanol (b) concentration and on the discharge gap width. Feeding voltage frequency f = 6.2 kHz, voltage amplitude was maintained at the minimal possible value (equal to burning voltage).

It can be seen that the diffuse form of the DBD is observed in a rather limited range of concentrations of organic compound in argon and for broad discharge gap width. Due to the continuous transition from one combustion mode to another with increasing discharge gap width in some cases it was difficult to distinguish between them, that is why we denoted such DBD operation mode as "transition mode". The experimental conditions under which diffuse mode of DBD can be operated are practically similar for all substances under investigation: concentration of methanol 0.02% − 1% and d≥3 mm; 0.02% − 0.7% of ethanol in argon and d≥4 mm; 0,02% − 0,3% of isopropanol in argon and≥4 mm; 0,04% − 0,3% of ethyl acetate and d ≥ 4-5 mm.

It should be noted that the ionization potentials of methanol, ethanol, isopropanol and ethyl acetate are 10.85 eV, 10.48 eV, 10.16 eV and 10.1 eV respectively, which are less than the energies of the metastable states of the argon atom (11 - 12 eV). But opposite the ionization potential of acetonitrile is higher than the energies of metastable states of argon and is equal to 12.2 eV. Apparently, such a difference of the IP of the molecular impurity and the energies of the excited metastable states of the carrier gas is also the determining factor for the possibility of developing a barrier discharge in the diffuse mode. So that, it is reasonable to expect the formation of a diffuse barrier discharge in other different gas mixtures in which the ionization potential of a volatile molecular compound is lower than the energy of metastable excited states of noble gas atoms.

References

1. P. Heyse, R. Dams, S. Paulussen et al., Plasma Process. Polym. 4, 145-157 (2007)
2. R. Brandenburg, Plasma Sources Sci. Technol. 26, 053001 (2017)
3. K. Urabe, K. Yamada, O. Sakai , Jap. J. Appl. Phys. 50, 11R, 116002 (2011)
4. K.V. Kozlov, E.A.Abramovskaia in *Proceedings of the 15th International Symposium on High Pressure Low Temperature Plasma Chemistry (HAKONE-XV)*, Brno, Czech Republic, 2016, p. 184

Multi-channel plasma igniter and plasma fuel injector for aero engine

Bingxuan LIN[1], Yun WU[2], Yifei Zhu[1], Shengfang Huang[1], Di JIN[1], Min JIA[1]
[1] *Science and Technology on Plasma Dynamics Laboratory, Air Force Engineering University, Xi'an, China*
[2] *Institute of Aero-engine, School of Mechanical Engineering, Xi'an Jiaotong University, Xi'an, China*
E-mail:244146596@qq.com

Extensive lean blow-out (LBO) limit of combustor and reliable relight in the event of flame out are crucial for both safety and aircraft engine performance requirement [1]. The low pressure and temperature at high altitude degrades spray atomization, vaporization, and ignition chemistry, resulting in lean flame instability and extremely difficult relight [2]. Plasma provides an unprecedented opportunity for combustion owing to its unique capability and has been applied to aerospace propulsion systems [3].

There is a minimum ignition energy (MIE) deposited into the combustible mixture to achieve successful ignition. Chen et al. found that MIE is governed by a critical flame initiation radius (Rc) [4]. Successful ignition is achieved only when the ignition kernel can reach the critical flame initiation radius. At high altitude with low pressure, the critical flame initiation radius becomes large and it cannot be easily reached by the ignition kernel. In this study, a multi-channel plasma igniter (MCPI) was proposed to induce a large ignition kernel and to achieve successful ignition as shown in Fig.1. The discharge energy of MCPI with five channels is about five times more than that of conventional spark igniter (SI). As is seen in Fig.2, MCPI can generate much larger plasma volume and forming a larger initial flame kernel compared to SI. Cavity ignition experiments in an ethylene-fueled model scramjet combustor were conducted with SI and MCPI. The ignition processes of SI and MCPI at different fuel injection schemes were captured by CH* chemiluminescence imaging. The lean ignition limit of scramjet combustor using MCPI can be extended by 20%~26% than that through SI. The ignition time was also reduced by approximately 50%.

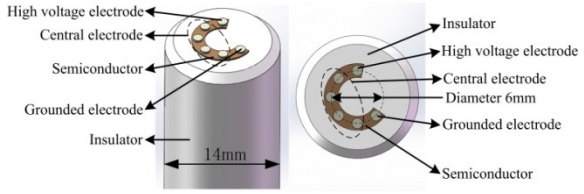

Fig. 1: Multichannel plasma igniter setup.

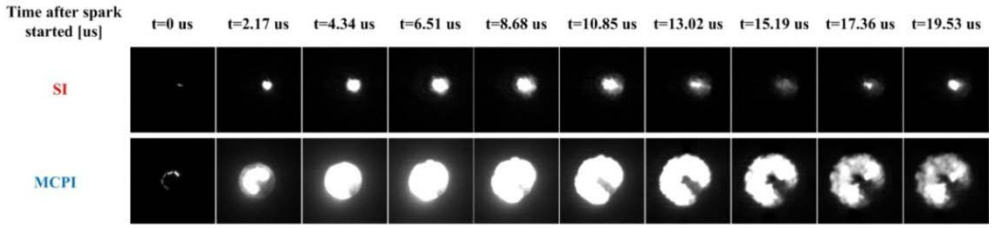

Fig. 2: Spark plasma volume and activated area development of SI and MCPI at atmospheric pressure from top view.

In order to combine plasma source and fuel atomizer into one device, a plasma fuel nozzle using transient DC discharge as shown in Fig.3 was proposed to obtain reliable altitude relight performance and wider LBO limits. The ignition and extinction experiments of GAPFI using normal and low-temperature kerosene (RP-3) were conducted. A thin and string-like gliding

arc plasma column was observed with repeating phases of breakdown between the fuel atomizer and venturi nozzle, extension with rotating airflow and column quenching. The optical emission spectroscopy of gliding arc plasma in GAPFI indicated the heating effect of the arc column.

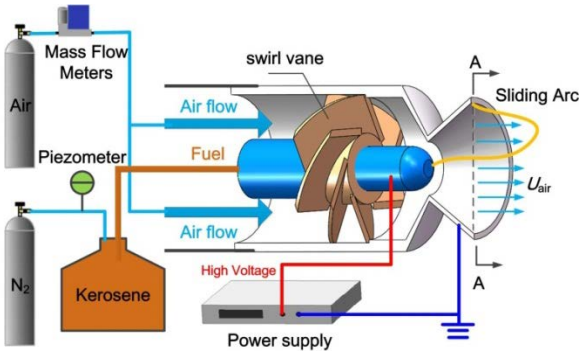

Fig. 3. A schematic of the GAPFI and supply system.

Based on the analysis of GA discharge, the effects of GAAFI on kerosene spray characteristics and hydrocarbon compounds productions were investigated. The ignition limit was largely extended using GAPFI almost the same with the LBO limits, especially for the low temperature fuel. Low temperature and low injection pressure leads to much larger droplets and irregular injection cone. Influenced by heating and hydrodynamic effect of gliding arc plasma, the drop size of -30 ℃ kerosene spray decreases from around 150 μm to 30 μm with GAPFI, which is a main reason for ignition range extension. The equivalence ratios of LBO were extended by up to 48% and 47% using 5 ℃ and -30 ℃ kerosene, respectively. Several light hydrocarbons, such as CH_4 (1.26 SLM), C_2H_4 (1.31 SLM) and C_2H_2 (2.30 SLM) with a larger laminar flame propagation velocity, were detected as reforming products. Both heating and reforming effects contribute to the LBO limit extension. The residence time of kerosene sprays in GAAFI is the determining factor for conversion capability.

Acknowledgement:
This work is supported by National Natural Science Foundation of China (NSFC, 91541120, 91641204, 51336011).

Reference:
[1] Serbin S I, Matveev I B, Mostipanenko G B. Investigations of the working process in a “Lean-Burn” gas turbine combustor with plasma assistance[J]. IEEE Transactions on Plasma Science, 2011, 39(12): 3331-3335.
[2] Pucher G, Allan W D. Turbine fuel ignition and combustion facility for extremely low temperature conditions[C]//ASME Turbo Expo 2004: Power for Land, Sea, and Air. American Society of Mechanical Engineers, 2004: 385-392.
[3] Ju Y, Sun W. Plasma assisted combustion: Dynamics and chemistry[J]. Progress in Energy and Combustion Science, 2015, 48: 21-83.
[4] Chen Z, Burke M P, Ju Y. On the critical flame radius and minimum ignition energy for spherical flame initiation[J]. Proceedings of the Combustion Institute, 2011, 33(1): 1219-1226.

Lean Flammability Characteristics of Plasma-actuated Swirl Flames under Pulsating Flow Disturbances

Wei Cui, Hu Wu, Shuiqing Li*

Department of Energy and Power Engineering, Tsinghua University, Beijing, China

E-mail: cw14@mails.tsinghua.edu.cn

Flow pulsations obviously affect the lean flammability limits of premixed flames. In contrast to positive pulse, the negative pulse deteriorates the lean flammability limits more severely. The flammability limits are obviously extended by the plasma with a proper time delay between discharges and flow pulses, and further destabilizes the flame with improper time delays. The flame front is highly wrinkled and stretched by the shockwaves and aerodynamic actuations induced by the plasma. The high stretched flame is prone to extinction, which partially explain the plasma-deterioration mechanism.

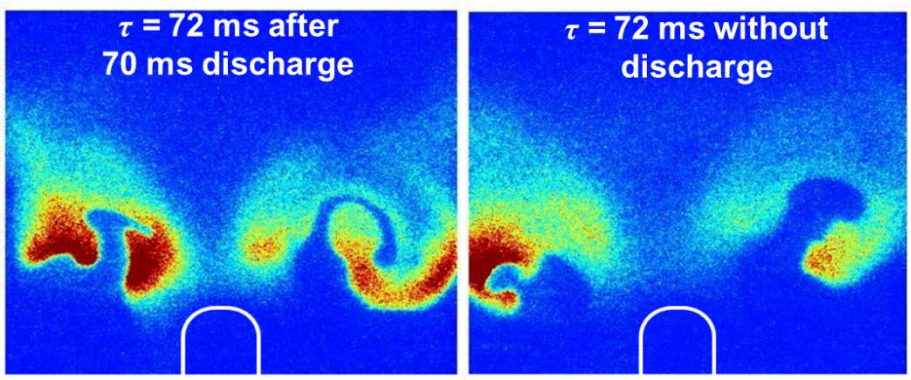

Fig. 1: Single-shot OH-PLIF images: 2 ms later after τ = 70 discharge / without discharge

Electrohydrodynamic flame instability under manipulations of AC and DC electric fields

Yihua Ren, Wei Cui, Shuiqing Li*

Department of Energy and Power Engineering, Tsinghua University, Beijing, China

E-mail: ryh13@mails.tsinghua.edu.cn

Sub-breakdown electric fields have been intensively investigated to drive convections, stabilize flames, and control flame-synthesized nanoparticles, etc. The electric fields affect flame front structures by electric body forces in a complex way. The two-way coupling between the flame hydrodynamic behaviors and the electric responses of the flame plasmas can induce a novel electrohydrodynamic flame instability which can be well demonstrated in a premixed stagnation flame setup.

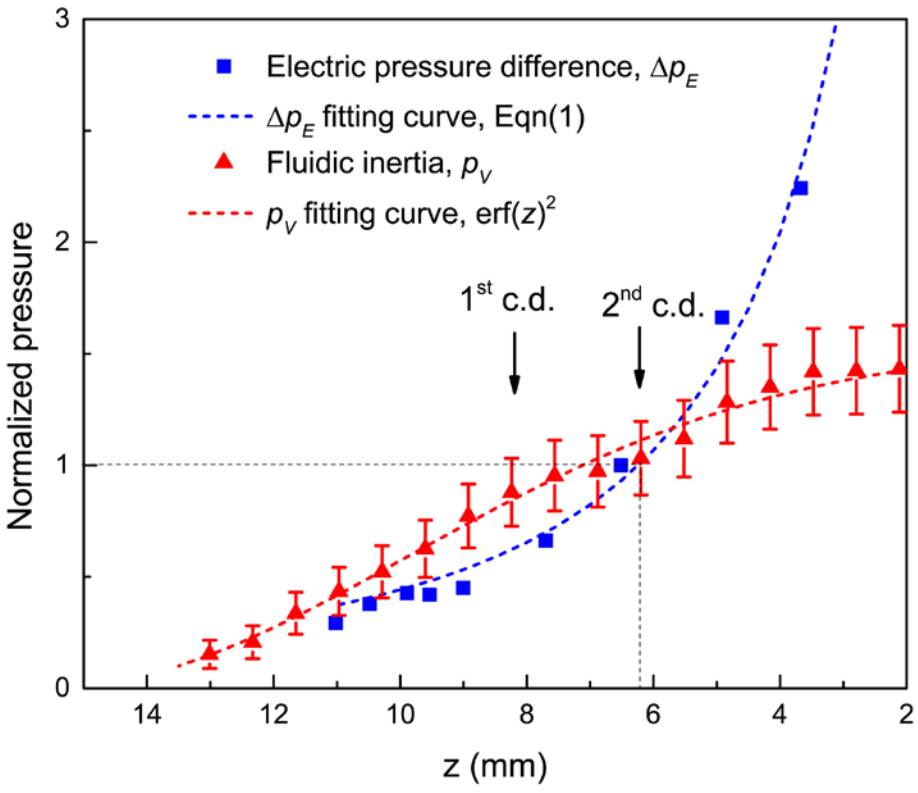

Fig. 1: Growth rates comparison between fludic inertia and electric pressure

Phase-selective Laser-induced Breakdown Spectroscopy

Yihua Ren, Yiyang Zhang, Shuiqing Li*

Department of Energy and Power Engineering, Tsinghua University, Beijing, China

E-mail: ryh13@mails.tsinghua.edu.cn

Phase-selective laser induced breakdown spectroscopy (PS-LIBS) has shown the ability to be a diagnostic for gas-to particle conversion, volume fraction measurement,and bandgap variation in mixed crystal structures. Briefly, nano particles are selectively broken down into plasma, with no gas phase breakdown because of the different thresholds between gas and particle phase, such that atomic spectroscopy can be made of only atoms originating from the particulate phase. Therefore, it can be applied to examine the gas-to-particle conversion process in flame aerosol synthesis, as well as sodium release during coal combustion. When PS-LIBS signals reach saturation with laser intensity, the signal intensity is linear with volume fraction of particles, enabling quantitative measurement of volume fraction.

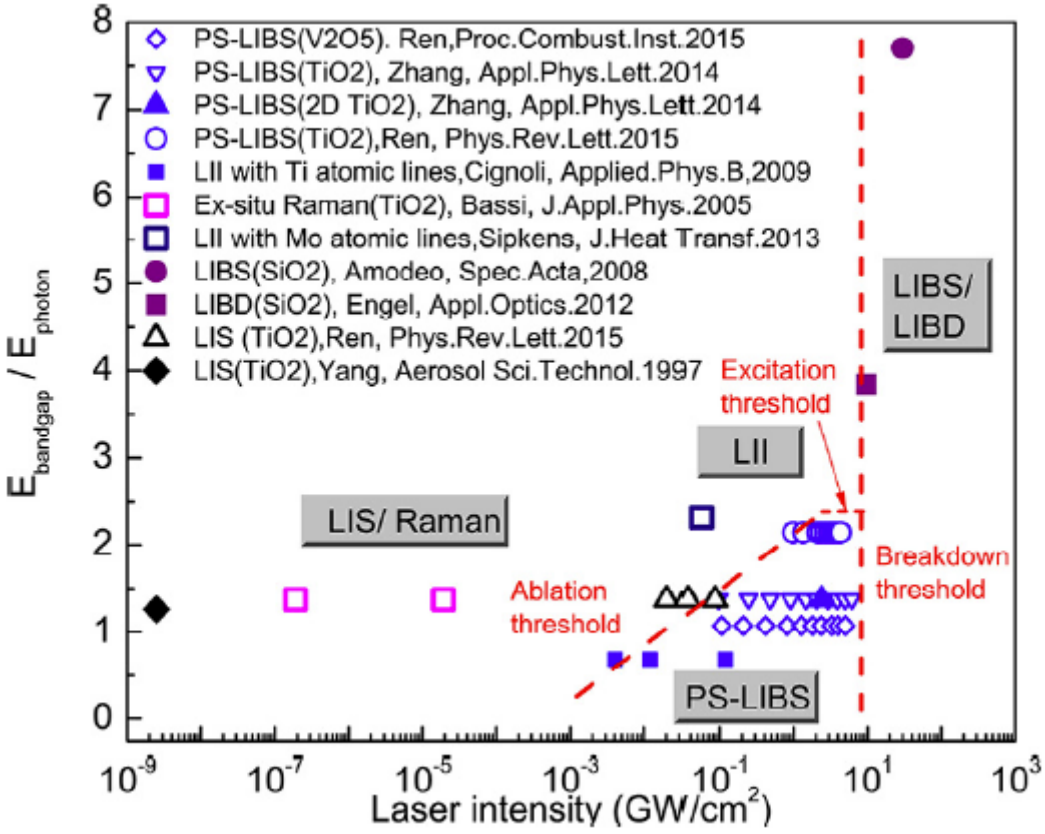

Fig. 1: Map of different laser–matter interactions of various laser-based diagnostic methods.

FLOW FLUCTUATION INDUCED BY COAXIAL PLASMA DEVICE AT ATMOSPHERIC PRESSURE

Yong Tang[1], Qiang Yao[1], Wei Cui[1], Shui-Qing Li[1], Yi-Kang Pu[2]
[1]*Department of Energy and Power Engineering, Tsinghua University, Beijing 100084, China*
[2]*Department of Engineering Physics, Tsinghua University, Beijing 100084, China*

E-mail: tang-y15@mails.tsinghua.edu.cn

With a novel flow configuration, the flow structure and velocity fluctuation generated downstream from a coaxial geometry Dielectric-Barrier-Discharges are investigated at atmospheric pressure. The discharges are characterized using in-situ electrical measurements and optical diagnostics. Both streamers and glow-like discharges are detected in each alternating-current cycle. The flow structure is temporally and spatially resolved using tracer particles, and large vortices are visualized in planar velocity distribution patterns (Fig.1). The flow upstream of the discharge is laminar; however, we discover that the spectrum of downstream fluctuation velocity exhibits a nearly Kolmogorov −5/3 slope (Fig.2), which is a typical feature for high Reynolds number turbulent flows. Based on the electron density measured through a line-ratio method, the dimensionless pressure and electrical body force derived from Navier-Stokes equation is estimated to illustrate the generation of Reynolds stress.

$$\mathrm{Eu}(p) = \frac{\langle p \rangle}{\rho U_0^2}, \mathrm{Re}_l = \frac{\rho U_0 l}{\mu}, \mathrm{Fr}_e^2 = \frac{\rho U_0^2}{q n_* E_0 l} \quad (1)$$

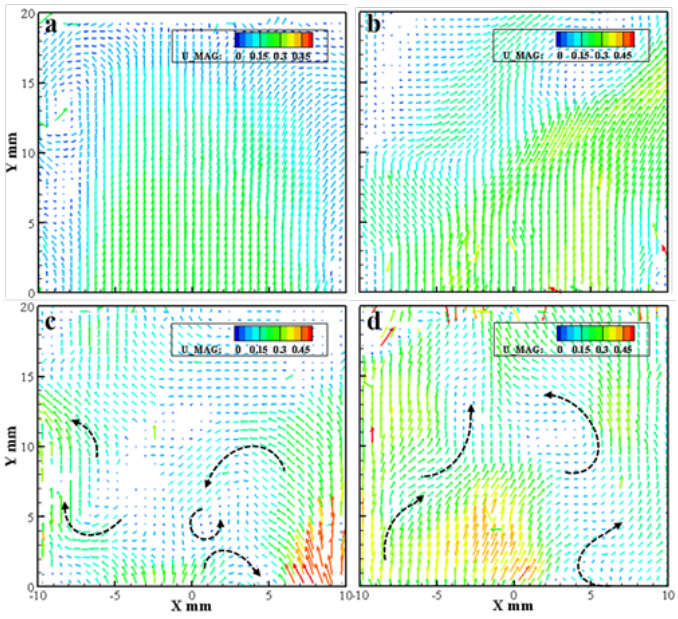

Fig. 1: Typical PIV (Particle Image Velocimetry) image of the flow field at the exit of the nozzle in ambient air: a) plasma off; b) 0.4 kHz; c) 6.5 kHz; d) 25 kHz. Dashed lines indicate vortices. (Velocity is in m/s).

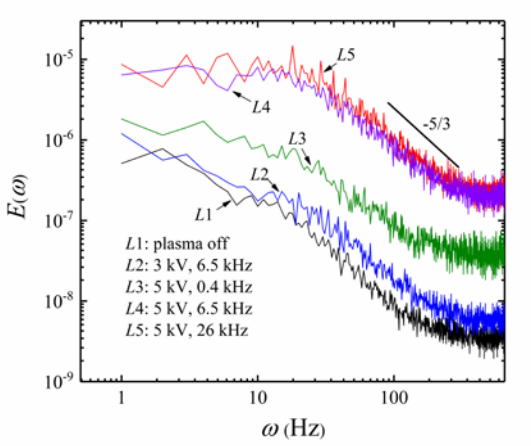

Fig. 2: Frequency energy spectrum in plasma-affected flow at different discharge voltages and frequencies. The flow rate of argon was fixed at 4 slm. The focal sampling point is on the centerline and 2 mm away from the nozzle exit plane.

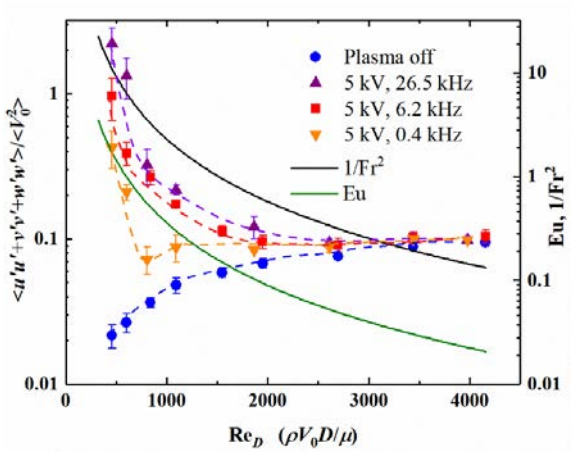

Fig. 3: Time-averaged Reynolds stress, Eu(p) , and $1/Fr^2$ versus the Reynolds number of the bulk flow. It shows a positive correlation between the Reynolds stress and the operating frequency. At high frequency, the plasma-induced body force plays an important role on Reynolds stress when bulk Reynolds number is less than 2000.

Fig.3 illustrates that the fluctuation intensity of the neutral flow increases at first, and then remains nearly constant. However, the plasma-induced Reynolds stress decreases dramatically at first, and subsequently approaches that of the neutral flow. In other words, the inertial force become dominant as the flow rate increases. $1/Fre^2$ for the transition also increases with operating frequency.

For Reynolds numbers over a range of 400 to 2000, flow fluctuations generated downstream of a high-frequency discharge are prominent, and a positive correlation is observed between the fluctuation intensity and the operating frequency. The measured discharge power varies with frequency but remains nearly constant for different flow rates. For a 0.3 m/s bulk flow and 6.5 kHz discharge (with the power of ~ 1 W), the fluctuation velocity is about 0.3 m/s, and the turbulent kinetic power is less than 10-4 W. The temperature of the argon flow downstream of the discharge, measured by employing a K-type thermocouple, increased by about 2 K after plasma treatment. The gas heating power is above 0.1 W since the heat loss is not included. Thus, energy transfer to the kinetic energy of the flow is a very small fraction of the input power, which is mainly converted into Joule heating or chemical energy.